

Spectral and nonlinear optical characterization of ZnO nanocomposites

Litty Mathew Irimpan

International School of Photonics
Cochin University of Science and Technology
Cochin – 682 022, Kerala, India

Ph D Thesis submitted to Cochin University of Science and Technology in
partial fulfilment of the requirements for the award of the degree of

Doctor of Philosophy

June 2008

Spectral and nonlinear optical characterization of ZnO nanocomposites

Thesis in the field of Photonics

Author:

Litty Mathew Irimpan

Research Fellow, International School of Phonics,
Cochin University of Science and Technology,
Cochin-682 022, Kerala, India

Email: littyirimpan@yahoo.co.in, lit.irimpan@gmail.com

Research Advisors:

Dr. P Radhakrishnan

Professor, International School of Phonics,
Cochin University of Science and Technology,
Cochin-682 022, Kerala, India

Email: radhak@cusat.ac.in

Dr. V P N Nampoori

Professor, International School of Phonics,
Cochin University of Science and Technology,
Cochin-682 022, Kerala, India

Email: nampoori@gmail.com

International School of Phonics, Cochin University of Science and
Technology, Cochin-682 022, Kerala, India

URL:www.photonics.cusat.edu

June 2008

Front cover: saturable and reverse saturable absorption

Background: SEM image of ZnO self assembled film

Cover design: Aneesh Krishnan

Dedicated to

My loving parents

Life is...

Life is an opportunity, benefit from it.

Life is beauty, admire it.

Life is a dream, realize it.

Life is a challenge, meet it.

Life is a duty, complete it.

Life is a game, play it.

Life is a promise, fulfill it.

Life is sorrow, overcome it.

Life is a song, sing it.

Life is a struggle, accept it.

Life is a tragedy, confront it.

Life is an adventure, dare it.

Life is luck, make it.

Life is too precious, do not destroy it.

Life is life, fight for it.

Mother Theresa

CERTIFICATE

Certified that the work presented in the proposed thesis entitled "*Spectral and nonlinear optical characterization of ZnO nanocomposites*" is based on the original work done by Smt. Litty Mathew Irimpan under my guidance and supervision at the International School of Photonics, Cochin University of Science and Technology, Cochin–22, India and has not been included in any other thesis submitted previously for award of any degree.

Cochin–22
30th June 2008.

Prof. P Radhakrishnan
(Supervising Guide)

DECLARATION

Certified that the work presented in the thesis entitled “*Spectral and nonlinear optical characterization of ZnO nanocomposites*” is based on the original work done by me under the guidance of Dr. P Radhakrishnan, Professor, International School of Photonics, Cochin University of Science and Technology, Cochin–22, India and the co-guidance of Dr. V P N Nampoori, Professor, International School of Photonics, Cochin University of Science and Technology, Cochin–22, India and it has not been included in any other thesis submitted previously for award of any degree.

Cochin–22

30th June 2008.

Litty Mathew Irimpan

Preface

Semiconductor nanoparticles have been the subject of scientific interest because of their unique quantum confinement nature, which changes the optical and electronic properties of materials. The study of these properties constitutes new perspectives for basic and applied research in nanophotonics. Amongst the different semiconductors, ZnO has gained substantial interest because of its large exciton binding energy which could lead to lasing action based on exciton recombination even above room temperature. Nonlinear optics offers to these classes of nanomaterials numerous new functionalities such as spectral tunability and ultrafast nonlinear response. The thesis has seven chapters and it reports the results obtained from the systematic studies carried out on the spectral and nonlinear optical properties of ZnO nanocomposites.

Chapter 1 gives a glimpse of the potentials of the marriage between nonlinear optics and nanotechnology. Blue shift of the absorption edge, size dependent luminescence, enhanced oscillator strength and nonlinear optical properties are some of the interesting properties exhibited by most of the nanomaterials. All these properties are various manifestations of the quantum confinement effect, which arises due to the increasing proximity of electrons and holes with the diminishing size of the crystallites and the consequent changes in the electronic structure. This is an exciting area of research, which makes it possible to tune the properties of nanoparticles to suit any application by tailoring size and may find tremendous technological applications. In this chapter, the applications of ZnO nanocomposites along with some important optical properties exhibited by them have been introduced. This chapter also includes the theory and experimental details of the z-scan technique used to study the nonlinear optical properties of ZnO nanocomposites.

Chapter 2 describes the fluorescence spectroscopy of nano colloids of ZnO. The fluorescence behaviour has been studied as a function of the excitation wavelength and there is a red shift in emission peak with excitation wavelength. In essence, the inefficient energy transfer between the

upper and the lower vibrational levels of the excited state of these particles owing to short fluorescence lifetime is primarily responsible for the excitation wavelength dependent spectral shift of ZnO colloids. Fluorescence spectra consist of emissions in the UV and visible regions. Apart from the known band gap emissions at 380 nm and impurity dominated emissions at 530 nm, emissions at 420 and 490 nm are also observed with change in particle size. Systematic studies on nano ZnO have indicated the presence of luminescence due to excitonic emissions when excited with 255 nm as well as significant contribution from surface defect states when excited with 325 nm. The relevant energy levels showing the transitions corresponding to the observed peaks in the emission spectrum of ZnO of particle size 18 nm under 255 nm excitation are identified. The luminescence mechanism and a correlation analysis between the particle size and spectroscopic observations are discussed.

Chapter 3 discusses the size dependent enhancement of nonlinear optical properties in nano colloids of ZnO. ZnO nano colloids show negative nonlinearity and good nonlinear absorption behaviour at 532 nm. The observed nonlinearity is explained through two photon absorption followed by weak free carrier absorption. The third-order optical susceptibility ($\chi^{(3)}$) increases with increasing particle size (R) due to the size dependent enhancement of exciton oscillator strength. In the weak confinement regime, R^2 dependence of $\chi^{(3)}$ is obtained for ZnO nano colloids. Nonlinear susceptibility is highly fluence dependent and it becomes quadratic in nature for large particle size. The optical limiting response of ZnO nano colloids, in the range of 6–18 nm, increases with the increase of particle size.

Chapter 4 presents the third order nonlinear optical properties of self assembled films formed from ZnO colloidal spheres are investigated and are compared with those of ZnO thin films deposited by sol-gel process as well as pulsed laser ablation. Both ZnO colloids and films clearly exhibit a negative nonlinear index of refraction. However there is a change in the sign of the absorptive nonlinearity of the self assembled films compared to others.

The colloids and the films developed by dip coating and pulsed laser ablation exhibit reverse saturable absorption whereas the self assembled films exhibit saturable absorption. These different nonlinear characteristics can be mainly attributed to ZnO defect states and electronic effects when the colloidal solution is transformed into self assembled films. We report our investigations on the intensity, wavelength and size dependence of saturable and induced absorption of ZnO self assembled films and colloids. Values of the imaginary part of third order susceptibility are calculated for particles of size in the range 20-300 nm at different intensity levels ranging from 40 to 325 MW/cm² within the wavelength range of 450–650 nm. The wavelength dependence of figure of merit, which specifies the magnitude of nonlinear absorption for unit value of linear absorption, is calculated and this helps in comparing the absorptive nonlinearities at various excitation wavelengths.

Chapter 5 explains the effect of annealing on the spectral and nonlinear optical characteristics of ZnO thin films deposited on quartz substrates by sol gel process. As the annealing temperature increases from 300-1050°C, there is a decrease in the band gap which indicates the changes of the interface of ZnO. In the fluorescence spectra we have observed two principal bands: UV band and visible band. Systematic studies on nano crystallites have indicated the presence of luminescence due to excitonic emissions when excited with 255 nm as well as significant contribution from surface defect states when excited with 325 nm. The intensity of UV peak remains the same while the intensity of the visible peak increases with increase in post-annealing temperature. Nonlinear optical response of these samples is studied using nanosecond laser pulses at off-resonance wavelengths for optical limiting applications. The nonlinear susceptibility increases from 2.3×10^{-6} to 1.3×10^{-5} esu when the annealing temperature rises from 300°C to 1050°C, mainly due to the enhancement of interfacial state and exciton oscillator strength. We have experimentally studied the optical nonlinearity as a function of temperature and a $T^{2.5}$ dependence of nonlinear susceptibility is obtained for thin films of nano ZnO. Optical limiting response is temperature dependent and the film annealed at higher

temperature and having larger particle size is a better nonlinear absorber and hence a good optical limiter.

Chapter 6 explains the spectral and nonlinear optical properties of ZnO based nanocomposites prepared by colloidal chemical synthesis. Very strong UV emissions at room temperature are observed from ZnO-Ag, ZnO-Cu and ZnO-SiO₂ nanocomposites. The strongest visible emission of a typical ZnO-Cu nanocomposite is over ten times stronger than that of pure Cu due to transition from deep donor level to the copper induced level. The optical band gap of ZnO-CdS and ZnO-TiO₂ nanocomposites is tunable and emission peaks changes almost in proportion to changes in band gap. It is possible to obtain a desired luminescence colour from UV to green by simply adjusting the composition. Nonlinear optical response of these nanocomposites is studied using nanosecond laser pulses from a tunable laser in the wavelength range of 450-650 nm at resonance and off-resonance wavelengths. The nonlinear response is wavelength dependent and switching from induced absorption to SA has been observed at resonant wavelengths. Such a change-over is related to the interplay of plasmon/exciton band bleach and optical limiting mechanisms. ZnO based nanocomposites show self-defocusing nonlinearity and good nonlinear absorption behaviour at 532 nm. The observed nonlinear absorption is explained through two photon absorption followed by weak free carrier absorption, interband absorption and nonlinear scattering mechanisms. The nonlinearity of the silica colloid is low and its nonlinear response can be improved by making composites with ZnO and ZnO-TiO₂. The enhancement of the third-order nonlinearity in the composites can be attributed to the concentration of exciton oscillator strength. This study is important in identifying the spectral range and composition over which the nonlinear material acts as an RSA based optical limiter. These materials can be used as optical limiters and are potential nanocomposite material for the light emission and for the development of nonlinear optical devices with a relatively small limiting threshold.

Chapter 7 deals with the summary of the present work along with a brief report of the future prospects.

List of Publications

I. Journal Publications

- 1 **Litty Irimpan**, V P N Nampoori and P Radhakrishnan; “*Spectral and nonlinear optical characteristics of nanocomposites of ZnO-CdS*” Journal of Applied Physics [American Institute of Physics] **103**, 094914 (2008)
- 2 **Litty Irimpan**, V P N Nampoori and P Radhakrishnan; “*Spectral and nonlinear optical characteristics of nanocomposites of ZnO-Ag*” Chemical Physics Letters [Elsevier] **455** (4-6), 265-269 (2008)
- 3 **Litty Irimpan**, A Deepthy, Bindu Krishnan, V P N Nampoori and P Radhakrishnan; “*Nonlinear optical characteristics of self assembled films of ZnO*” Applied Physics B: Lasers and Optics [Springer] **90** (3-4), 547-556 (2008)
- 4 Litty Irimpan, Bindu Krishnan, V P N Nampoori and P Radhakrishnan; “*Luminescence tuning and enhanced nonlinear optical properties of nanocomposites of ZnO-TiO₂*” Journal of Colloid and Interface Science [Elsevier] **324** (1-2), 99-104 (2008)
- 5 **Litty Irimpan**, A Deepthy, Bindu Krishnan, L M Kukreja, V P N Nampoori and P Radhakrishnan; “*Effect of self assembly on the nonlinear optical characteristics of ZnO thin films*” Optics Communications [Elsevier] **281** (10), 2938-2943 (2008)
- 6 **Litty Irimpan**, Bindu Krishnan, A Deepthy, V P N Nampoori and P Radhakrishnan; “*Size dependent enhancement of nonlinear optical properties in nano colloids of ZnO*” Journal of Applied Physics [American Institute of Physics] **103**, 033105 (2008), Virtual Journal of Nanoscale Science & Technology, February 25 issue, 2008
- 7 **Litty Irimpan**, A Deepthy, Bindu Krishnan, V P N Nampoori and P

- Radhakrishnan, ‘Size dependent fluorescence spectroscopy of nanocolloids of ZnO’, Journal of Applied Physics [American Institute of Physics] **102**, 063524 (2007)
- 8 **Litty Irimpan**, Bindu Krishnan, A Deepthy, V P N Nampoori and P Radhakrishnan; “Excitation wavelength dependent fluorescence behaviour of nano colloids of ZnO” Journal of Physics D: Applied Physics [Institute of Physics] **40**, 5670-5674 (2007)
- 9 **Litty Irimpan**, V J Dann, Bindu Krishnan, A Deepthy, V P N Nampoori and P Radhakrishnan; “Backscattering of laser light from colloidal silica” Laser Physics [Springer] **18** (7), 882-885 (2008)
- 10 **Litty Irimpan**, Bindu Krishnan, V P N Nampoori and P Radhakrishnan; “Nonlinear optical characteristics of nanocomposites of ZnO-TiO₂-SiO₂” Optical Materials [Elsevier] DOI:10.1016/j.optmat.2008.05.009 (2008)
- 11 **Litty Irimpan**, V P N Nampoori and P Radhakrishnan; “Enhanced luminescence and nonlinear optical properties of nanocomposites of ZnO-Cu” Journal of Materials Research [Materials Research Society] 2008 (in press)
- 12 **Litty Irimpan**, D Ambika, V Kumar, V P N Nampoori and P Radhakrishnan; “Effect of annealing on the spectral and nonlinear optical characteristics of thin films of nano ZnO” Journal of Applied Physics [American Institute of Physics] 2008 (in press)
- 13 **Litty Irimpan**, Bindu Krishnan, V P N Nampoori and P Radhakrishnan; “Linear and nonlinear optical characteristics of ZnO-SiO₂ nanocomposites” Applied Optics [Optical Society of America] 2008 (in press)
- 14 **Litty Irimpan**, V P N Nampoori and P Radhakrishnan; “Visible

luminescence mechanism in nano ZnO under weak confinement regime”
communicated to Optics Letters

- 15 Bindu Krishnan, **Litty Irimpan**, V. P. N. Nampoori and V. Kumar; "Synthesis and nonlinear optical studies of nano ZnO colloids" Physica E [Elsevier] **40**, 2787 (2008)
- 16 Bindu Krishnan, A Deepthy, **Litty Irimpan**, V J Dann and V P N Nampoori; "Back scattering from nano-sized ZnO colloids" Physica E [Elsevier] **35**, 23-26 (2006)
- 17 Annieta Philip K, Lyjo K. Joseph, **Litty M. Irimpan**, Bindu Krishnan, P. Radhakrishnan, V. P. N. Nampoori and Raghu Natarajan "Thermal Characterization of Ceramic Tapes using Photoacoustic Effect" Physica Status Solidi (a) [Wiley Interscience] **204** (3), 737 (2007)
- 18 Annieta Philip K, Lyjo K Joseph, **Litty Mathew Irimpan**, P. Radhakrishnan and V.P.N Nampoori; "Photoacoustic study on the photostability of polymethyl methacrylate (PMMA) films doped with Rhodamine 6G-Rhodamine B dye mixture systems", Journal of Physics D: Applied Physics [Institute of Physics] **38**, 2904 (2005)

II. Conference Publications

- 1 **Litty Irimpan**, Bindu Krishnan, A Deepthy, V P N Nampoori and P Radhakrishnan; "Excitation wavelength dependent fluorescence behaviour of nano colloids of ZnO" Proceedings of national conference on Current Trends in Chemistry, CTriC-2008, Cochin, India, 18-19 January, 2008, OP-26, P 21
- 2 **Litty Irimpan**, A Deepthy, Bindu Krishnan, V P N Nampoori and P

Radhakrishnan; “*Size dependent fluorescence spectroscopy of nano ZnO colloids*” Proceedings of International Conference on Materials for the Millennium, *MatCon 2007*, Cochin, India, 1-3 March, 2007, P 115

- 3 **Litty Irimpan**, Bindu Krishnan, A Deepthy, V P N Nampoori and P Radhakrishnan; “*Size dependent enhancement in nonlinear optical properties of nano ZnO colloids using z-scan technique*” Proceedings of Eighth International Conference on Optoelectronics, Fiber Optics and Photonics, *Photonics 2006*, Hyderabad, 13-16 December 2006, NLO 5, P 188.
- 4 **Litty Irimpan**, A Deepthy, Bindu Krishnan, V P N Nampoori and P Radhakrishnan; “*Nonlinear optical characterization of self-assembled 3D photonic crystals from ZnO colloidal spheres*” Proceedings of Eighth International Conference on Optoelectronics, Fiber Optics and Photonics, *Photonics 2006*, Hyderabad, 13-16 December 2006, NLO 18, P 346.
- 5 **Litty Irimpan**, Deepthy A, Nampoori V.P.N, Radhakrishnan P; “*Optical nonlinearities in silicon quantum dots*”; Proceedings of International Conference on Optics & Optoelectronics, *ICOL-2005*, Dehradun, Uttarakhand, India, 12-15 December 2005, NLO 17, P260.
- 6 **Litty Irimpan**, V.J Dann, Bindu Krishnan, A. Deepthy, V.P.N Nampoori and P. Radhakrishnan; “*Studies on backscattering of laser light in colloidal silica*”; Proceedings of Seventh International conference on Optoelectronics, Fiber optics and Photonics, *Photonics 2004*, Cochin, India, 9-11 December 2004, LTW P10, P207.
- 7 Bindu Krishnan, **Litty Irimpan** and V. P. N. Nampoori; “*Nonlinear optical studies in PEI-capped ZnO colloids*”, National conference on photonics for advanced technology (NCPAT 2007), Thanjavur, Tamil

Nadu, March 22-25, 2007

- 8 Ritty J Nedumpara, Thomas K J, **Litty Mathew**, V P N Nampoori and P Radhakrishnan; “*Nonlinear absorption in dye doped polymer matrices*”; Proceedings of Eighth International Conference on Optoelectronics, Fiber Optics and Photonics, *Photonics 2006*, Hyderabad, 13-16 December 2006, NLO 21, P 349.
- 9 Bindu Krishnan, **Litty Irimpan** and V P N Nampoori; “*Flexible nanocomposite films with selective optical filtering*”; Proceedings of International Conference on Optoelectronic Materials and Thin films for Advanced Technology, *OMTAT 2005*, Cochin, India, 24-27 October 2005, NT020, P 63.
- 10 Bindu Krishnan, **Litty Irimpan**, V. P. N Nampoori and V. Kumar; “*Stable nano ZnO colloid using a novel capping agent*” Proceedings of First National Conference on Nanoscience and Technology, NPL, Pune, March 2005
- 11 Lyjo K Joseph, **Litty Mathew Irimpan**, Dann V J, Radhakrishnan P and V P N Nampoori; “*Fluorescence Study of Lanthanum Titanate*”; Proceedings of DAE- BRNS *NLS-5*, Vellore, P181-2 (2005)
- 12 Bindu Krishnan, **Litty Irimpan**, Deepthy A, Dann V.J and V.P.N. Nampoori; “*Non linear optical properties of nano-ZnO colloids using z-scan technique*”; Proceedings of National Laser Symposium, *NLS-4*, BARC, Mumbai, 10-13 January 2005, F7, P-418
- 13 Annieta Philip K, Lyjo K Joseph, **Litty M. Irimpan**, P. Radhakrishnan and V.P.N Nampoori; “*Concentration dependent photostability of dye doped olymer films- A PA study*”, Proceedings of National Laser Symposium, *NLS-4*, BARC, Mumbai, 10-13 January 2005, C3, P-300

- 14 Annieta Philip K, Lyjo K. Joseph, **Litty M. Irimpan**, Bindu Krishnan, P. Radhakrishnan, V. P. N. Nampoori and Raghu Natarajan “*Thermal characterization of zirconia and alumina-zirconia ceramic tapes using photoacoustic technique*”; Proceedings of National Laser Symposium, *NLS-4*, BARC, Mumbai, 10-13 January 2005, D5, P-342
- 15 P. Nandi, **Litty Irimpan**, P. Radhakrishnan, V.P.N. Nampoori and G. Jose; “*Spectroscopic properties of Ag-Na ion exchanged, Er-Yb codoped phosphate glasses*”; Proceedings of National Laser Symposium, *NLS-4*, BARC, Mumbai, 10-13 January 2005, G28, P515
- 16 Bindu Krishnan, A. Deepthy, **Litty Irimpan**, Dann V.J and V.P.N Nampoori; “*Coherent backscattering from nano-sized ZnO suspensions*”; Proceedings of Seventh International conference on Optoelectronics, Fiber optics and Photonics, *Photonics 2004*, Cochin, India, 9-11 December 2004, LTW P10, P208
- 17 Annieta Philip K, Lyjo K Joseph, **Litty Irimpan**, P. Radhakrishnan and V.P.N Nampoori; “*Photosensitivity of Laser Dye Mixtures in Polymer Matrix-A Photoacoustic Study*”; Proceedings of Seventh International conference on Optoelectronics, Fiber optics and Photonics, *Photonics 2004*, Cochin, India, 9-11 December 2004, PMR P7, P440

*“Live as though you will die tomorrow,
but learn as though you live forever”
: Gandhiji*

Acknowledgments

No matter how this thesis is attributed, its contents are actually the fortunate product of the insights and direction of several people whose contributions I gratefully acknowledge. I would like to express my sincere gratitude to my guide, Prof. P Radhakrishnan, for all of his instructive comments and evaluation at every stage of the thesis process. His unwavering support throughout the research period as well as his pain-staking effort in reviewing the thesis is greatly appreciated. His involvement in research has triggered and nourished my intellectual maturity that I will benefit from, for a long time to come. My co-guide, Prof. V P N Nampoori, has been everything that one could want in an advisor. His truly scientist intuition has made him as a constant oasis of ideas and passions in science, which exceptionally inspire and enrich my growth as a student and a researcher. Besides providing useful comments and contributing his all important signatures to my thesis, his contribution in the role of a more experienced friend and well-wisher was a great support. I am indebted to him more than he knows. My sincere thanks go to Prof. C P G Vallabhan and Prof. V M Nandakumaran for providing me intellectual advice. I also thank Prof. N V Unnikrishnan, Prof. Prathap, Prof. Unnikrishnan Nayar, Mr. Kailasnath, Dr. Sheenu and all teaching staff of ISP and CELOS. I take this opportunity to thank all my school and college teachers.

I would like to acknowledge the financial support of University Grants Commission, UGC. It is a pleasure to pay tribute also to the sample collaborators. I thank Dr. L M Kukreja, RRCAT, Indore and Dr. Kumar, CMET, Thrissur for ZnO films. Special thanks to Ambika who prepared ZnO spin coated samples at C-MET for my investigation. The fruitful discussions with Dr. Reji Philip, Prof. D Narayana Rao and Dr. Soma Venugopal Rao are greatly acknowledged. I wish to thank the reviewers of my articles, their critical comments helps to improve the quality of the work presented in the thesis.

Some debts are hard to put into words. I would express my sincere thanks to Dr. Deepthi for her consistent efforts and true desire to keep me on track. I doubt that I will ever be able to convey my appreciation fully, but I owe her my eternal gratitude. A

special thanks goes out to Dr. Bindu Krishnan. I learnt the tricks of the trade from her, and partly because of this, I was able to do large parts of my work independently. I would like to acknowledge Mathew for proof reading this thesis and providing valuable feedback. My thanks also goes to Aneesh for the cover design.

All the friends of the photonics family helped me, one way or another, in my struggle to complete Ph.D. I am grateful to Lyjo, Parvathi, Murali and Prabhath for their timely help and advice. I thank Sr. Ritty and Annieta chechi for being great friends. The automated z-scan set up would not have been existed without the efforts of Vinu and Santhi. Many thanks to Pramod chetan, Unnikrishnan, Achamma teacher, Pravitha, Rekha, Thomas Lee, Jyotsana, Binoy, Aneesh, Prasantha, Sajeet, Rajesh S, Geetha, Sajan, Rajesh M, Sheeba, Manu, Jijo, Dann, Thomas, Jayasree teacher, Saritha A C, Saritha M, Linesh, Jinesh, Nithyaja, Sreelekha, Sithara, Tintu, Vasuja, Sudeesh, Sony, Ambili, Reetha teacher, Annie teacher, Samuel, Radhakrishnan, Bindu Murali, Suresh, Jibu Kumar and Swapna. I would like to thank the office staff for the assistance they provided throughout my research period.

Where would I be without my family? My parents deserve special mention for their inseparable support and prayers- in any case I wish not to attract severe penalty they would impose on expressing formal "thanks". My two sisters, Sr. Roslin and Linta, have provided invaluable moral support. Special thanks to my in laws and all relatives. I am deeply and forever indebted to my loving husband, Albino Chazhoor, who has been a great source of strength all through this work. Akhil John came into our world during the time of my research carrier who always provides me a good company, a break now and then and made this entire endeavor worthwhile.

Finally, I would like to thank everybody who was important to the successful realization of thesis, as well as expressing my apology that I could not mention personally one by one. Thank God for the wisdom and perseverance that he has been bestowed upon me during this research period, and indeed, throughout my life.

Litty

"I can do everything through him who give me strength." (Philippians 4: 13)



Contents

1	Nanophotonics	25
1.1	Nanophotonics	26
1.2	Nanosemiconductors	27
1.3	ZnO: Potential nanophotonic material	28
1.3.1	Applications of nano ZnO	31
1.4	Synthesis	32
1.4.1	Colloidal chemical synthesis	32
1.4.2	Size selection techniques	33
1.4.3	The effect of substrate temperature on the formation of quantum structures	33
1.4.4	Self assembly	34
1.5	Doping and defects in ZnO	34
1.6	ZnO based composites	35
1.7	Exciton	37
1.8	Quantum confinement effects	38
1.9	Exciton oscillator strength	39
1.10	Optical properties	40
1.10.1	Size dependence	41
1.10.2	Temperature dependence	42
1.11	Absorption	43
1.12	Optical bandgap	44
1.12.1	Bandgap engineering	44
1.13	Photoluminescence	45
1.14	Nonlinear optical (NLO) properties	45
1.15	Nonlinear absorption	46
1.15.1	Two photon absorption (TPA)	46
1.15.2	Multiphoton absorption	47

1.15.3	Excited state absorption (ESA)	47
1.15.4	Saturable absorption (SA)	48
1.15.5	Reverse saturable absorption (RSA)	48
1.15.6	Free carrier absorption (FCA)	48
1.15.7	Two photon induced free carrier absorption	49
1.16	Optical limiting	49
1.17	Nonlinear refraction (NLR)	50
1.18	Measurement techniques for NLO characterization	51
1.19	Z-scan technique	51
1.19.1	Open aperture z-scan	53
1.19.2	Theory of open aperture z-scan technique	54
1.19.3	Closed aperture z-scan	55
1.19.4	Theory of closed aperture z-scan technique	57
1.19.5	Merits and demerits of z-scan technique	61
1.20	Conclusions	62
1.21	References	62
2	Fluorescence spectroscopy of nano colloids of ZnO	65
2.1	Introduction	66
2.2	Theory	67
2.2.1	Weak confinement regime ($R >> a_B$)	69
2.2.2	Strong confinement regime ($R \ll a_B$)	70
2.2.3	Intermediate regime ($R \sim a_B$)	71
2.3	Synthesis of nano colloids of ZnO	74
2.3.1	Polyol method	74
2.3.2	Capping	75
2.4	Absorption spectroscopy	75
2.5	X-ray diffraction (XRD)	78
2.6	Optical bandgap	79
2.7	Fluorescence spectroscopy	82
2.7.1	Excitation spectrum	82
2.7.2	Excitation wavelength dependent fluorescence	83

spectroscopy		
2.7.3	Factors contributing to REE	88
2.7.4	Size dependent fluorescence spectroscopy	92
2.7.5	UV emission	95
2.7.6	Visible emission	97
2.7.7	Luminescence mechanism	100
2.8	Conclusions	101
2.9	References	102
3	Size dependent enhancement of nonlinear optical properties in nano colloids of ZnO	107
3.1	Introduction	108
3.2	Theory	109
3.3	Nonlinear optical properties of nano colloids of ZnO	113
3.4	Size dependent enhancement of third order nonlinear susceptibility	114
3.4.1	Open aperture z-scan	114
3.4.2	Closed aperture z-scan	115
3.5	Fluence dependence of third order nonlinear susceptibility	117
3.6	Optical limiting	122
3.6.1	Optical limiting and open aperture z-scan	122
3.7	Conclusions	124
3.8	References	124
4	Spectral and NLO characteristics of Self assembled films of ZnO	127
4.1	Introduction	128
4.2	Theory	131
4.2.1	Induced absorption	132
4.2.2	Saturable absorption	132
4.3	Synthesis	133
4.3.1	Self assembled films of ZnO	133
4.3.2	Thin films of ZnO through sol-gel process	133

4.3.3	Thin films of ZnO through pulsed laser ablation	133
4.4	Absorption spectroscopy	134
4.5	Optical bandgap	135
4.6	X-ray diffraction	137
4.7	Scanning electron microscopy	139
4.8	Fluorescence spectroscopy	139
4.9	Nonlinear optical characterization	140
4.9.1	Open aperture z-scan	140
4.9.2	Closed aperture z-scan	143
4.9.3	Nonlinear optical parameters	145
4.9.4	Size dependence	146
4.9.5	Fluence dependence	148
4.9.6	Spectral dependence	149
4.9.7	Variation of imaginary part of susceptibility	151
4.9.8	Figure of merit	152
4.10	Conclusions	153
4.11	References	154
5	Effect of annealing on the spectral and nonlinear optical characteristics of thin films of nano ZnO	157
5.1	Introduction	158
5.2	Theory	158
5.3	Synthesis	160
5.4	Absorption spectroscopy	160
5.5	Optical bandgap	162
5.6	Fluorescence spectroscopy	164
5.6.1	Luminescence mechanism	169
5.7	Nonlinear optical characterization	170
5.8	Optical limiting	176
5.9	Conclusions	177
5.10	References	178

6 ZnO nanocomposites	181
6.1 Introduction	183
6.2 Theory	186
6.3 ZnO-Ag	187
6.3.1 Synthesis	187
6.3.2 Absorption spectroscopy	188
6.3.3 Fluorescence spectroscopy	190
6.3.4 Nonlinear optical characterization	192
6.3.5 Optical limiting	197
6.4 ZnO-Cu	198
6.4.1 Synthesis	198
6.4.2 Absorption spectroscopy	198
6.4.3 Fluorescence spectroscopy	199
6.4.4 Nonlinear optical characterization	202
6.4.5 Optical limiting	208
6.5 ZnO-CdS	209
6.5.1 Synthesis	209
6.5.2 Absorption spectroscopy	210
6.5.3 Optical bandgap	211
6.5.4 Fluorescence spectroscopy	212
6.5.5 Nonlinear optical characterization	213
6.5.6 Optical limiting	217
6.6 ZnO-TiO ₂	218
6.6.1 Synthesis	218
6.6.2 Absorption spectroscopy	219
6.6.3 Optical bandgap	220
6.6.4 Fluorescence spectroscopy	221
6.6.5 Nonlinear optical characterization	222
6.6.6 Optical limiting	225
6.7 ZnO-SiO ₂	226
6.7.1 Synthesis	226
6.7.2 Absorption spectroscopy	226

6.7.3	Fluorescence spectroscopy	227
6.7.4	Nonlinear optical characterization	229
6.7.5	Optical limiting	233
6.8	ZnO-TiO ₂ -SiO ₂	234
6.8.1	Synthesis	234
6.8.2	Absorption spectroscopy	234
6.8.3	Nonlinear optical characterization	235
6.8.4	Optical limiting	237
6.9	Conclusions	238
6.10	References	240
7	Conclusions and Future prospects	245
7.1	Synthesis	246
7.2	Optical properties	248
7.2.1	Fluorescence spectroscopy	248
7.2.2	Nonlinear optical properties	249
7.3	Device applications	252
7.3.1	ZnO based devices	254



Chapter 1

Nanophotonics

Abstract

This chapter gives a glimpse of the potential of tying the knot between nonlinear optics and nanotechnology. Nanophotonics is an exciting area of research, which makes it possible to tune the optical properties of nanoparticles to suit any application by tailoring size, composition etc. and may find tremendous technological applications. In this chapter, the applications of ZnO nanocomposites along with some important optical properties exhibited by them have been introduced. The theory and experimental details of the z-scan technique used to study the nonlinear optical properties of ZnO nanocomposites are also discussed.

"So how do you go about teaching them something new? By mixing what they know with what they don't know. Then, when they see in their fog something they recognize they think, 'Ah, I know that'. And then it's just one more step to, 'Ah, I know the whole thing'. And their mind thrusts forward into the unknown and they began to recognize what they didn't know before and they increase their powers of understanding".

: Picasso

As the present electronics related technologies are beginning to show their limitations in speed and capacity, the quantum technology is being given increased attention as an alternate mode of doing telecommunications and information processing¹. Nanotechnology is outcome of a tangible nanoscience which deals with the description of matter at quantum level. Nanotechnology is based on the realization of the fact that at nanoscale, material properties are size dependent. It is in this context that nanoscale semiconductor devices are being given increased attention, as they have novel electrical properties that can be utilized for many of the practical applications. The emergent field of nanophotonics deals more particularly with the interaction of optical fields with matter at nano regime².

1.1 Nanophotonics

One year after the invention of the laser³, the observation of second harmonic generation⁴ marked the starting point of a new field in optics: nonlinear optics. This observation constituted a demonstration of the possibility of changing the wavelength of laser radiation via second order nonlinear processes and realization of tunable laser sources based on the nonlinear processes such as parametric oscillation and parametric amplification. Third order nonlinear effects such as optical Kerr effect can be used in optical fiber communication systems in order to compensate chromatic dispersion and propagate optical solitons. However, break throughs are still awaited in nonlinear optics, especially their capability to be used for ultrafast data processing for future optical integrated circuits.

On the other hand, in the domain of nanotechnology, the tremendous progress achieved in material processing, such as in growing, lithography and etching are revolutionizing optoelectronics and integrated optics because they enable the fabrication of nanostructures that can be used to manufacture completely new miniaturized optical components⁵.

Despite pioneering experiments, it is only since the 1990's that the study of nonlinear effects in nanostructured materials has become a very active research domain². This chapter describes an overview of the potentials of the marriage between nanotechnology and optics. Nanocrystal semiconductors, composed of a few hundred to a few thousand atoms, belong to the category of nano objects of great interest for small scale optics. Optics offers to these classes of nanomaterials numerous new functionalities such as spectral tunability and ultrafast nonlinear response.

1.2 Nanosemiconductors

Since the invention of the first semiconductor transistor in 1947 by the scientists of Bell Labs, the semiconductor industry has grown at an incredible pace, fabricating faster, smaller, more powerful devices while manufacturing in larger volume at lower costs⁶. Even though the very first semiconductor transistor was made from germanium (Ge), silicon (Si) became the semiconductor of alternate choice as a result of the low melting point of Ge that limits high temperature processes and the lack of a naturally occurring germanium oxide to prevent the surface from electrical leakage. GaAs is a direct bandgap semiconductor, whereas Si is indirect, making GaAs better suited for optoelectronic devices. However, physical properties required for high power, high temperature electronics and UV/blue light emitter applications are beyond the limits of Si and GaAs. It is essential to investigate alternate materials and their growth and processing techniques in order to achieve such devices. Wide bandgap semiconductors exhibit inherent properties such as larger bandgap, higher electron mobility and higher breakdown field strength. Therefore, they are suitable for high power, high temperature electronic devices and short wavelength optoelectronics.

Wide gap II-VI compounds are characterized by the direct bandgap with either zinc blend or wurtzite structures and large exciton binding energy. Table 1.1 summarizes bandgap energy and exciton binding energy of

typical II-VI compounds and some other III-V compounds which have similar bandgap energies⁷.

Materials	Energy Bandgap (eV)	Exciton Binding energy (meV)
ZnO	3.37	60
ZnS	3.54	39
ZnSe	2.7	20
CdSe	1.74	16
GaAs	1.43	4.2
GaN	3.39	21

Table 1.1: Energy bandgap at room temperature and exciton binding energy of II-VI compounds and other materials

As a general tendency, the exciton binding energy of II-VI compounds is larger than that of III-V compounds with similar bandgap energy. Among II-VI semiconductors, ZnO possesses very large binding energy which makes the material very attractive both from scientific point of view and optical device application aspects.

1.3 ZnO: Potential nanophotonic material

ZnO is a direct, wide bandgap semiconductor material with many promising properties for blue/UV optoelectronics, transparent electronics, spintronic devices and sensor applications. Its research interest has waxed and waned as new perspective applications revive interest in the material, but the applications have been limited by the technology available at the time⁶. The first utilization of ZnO for its semiconductor properties was detectors in build-your-own radio sets in the 1920s. In 1957, the New Jersey Zinc

Company published a book entitled “Zinc Oxide Rediscovered” to promote the material’s frontier properties (semiconductor, luminescent, catalytic, ferrite, photoconductive and photochemical properties) and illustrative applications. Research focused mainly on growth, characterization and applications that do not require single crystals such as varistors, surface acoustics wave devices and transparent conductive films. Nanotechnology has provided new vitality in the area of ZnO based studies.

With a wide bandgap of 3.37 eV and a large exciton binding energy of 60 meV at room temperature, ZnO, like GaN, will be proved to be important for UV/blue optical devices. ZnO has several advantages over GaN in this application range; the most important being its large exciton binding energy and the ability to grow single crystal substrates. The large exciton binding energy paves the way for an intense near band edge excitonic emission at room and even high temperatures since this value is 2.4 times that of room temperature thermal energy ($k_B T=25\text{meV}$). In this vein, there have also been a number of reports on laser emission from ZnO based structures at room temperature and beyond. Moreover ZnO has exhibited better radiation resistance than GaN for possible devices used in space and nuclear applications. Other favorable aspects of ZnO include its broad chemistry leading to many opportunities for wet chemical etching, low power threshold for optical pumping, radiation hardness and biocompatibility. ZnO can be grown on inexpensive substrate, such as glass, at relatively low temperatures. Nanostructures, such as nanowires and nanorods, have been demonstrated. These structures are ideal for detection applications due to their large surface to volume ratio. One main attractive feature of ZnO is its bandgap tuning via divalent substitution on the cation site to form heterostructures. Bandgap energy of 3 eV can be achieved by doping with Cd, while Mg increases the bandgap energy to 4 eV. These properties of ZnO make it an ideal candidate for a variety of devices ranging

from sensors to UV laser diodes and nanotechnology based devices such as displays. Some of the key properties⁶ of ZnO are shown in table 1.2.

Properties	Values
E_g (eV)	3.37 eV
Exciton binding energy	60 meV
Dielectric constant	3.7
Refractive index	2.008
m_e	0.24m ₀ where m ₀ being the rest mass of electron
m_h	0.59m ₀
Stable crystal structure	Wurtzite
Lattice parameters	$a=3.25\text{Å}^0$ and $c=5.12\text{Å}^0$
Face terminations	(0001) - Zn terminated (c axis oriented) Polar $(000\bar{1})$ - O terminated (c axis oriented) $(10\bar{1}0)$ - Equal number of Zn and O atoms $(11\bar{2}0)$ - “ (a axis) Non Polar
thermal conductivity	$0.6-1.2 \text{ Wcm}^{-1}\text{K}^{-1}$
thermal expansion coefficients	$\alpha_a = 4.31 \times 10^{-6} K^{-1}$ and $\alpha_c = 2.49 \times 10^{-6} K^{-1}$ at 300K
specific heat capacity	$C_p=40.3 \text{ J mol}^{-1}\text{K}^{-1}$

Table 1.2: Important parameters of ZnO

As intense research into ZnO continues, difficulties such as the fabrication of p-type ZnO that have so far stalled the development of devices are being overcome. We are thus moving ever close to the future in which ZnO will be a viable and integral part of many functional and exotic devices.

1.3.1 Applications of nano ZnO

ZnO has been commonly used in our society in its polycrystalline form for over a hundred years in a wide range of applications such as facial powders, ointments, sunscreens, catalysts, lubricant additives, piezoelectric transducers, varistors and as transparent conducting electrodes⁶. ZnO is a key element in many industrial manufacturing processes including paints, cosmetics, pharmaceuticals, plastics, batteries, electrical equipment, rubber, soap, textiles, floor coverings to name just a few. With improvements in growth technology of ZnO nanostructures, epitaxial layers, single crystals and nanoparticles, we are now moving into an era where ZnO devices will become increasingly functional and exotic.

ZnO based nanostructures including nanowire arrays hold a host of opportunities for flat screen displays, field emission sources, gas, chemical and biological sensors and as UV light emitters and switches⁸. Epitaxial layers and single crystals will be important for the development of optoelectronic (UV/blue light emitters and detectors), piezoelectric and spintronic devices and together with GaN may form the light source of the 21st century⁶. ZnO holds as a semi-conducting transparent thin film which will be important for solar cells, gas sensors, displays and wavelength selective applications⁹.

Existing technologies are also being revolutionized with ZnO nanoparticles, which have led to the development of improved sunscreens, paints and coatings to name just a few. Additionally, the radiation hardness of ZnO to MeV proton irradiation makes it an ideal candidate for space applications⁶. Thus ZnO whilst already possessing a wide application base,

has enormous opportunities for society and industry alike due to its unique properties which are now being explored and applied. The future in which ZnO devices become part of our everyday lives is already approaching reality.

1.4 Synthesis

The concept of quantum confinement, and its use in the distinction between the colouring of glasses by changes in stoichiometry of $\text{CdS}_x\text{Se}_{1-x}$ mixed crystals or by size changes of the binary nanocrystals, was introduced by Efros and Efros¹⁰, and confirmed experimentally by Ekimov and Onushenko¹¹. At the same time, the change of colour of semiconductor colloidal solutions has been discussed in the context of quantum confinement effects by Rosetti et.al.¹². A period of control of the growth process of these nanocrystalline semiconductors followed in the 1980's combined with a detailed investigation of their linear and nonlinear optical behaviour¹³.

The understanding of the growth process of nanocrystals is a prerequisite for the understanding of all basic properties of three-dimensional confinement in semiconductors¹⁴. The most important information to be obtained from growth analysis concerns the sizes, the size distribution, stoichiometry, structure and the interface configuration of the nanocrystals. The development of nanocrystals is supposed to proceed only by the thermodynamic nucleation followed by diffusion in the direct surrounding of the nanocluster and without interaction between them.

1.4.1 Colloidal chemical synthesis

Both fast nucleation and slow growth dynamics should be adjusted to obtain monodisperse nanocrystals¹³. One of the ways to accomplish this is to grow the crystallites by chemical reactions in liquid or micelle media or in polymers. Here, the matrix acts not only as the stabilizer; but also determines the chemical interface configuration and therefore controls the sizes via chemical equilibrium conditions. The growth of nanocrystals can be

controlled by the choice of the solvent and the concentration of the reacting species as well as the reaction temperature and duration. Compared to glass technologies, the obvious advantage of these methods is the low preparation temperature (usually not more than 200°C), and the realization of very narrow size distributions (<5%).

One of the first attempts to produce II-VI nanocrystals is the manufacture of colloidal suspensions¹³. The nature of the different stabilizing groups strongly influences the electronic states. Drastic changes in the optical spectra have been observed when using different solvents. The shift of the absorption peaks can be explained by different sizes and probably also by different charge states at the interface.

1.4.2 Size selection techniques

Large efforts are presently being made to prepare highly monodisperse nanocrystals¹³. The reduction of the nucleation process to a short time interval is attained by a rapid increase of the supersaturation upon injection of room temperature reagents into a hot coordinating solvent. The sudden temperature drop and the fast decrease in the concentration of the reagents prevent further nucleation. The onset of the slow growth process is promoted by moderate reheating. Simultaneously to the growth, the absorption spectra are used to monitor the size changes of the crystallites.

1.4.3 The effect of substrate temperature on the formation of quantum structures

The formation of quantum structures is controlled by the interplay of energetics and kinetics. From the consideration of total free energy, the high temperature growth would promote the spontaneous formation of quantum structures. A change in substrate temperature may induce substantial changes in the formation of quantum structures. As the substrate temperature increases, the migration of atoms is enhanced to form more energetically favourable interface structures, which results in the formation of quantum

dots with better uniformity in size¹³. The production of nanocrystals with larger sizes covering also the weak confinement range (quantum description of nanomaterials explains the confinement strength as strong or weak with respect to the ratio of the size of the nanocrystal to the Bohr radius of the exciton in the corresponding bulk material, details of which are given in chapter 2) has been achieved by the use of higher reaction temperatures.

1.4.4 Self assembly

Self assembly is an important phenomenon which results in the spontaneous organization of structures and pattern formation. In the context of nanotechnology, the process of self assembly allows us to tune the quantum dot size and improve the size and shape uniformity of the optically active quantum dots. Self organized quantum dots are easily incorporated in conventional device structures. Additionally, the inhomogeneous broadening of the discrete density of states for the self organized quantum dot ensembles hampers detailed investigations of the excited state spectrum and of energy relaxation (and recombination) processes, which are both of basic physical interest and critical for design and performance of devices. In recent years, extensive work has been devoted to the study of the excited states as well as the temperature dependence and dynamical behaviour of the optical properties of self organized quantum dots⁷.

1.5 Doping and defects in ZnO

Since most of the ZnO samples are grown under Zn rich conditions, the dominant donor type point defects⁶ in ZnO are oxygen vacancy (V_O) and Zn interstitial (Zn_I). In the year 2000, Van de Walle suggested that hydrogen is likely to be a dominant background donor in ZnO materials that were exposed to hydrogen during growth¹⁵. Donors which have been identified by Hall effect and PL measurements include interstitial hydrogen, substitutional Al and Ga, Zn interstitial complex ($Zn_I\text{-}X$) and the oxygen vacancy. For the

acceptors, substitutional N, P, As, Sb and the Zn vacancy (V_{Zn}) seem to be the most important species⁶.

Besides Zn_I and V_O , the antisite Zn_O should also be a donor, although there is some disagreement among theoreticians on whether its level is shallow or deep. In any case, right now, there is little evidence for any optical or electrical activity caused by Zn_O . According to the theory, the oxygen interstitial (O_I) and Zn vacancy (V_{Zn}) should behave as acceptors and V_{Zn} should be prevalent in n-type ZnO , especially in materials created under oxygen-rich conditions. Experimentally, little is known about O_I , which can exist in both tetrahedral and octahedral positions.

All of the defects mentioned such as V_{Zn} , V_O or Zn_I-X , are quite small and qualify as point defects. However, there are also much larger defects that are present and important. For example, many ZnO samples contain line defects such as threading dislocations and surface defects such as stacking faults.

The common techniques that can deliver quantitative information about donor and acceptor concentrations and energies include PL measurements and optical absorption measurements. Other characterization techniques such as transmission electron microscopy (TEM), x-ray diffraction (XRD), Secondary ion mass spectroscopy (SIMS) and Hall effect (T-Hall) have also contributed much to the understanding of defect states in ZnO .

1.6 ZnO based composites

The field of nanocomposite materials has been widely recognized as one of the most promising and rapidly emerging research areas¹⁵. It is found that a common cation quantum structure such as $ZnS/ZnSe$ lead to an island interface which ensures localization at the interface thereby facilitating the growth of quantum dots at the heterointerface⁷. Such quantum structures show a broad exciton luminescence band with developed low-energy tail,

which is characteristic for a quantum dot system with random distribution of lateral confinement. The emissions are stronger in nanocomposites than quantum dots and this might be caused by the exciton localization at the ZnSe/ZnS interfaces. In contrast, the common anion interface such as ZnSe/CdSe ultrathin quantum wires leads to interface alloying due to large interdiffusivity of metal atoms⁷.

Luminescent centres in a nanocomposite material can be excited either via direct pumping the centres or indirectly through energy transfer from the host materials⁷. The latter is of more importance for practical applications because it allows the realization of light emitting devices through current injections. Neglecting the non-radiative carrier loss channels,

the energy transfer rate should be proportional to $\frac{\tau_{rh}}{(\tau_{rh} + \tau_T)}$ with τ_{rh} as the radiative lifetime of the host carriers and τ_T the energy transfer time respectively⁷. This relationship implies that there are two ways to enhance the energy transfer, i.e. either increasing τ_{rh} or reducing τ_T . A quantum dot is an ideal system for achieving this purpose because τ_{rh} is expected to be much longer than those of bulk materials if the relaxation time is also taken into account and τ_T can be expected to be shorter due to the strong spatial coupling between the host and the luminescence centres. The latter can even be made shorter by choosing an appropriate host material and controlling the dot size. This idea is depicted in figure 1.1, where the excited carriers should have three major recombination or loss channels, i.e. (1) recombination radiatively and emit photons with an energy equal to the effective bandgap of host materials, (2) trapped by defects and (3) transfer energy to radiative centres. The phonon bottleneck problem and relatively longer intrinsic lifetime in quantum dots⁷ can be effectively used to enhance the energy transfer from host to luminescence centers.

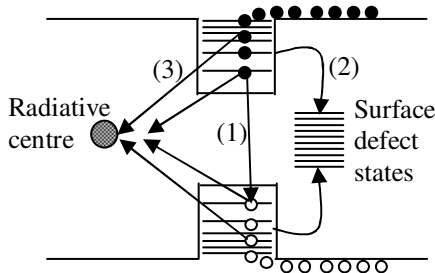


Figure 1.1: The phonon bottleneck problem and three major carrier recombination or loss channels in doped quantum dots

Chemically synthesized semiconductor nanocomposites offer necessary and basic materials promising color-tunable, flexible, all-purpose chromophore systems, in which the strong quantum confinement effect of the carriers leads to unique, size dependent linear and nonlinear optical properties¹⁶. Optical nonlinearity of metal nanoparticles in a semiconductor has attracted much attention because of the high polarisability and fast nonlinear response that can be utilised in making them as potential optical devices¹⁵.

1.7 Exciton

In optical responses of semiconductors or insulators, an electron and a hole excited respectively in a conduction and a valence band, or their composite particle called exciton, play central roles. In low-dimensional structures, the coulomb correlational effects or the excitonic effects become more prominent than in bulk structures, leading to peculiar optical characteristics combined with the geometrical confinement effects. When we define exciton as a bound state of an electron in a conduction band and a hole in a valence band, there are two limiting types of excitons: the Wannier exciton and the Frenkel exciton⁷. Generally, the wavefunction of the electron-hole relative motion of the Wannier exciton is more sensitively affected by a spatial geometry than that of the Frenkel excitons¹⁷.

The Wannier exciton has three degrees of freedom: a centre of mass motion, an electron-hole relative motion and a spin configuration, where the latter two are internal degrees of freedom⁷. In perfect rigid crystals in d dimensions (d=1, 2, 3), the centre of mass motion is well described by a plane wave with a d-dimensional wave vector K. Since only the centre of mass state of K~0 contributes to the optical responses, the electron-hole relative motion and subband (sublevel) structures mainly determine the optical properties of low-dimensional exciton systems.

The relation between number of excitons and the optical responses is a long standing problem in exciton physics. Under a weak excitation condition, only an electron and a hole are created, which form a bound state due to the coulomb attraction. This is just a two-body problem, which can be solved with the use of effective mass approximation. However, in the case of stronger excitation where many electrons and holes are excited in semiconductors, many body effects should be taken into account and the inter-particle coulomb interaction plays an essential role.

The dimensionality of exciton systems depends on the ratio of the particle size R to the exciton effective Bohr radius, a_B . The Bohr radius corresponding to nano ZnO is 2 nm. Geometrical confinement of excitons and the dielectric image-charge effects as well as the single-electron band structures are keys for designing novel materials with new optical functions.

1.8 Quantum confinement effects

Quantum confinement describes the confinement of the exciton within the physical boundaries of the semiconductor. The effective coulomb potential include the dielectric image-charge effect arising from the difference in the dielectric constant between the material (ϵ) and the surroundings (ϵ_l). This is a confinement effect of the coulomb interaction. If the surrounding materials have a smaller dielectric constant and a larger

energy gap than the relevant material ($\epsilon_l < \epsilon$), the electron-hole coulomb attraction in the relevant material works very effectively through the surroundings with reduced screening⁷. As a result, the exciton binding energy is expected to increase much more than in a normal low-dimensional system without this effect. Quantum confinement effects arise as soon as the dimension of a nanocrystal (R) becomes comparable to the Bohr radius (a_B) of the exciton wave function, leading to significant changes in the electronic and optical properties. Details are given in chapter 2.

1.9 Exciton oscillator strength

The quantum confinement and the piezoelectricity in quantum dots result in an enhanced coupling strength. The oscillator strength is one of the main excitonic characteristics, providing unique information about the geometry of the exciton wave function in a structure. As a figure of merit for the recombination of an exciton, we use the oscillator strength and excitonic optical transition is characterized by large oscillator strength. Nonlinear optical effects are enhanced when the associated optical transition has a large optical oscillator strength. One of such examples can be seen in room temperature excitonic lasing¹⁸ and high-temperature stimulated emission upto 550K due to an excitonic mechanism from ZnO epilayers grown by plasma assisted molecular beam epitaxy¹⁹. The characteristic temperature for the threshold intensity of stimulated emission is as large as 90K, which is very large for a structure without carrier and optical confinement⁷. This large oscillator strength would even be enhanced when biexcitons are participated in the optical transition process due to giant oscillator strength effects.

The binding energies of exciton and biexciton increase due to quantum confinement effects in low-dimensional quantum structures, which is favourable for room temperature operation of nonlinear optical devices. As the quantum-confined exciton system can be modeled as a two level atomic system, the imaginary part of $\chi^{(3)}$ is given by

$$\text{Im}(\chi^{(3)}) = \left[\frac{e^2}{2m_0\omega} \right]^2 \hbar N F_n^2 \frac{T_1}{\Gamma_h^2} \quad (1.1)$$

where T_1 and Γ_h are the longitudinal relaxation time and homogeneous width respectively, ω is the angular frequency and F_n and N are the oscillator strength and the number density of nanocrystals, respectively. The oscillator strength is also increased due to an increase in density of states at around the bandgap energy⁷. These properties would contribute to realization of low threshold nonlinear optical devices at room temperature or even at higher temperatures.

1.10 Optical properties

The optical properties of a semiconductor have their genesis in both intrinsic and extrinsic effects. Intrinsic optical transitions take place between the electrons in the conduction band and holes in the valence band, including excitonic effects due to the coulomb interaction. Excitons are classified into free and bound excitons. In high quality samples with low impurity concentrations, the free excitons can also exhibit excited states, in addition to their ground state transitions. Extrinsic properties are related to dopants/impurities or point defects and complexes, which usually create electronic states in the bandgap, and therefore influence both optical absorption and emission processes. The electronic states of the bound excitons, which may be bound to neutral or charged donors and acceptors, depend strongly on the semiconductor material, in particular the band structure. Other extrinsic transitions could be seen in the optical spectra such as free to bound (electron-acceptor), bound to bound (donor-acceptor) and yellow/green luminescence due to surface defect states.

The optical properties of ZnO are heavily influenced by the energy band structure and lattice dynamics. Optical transitions in ZnO have been studied by a variety of experimental techniques such as optical absorption,

transmission, reflection, photo-reflection, spectroscopic ellipsometry, photoluminescence, cathodoluminescence, calorimetric spectroscopy etc. Many body effects such as bandgap renormalization, enhancement of optical gain due to the attractive electron-hole interaction (coulomb or exciton enhancement) and the plasma screening are also considered important in the description of the optical properties of semiconductors⁷.

1.10.1 Size dependence

Semiconductor nanoparticles exhibit a change in their electronic properties relative to that of the bulk material; as the size of the solid becomes smaller, the band gap becomes larger²⁰. This allows material scientists the unique opportunity to change the properties of a material simply by controlling its particle size which leads to the fabrication of a number of devices. The size-dependence of the optical properties of quantum dots has been one of the main subjects of research work during the last decade.

There are three types of nanometer-size semiconductors having zero, one and two dimensional structures. Electrons, holes and/or excitons are confined in these semiconductors resulting in size quantization of their momenta and energies. In many semiconductors, these size quantization have been studied. In a weak confinement regime, a translational motion of an exciton is size quantized. One typical example is a CuCl dot where the nanocrystal size is larger than the exciton Bohr radius⁷. In a strong confinement regime, motions of electrons and holes are individually quantized. The typical examples are seen in CdSe dots and GaAs wells, where the spatial size is smaller than the exciton Bohr radius⁷. On the other hand, in the very small structures of atomic size, the effective mass approximation breaks down and the electronic band structure may be changed. Hence it is important to show an example in the whole range of the crystal size.

1.10.2 Temperature dependence

One main driving force for device applications of quantum dots is the temperature stability of their properties resulting from the combination of the discrete density of states and a potentially large substrate splitting. The temperature dependent energy shift of bulk bandgaps is phenomenologically described by Varshni's formula²¹.

$$E_g(T) = E_g - \frac{AT^2}{B+T} \quad (1.2)$$

For ZnO, the empirical Varshini parameters A and B are calculated to be 5.05×10^{-4} and 900 respectively²⁶ upto 300K. A detailed understanding of the temperature dependence of the ground state transition energy of the self organized quantum dots would require numerical calculations with temperature dependent material parameters, which are not available yet.

The average size of quantum dots can be controlled by deposition temperature as well as annealing temperature. Quantum dots exhibit a shift of the band edge due to carrier confinement and the extent of the confinement is a function of the average dot size.

1.11 Absorption

A first approach in understanding the behaviour of quantum dots is mainly the investigation of their optical properties, in particular their absorption spectra. The spectrum is characterized by the sharp band-edge and close to that, by the series of exciton states. The spectral positions of the absorption peaks shift to higher energies and the lines become broader with decreasing sizes of the nanocrystals. The explanation for these spectral changes in the absorption spectra by a size-dependent effect was the beginning of the intensive research on three-dimensional quantum confinement in solid-state semiconductor composite materials.

Considering the absorption coefficient of an ensemble of quantum

dots inside a transparent matrix, the averaged absorption spectrum $\alpha(\omega)$ can be expressed by¹³,

$$\alpha(\omega) = \frac{p}{V_{QD}} \int dR \frac{4\pi}{3} R^3 P(R) \alpha_{QD}(\omega, R) \quad (1.3)$$

with p the volume fraction of the semiconductor material, V_{QD} the average quantum dot volume, R the radius and $P(R)$ a characteristic distribution function for the dot sizes, as well as $\alpha_{QD}(\omega, R)$ the absorption coefficient of a single quantum dot. As a result of the quantum confinement effect, the absorption coefficient α_{QD} is strongly dependent on the radius R of the dot. The absorption spectrum is given by a series of Lorentzian lines for the ground and excited states at energies $E_{QD}^j = \hbar\omega_j$ with homogeneous line widths Γ_j and oscillator strengths f_j

$$\alpha_{QD}(\omega, R) = \sum_j f_j(R) \frac{\frac{\hbar\Gamma_j(R)}{2}}{\left(E_{QD}^j(R) - \hbar\omega\right)^2 + \left(\frac{\hbar\Gamma_j(R)}{2}\right)^2} \quad (1.4)$$

Equations (1.1) and (1.2) show that one needs information about the radius R , the size distribution $P(R)$, and the semiconductor volume fraction p to correlate the appearance of structures in the absorption spectrum to electronic states of the quantum dots as well as suitable relations for the size dependence of $E(R)$, $\Gamma(R)$ and $f(R)$, the energy, homogeneous line broadening and oscillator strength, respectively¹³.

The widespread quantum dot systems based on II-VI materials show absorption structures in the visible and near ultra violet part of the spectrum and therefore compatible with a great number of laser sources used in experiments.

1.12 Optical bandgap

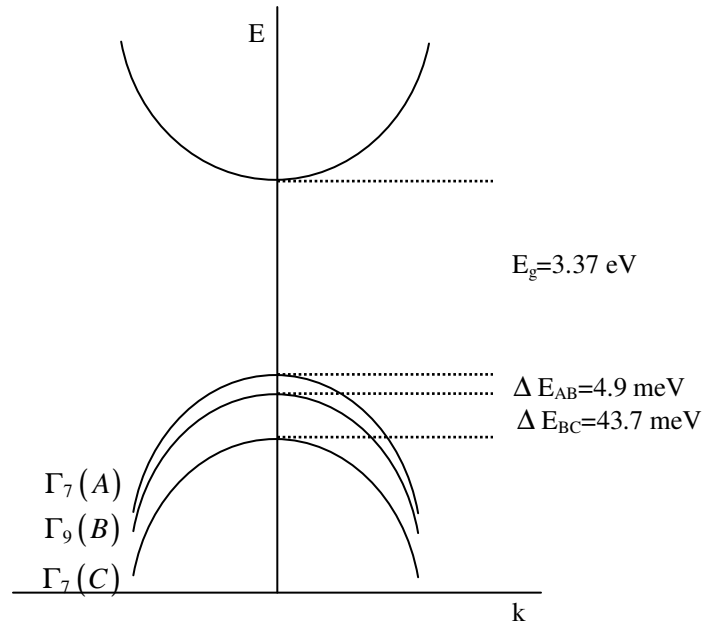


Figure 1.2: Schematic diagram representing the crystal-field and spin-orbit splitting of the valence band of ZnO into 3 subband states A, B and C at 4.2K

ZnO is a direct wide bandgap material. ZnO valence band is split into three band states, A, B and C by spin-orbit and crystal-field splitting. This splitting is schematically illustrated in figure 1.2. The A and C subbands are known to possess Γ_7 symmetry, whilst the middle band, B, has Γ_9 symmetry⁶.

1.12.1 Bandgap engineering

For a semiconductor to be useful, particularly with reference to optoelectronic devices, bandgap engineering is a crucial step in device development. By alloying the starting semiconductor with another material of different bandgap, the bandgap of the resultant alloy material can be fine tuned, thus affecting the wavelength of exciton emissions. ZnO has been identified as a promising candidate for UV optoelectronic devices and the

main emphasis is on bandgap engineering for the design of ZnO based short wavelength transparent optoelectronic devices. Alloying ZnO with MgO and CdO is an effective means of increasing or decreasing the energy bandgap respectively⁶.

Currently however only limited experimental and theoretical work has been done for these materials, and thus the information available is both incomplete and not well verified. In this context, we concentrate on the spectral and nonlinear optical properties of ZnO nanocomposites²²⁻³⁴.

1.13 Photoluminescence

The decades-old promise of light emission from intersubband transitions in semiconductors is beginning to reach its potential. The past ten years have seen major advances in growth technology which have enabled the design of emission sources operating at wavelengths ranging from a few micrometers to a few hundred micrometers. The advantage of using bandgap engineering is to tailor emission frequencies, even though many interesting challenges remain, particularly at longer wavelengths (20-100 micrometer).

B K Meyer et.al.³⁵ gives a comprehensive review on the optical properties of excitonic recombinations in bulk, n-type ZnO. Excitonic emissions of ZnO are observed even above room temperature. A broad defect related peak extending from 1.9 to 2.8 eV is a common optical feature of ZnO, known as the green band. The origin of this luminescence band is still not well understood and has in the past been attributed to a variety of different impurities and defects.

1.14 Nonlinear optical properties

Optical nonlinearity is very important in the semiconductor nanocrystals, because it becomes considerably large compared to the bulk³⁶. Studies on optical nonlinearity and related dynamics are useful for the development of new materials for applications in ultrafast optical devices.

Nonlinear optical responses have also been studied for a long time in relation to the photonic device application and the laser operation. In particular, the third order nonlinear processes are of special importance because they belong to the nonlinearity which is the lowest-order nonlinear effect in majority of the materials. When the energy of the incident light is tuned at the exciton level, the nonlinearity results from the enhancement of exciton oscillator strength. Recently, relations between the $\chi^{(3)}$ nonlinearity and the interaction between the excitons are investigated theoretically⁷. In the nano regime, quantum confinement effects produce exciton resonances that are sharper than the corresponding ones in bulk semiconductors and this results in large optical nonlinearities.

1.15 Nonlinear absorption

Nonlinear absorption refers to the change in transmittance of a material as a function of intensity or fluence³⁷. At sufficiently high intensities, the probability of a material absorbing more than one photon before relaxing to the ground state can be greatly enhanced. In addition, population redistribution induced by intense laser fields leads to interesting counterplays of stimulated emission and absorption, complicated energy transitions in complex molecular systems and the generation of free carriers in solids. These phenomena are manifested optically in a reduced (saturable) or increased (reverse saturable) absorption.

1.15.1 Two photon absorption (TPA)

Two photon absorption involves a transition from the ground state of a system to a higher-lying state by the simultaneous absorption of two photons from an incident radiation field or fields³⁷. TPA spectroscopy complements linear absorption spectroscopy in studying the excited states of systems. Figure 1.3 shows the schematic representation of TPA. The intermediate state is not real and hence the system must absorb two photons

simultaneously. This makes the process sensitive to the instantaneous optical intensity.

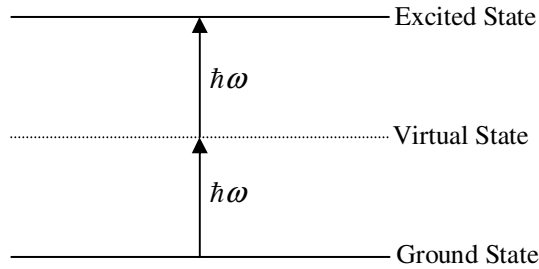


Figure 1.3: Schematic diagram of two photon absorption

The nonlinear absorption in this case is proportional to the square of the instantaneous intensity and is given by³⁷

$$\frac{dI}{dz} = -\alpha I - \beta I^2 \quad (1.5)$$

where α is the linear absorption coefficient and β is the two photon absorption coefficient.

1.15.2 Multiphoton absorption

Multiphoton absorption refers to the simultaneous absorption of n photons from a single beam or multiple beams. The absorption of $(n+1)$ photons from a single optical beam is given by

$$\frac{dI}{dz} = -(\alpha + \gamma^{(n+1)} I^n) I \quad (1.6)$$

where $\gamma^{(n+1)}$ is the $(n+1)$ photon absorption coefficient.

1.15.3 Excited state absorption (ESA)

In systems such as polyatomic molecules and semiconductors, there is a high density of states near the state involved in the excitation³⁷. The excited electron can rapidly make a transition to one of these states before it

eventually make transitions back to the ground state. There are also a number of higher lying states that may be radiatively coupled to these intermediate states, and for which the energy differences are in near-resonance with the incident photon energy. Therefore, before the photon relaxes to the ground state, it may experience absorption that promotes it to a higher-lying state. This process is called excited state absorption.

1.15.4 Saturable absorption (SA)

When the absorption cross-section from excited state is smaller than that from the ground state, the transmission of the system will be increased when the system is pumped with high intensity laser beam. This process is called saturable absorption.

1.15.5 Reverse saturable absorption (RSA)

When the absorption cross-section from excited state is larger than that from the ground state, the transmission of the system will be less under intense laser fields. This process is called reverse saturable absorption.

1.15.6 Free carrier absorption (FCA)

In semiconductors, the absorption of a photon with energy greater than the bandgap will promote an electron to the conduction band, where it is a free carrier and can contribute current flow when a field is applied. The excited electron will rapidly thermalize and relax to the bottom of the conduction band. From there it will recombine with an excited hole in the valence band after a characteristic recombination time. However, at sufficiently high intensities, it can, with high probability, absorb another photon while it is still in the conduction band. This process is called free carrier absorption.

In the weak absorption regime, the attenuation may be described by³⁷

$$\frac{dI}{dz} = -\alpha I - \sigma_c N_C(I) I \quad (1.7)$$

where $N_C(I)$ is the intensity dependent carrier density and σ_c is the free carrier absorption cross-section.

1.15.7 Two photon induced free carrier absorption

When two photon absorption is particularly strong in a material, it can lead to significant population of a two photon allowed state. If a semiconductor is exposed to light of photon energies greater than the half of E_g , both bound electronic and free carrier nonlinearity occur simultaneously. Thus two photon induced free carrier absorption is the dominant mechanism in semiconductors. Then the attenuation may be described by³⁷

$$\frac{dI}{dz} = -\alpha I - \beta I^2 - \sigma_c N_C(I) I \quad (1.8)$$

In general, induced absorption can occur due to a variety of processes. However, the dominant mechanism is decided by factors such as duration of the excitation pulse, lifetimes of excited singlet and triplet states and intersystem crossing time, crossing yield, etc. TPA is an irradiance dependent process whereas ESA is fluence dependent. This means that the same fluence for two different pulse widths will give the same nonlinear absorption if the mechanism is ESA. By measuring the nonlinear absorption for various pulse durations, it is possible to confirm whether ESA or TPA dominates in contributing to the induced absorption. As a rule, transmittance change ΔT at a fixed pulse energy will be independent of pulse width if the mechanism is ESA but will depend on pulse width if it is TPA.

1.16 Optical limiting

Optical limiters are devices that transmit light at low input fluences or intensities, but become opaque at high inputs. Optical limiters have applications in optical pulse shaping, pulse compression and protection of human eye and optical sensors from intense laser pulses. Several reviews³⁸⁻³⁹ of optical limiter materials and devices have been published since 1989. One

of the desirable attributes of an optical limiter is low threshold. An ideal optical limiter will have a linear transmission upto a threshold input fluence I_{th} , which varies for different materials. If incident fluence is increased beyond I_{th} , the transmittance remains a constant as shown in figure 1.4.

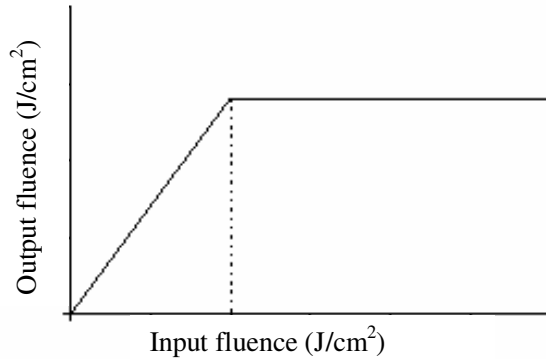


Figure 1.4: Ideal optical limiting curve

The important processes causing optical limiting effects are reverse saturable absorption, two photon absorption, free carrier absorption, nonlinear refraction, photorefraction and induced scattering. TPA and TPA induced FCA has been extensively studied for optical limiting³⁹. Thresholds of TPA materials depend on β and are generally much higher than those observed in RSA materials. However TPA materials do not saturate as RSA materials.

1.17 Nonlinear refraction (NLR)

Nonlinear index of refraction is the change in refractive index or the spatial distribution of the refractive index of a medium due to the presence of optical waves and has generated significant and technological interest. It has been utilized for a variety of applications such as nonlinear spectroscopy, correcting optical distortions, optical switching, optical logic gates, optical data processing, optical communications, optical limiting, passive laser

mode-locking, wave guide switches and modulators. The general dependence of the NLR on intensity is given by³⁷

$$n(r,t) = n_0(r,t) + \Delta n[I(r,t)] \quad (1.9)$$

This equation indicates that the change in the refractive index, Δn over its value at low intensities, n_0 , has a functional dependence on intensity, $I(r,t)$. Several physical mechanisms that contribute to the NLR include electronic polarization, Raman induced kerr effect, molecular orientational effects, electrostriction, population redistribution, thermal contributions, cascaded second order effects and photorefractive effect.

1.18 Measurement techniques for NLO characterization

Some of the characterization methods for studying materials exhibiting NLO properties are z-scan, degenerate four wave mixing, three wave mixing, optical Kerr effect, ellipse rotation, interferometric methods, beam self bending, third harmonic generation, two photon fluorescence, photothermal and photoacoustic techniques and beam distortion measurements³⁷. Z-scan technique has been employed in investigating the NLO properties of ZnO nanocomposites reported in this thesis.

1.19 Z-scan technique

Z-scan is a single beam technique developed by Sheik Bahae to measure the magnitude of nonlinear absorption as well as the sign and magnitude of nonlinear refraction⁴⁰⁻⁴¹. The technique is based on the principle of spatial beam distortion, but offers simplicity as well as high sensitivity comparable to interferometric methods. When a high irradiance laser beam propagates through any nonlinear material, photoinduced refractive index variations may lead to self-focusing of the beam. The propagation of laser beam inside such a material and the ensuing self refraction can be studied using the z-scan technique. It enables one to

determine the third order nonlinear properties of solids, ordinary liquids, and liquid crystals.

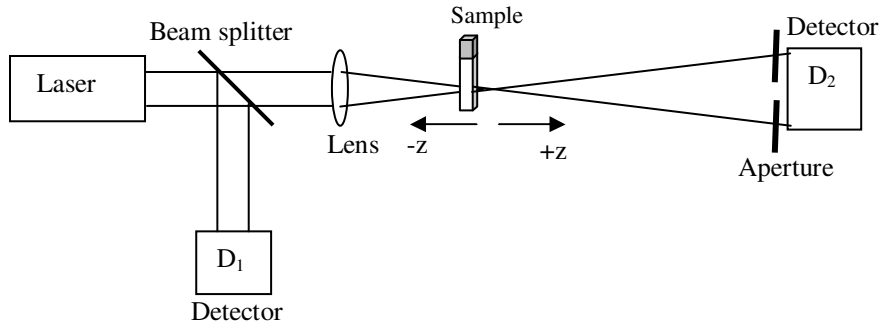


Figure 1.5: Schematic representation of the experimental setup for z-scan technique

The experimental set up for single beam z-scan technique is given in figure 1.5. In the single beam configuration, the transmittance of the sample is measured, as the sample is moved along the propagation direction of a focused gaussian beam. A laser beam propagating through a nonlinear medium will experience both amplitude and phase variations. If transmitted light is measured through an aperture placed in the far field with respect to focal region, the technique is called closed aperture z-scan⁴⁰⁻⁴¹. In this case, the transmitted light is sensitive to both nonlinear absorption and nonlinear refraction. In a closed aperture z-scan experiment, phase distortion suffered by the beam while propagating through the nonlinear medium is converted into corresponding amplitude variations. On the other hand, if transmitted light is measured without an aperture, the mode of measurement is referred to as open aperture z-scan⁴¹. In this case, the throughput is sensitive only to nonlinear absorption. Closed and open aperture z-scan graphs are always normalized to linear transmittance i.e., transmittance at large values of $|z|$. Closed and open aperture z-scan methods yield the real part and imaginary

part of nonlinear susceptibility $\chi^{(3)}$ respectively. Usually closed aperture z-scan data is divided by open aperture data to cancel the effect of nonlinear absorption contained in the closed aperture measurements⁴¹. The new graph, called divided z-scan, contains information on nonlinear refraction alone.

In a z-scan measurement, it is assumed that the sample thickness is much less than Rayleigh's range z_0 (diffraction length of the beam), defined as $z_0 = k\omega_0^2/2$ where k is the wave vector and ω_0 is the beam waist radius given by $\omega_0 = \frac{f\lambda}{D}$ where f is the focal length of the lens used, λ is the wavelength of the source and D is the beam radius at the lens.

Z-scan technique is highly sensitive to the profile of the beam and also to the thickness of the sample. Any deviation from gaussian profile of the beam and also from thin sample approximation will give rise to erroneous results. For ensuring that the beam profile does not vary appreciably inside the sample, the sample thickness should always be kept less than the Rayleigh's range. The sensitivity of this z-scan method is used to monitor nonlinear refraction at low irradiance levels, where a third order nonlinearity attributed to n_2 caused by bound electrons can be observed. At higher irradiance levels the refraction caused by two photon absorption induced free charge carriers becomes significant. Thus the electronic Kerr effect will be dominant at low irradiance levels whereas TPA induced FCA will be dominant at high irradiance levels⁴².

1.19.1 Open aperture z-scan

Open aperture z-scan technique is employed to measure nonlinear absorption in the sample. If nonlinear absorption such as two photon absorption is present, it is manifested in the measurements as a transmission minimum at the focal point⁴¹. On the other hand, if the sample is a saturable absorber, transmission increases with increase in incident intensity and

results in a transmission maximum at the focal region⁴³. Brief description of the theory described by *Sheik Bahae et al.* is given below⁴¹.

1.19.2 Theory of open aperture z-scan technique

In the case of an open aperture z-scan, the transmitted light measured by the detector is sensitive only to intensity variations. Hence, phase variations of the beam are not taken into consideration. The intensity dependent nonlinear absorption coefficient $\alpha(I)$ can be written in terms of linear absorption coefficient α and TPA coefficient β as

$$\alpha(I) = \alpha + \beta I \quad (1.10)$$

The irradiance distribution at the exit surface of the sample can be written as

$$I_r(z, r, t) = \frac{I(z, r, t) e^{-\alpha l}}{1 + q(z, r, t)} \quad (1.11)$$

$$\text{where } q(z, r, t) = \beta I(z, r, t) L_{\text{eff}} \quad (1.12)$$

L_{eff} is the effective length and is given in terms of the length of the sample (l) by the relation

$$L_{\text{eff}} = \frac{(1 - e^{-\alpha l})}{\alpha} \quad (1.13)$$

The total transmitted power $P(z, t)$ is obtained by integrating equation (1.11) over z and r and is given by

$$P(z, t) = P_l(t) e^{-\alpha l} \frac{\ln[1 + q_0(z, t)]}{q_0(z, t)} \quad (1.14)$$

where $P_l(t)$ and $q_0(z, t)$ are given by

$$P_l(t) = \frac{\pi \alpha_0^2 I_0(t)}{2} \quad (1.15)$$

$$q_0(z, t) = \frac{\beta I_0(t) L_{\text{eff}} z_0^2}{z^2 + z_0^2} \quad (1.16)$$

For a pulse of gaussian temporal profile, equation (1.14) can be integrated to give the transmission as

$$T(z) = \frac{1}{q_0 \sqrt{\pi}} \int_{-\infty}^{\infty} \ln(1 + q_0 e^{-t^2}) dt \quad (1.17)$$

If $|q_0| < 1$, equation (1.17) can be simplified as

$$T(z, S=1) = \sum_{m=0}^{\infty} \frac{[-q_0(z, 0)]^m}{(m+1)^{\frac{3}{2}}} \quad (1.18)$$

where m is an integer. Once an open aperture z-scan is performed, the parameter q_0 can be obtained by fitting the experimental results to equation (1.17). Then the nonlinear absorption coefficient β can be unambiguously deduced using equation (1.12). The imaginary part of third order susceptibility ($\chi^{(3)}$) determines the strength of the nonlinear absorption. The TPA coefficient is related to $\text{Im}(\chi^{(3)})$ by the relation

$$\text{Im}(\chi^{(3)}) = \frac{\epsilon_0 n_0^2 c^2 \beta}{\omega} \quad (m^2 V^{-2}) = \frac{n_0^2 c^2 \beta}{240 \pi^2 \omega} \quad (\text{esu}) \quad (1.19)$$

where λ is the excitation wavelength, n_0 is the linear refractive index, ϵ_0 is the permittivity of free space and c the velocity of light in vacuum.

1.19.3 Closed aperture z-scan

The basis of closed aperture z-scan is the self refraction and self phase modulation effects. The technique relies on the transmittance measurement of a nonlinear medium through a finite aperture in the far field as a function of the sample position z with respect to the focal plane using a single gaussian beam in a tight focus geometry.

Consider, for instance, a material with a negative nonlinear refraction and thickness smaller than the diffraction length ($k\omega_0^2/2$) of the focused beam being positioned at various points along the z -axis. This assumption implies that the sample acts as a thin lens of variable focal length due to the change in refractive index at each position ($n = n_0 + n_2 I$).

Suppose that the sample is kept at a distance far away from the focus ($-z$). The irradiance is low and there is negligible nonlinear refraction. Hence the transmittance characteristics are linear. As the sample is moved close to the focus, the beam irradiance increases, leading to self lensing in the sample. A negative self lensing prior to focus will tend to collimate the beam, causing a beam narrowing at the aperture which results in an increase in the measured transmittance. As the scan in z direction continues and passes the focal plane, the sample which acts as a negative lens increases the defocusing effect thus increasing the beam divergence, leading to beam broadening at the aperture. Hence the transmittance decreases. Thus there is a null as the sample crosses the focal plane (z_0). The z -scan is completed as the sample is moved away from focus ($+z$) such that the transmittance becomes linear since the irradiance is again low. A prefocal transmittance maxima (peak) followed by a post focal transmittance minima (valley) is the z -scan signature of negative refraction nonlinearity.

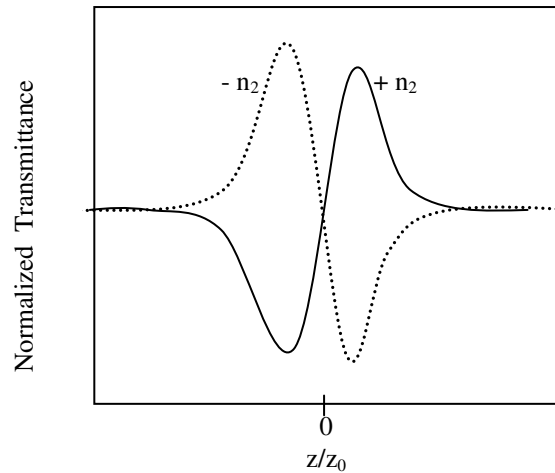


Figure 1.6: Typical closed aperture z-scan curves of samples having positive (solid line) and negative (dashed line) nonlinearity.

The curves for closed z-scan in the case of positive nonlinearity and negative nonlinearity shows opposite effects as depicted in figure 1.6. This is the case of purely refractive nonlinearity where nonlinear absorption is absent. In the presence of multiphoton absorption, there is a suppression of the peak and enhancement of the valley, whereas the opposite effect occurs if there is a saturation of absorption⁴¹.

1.19.4 Theory of closed aperture z-scan technique

In a cubic nonlinear medium the index of refraction (n) is expressed in terms of nonlinear indices n_2 (m^2/W) through

$$n = n_0 + n_2 |E|^2 = n_0 + n_2 I \quad (1.20)$$

where n_0 is the linear index of refraction, E is the peak electric field, n_2 the intensity dependent refractive index and I denotes the irradiance of the laser beam within the sample. Assume a TEM₀₀ beam of waist radius w_0 travelling in the +z direction. E can be written as⁴¹

$$E(z, r, t) = E_0(t) \frac{w_0}{w(z)} \exp \left[-\frac{r^2}{w^2(z)} - \frac{ikr^2}{2R(z)} e^{i\phi(z,t)} \right] \quad (1.21)$$

where $w^2(z) = w_0^2(1 + z^2/z_0^2)$ is the beam radius, $R(z) = z(1 + z^2/z_0^2)$ is

the radius of curvature of the wave front at z , $z_0 = \frac{k\omega_0^2}{2}$ is the diffraction

length of the beam and $k = \frac{2\pi}{\lambda}$ is the wave vector. $E_0(t)$ denotes the radiation electric field at the focus and contains the temporal envelope of the laser pulse. The term $e^{i\phi(z,t)}$ contains all the radially uniform phase variations. For calculating the radial phase variations $\Delta\phi(r)$, the slowly varying envelope approximation (SVEA) is used and all other phase changes that are uniform in r are ignored. $L \ll z_0/\Delta\phi(0)$, where L is the sample

length, the amplitude \sqrt{I} and the phase ϕ of the electric field as a function of z' are now governed in the SVEA by a pair of simple equations

$$\frac{d\Delta\phi}{dz} = \Delta n(I)k \quad (1.22)$$

$$\text{and} \quad \frac{dI}{dz} = -\alpha(I)I \quad (1.23)$$

where z' is the propagation depth in the sample and $\alpha(I)$ in general includes linear and nonlinear absorption terms. In the case of cubic nonlinearity and negligible nonlinear absorption, equation (1.22) and equation (1.23) can be solved to get the phase shift $\Delta\phi$ at the exit of the sample and is given by

$$\Delta\phi(z, r, t) = \Delta\phi(z, t) \exp\left[-\frac{2r^2}{w^2(z)}\right] \quad (1.24)$$

$$\text{with} \quad \Delta\phi(z, t) = \frac{\Delta\phi_0(t)}{\left[1 + \frac{z^2}{z_0^2}\right]} \quad (1.25)$$

where $\Delta\phi_0(t)$ is the on axis phase shift at the focus which is defined as

$$\Delta\phi_0(t) = k\Delta n_0(t)L_{eff} = \frac{2\pi}{\lambda}n_2 I_0(t)L_{eff} \quad (1.26)$$

where $I_0(t)$ is the on axis irradiance at focus (i.e. at $z=0$). The complex electric field exiting the sample E_e now contains the nonlinear phase distribution

$$E_e(z, r, t) = E(z, r, t) e^{-\frac{\alpha l}{2}} e^{i\Delta\phi[z, r, t]} \quad (1.27)$$

By virtue of Huygen's principle and making use of gaussian decomposition method [GD] one can show that

$$e^{i\Delta\phi(z, r, t)} = \sum_{m=0}^{\infty} \frac{[i\Delta\phi_0(z, r, t)]^m}{m!} e^{-2mr^2/w^2(z)} \quad (1.28)$$

Each gaussian beam can be simply propagated to the aperture plane and they will be resummed to reconstruct the beam. After including the initial beam curvature for the focused beam, the resultant electric field pattern at the aperture is

$$E_a(r, t) = E(z, r=0, t) e^{-\alpha l/2} \times \sum_{m=0}^{\infty} \frac{[i\Delta\phi_0(z, t)]^m}{m!} \frac{w_{m0}}{w_m} \exp\left[-\frac{r^2}{w_m^2} - \frac{ikr^2}{2R_m} + i\theta_m\right] \quad (1.29)$$

Defining d as the propagation distance in free space from the sample to the aperture plane and $g=1+\frac{d}{R(z)}$, the remaining parameters in equation (1.29) are expressed as

$$w_{mo}^2 = \frac{w^2(z)}{(2m+1)} \quad d_m = \frac{kw_{mo}^2}{2} \quad \theta_m = \tan^{-1}\left[\frac{d/d_m}{g}\right]$$

$$w_m^2 = w_{mo}^2 \left[g^2 + \frac{d^2}{d_{mo}^2}\right] \quad \text{and} \quad R_m = d \left[1 - \frac{g}{g^2 + d^2/d_m^2}\right]^{-1}$$

The on-axis electric field at the aperture plane can be obtained by putting $r=0$ in equation (1.29). In the limit of small nonlinear phase change ($[\Delta\phi_0 \ll 1]$) and small aperture, only two terms in the sum in equation (1.29) needs to be retained. The normalized z-scan transmittance can be written as

$$T(z, \Delta\phi_0) = \frac{|E_a(z, r=0, \Delta\phi_0)|^2}{|E_a(z, r=0, \Delta\phi_0=0)|^2} = \frac{\left|(g + id/d_0)^{-1} + i\Delta\phi_0(g + id/d_1)^{-1}\right|^2}{\left|(g + id/d_0)^{-1}\right|^2} \quad (1.30)$$

The far field condition $d \gg z_0$ can give a geometry-independent normalized transmittance as

$$T(z, \Delta\phi_0) = 1 - \frac{4\Delta\phi_0 x}{(x^2 + 9)(x^2 + 1)} \quad \text{where } x = z/z_0 \quad (1.31)$$

For a cubic nonlinearity, the peak and valley of the z-scan transmittance can be calculated by solving the equation

$$\frac{dT(z, \Delta\phi_0)}{dz} = 0 \quad (1.32)$$

Solution to this equation (1.32) yields the peak valley separation as

$$\Delta Z_{p-v} = 1.7 z_0 \quad (1.33)$$

Then the peak valley transmittance change is

$$\Delta T_{p-v} = 0.406 \Delta\phi_0 \quad (1.34)$$

Numerical calculations show that this relation is accurate to 0.5% for $|\Delta\phi_0| \leq \pi$. For large aperture, this equation is modified within a $\pm 2\%$ accuracy and is given by

$$\Delta T_{p,v} \approx 0.406 (1 - S)^{0.25} |\Delta\phi_0| \quad \text{for } |\Delta\phi_0| \leq \pi \quad (1.35)$$

where S is the linear transmittance of the far field aperture. From the closed aperture z-scan fit, $\Delta\phi_0$ can be obtained. Then the nonlinear refractive index n_2 can be determined using equation (1.26) and is given by

$$\begin{aligned} n_2 & \quad (\text{m}^2/\text{W}) = \frac{\lambda}{2\pi I_0 L_{\text{eff}}} \Delta\phi_0 \\ n_2 & \quad (\text{esu}) = \frac{cn_0}{40\pi} \frac{\lambda}{2\pi I_0 L_{\text{eff}}} \Delta\phi_0 \end{aligned} \quad (1.36)$$

The n_2 is related to $\text{Re}(\chi^{(3)})$ by the relation,

$$\text{Re}(\chi^{(3)}) = \frac{n_0 n_2 (\text{esu})}{3\pi} \quad (1.37)$$

From the real and imaginary part of $\chi^{(3)}$, the modulus of third order nonlinear susceptibility can be found out.

$$|\chi^{(3)}| = \sqrt{\left[\operatorname{Re}(\chi^{(3)}) \right]^2 + \left[\operatorname{Im}(\chi^{(3)}) \right]^2} \quad (1.38)$$

The magnitude of $\chi^{(3)}$ is significantly affected by the molecular orientation and it determines the strength of nonlinearity of the material.

1.19.5 Merits and demerits of z-scan technique

This technique has several advantages, some of which are

1. Simplicity of the technique as well as simplicity of interpretation
2. Simultaneous measurement of both sign and magnitude of nonlinearity
3. Possibility of isolating the refractive and absorptive parts of nonlinearity
4. High sensitivity, capable of resolving a phase distortion of $\lambda/300$
5. Close similarity between z-scan and the optical limiting geometry

Some of the disadvantages include,

1. Stringent requirement of high quality gaussian TEM_{00} beam for absolute measurements
2. Beam walk-off due to sample imperfections, tilt, or distortions
3. Not suitable for measurements of off diagonal elements of the susceptibility tensor, except when a second non-degenerate frequency beam is employed
4. The determination of the nonlinear coefficients depend on the temporal and spatial profiles, power or energy content and stability of the laser source

1.20 Conclusions

The importance of ZnO nanocomposites have been reviewed with emphasis placed upon its spectral and nonlinear optical properties. Among II-VI semiconductors, ZnO possesses very large exciton binding energy which makes the material very attractive both from scientific point of view and optical device application aspects. One of the first attempts to produce II-VI nanocrystals is by the method of colloidal chemical synthesis. The blue shift of the absorption edge can be explained by different sizes and probably also by different charge states at the interface. Size dependent luminescence, enhanced exciton oscillator strength and nonlinear optical properties are some of the interesting properties exhibited by most of the quantum dots due to quantum confinement effects. Thus nanophotonics is an exciting area of research, which makes it possible to tune the optical properties of nanoparticles to suit any application just by tailoring size, composition etc. and may find tremendous technological applications. The theory and experimental details of z-scan technique used to investigate the NLO properties of ZnO nanocomposites is discussed.

1.21 References

- 1 Lee E-H, “*Physics of semiconductor device*”, New Delhi: Narosa, (1993)
- 2 Herve Rigneault, Jean-Michel Lourtioz, Claude Delalande and Ariel Levenson; “*Nanophotonics*”, ISTE Ltd. London, UK
- 3 Mainman T H; “*Stimulated optical radiation in ruby*”, Nature **87**, 493 (1960)
- 4 Franken P A, Hill A E, Peters C W and Weinrich G; “*Generation of optical harmonics*”, Phys. Rev. Lett. **7**, 118 (1961)
- 5 Joannopoulos J D, Villeneuve P R, Fan S; “*Photonic crystals: putting a new twist on light*”, Nature **386**, 143 (1997)
- 6 Chennupati Jagadish and Stephen J Pearton; “*Zinc oxide: bulk, thin films and nanostructures: Processing, properties and applications*” Elsevier (2006)
- 7 T Yao and J C Woo; “*Physics and applications of semiconductor quantum structures*” IOP publishing Bristol and Philadelphia (2001)
- 8 L Liao, J C Li, D F Wang, C Liu, C S Liu, Q Fu and L X Fan; “*Field emission property*

- improvements of ZnO nanowires coated with amorphous carbon and carbon nitride films”, Nanotech. **16**, 985, 2005*
- 9 H Hartnagel, A L Dawar, A K Jain, C Jagadish; “Semiconducting transparent thin films”, IOP publishing, Bristol and Philadelphia (1995)
 - 10 Al L Efros and A L Efros; “*Interband Absorption of Light in a Semiconductor Sphere*”, Sov. Phys. Semicond. **16**, 772 (1982)
 - 11 Ekimov A I and A A Onushenko JETP Lett. **40**, 1137 (1984)
 - 12 R Rossetti, J L Ellison, J M Gibson and L E Brus; “*Size effects in the excited electronic states of small colloidal CdS crystallites*”, J. Chem. Phys. **80**, 4464 (1984)
 - 13 U Woggon; “optical properties of semiconductor quantum dots” Springer Veralag Berlin Heidelberg (1997)
 - 14 A K Bandyopadhyay “nanomaterials” New Age International (P) Ltd (2007)
 - 15 Kreibig U, Vollmer M; “*Optical Properties of Metal Clusters*”; Springer: Berlin (1995)
 - 16 A Nakamura, Y L Lee, T Kataoka, and T Tokizaki; ”*Mesoscopic enhancement of optical nonlinearity in semiconducting quantum dots: CuCl and CuBr microcrystals*” J. Lumin., **60–61**, 376 (1994)
 - 17 S Ogawa, H Nagano and H Petek; “*Optical Intersubband Transitions and Femtosecond Dynamics in Ag /Fe(100) Quantum Wells*”, Phys. Rev. Lett. **88**, 116801 (2002)
 - 18 D. M. Bagnall, Y. F. Chen, Z. Zhu, T. Yao, S. Koyama, M. Y. Shen and T. Goto; “*Optically pumped lasing of ZnO at room temperature*”, Appl. Phys. Lett. **70**, 2230 (1997)
 - 19 Yefan Chen, D. M. Bagnall, Hang-jun Koh, Ki-tae Park, Kenji Hiraga, Ziqiang Zhu, and Takafumi Yao; “*Plasma assisted molecular beam epitaxy of ZnO on c -plane sapphire: Growth and characterization*”, J. Appl. Phys. **84**, 3912 (1998)
 - 20 Joachin Piprek; “*Semiconductor optoelectronic devices: Introduction to physics and simulation*”, Academic press, Elsevier Science-USA (2003)
 - 21 Y P Varshni; “*Temperature dependence of the energy gap in semiconductors*”, Physica, **34**, 149 (1967)
 - 22 Litty Irimpan et.al.; “Nonlinear optical characteristics of nanocomposites of ZnO-TiO₂-SiO₂” *Optical Materials*(2008) (in press)
 - 23 Litty Irimpan et.al.; “Enhanced luminescence and nonlinear optical properties of nanocomposites of ZnO-Cu” *Journal of materials research*(2008) (in press)
 - 24 Litty Irimpan et.al.; “Effect of annealing on the spectral and nonlinear optical characteristics of thin films of nano ZnO” *Journal of Applied Physics* (2008) (in press)
 - 25 Litty Irimpan et.al.; “Luminescence tuning and enhanced nonlinear optical properties of nanocomposites of ZnO-TiO₂” *Journal of colloids and interface science* (2008) DOI:10.1016/j.jcis.2008.04.056
 - 26 Litty Irimpan, V P N Nampoori and P Radhakrishnan; “*Spectral and nonlinear optical characteristics of nanocomposites of ZnO-CdS*” J. Appl. Phys. **103**, 094914 (2008)

- 27 Litty Irimpan et.al.; “*Spectral and nonlinear optical characteristics of nanocomposites of ZnO-Ag*” Chemical physics letters, **455** (4-6), 265-269 (2008)
- 28 Litty Irimpan et.al.; “*Nonlinear optical characteristics of self assembled films of ZnO*” Applied Physics B: Lasers and Optics, **90** (3-4), 547-556 (2008)
- 29 Litty Irimpan et.al.; “*Effect of self assembly on the nonlinear optical characteristics of ZnO thin films*” Optics Communications, **281** (10), 2938-2943 (2008)
- 30 Litty Irimpan et.al.; “*Size dependent enhancement of nonlinear optical properties in nano colloids of ZnO*” Journal of applied physics **103**, 033105 (2008), Virtual Journal of Nanoscale Science & Technology, February 25 issue, 2008
- 31 Litty Irimpan et.al.; ‘*Size dependent fluorescence spectroscopy of nanocolloids of ZnO*’, J. Appl. Phys. **102**, 063524 (2007)
- 32 Litty Irimpan, Bindu Krishnan, A Deepthy, V P N Nampoori and P Radhakrishnan; J. Phys. D: Appl. Phys. **40**, 5670 (2007)
- 33 Litty Irimpan et.al.; “Visible luminescence mechanism in nano ZnO under weak confinement regime” Communicated to *Optics letters*
- 34 Litty Irimpan et.al.; “Linear and nonlinear optical characteristics of ZnO-SiO₂ nanocomposites” Communicated to *Applied Optics*
- 35 B K Meyer et.al.; “*Bound exciton and donor-acceptor pair recombinations in ZnO*”, Phys. Stat.Sol. (b), **241**, 231 (2004)
- 36 Hari Singh Nalwa and Seizo Miyata; “Nonlinear optics of organic molecules and polymers”, CRC press (1997)
- 37 Richard L Sutherland; “*Handbook of nonlinear optics*”,CRC press (2003)
- 38 J A Herman and J Staromlynska; “*Trends in optical switches, limiters and discriminators*”, Int. J. Nonlinear Opt. Phys. **2**, 271 (1993)
- 39 L W Tutt and T F Boggess; “*A review of optical limiting mechanisms and devices using organics, fullerenes, semiconductors and other materials*” Prog. Quant. Electr. **17**, 299 (1993)
- 40 M S Bahae, A A Said and E W van Stryland; “*High-sensitivity, single-beam n₂ measurements*”, Opt Lett, **14**, 955 (1989)
- 41 M S Bahae, A A Said, T H Wei, D J Hagan and E W Van Stryland; “*Sensitive measurement of optical nonlinearities using a single beam*”, IEEE J. Quantum Electron. **14**, 760 (1990)
- 42 Said A A, Bahae M S, Hagan D J, Wei T H, Wang J, Young J and Van Stryland E W; “*Determination of bound-electronic and free-carrier nonlinearities in ZnSe, GaAs, CdTe, and ZnTe*” JOSA B; **9**, 405 (1992)
- 43 Tai-Huei Wei, Tzer-Hsiang Huang, Huang-Der Lin and Sheng-Hsien Lin; “*Lifetime determination for high-lying excited states using Z-scan*”, Appl. Phys. Lett. **67**, 2266 (1995)



Chapter 2

Fluorescence spectroscopy of nano colloids of ZnO

Abstract

The fluorescence characteristics of nano colloids of ZnO have been studied as a function of the excitation wavelength and particle size. We have found that emission shifts with the change of the excitation wavelength. The excitation wavelength dependent shift of the fluorescence maximum is measured to be between 60 and 100 nm for a change in excitation wavelength from 230 to 355 nm. ZnO is reported to show two emission bands namely an ultraviolet (UV) emission band (380 nm) and another in the green region (530 nm). Apart from the observation of these reported emissions due to near bandgap emission and impurity related emissions, we have found some peculiar features in the fluorescence spectra that are consistent with the nanoparticle size distribution. Results reveal that additional blue emissions at 420 nm and 490 nm are developed with increasing particle size. Systematic studies on nano ZnO have indicated the presence of luminescence due to excitonic emissions when excited with 255 nm as well as significant contribution from surface defect states when excited with 325 nm. The relevant energy levels showing the transitions corresponding to the observed peaks in the emission spectrum of ZnO of particle size 18 nm under 255 nm excitation are identified. The luminescence mechanism and a correlation analysis between the particle size and spectroscopic observations are discussed.

The results of this chapter are published in
Litty Irimpan et.al., Journal of Applied Physics **102**, 063524 (2007)
Litty Irimpan et.al., Journal of Physics D: Applied Physics **40**, 5670 (2007)

2.1 Introduction

Recently, the interest on the short wavelength display device is more increasing¹. Although laser diode or light emitting diode using GaN was already reported, ZnO has several fundamental advantages over its chief competitor, GaN: (1) its free exciton is bound with energy 60 meV, much higher than that of GaN (21–25 meV); (2) it has a native substrate; (3) wet chemical processing is possible and (4) it is more resistant to radiation damage². Optical UV lasing, at both low and high temperatures, has already been demonstrated, although efficient electrical lasing must await the additional development of good *p*-type material³. The growth mechanisms and potential applications of these nanostructures have been reviewed by Wang⁴.

The ZnO bulk or nano particles have various luminescence transitions since different preparation techniques lead to varying structures and surface properties in ZnO. Generally, ZnO exhibits two kinds of emissions: one is in the ultraviolet region corresponding to near band edge emission and the other in the visible region corresponding to deep level emissions⁵⁻⁶ with a peak in the range from 450 to 730nm. Out of the different reported emission peaks, the origin of the green emission is the most controversial.

Stoichiometric zinc oxide is an insulator that crystallizes with the wurtzite structure to form transparent needle-shaped crystals. The structure contains large voids which can easily accommodate interstitial atoms. Consequently, it is virtually impossible to prepare really pure crystals. Moreover, when these crystals are heated, they tend to lose oxygen⁷. For these reasons, ZnO shows *n*-type semiconducting properties with many defects, such as lack of oxygen and the excess of zinc. It is known that visible luminescence is mainly due to defects which are related to deep level emissions, such as Zn interstitials and oxygen vacancies. Vanheusden *et al.*

found that oxygen vacancies are responsible for the green luminescence in ZnO⁸. Oxygen vacancies occur in three different charge states: the neutral oxygen vacancy (Vo^0), the singly ionized oxygen vacancy (Vo^*) and the doubly ionized oxygen vacancy (Vo^{**}) of which only Vo^* can act as the so-called luminescent center⁹.

2.2 Theory

Optical properties of semiconductor nanocrystals depend on the structure of valence and conduction electronic states. One of the most interesting effects of low dimensional semiconductor quantum structures¹⁰⁻¹³ is the size dependent bandgap. The oldest and less computationally demanding approach is the effective mass approximation (EMA) model mostly relying on infinite-well confining potentials^{14, 15}. In 1990 Kayanuma and Momiji¹⁶ introduced the finite depth square well effective mass approximation (FWEMA). Recently, a more refined method has been adopted by other researchers. It has been shown that the refined method considerably improves the model which is suitable for quantitative predictions^{13, 17}. Moreover, Pellegrini et al.¹⁸ systematically investigated the applicability and limitations of the finite depth square well effective mass approximation (FWEMA), applying it to several semiconductor quantum dots (QD) and the numerical results on these systems is obtained recently using the potential morphing method¹² (PMM). Using the PMM, the effective bandgap of colloidal QDs can be estimated using the FWEMA. FWEMA can be extended even to the case of narrow bandgap semiconductor QDs assuming a size dependent dielectric constant.

Brief description of the model described by *S Baskoutas et al.* is given below. In the effective mass approximation, the Hamiltonian for the electron–hole system contains kinetic energy of electron and hole, confinement potential for electron and hole and their coulomb interaction energy¹⁵. It can be written as,

$$H = -\frac{\hbar^2}{2m_e^*} \vec{\nabla}_e^2 - \frac{\hbar^2}{2m_h^*} \vec{\nabla}_h^2 + V_0^e(\vec{r}_e) + V_0^h(\vec{r}_h) - \frac{e^2}{\epsilon} \frac{1}{r_{eh}} \quad (2.1)$$

where m_e^* (m_h^*) is the effective electron (hole) mass, ϵ is the effective dielectric constant, $r_{eh} = |\vec{r}_e - \vec{r}_h|$ is the electron-hole distance in three dimensions and $V_0^e(\vec{r}_e)[V_0^h(\vec{r}_h)]$ is the confinement potential of electron (hole). For QDs the potential is assumed to be centro-symmetric; it has a constant value $V_0^e[V_0^h]$ for distances larger than the QD radius and it vanishes inside the dot. The Bohr radius of Hydrogen atom, a_B^H and that of the electron and hole pair, a_B^{QD} are given by

$$a_B^H = \frac{\hbar^2 \epsilon}{\pi m_e e^2} \quad \text{and} \quad a_B^{QD} = \frac{\hbar^2 \epsilon}{2\pi \mu e^2} \quad (2.2)$$

where μ is the effective mass and $\frac{1}{\mu} = \frac{1}{m_e^*} + \frac{1}{m_h^*}$. In order to appreciate the different Bohr radius of quantum dots (a_B^{QD}) with that of hydrogen atom (a_B^H), let us evaluate the respective numerical values.

$$a_B^H = \frac{\hbar^2 \epsilon}{\pi m_e e^2} = \frac{(6.63 \times 10^{-34})^2 \times 8.85 \times 10^{-12}}{3.14 \times 9.1 \times 10^{-31} \times (1.6 \times 10^{-19})^2} \sim 0.5 A^0$$

$$\text{For ZnO, } \mu = \frac{m_e}{2} \quad \text{and} \quad \epsilon = 3.7 \epsilon_0$$

$$a_B^{ZnO} = \frac{\hbar^2 \epsilon}{2\pi \mu e^2} = 3.7 a_B^H = 3.7 \times 0.52 A^0 = 2 nm$$

Charged particles, electrons and holes have two potentials: the interaction Coulomb potential and the spherical well potential that quantifies the kinetic energies of the electron-hole pair. The Coulomb energy scales as

$\frac{e^2}{\varepsilon R}$ where as electron-hole pair (e-h pair) kinetic energy in the well of radius R scales as $\frac{\hbar^2}{2\mu R^2}$. The relative importance of these two potentials

enables us to distinguish three different confinement regimes.

2.2.1: Weak confinement regime ($R>>a_B$)

When the Coulomb energy is much larger than the confinement energy, the regime is called weak confinement and the particle size is much larger than Bohr radius. In this case, the e-h pair is confined as a whole and the quantification of the movement of the centre of mass is accomplished. Then the envelope wavefunction of the e-h pair is the product of two wavefunctions describing the movement of the e-h pair with respect to center of mass and the movement of the centre of mass confined in the infinite spherical well. On solving the Schrodinger equation, we get the energies of possible related optical transitions as,

$$E_n = E_g - E_{exc} + \frac{\hbar^2 \pi^2 n^2}{2MR^2} \quad (2.3)$$

where $M = m_e^* + m_h^*$ is the total mass of the e-h pair, $R = \frac{m_e^* \vec{r}_e + m_h^* \vec{r}_h}{m_e^* + m_h^*}$ is

the position of the centre of mass, E_g denotes the bulk bandgap energy, E_{exc} is the exciton binding energy and n is quantum number. The energy of $(n+1)^{th}$ optical transition is,

$$E_{n+1} = E_g - E_{exc} + \frac{\hbar^2 \pi^2 (n+1)^2}{2MR^2} \quad (2.4)$$

$$E_{n+1} - E_n = \frac{\hbar^2 \pi^2}{2MR^2} (2n+1) = \frac{\hbar^2}{4MR^2} \left(n + \frac{1}{2} \right) = \alpha \left(n + \frac{1}{2} \right) \quad (2.5)$$

$$\text{where } \alpha = \frac{\hbar^2}{4MR^2} \quad (2.6)$$

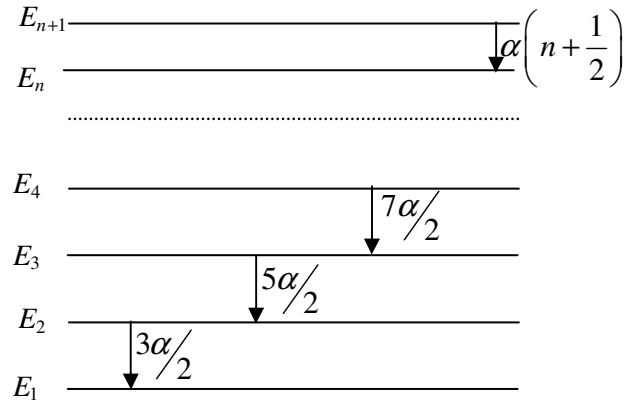


Figure 2.1: Energy level diagram of the excitons in ZnO under weak confinement regime ($R>>a_B$)

For ZnO colloids of particle size, $R=18$ nm,

$$\alpha = \frac{h^2}{8m_e R^2} = 1.85 \times 10^{-22} J = 0.0012 eV = 9.6 cm^{-1} \quad (2.7)$$

When $n=1$, The energy of first optical transition is,

$$E_B = E_g - E_{exc} + \frac{\hbar^2 \pi^2}{2MR^2} = E_g - E_{exc} + \frac{\alpha}{2} = 3.31 eV \quad (2.8)$$

where the bulk bandgap energy of ZnO is 3.37 eV and the exciton binding energy is 60 meV.

2.2.2: Strong confinement regime ($R << a_B$)

Here the Coulomb energy is negligible with respect to confinement energy and this regime appears when the particle size is much smaller than Bohr radius. In this case, both electron and hole are confined separately. The movement of both the carriers is independent and they are considered separately confined in the infinite spherical potential. Confinement energies of the electron and hole depend only on n and l quantum numbers and can be written as

$$E_{n,l}^{e,h} = \frac{\hbar^2 \alpha_{n,l}^2}{2m_{(e,h)}^* R^2} \quad (2.9)$$

with $\alpha_{1,0} = \pi$, $\alpha_{1,1} \approx 1.43\pi$, $\alpha_{2,1} \approx 1.83\pi$, etc...

Calculation of selection rules for dipolar transitions shows that in the optically allowed transitions, the quantum numbers n and l are preserved. By perturbation approach, the Coulomb energy is calculated and the total energy of the first optical transition, 1S-IS ($n_e=n_h=1$, $l_e=l_h=0$, $m_e=m_h=0$) is written as

$$E_{1S-1S} = E_g + \frac{\hbar^2 \pi^2}{2\mu R^2} - \frac{e^2}{\epsilon} \frac{1.8}{R} \quad (2.10)$$

2.2.3: Intermediate regime ($R \sim a_B$)

Here, the Coulomb energy is no longer negligible with respect to confinement energy. In general, the electron and hole have different effective masses. The electron is the lightest particle, and only its movement is confined. To solve the problem in this situation, the results of strong confinement are taken as a departure point to diagonalize the Hamiltonian and to use a variational calculation or a perturbative calculation to take into account the Coulomb interaction.

In any case, the boundaries of the different regimes are not really strict and it is common to extend the theory of strong confinement to describe transitions near the threshold of optical absorption. The main results in the effective mass approximation (EMA) are the transformation of a band structure into a series of discrete levels for which their energy depends on nanocrystal size and increase of first optical transition energy with respect to the bulk gap energy. For very small nanocrystals, this EMA cannot be applicable since it is based on weak confinement regime. A theoretical model has been proposed by *Grigorian G B et al.* taking into account of the complexity of the electronic structure of conduction and valence bands in the strong confinement regime which gives a better result¹⁹⁻²³.

The Hartree-Fock formulation for two particles (electron and hole) results in the following coupled equation²⁴

$$\left[\frac{\vec{p}_i^2}{2m_i} + U_i(\vec{r}_i) \right] \Phi_i(\vec{r}_i) = E_i \Phi_i(\vec{r}_i) \quad (2.11)$$

where $i=e$ or h and the e and h indices refer to the electron and the hole, respectively. The self-consistent effective field $U_i(r_i)$ that acts on the electron is given by

$$U_e(\vec{r}_e) \Phi_e(\vec{r}_e) = \left[V_0^e(\vec{r}_e) - \frac{1}{2} \frac{e^2}{\epsilon} \int d\vec{r}_h \frac{|\Phi_h(\vec{r}_h)|^2}{|\vec{r}_e - \vec{r}_h|} \right] \Phi_e(\vec{r}_e) + \frac{1}{2} \frac{e^2}{\epsilon} \int d\vec{r}_h \frac{\Phi_h^*(\vec{r}_h) \Phi_e(\vec{r}_h)}{|\vec{r}_e - \vec{r}_h|} \Phi_h(\vec{r}_e) \quad (2.12)$$

while the self-consistent effective field that acts on the hole takes the form

$$U_h(\vec{r}_h) \Phi_h(\vec{r}_h) = \left[V_0^h(\vec{r}_h) - \frac{1}{2} \frac{e^2}{\epsilon} \int d\vec{r}_e \frac{|\Phi_e(\vec{r}_e)|^2}{|\vec{r}_e - \vec{r}_h|} \right] \Phi_h(\vec{r}_h) + \frac{1}{2} \frac{e^2}{\epsilon} \int d\vec{r}_e \frac{\Phi_e^*(\vec{r}_e) \Phi_h(\vec{r}_e)}{|\vec{r}_h - \vec{r}_e|} \Phi_e(\vec{r}_h) \quad (2.13)$$

In order to solve the iterative Hartree-Fock equations, the potential morphing method is applied, using the three-dimensional harmonic oscillator as reference system. Once the Hartree-Fock iteration scheme converges, the total energy of the exciton is estimated by the following expression

$$E(X) = E_e + E_h \quad (2.14)$$

and the corresponding effective bandgap is given by

$$E_g^{eff}(X) = E_g + E(X) \quad (2.15)$$

As a first order approximation, the electrons and the holes are assumed to be confined by the same finite square well potential in three-dimensions¹⁸. The form of the lateral confinement potential is (where the indices for both electrons and holes are omitted)

$$\begin{aligned} V_0^{e(h)}(r_{e(h)}) &= 0, \quad r_{e(h)} \leq R \\ &= V_0, \quad r_{e(h)} > R \end{aligned} \quad (2.16)$$

where R is the QD radius and $\overrightarrow{r_{e(h)}} = (x_{e(h)}, y_{e(h)}, z_{e(h)})$ is the three dimensional position vector of the electron (hole). The height of the finite depth well confining potential is independent of the specific type of the semiconductor QD and depends exclusively on the matrix energy bandgap by a simple linear relation of the form

$$V_0 = 0.08E_g(M) \quad (2.17)$$

where $E_g(M)$ is the matrix energy bandgap. The material parameters used in the potential morphing method calculations for ZnO such as effective masses

and dielectric constants are $\frac{m_e^*}{m_e} = 0.24, \frac{m_h^*}{m_e} = 0.45$ and $\epsilon = 3.7$.

Thus the energy shift of the optical absorption edge is size dependent and luminescence experiments give complementary information. The red shift in bandgap fluorescence with particle size closely follows the red shift in the absorption band edge. When particle size decreases, the overlap of the electron and hole wavefunctions increase and the Coulomb interaction between particles also increases. If two or more e-h pairs are present in the nanocrystal, a phenomenon known as Auger ionization becomes important. Theoretical treatment of this process is complex²⁵. Auger effect efficiency is related to e-h pair Coulomb interaction. Auger ionization consists of an energy transfer from one e-h pair, which relaxes non-radiatively, to the other pair in the nanocrystal. Then the ejection of an

electron or a hole belonging to the second pair to the surrounding matrix occurs and the lifetime of e-h pairs become shorter and shorter as the number of e-h pairs increases for a given size. As the particle size decreases, the electronic confinement increases the Coulomb interaction and decreases lifetime. For example, the fluorescence life time of CdSe nanocrystal is reported to be reduced from 360ps to 6ps when the particle size reduces from 4.1 nm to 1.2 nm²⁶. This reduction in fluorescence lifetime leads to excitation wavelength dependent emission behaviour in nanocrystals. This behaviour is less important in semiconductors with large particle size because of the reduction in e-h interaction and because of the restrictions imposed by energy and momentum conservation.

2.3 Synthesis of nano colloids of ZnO

ZnO is prepared by two different chemical routes and different capping agents like Poly Vinyl Pyrrolidone(PVP) and Poly Ethylene Imine(PEI) have been used.

2.3.1 Polyol method

In the present investigation, colloids of ZnO are synthesized by a modified polyol precipitation method²⁷⁻³⁰. The monodisperse ZnO colloidal spheres are produced by a two-stage reaction process. The method of preparation involves the hydrolysis of zinc acetate dihydrate (ZnAc) in diethylene glycol medium (DEG). Among the different polyols, diethylene glycol (DEG) is chosen because it is reported to give particles with uniform shape and size distribution. The size of the particles and hence the stability of this colloidal suspension depend on the concentration of zinc acetate as well as on the rate of heating. The molar concentration of precursor solution is varied from 0.01mM to 0.1M and a heating rate of 4°C per minute is employed for the formation of ZnO at a temperature of 120°C. The product from the primary reaction is placed in a centrifuge and the supernatant (DEG, dissolved reaction products, and unreacted ZnAc and water) is decanted off

and saved. A secondary reaction is then performed which is similar to the above procedure to produce the monodisperse ZnO spheres. Prior to reaching the working temperature, typically at 115°C , some volume of the primary reaction supernatant is added to the solution. After reaching 120°C , it is stirred for one hour, to get a monodisperse stable colloid.

2.3.2 Capping

In the second method that we adopted, 1mM zinc acetate is dissolved in isopropyl alcohol (IPA-Merck, HPLC grade) by stirring at 50°C in the presence of capping agent poly vinyl pyrrolidone (PVP-Sisco)³⁰. ZnO colloid is formed when it is hydrolysed with sodium hydroxide under ultrasonification for 2 hours. In the third method, we used another cationic dispersant poly ethylene imine (PEI- Sigma Aldrich] as capping agent³¹. PEI is a polyelectrolyte and it makes the surface positively charged. The positive charges keeps the particles repelled from each other and prevent agglomeration. The long polymeric chains of PEI on the other hand effectively cap the surface as soon as nucleation occurs and prevents growth. Thus, a polyelectrolyte can make a stable nano semiconductor crystal colloid by these two mechanisms.

2.4 Absorption spectroscopy of nano colloids of ZnO

The ZnO colloids are characterized by optical absorption measurements recorded using a spectrophotometer (JascoV-570 UV/VIS/IR). Figure 2.2 gives the room temperature absorption spectra of the ZnO colloids prepared by polyol method. The excitonic peak is found to be blue shifted with decrease in particle size (370-350 nm) with respect to that of bulk ZnO (395 nm) and this could be attributed to the confinement effects³².

In the case of nanocrystallites, the electrons, holes and excitons have limited space to move and their limited motion becomes possible only for definite values of energy. The highest occupied valence band and lowest unoccupied conduction band are shifted to a more negative and positive

values respectively resulting in widening of bandgap. This leads to a blue shift of absorption band which can be observed through optical absorption and transmission studies. This size dependent shifts in absorption band edge are shown in figure 2.2. From the figure, it is clear that ZnO colloids of size 4.5 nm to 6 nm lies in one regime called intermediate regime ($R \sim a_B$) and ZnO colloids of size 10 nm to 18 nm lies in the other regime called weak confinement regime ($R > a_B$).

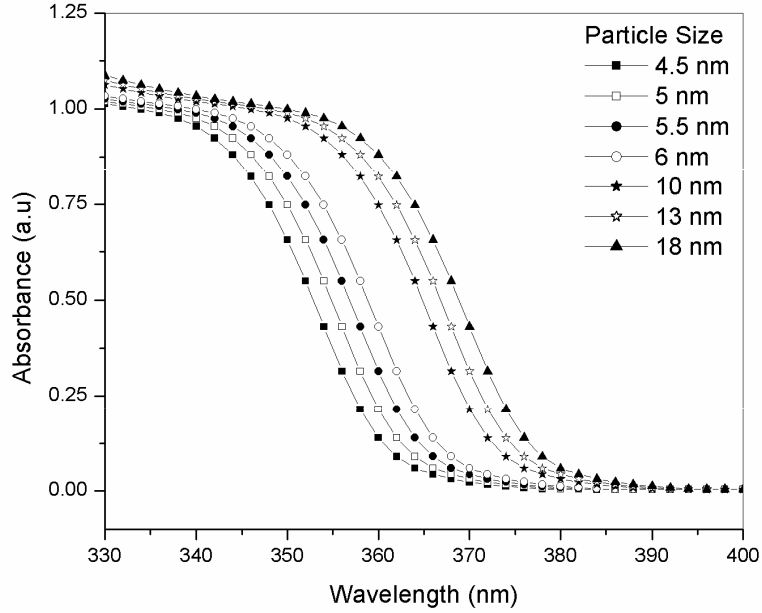


Figure 2.2: Size dependent absorption spectroscopy of ZnO colloids prepared by modified polyol method

The pronounced dependence of the absorption bandgap on the size of ZnO nano crystals is used to determine the particle size. The cluster sizes are calculated from the absorption spectra using the analytical formula given by Ranjani Viswanatha et al³³. To get a precise measure of the shift, the first

derivative curve of the absorption spectrum is taken and the point of inflection is taken as the cut-off wavelength and is shown in figure 2.3.

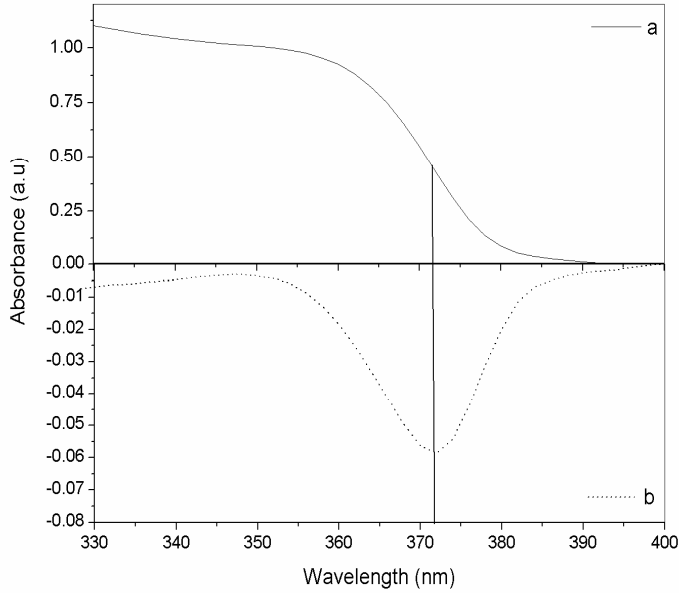


Figure 2.3 (a): Absorption spectrum (b): first derivative of the absorption spectrum of ZnO colloids of size 18 nm.

From the cut-off wavelength, the corresponding E_g is calculated. The deviation of this from the E_g of bulk ZnO gives ΔE_g and the particle size, d is determined using the equation,

$$\Delta E_g = 100(18.1d^2 + 41.4d - 0.8)^{-1} \quad (2.18)$$

Figure 2.4 gives the room temperature absorption spectra of the ZnO colloids prepared by different chemical routes in which the effect of capping is clearly seen.

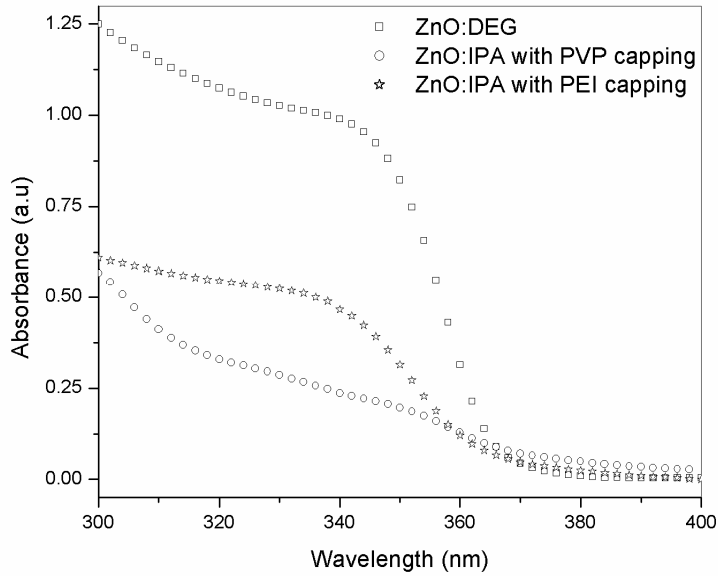


Figure 2.4: Absorption spectra of the ZnO colloids prepared by different chemical routes

2.5 X-ray diffraction (XRD)

The powder extracted from the colloid of large particle size is characterized by x-ray diffraction. Typical XRD pattern of ZnO colloid is given in figure 2.5. The diffraction pattern and interplane spacings can be well matched to the standard diffraction pattern of wurtzite ZnO, demonstrating the formation of wurtzite ZnO nanocrystals³⁴. The particle diameter d is calculated using the Debye–Scherer formula

$$d = \frac{0.89\lambda}{\beta \cos \theta} \quad (2.19)$$

where λ is the x-ray wavelength (1.5406 \AA), θ is the Bragg diifraction angle, and β is the peak width at half maximum³⁵. The XRD peak at 36° in

figure 2.5 gives the ZnO particle diameter of 18 nm and matches well with the size calculated from absorption spectrum.

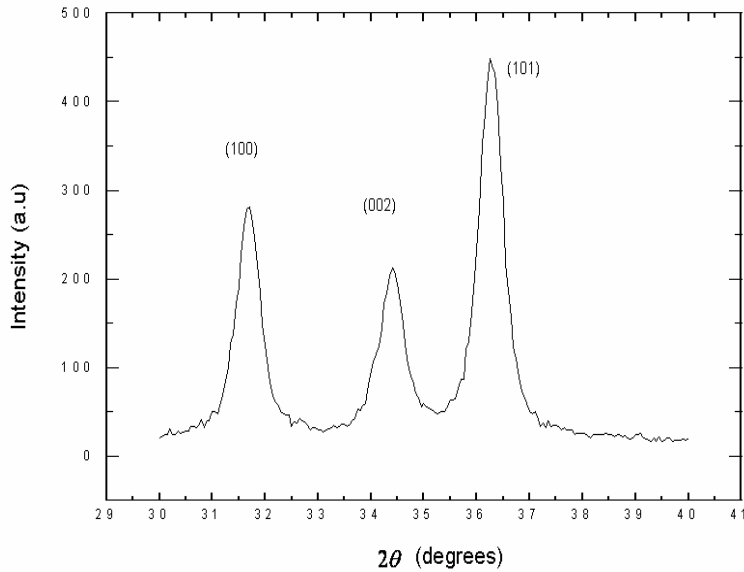


Figure 2.5: XRD pattern of the powder extracted from ZnO colloid of size 18 nm

2.6 Optical bandgap

The absorption of a photon, leading to excitation of an electron from the valence band to the conduction band, is associated with the bandgap energy. The direct bandgap of ZnO colloids are estimated from the graph of $h\nu$ vs $(\alpha h\nu)^2$ for the absorption coefficient α which is related to the bandgap E_g as $(\alpha h\nu)^2 = k(h\nu - E_g)$, where $h\nu$ is the incident light energy and k is a constant. Extrapolation of the linear part until it intersects the $h\nu$ axis gives E_g . The optical bandgap (E_g) is found to be size dependent and there is an increase in the bandgap of the semiconductor with a decrease in the particle size as shown in figure 2.6.

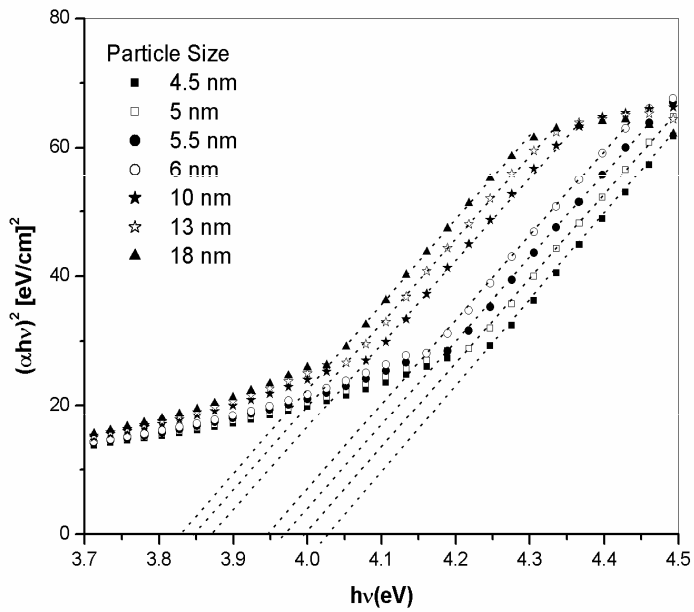


Figure 2.6 : Optical bandgap of ZnO colloids

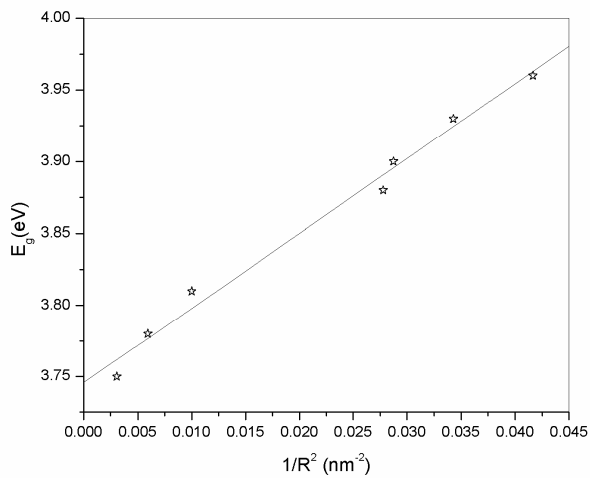


Figure 2.7: Variation of optical bandgap as a function of $1/R^2$

Figure 2.7 shows the optical bandgap energy as a function of $1/R^2$. The bandgap energy becomes larger with decreasing size. This effect is considered to be due to confinement of the exciton in the nanocrystal. When we apply equation (2.3) the y-intercept gives $E_B = E_g - E_{exc} = 3.75\text{eV}$ which is comparable with the theoretical value in equation (2.8).

The total change in the bandgap of the material is jointly contributed by shifts of the valence and the conduction band edges away from each other and is schematically shown in figure 2.8. In general, the shift of the top of the valence band (TVB) is not the same as that of the bottom of the conduction band (BCB). Moreover, there are recent studies, though few in number,³⁶ that report the individual shifts in top of the valence band and bottom of the conduction band as a function of the size employing various forms of high-energy spectroscopies, such as the photoemission and the x-ray absorption spectroscopies.

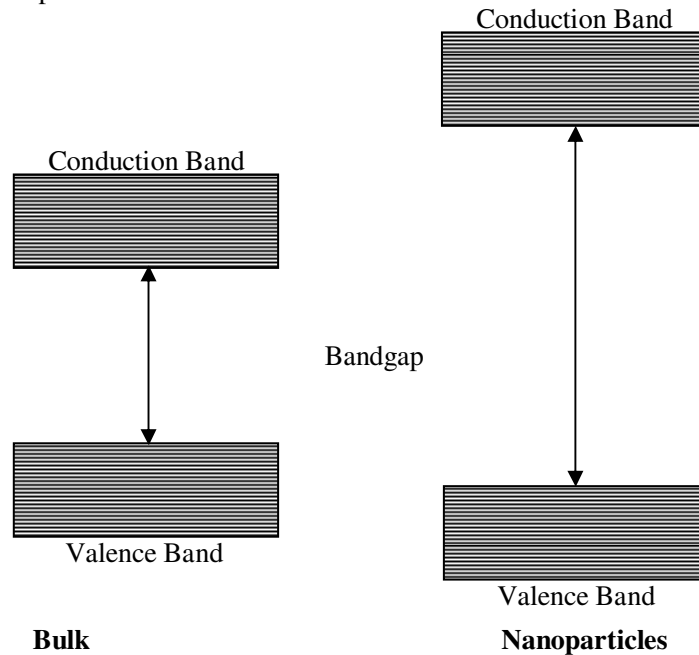


Figure 2.8: Schematic representation of bandgap in bulk and nanoparticles

Thus, it is desirable to compute these shifts of the individual band edges with the size of the nanocrystallite. The shifts of the band edges decrease smoothly to zero for large sized nanocrystals in every case and the shift in the bottom of the conduction band is in general much larger compared to the shift in the top of the valence band for any given size of the nanocrystal. This indicates that the shifts in the total bandgap as a function of the nanocrystal size are always dominated by the shifts of the conduction band edge in these systems. A larger shift for the bottom of the conduction band is indeed expected in view of the fact that the band-edge shifts are related inversely to the corresponding effective masses⁵ and the effective mass of the electron is always much smaller than that of the hole in these II-VI semiconductors. From this band edge shifts, the electronic structure as a function of the nanocrystallite size can be calculated for semiconductors³⁷. The bandgap is found to be in the range 3.5-4 eV for the range of particles from 4.5-18 nm which is in agreement with the reported value³⁸.

2.7 Fluorescence spectroscopy

The fluorescence emission from ZnO colloids is recorded using a Cary Eclipse fluorescence spectrophotometer (Varian). The fluorescence behaviour of nano colloids of ZnO has been studied as a function of the excitation wavelength and particle size. The reduction in fluorescence lifetime with decrease in particle size leads to excitation wavelength dependent emission behaviour in nanocrystals. This behaviour is less important in semiconductors with large particle size because of the reduction in electron-hole interaction and because of the kinetic restrictions imposed by energy and momentum conservation.

2.7.1 Excitation spectrum

Figure 2.9 shows the excitation spectrum corresponding to the emission peak at 390 nm and exhibiting two excitation wavelengths at

$\lambda_{ex}^{(1)}=255$ nm and $\lambda_{ex}^{(2)}=325$ nm. Since ZnO has a broad band absorption, excitation spectrum is very significant in finding the excitation wavelengths at which it has maximum emission.

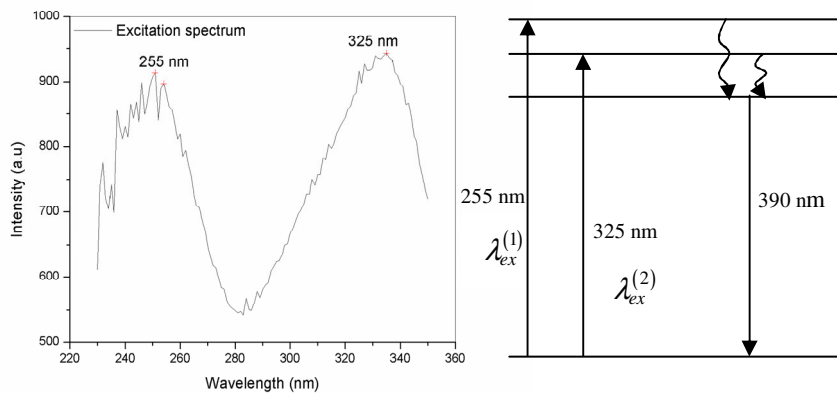


Figure 2.9: Excitation spectrum of ZnO colloid for an emission peak of 390 nm

2.7.2 Excitation wavelength dependent fluorescence spectroscopy

The steady state absorption and fluorescence behaviour of nano colloids of ZnO, in which spectra are sensitive to the polarity of the surrounding environment, has been studied with a view to obtaining information on how the polarity of these liquids influence the fluorescence behaviour. Time-resolved fluorescence studies on dipolar solutes, which have revealed wavelength dependence of the fluorescence decay profiles and dynamic fluorescence Stokes shift in the ps–ns time scale³⁹⁻⁴², have thrown insight into the mechanism of solvation. The excitation at the tail of the absorption band gives rise to an emission that shifts with the change of the excitation wavelength⁴³. This kind of excitation wavelength dependent fluorescence behaviour has also been reported for some dipolar solutes in ionic liquids⁴⁴. The excitation wavelength dependent emission behaviour of

nano colloids of ZnO is considered unusual as the literature suggests that ZnO does not exhibit excitation wavelength dependent behaviour^{6, 45} and the observed behaviour is contrary to what is prescribed by the well-known Kasha's rule of excitation wavelength independence of the emission spectrum⁴⁶ (figure 2.10).

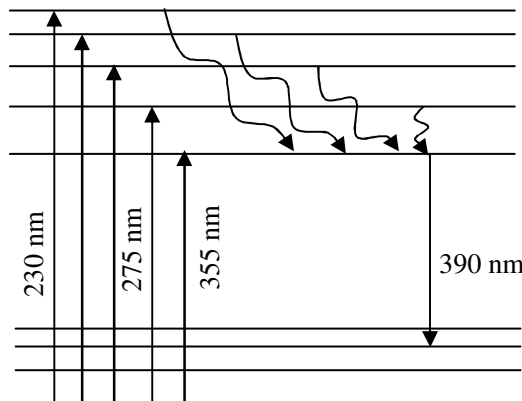


Figure 2.10: Schematic representation of Kasha's rule of excitation wavelength independence of the emission spectrum

To understand the origin of this behaviour, we have undertaken the present investigation on nano ZnO colloids prepared in two different media of different viscosities. The behaviour of these systems that show excitation wavelength dependent fluorescence spectra is also examined by capping them with two different capping agents. Figure 2.11 shows the excitation wavelength dependent fluorescent behaviour in nano colloids of ZnO prepared by polyol method. When ZnO prepared in diethylene glycol medium is excited at the UV side (say, at 230-240 nm) of the absorption maximum, the fluorescence maximum (λ_{em}^{\max}) of ZnO is observed at 346 nm. Interestingly, as can be seen from figure 2.11, as the excitation wavelength is progressively shifted towards the red side, there is a shift in the fluorescence

maximum. The shift in the fluorescence maximum is small and steady when the excitation wavelength changes from 275 nm to 325 nm whereas the shift is significant when the excitation wavelength varies near the edge of $\lambda_{ex}^{(1)}$ and $\lambda_{ex}^{(2)}$.

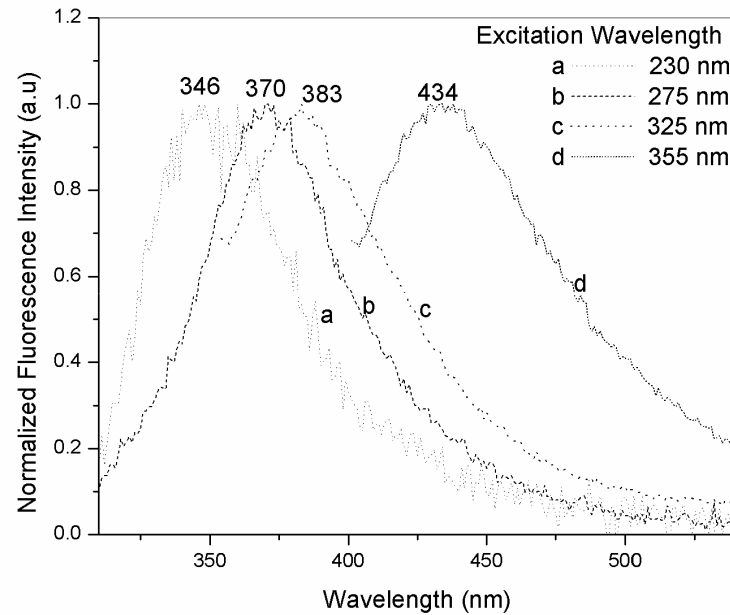


Figure 2.11: Normalized fluorescence spectra of ZnO nano colloids of size 6 nm as a function of excitation wavelength. The fluorescence spectra have been corrected for the instrumental response.

The dependence of λ_{em}^{\max} of ZnO of different particle size prepared by polyol method on the excitation wavelength (λ_{ex}) is shown in figure 2.12. The extent of the shift, as measured from λ_{em}^{\max} , is around 90 nm for the range of excitation wavelength studied.

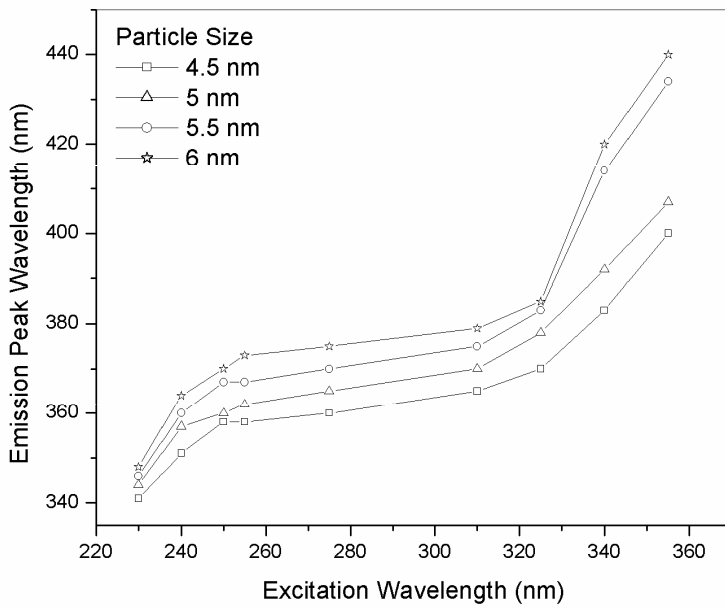


Figure 2.12: λ_{em}^{\max} vs λ_{ex} plots of nano colloids of ZnO of different sizes prepared by modified polyol synthesis

Figure 2.13 shows the dependence of λ_{em}^{\max} on the excitation wavelength of nano colloids of ZnO prepared in different media by using different capping agents. The excitation wavelength dependence of emission maxima is different for colloids prepared in different media. Although both the absorption and emission band positions are dependent on the polarity of the medium, the fluorescence spectrum is much more sensitive to the medium than the absorption spectrum. This is evident from the fact that, when the solvent is changed from isopropyl alcohol to polar diethylene glycol, the absorption maximum shifts by only 7-8 nm, whereas the emission maximum shifts by more than 20 nm. This behaviour is suggestive of an

emitting state that is more polar than the ground state. The shift remains the same when we change the capping agent in the same medium. ZnO exhibits more pronounced excitation wavelength dependence in relatively more viscous and more polar diethylene glycol medium compared to isopropyl alcohol medium. Viscosity and polarity of the medium plays a major role in the excitation wavelength dependent shift of emission maxima.

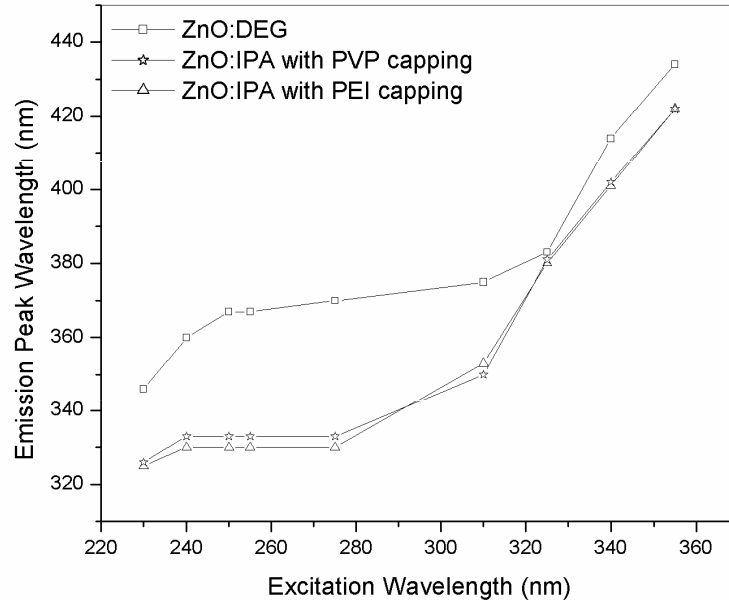


Figure 2.13: λ_{em}^{\max} vs λ_{ex} plots of nano colloids of ZnO prepared in different media using different capping agents

To the best of our knowledge, this is the first report on the excitation wavelength dependent emission behaviour in nano colloids of ZnO. When the homogeneous nature of the ZnO colloids and the literature data of fluorescence emission behaviour already studied are taken into consideration,

the present observation appears to be quite unusual. However, when excited at the long wavelength edge of the first absorption band, a red shift of λ_{em}^{\max} of the dipolar molecules is often observed in low-temperature glasses; polymer matrixes; and organized assemblies such as micelles, vesicles, proteins, and membranes^{47, 48}. This is primarily due to the fact that (i) the probe molecules absorbing at the red edge of the absorption band have greater interaction with the solvent molecules than those absorbing in the blue side and (ii) the inhomogenous broadening can only be probed at the red excitation edge where the excitation to the higher vibrational levels does not interfere with this selection. This phenomenon is termed as the “red-edge effect” (REE)^{49,50}. This is also called the edge excitation shift (EES)⁴⁸ or the edge excitation red shift (EERS)^{51, 52} or the red-edge excitation shift (REES)^{53, 54}. We prefer to use the REE terminology, as there is red shift in emission peak with respect to excitation wavelength and this happens to be the first accepted abbreviation for the observed phenomenon^{49, 50}.

2.7.3 Factors contributing to REE

The excitation wavelength dependence can arise when there exists a distribution of the molecules in the ground state that differ in their solvation sites and, hence, their energies. This inhomogeneity can originate from the difference in the interaction energies between the medium and the nano particles. However, the presence of an ensemble of energetically different molecules in the ground state *alone* does not guarantee an excitation wavelength dependent fluorescence behaviour because rapid relaxation of the excited state, such as the solvation of the fluorescent state or energy transfer between the energetically different excited states of the molecules, is expected to result in emission from the lowest energy state irrespective of the excitation. It is only when a system allows selective excitation of the

energetically different species and the relaxation of the fluorescent state is slow (hence, incomplete) that REE can be expected.

Since inhomogeneous broadening, which dictates photo-selection of the energetically different species, is directly proportional to the change of dipole moment ($\Delta\mu$) due to electronic excitation, the probe molecules with large $\Delta\mu$ values are the most suitable candidates to exhibit REE. The change in the dipole moment of ZnO upon electronic excitation is reported to be high⁵⁵. The second factor, which is even more important than the first, is that ZnO has a rather short fluorescence lifetime (τ_f). The bandgap fluorescence of ZnO has an extremely short lifetime which is reported to be 100 ps⁵⁶. On the other hand, recent studies on solvation dynamics suggest that solvation is a rather slow process⁵⁷. The solvent relaxation time (τ_{sol}) of the medium is of the order of nanoseconds. Because τ_{sol} around the photoexcited molecule is an order of magnitude higher than the τ_f value, it is not difficult to understand why unrelaxed fluorescence, which gives rise to the excitation wavelength dependent emission behavior, could be observed in the case of nano colloids of ZnO. When the τ_f values are higher than the τ_{sol} value of the solvent, the fluorescence occurs from a fully solvated state. Potentially, lifetime shortening with decrease in particle size has been recently found in KrN clusters³¹. This model also explains why the more short wave emission with a shorter lifetime originates from smaller clusters. Due to the low concentration of ZnO colloids of small particle size, the energy transfer between the upper vibrational level and the lower vibrational level of the excited state of these particles is inefficient owing to short fluorescence lifetime and thus the emission characteristics changes with excitation wavelength.

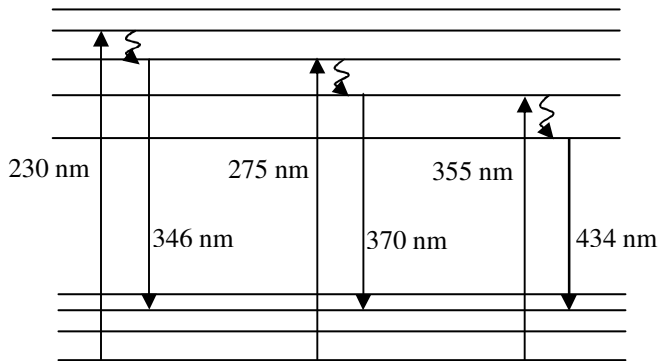


Figure 2.14: Schematic representation of excitation wavelength dependence of emission spectrum

Probe molecules with short fluorescence lifetimes are more likely to exhibit REE than those with long lifetimes. The larger the polarity and nuclear polarizability of the medium, the stronger is the interaction of the probe molecule with the solvent and higher is the chance to observe REE. The more viscous is the medium, the slower is the excited state relaxation process (intramolecular) and higher is the possibility to observe REE. The molecule fluoresces efficiently and the quantum yield increases strongly with increase in viscosity. This dependence of the fluorescence yield on viscosity and polarity has been studied previously⁵⁸. The viscosity and possibly hardness of the medium plays a dominant role in the fluorescence efficiency of the molecule. These data can be understood by considering the effect of viscosity on the rotation of the active molecule. When these levels (modes) are hindered because of the increase in the viscosity, the rates of rotation and vibration decrease with the eventual cessation of several modes of rotation and vibration in viscous medium and solid matrices. This decrease in the active modes leads to a weaker coupling of the excited electronic states with upper levels of the ground state, which results in a decrease in the energy dissipation rate of the excited state by means of internal radiationless

channels to the ground states. Consequently the rate of population decay via radiative transitions increases and there is higher possibility to observe REE. Thus the high viscosity of the medium and short fluorescence lifetime, which makes the relaxation of the photo-excited species inefficient, contributes to REE-like behaviour in nano colloids of ZnO with smaller particle size.

The excitation wavelength dependent emission behaviour in nano colloids of ZnO is not due to any specific interaction between the medium and ZnO, but is due to incomplete solvation of the fluorescent state in the viscous medium. This is evident from the fact that ZnO exhibits shift of the λ_{em}^{\max} in two media prepared by different methods. Therefore, it can be concluded that it is the incomplete solvation (relaxation) in these viscous media that is primarily responsible for the excitation wavelength dependent spectral shift of nano colloids of ZnO.

In the case of ZnO, the electrostatic interaction is expected to dominate the other interactions and probably plays the most important role in creating a distribution of energetically different molecules in the ground state that allows their photo-selection. Two factors responsible for the slow relaxation of the excited state are the retardation of solvation due to the electrostatic forces induced by charged ZnO and/or an inefficient energy transfer between the energetically different species. In the absence of any literature data on solvation dynamics, it is not possible to pinpoint at this stage whether one or both the factors contribute to REE in ZnO. Further studies, both theoretical and experimental, need to be carried out to obtain insight into this aspect. Regarding excited state relaxation, an inefficient energy transfer between the energetically different molecules takes place which presumably contributes to the excitation wavelength dependent fluorescence behaviour in this case. Thus we can conclude that the larger viscosity of the medium which slows down the excited state relaxation

process and the reduction in fluorescence lifetime due to small particle size are responsible for the excitation wavelength dependent spectral shift in nano ZnO colloids.

2.7.4 Size dependent fluorescence spectroscopy

The fluorescence spectra of nano ZnO colloids of different particle size for an excitation wavelength of 255 nm are shown in figure 2.15. Results show that additional emissions at 420 nm and 490 nm are developed with increase in particle size along with known bandgap emissions at 380 nm and impurity dominated emissions at 530 nm. The excitons can exhibit excited states, in addition to their ground state transitions which results in the additional emission peaks.

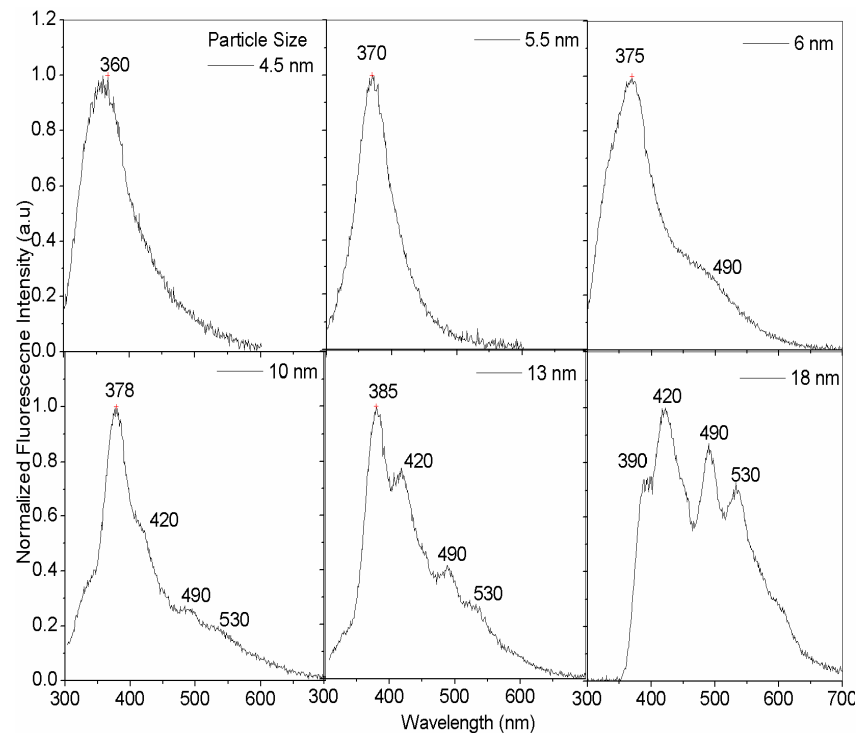


Figure 2.15:Steady state fluorescence spectra of nano ZnO colloids of different particle size for an excitation wavelength of 255 nm

Figure 2.16 shows the fluorescence spectrum of the powder extracted from ZnO colloid of 18 nm at an excitation wavelength of 255 nm. It exhibits all the characteristic emission peaks of the colloid. It confirms the fact that the emission peaks are of pure ZnO and there are no solvent effects. Figure 2.15 and 2.16 show multiple emission peaks at larger particle size. These may be attributed to transition from various excited state energy levels of exciton to the ground level corresponding to $R>>a_B$ case.

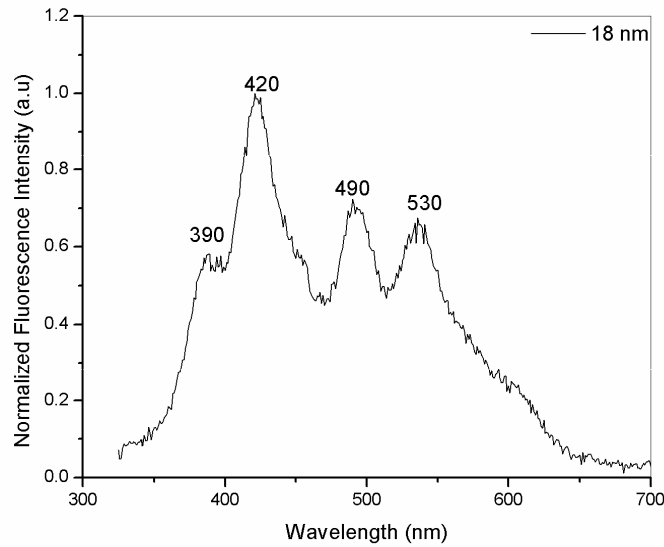


Figure 2.16: Fluorescence spectrum of the powder extracted from ZnO colloid of size 18 nm at an excitation wavelength of 255 nm

For ZnO colloids of particle size 18 nm, we get emission peaks at 390 nm, 420 nm, 490 nm and 530 nm. Additional shoulders at 455 nm, 570 nm and 600 nm are present along with the emission peaks. This series of peaks can be modelled as a particle in a box problem. Assume that the emission peak at 600 nm (2 eV) results from the transition from a higher

energy level corresponding to quantum number n to the lowest one corresponding to $n=1$. From equation (2.3), transition energy from n to 1 is

$$E_n - E_1 = \frac{\hbar^2 \pi^2}{2MR^2} (n^2 - 1) = \frac{\hbar^2}{2 \times 4MR^2} (n^2 - 1) = \frac{\alpha}{2} (n^2 - 1) \quad (2.20)$$

Therefore, $\frac{\alpha}{2} (n^2 - 1) = 2 \text{ eV}$ and $n=59$. Thus 600 nm transition corresponds to $n=59$ to $n=1$ level. Similarly for other emission peaks, transitions are identified based on this model and is shown in figure 2.17.

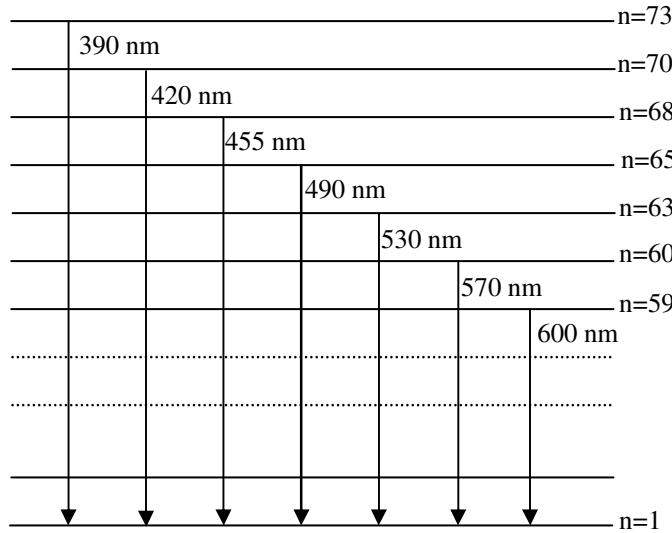


Figure 2.17: Relevant energy level diagram showing the transitions corresponding to the observed peaks in the emission spectrum of ZnO of particle size 18 nm under 255 nm excitation.

The results obtained support the fact that exciton levels in the weak confinement regime can be modelled as those related to particle in a box. The spectra are not of sufficient resolution to get the transition peaks from all the consecutive energy levels.

2.7.5 UV emission

The UV emission band is assigned to a direct *bandgap* transition. Like the absorption spectrum, this UV band undergoes a red shift with particle size. Such size dependent optical properties of semiconductor particle suspensions in the quantum regime are well known and similar observations have previously been made for several quantum particle systems⁵. For the intrinsic luminescence of ZnO nanoparticles, it is generally known that the formation of nanoparticles causes a red shift in the PL spectra due to quantum size effect⁵⁹. An analytical approximation for the lowest eigenvalue (i.e., the first excited electronic state) is described as follows⁵:

$$E^* = E_g + \frac{h^2}{8R^2} \left(\frac{1}{m_e} + \frac{1}{m_h} \right) - \frac{1.8e^2}{\epsilon R} + \text{smaller terms}, \quad (2.21)$$

where E_g is the bandgap, R is the radius of the ZnO nanoparticles, h is Plank's constant, $m_e = 0.24m_0$ is the electron effective mass, $m_h = 0.45m_0$ is the hole effective mass, ϵ is the dielectric constant of ZnO with an accepted value of 3.7. Results show that the fluorescence emission peak shifts from 360 nm to 370 nm as the particle size increases from 4.5nm to 6 nm as is evident from the above equation. The emission around 360 nm (3.4 eV) shown in the figure 2.14 is consistent with the bandgap of the ZnO nanoparticles. A red shift of UV emission is observed with the increase in the particle size which is attributed to quantum size effects.

With the increase in the particle size, the energy of UV luminescence is shifted from 3.5 eV (350 nm) to 3 eV (390 nm). The shift of bandgap energy is related to the structural property. Therefore, the energy of UV emission known as near band edge emission is decreased from 3.5 to 3 eV. The bandgap is found to be in the range 3.5-4 eV for the range of particles from 4.5-18 nm as shown in figure 2.5. The optical bandgap is shifted from 3.5 to 4 eV for different particle size and the shift is consistent

with the result of PL in the range of UV. The UV emission is shifted from 3.5 to 3 eV by the shift of optical bandgap from 4 to 3.5 eV and it clearly indicates that the origin of UV emission is the near band edge emission²⁹.

Mean cluster size could be principally derived from the absorption measurements and the enlargement effects are expected to be predominant when the particle size is less than about 6 nm as shown in figure 2.18 (a) where the band enlargement is plotted as a function of the average particle size. Figure 2.18 (b) shows the energy of the band to band transition as a function of the mean particle size. The red shift in the UV emission with particle size closely follows the red shift in the band edge, indicating that the two are related. The reconstructed size distribution curve from the fluorescence spectrum is shown below²⁹.

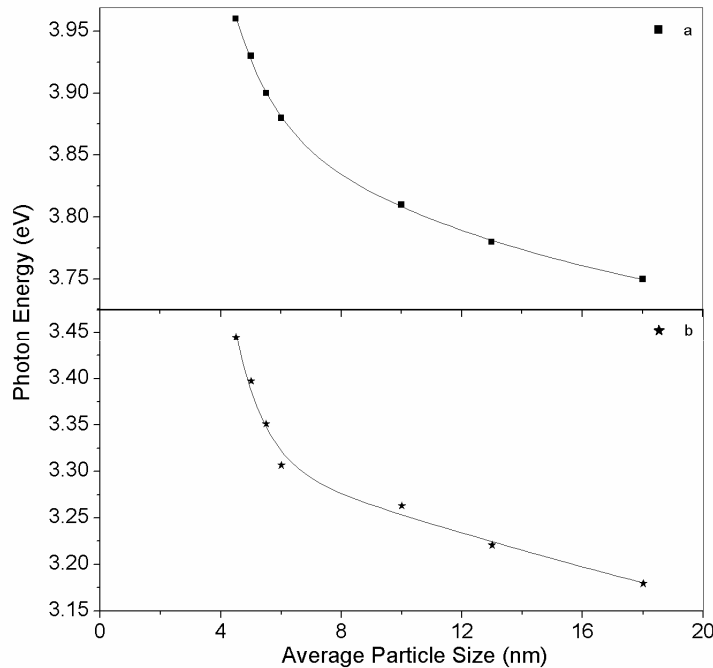


*Figure 2.18:The dependence of mean particle size on
 (a) bandgap (b) band to band emission*

Figure 2.19 shows the fluorescence spectra of nano ZnO colloids of different particle size for an excitation wavelength of 325 nm. We have observed that with the decrease of excitation energy, the blue band peaks get suppressed and UV and green fluorescence peak becomes dominant at larger particle size²⁹. The transitions from different excited states of excitons may be weakened at this higher excitation wavelength and a broad visible emission due to surface defect states become more pronounced at 325 nm excitation wavelength for ZnO colloids of size 18 nm.

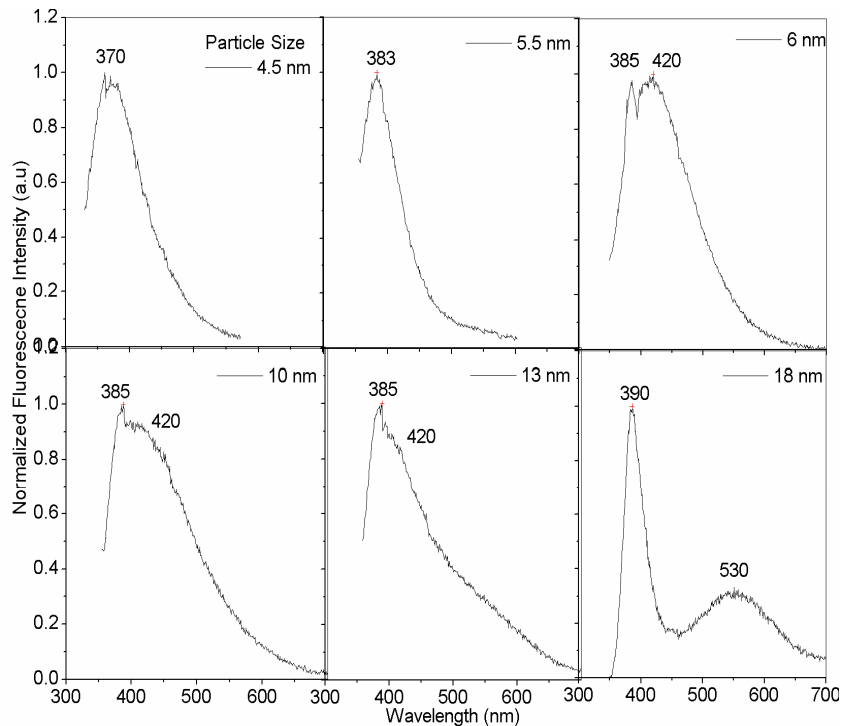


Figure 2.19: Fluorescence spectra of nano ZnO colloids of different particle size for an excitation wavelength of 325 nm

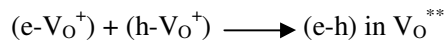
2.7.6 Visible emission

In contrast to the UV spectra, visible fluorescence spectra of ZnO particles are sensitive to the preparation procedure (and, therefore, to

environmental conditions). The well-known green fluorescence at 510 ± 50 nm appeared in colloids with larger particle size.

In ZnO, oxygen has tightly bound 2p electrons and Zn has tightly bound 3d electrons, which sense the nuclear attraction efficiently. The first principal calculation found that the Zn_{3d} electrons strongly interact with the O_{2p} electron in ZnO⁶⁰. Since the center energy of the green peak is smaller than the bandgap energy of ZnO, the visible emission cannot be ascribed to the direct recombination of a conduction electron in the Zn_{3d} band and a hole in the O_{2p} valence band. The green emission must be related to the localized level in bandgap. The PL of ZnO has been extensively investigated, and there is no consensus in the literature on the positions of the peaks in PL spectrum of ZnO nanostructures and thin films or on their origin.

The concept of surface fluorescence-centers seems to be more realistic for nanoparticles. Researches indicate that the surface passivation via surfactant and polymer capping is an effective method to enhance the UV emission and quench the defect-related visible photoluminescence (PL) from nanosized ZnO^{35, 61}. The effect of method of preparation and surface passivation itself is an indication that the green emission is due to surface states. For the uncapped ZnO nanoparticles, there exist abundant surface defects, the valence band hole can be trapped by the surface defects and then tunnels back into oxygen vacancies containing one electron to form V_O** recombination centre. The recombination of a shallowly trapped electron with a deeply trapped hole in a V_O** centre causes visible emission⁶².



The green emission is commonly referred to a deep-level or a trap-state emission attributed to the singly ionized oxygen vacancy and the emission results from the radiative recombination of photo-generated hole

with an electron occupying the oxygen vacancy⁹ and Vanheusden et al. observed a correlation between the intensities of g~1.96 electron paramagnetic resonance (EPR) peak and green PL. However, the assignment of g~1.96 signal to singly ionized oxygen vacancy is controversial. This signal was also assigned to shallow donors and its position appears to be independent on the shallow donor intensity⁶³. Recently, Djurisic et al.⁶⁴ found that there is no simple relationship between the intensity of g~1.96 EPR signal and the visible PL. The green PL is observed for the samples which do not show EPR line at g~1.96, and they concluded that the most likely explanation for the green luminescence involves multiple defects and/or defect complexes and the major part of the visible emission originates from the centers at the nanostructure surface. Xu et al.⁶⁵ calculated the levels of various defects including complex defects V_o:Zn_i and V_{Zn}:Zn_i. They found no states within the gap from V_{Zn}:Zn_i, while for V_o:Zn_i two levels 1.2 and 2.4 eV above the valence band were found and is depicted in figure 2.20. So this type of defect represents a possible candidate for green emission in ZnO.

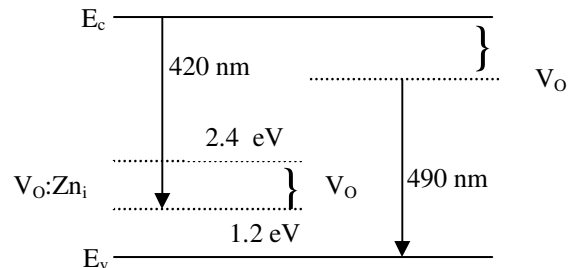


Figure 2.20: Representation of various defect levels in ZnO

ZnO is an *n*-type semiconductor and it means that most defects are Zn interstitials and oxygen vacancies. The crystal structure of ZnO as shown in figure 2.21 contains large voids which can easily accommodate interstitial

atoms⁷ and the appearance of blue emission at about 420 nm when excited with 325 nm may be due to the formation of Zn interstitial defects.

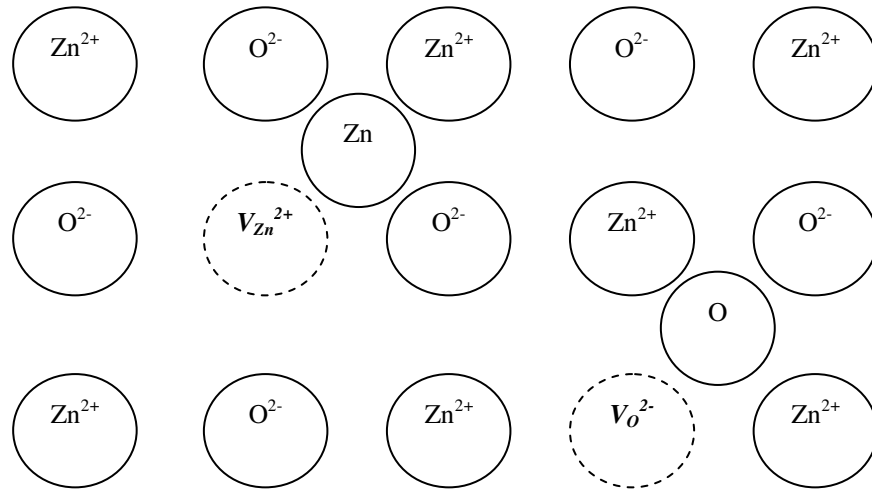


Figure 2.21: Crystal structure of ZnO

ZnO nanopowders and thin films also show green luminescence after they were annealed in oxygen, nitrogen or air⁶⁶. The appearance of a strong green emission is ascribed to the formation of oxygen vacancy defects or antisite defects (O_{Zn}). There exists many oxygen vacancies on the surface of the ZnO annealed in Ar at $900^{\circ}C$ and shows emission peak at 490 nm while the ZnO annealed in O_2 at $900^{\circ}C$ exhibits emission peak at 530 nm. So the appearance of visible emission may have originated from the oxygen vacancy defects⁶⁶.

2.7.7 Luminescence mechanism

Figure 2.22 shows the emission mechanism of UV and visible luminescence of ZnO colloids. UV luminescence at 3.5 eV is caused by the transition from near conduction band edge to valence band²⁹. As particle size increases, a shift of UV luminescence was observed from 3.5 to 3 eV because the optical energy gap decreases from 4 to 3.5 eV. The visible

luminescence in the range of 420–530 nm (2.9–2.4 eV) is mainly due to surface defect states. The UV luminescence center is not related to visible luminescence center.

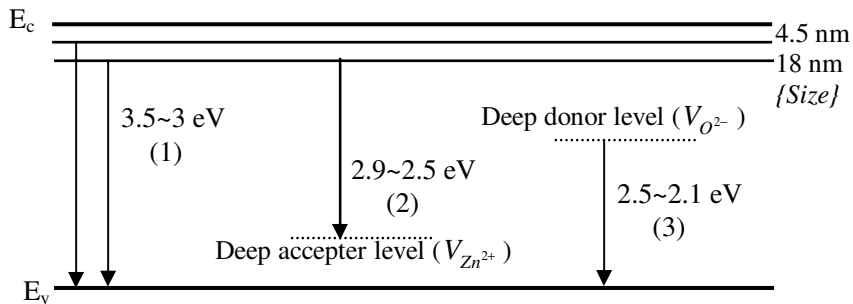


Figure 2.22: The UV and visible photoluminescence mechanism of ZnO:

- (1) transition from near conduction band edge to valence band
- (2) transition from near conduction band edge to deep acceptor level
- (3) transition from deep donor level to valence band

Based on these results, the green luminescence of ZnO colloid is not due to the transition from near band edge to deep acceptor level in ZnO but mainly due to the transition from deep donor level by oxygen vacancies in ZnO to valence band. If green luminescence is related to the deep acceptor level, UV luminescence should have decreased as green luminescence increased. Since the UV luminescence gets suppressed in the presence of blue band, the blue luminescence is related to the deep acceptor level. These results reveal that the mechanism of blue luminescence in ZnO is by the transition from near conduction band edge to deep acceptor level.

2.8 Conclusions

In this chapter, we have highlighted the size and excitation wavelength dependence of the fluorescence behaviour in nano colloids of ZnO. The size dependent optical bandgap is systematically investigated and

there is red shift in optical bandgap with increase in particle size. The fluorescence maximum shifts towards red as the excitation wavelength is increased. This observation has been attributed to the presence of energetically different associated forms of the constituent molecules and slow rate of the excited state relaxation process in these media. The high polarity and viscosity of the medium slows down the relaxation of the excited state. In essence, the inefficient energy transfer between the upper and the lower vibrational levels of the excited state of these particles owing to short fluorescence lifetime is primarily responsible for the excitation wavelength dependent spectral shift of ZnO colloids. Fluorescence spectra consist of emissions in the UV and visible regions. Apart from the known bandgap emissions at 380 nm and impurity dominated emissions at 530 nm, emissions in the 420-490 nm range are also observed with increase in particle size. This series of peaks are related to the transition from excited state energy levels of exciton to ground state by modelling it with a particle in a box problem. The UV band has been assigned to the *bandgap* fluorescence of clusters of different sizes. This allows us to reconstruct the size distribution curves from fluorescence spectroscopy. Systematic studies on nano crystallites have indicated the presence of luminescence due to excitonic emissions when excited with 255 nm as well as significant contribution from surface defect states when excited with 325 nm. The relevant energy levels showing the transitions corresponding to the observed peaks in the emission spectrum of ZnO of particle size 18 nm under 255 nm excitation are calculated. The luminescence mechanism is discussed.

2.9 References

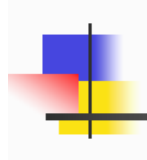
- 1 S A Studenikin, M Cocivera, W Kellner and H Pascher; “*Band-edge photoluminescence in polycrystalline ZnO films at 1.7 K*”, J. Lumin. **91**, 223 (2000)
- 2 S. Nakamura, *The Blue Laser Diode* (Springer, New York, 1997)
- 3 D. C. Reynolds, D. C. Look and B. Jogai; “*Optically pumped ultraviolet lasing from*

- ZnO*”, Solid State Commun. **99**, 873 (1996)
- 4 Zhong Ling Wang; “*Zinc oxide nanostructures: growth, properties and applications*”, J. Phys.: Condens. Matter. **16**, R829 (2004)
- 5 Louis Brus; “*Electronic wave functions in semiconductor clusters: experiment and theory*”, J. Phys. Chem. **90**, 2555 (1986)
- 6 R M Nyffenegger et.al.“*A Hybrid Electrochemical/Chemical Synthesis of Zinc Oxide Nanoparticles and Optically Intrinsic Thin Films*”, Chem. Mater. **10**, 1120 (1998)
- 7 L. V. Azaroff, *Introduction to Solids* (McGraw–Hill, New York, 1960)
- 8 K. Vanheusden, W. L. Warren, C. H. Seager, D. R. Tallant, J. A. Voigt, and B. E. Gnade; “*Mechanisms behind green photoluminescence in ZnO phosphor powders*”, J. Appl. Phys. **79**, 7983 (1996)
- 9 W. Li, D. Mao, F. Zhang, X. Wang, X. Liu, S. Zou, Y. Zhu, Q. Li, and J. Xu; “*Characteristics of ZnO:Zn phosphor thin films by post-deposition annealing*”, Nucl. Instrum. Methods Phys. Res. B, **169**, 59 (2000)
- 10 T Voddmeyer, D J Katsikas, M Giersig, I G Popovic, K Diesner, A Chemseddine, A Eychmuller and H Weller; “*Luminescent properties of local atomic order of Er³⁺ and Yb³⁺ ions in aluminophosphate glasses*” J. Appl. Phys. **90**, 265 (2001)
- 11 H Yu, J Li, R A Loomis, P C Gibbons, L W Wang and W E Buhro; “*Cadmium selenide quantum wires and the transition from 3D to 2D confinement*” J. Am. Chem. Soc. **125**, 16168 (2003)
- 12 S Baskoutas and A F Terzis; “*Size-dependent bandgap of colloidal quantum dots*”, J. Appl. Phys. **99**, 013708 (2006)
- 13 S Baskoutas; “*Excitons and charged excitons in InAs nanorods*” Chem. Phys. Lett. **404**, 107 (2005)
- 14 L E Brus; “*Electron–electron and electron-hole interactions in small semiconductor crystallites: The size dependence of the lowest excited electronic state*” J. Chem. Phys. **80**, 4403 (1984)
- 15 Efros A L, “*Interband absorption of light in semiconductor spheres*”, Sov. phys. semicond.**16**, 772 (1982)
- 16 Y Kyanuma and H Momiji; “*Incomplete confinement of electrons and holes in microcrystals*” Phys. Rev. B **41**, 10261 (1990)
- 17 K K Nanda, F E Kruis and H Fissan; “*Effective mass approximation for two extreme semiconductors: Bandgap of PbS and CuBr nanoparticles*” J. Appl. Phys. **95**, 5035 (2004)
- 18 G Pellegrini, G Mattei and P Mazzoldi, J. Appl. Phys. **97**, 073706 (2005)
- 19 Xia J B; “*Electronic structures of zero-dimensional quantum wells*”, Phys Rev. **40**, 8500 (1989)
- 20 Grigorian G B, Kazaryan E M, Efros A L and Yazeva T V; “*Quantized holes and the absorption edge in semiconductor nanocrystals with a complex valence band structure*”,

- Sov. Phys. Solid. State **32**, 1031 (1990)
- 21 Vahala K J and Sercel P C; “*Application of total angular momentum basis quantum dot structure*”, Phys. Rev.Lett, **65**, 239 (1990)
- 22 Ekimov A L et.al.; “*Absorption and intensity dependent photoluminescence measurements on CdSe quantum dots: assignment of the first electronic transitions*”, J. Opt. Soc. Am. B **10**, 100 (1993)
- 23 Richard T, Lefebvre P, Mathieu H and Allegre J; “*Effects of finite spin-orbit splitting on optical properties of spherical semiconductor quantum dots*”, Phys. Rev. B **53**, 7287 (1996)
- 24 S Baskoutas and A F Terzis; “*Size dependent exciton energy of various technologically important colloidal quantum dots*” Mater. Sci. Eng. B (2007), doi:10.1016/j.mseb.2007.09.041
- 25 Chepic D I, Efros A L, Ekimov A I, Ivanov M G, Kharchenko V A, Kudriavtsev I A and Yazeva T V; “*Auger ionization of semiconductor quantum dots in a glass matrix*”, J. of Lum. **47**, 113 (1990)
- 26 Klimov V I, Mikhailovsky A A, McBranch D W, Leatherrdale C A, Bawendi M G; “*Quantization of multiparticle Auger rates in semiconductor quantum dots*”, Science **287**, 1011 (2000)
- 27 Didier Jezequel, Jean Guenot, Noureddine Jouini, Fernand Fievet; “*Submicrometer zinc oxide particles: Elaboration in polyol medium and morphological characteristics*”, J.Mater.Res., **10**, 77, (1995)
- 28 Eric W. Seelig, Betty Tang, Alexey Yamilov, Hui Cao and R. P. H. Chang; “*Self-assembled 3D photonic crystals from ZnO colloidal spheres*”, Materials Chemistry and Physics, **80**, 257 (2002)
- 29 Litty Irimpan et.al.; ‘*Size dependent fluorescence spectroscopy of nanocolloids of ZnO*’, J. Appl. Phys. **102**, 063524 (2007)
- 30 Litty Irimpan, Bindu Krishnan, A Deepthy, V P N Nampoori and P Radhakrishnan; J. Phys. D: Appl. Phys. **40**, 5670 (2007)
- 31 S. Monticone, R. Tufeu, and A.V. Kanaev; “*Complex Nature of the UV and Visible Fluorescence of Colloidal ZnO Nanoparticles*”, J.Phys.Chem B, **102**, 2854 (1998)
- 32 D. Luna-Moreno, E. De la Rosa-Cruz, F. J. Cuevas, L. E. Regalado, P. Salas, R. Rodríguez and V. M. Castano; “*Refractive index measurement of pure and Er³⁺-doped ZrO₂–SiO₂ sol–gel film by using the Brewster angle technique*”, Opt. Mat., **19**, 275 (2002)
- 33 Ranjani Viswanatha, Sammer Sapra, B.Satpati, P.V.Satyam, B.N.Dev, D.D Sharma; “*Understanding the quantum size effects in ZnO nanocrystals*”, J.Mater.Chem,**14**, 661,(2004)
- 34 1999 JCPDS-International Centre for Diffraction Data.
- 35 Lin Guo, Shihe Yang, Chunlei Yang, Ping Yu, Jiannong Wang, Weikun Ge, and George

- K. L. Wong; “*Highly monodisperse polymer-capped ZnO nanoparticles: Preparation and optical properties*”, *Appl. Phys. Lett.*, **76** 2901 (2000)
- 36 V L Colvin, A P Alivisatos and J.G. Tobin; “*Valence-band photoemission from a quantum-dot system*”, *Phys. Rev. Lett.*, **66**, 2786 (1991)
- 37 S Sapra and D D Sarma; “*Evolution of the electronic structure with size in II-VI semiconductor nanocrystals*”, *Phys. Rev. B* **69**, 125304 (2004)
- 38 W. Zhang, H. Wang, K.S. Wong, Z.K. Tang, G.K.L. Wong, J. Ravinder, “*Third-order optical nonlinearity in ZnO microcrystallite thin films*”, *Appl. Phys. Lett.* **75**, 3321 (1999)
- 39 Rana Karmakar and Anunay Samanta; *J. Phys. Chem. A*, **107**, 7340 (2003)
- 40 S Saha, Prasun K. Mandal and Anunay Samanta; “*Solvation dynamics of Nile Red in a room temperature ionic liquid using streak camera*”, *Phys. Chem. Chem. Phys.*, **6**, 3106 (2004)
- 41 Debdeep Chakrabarty, Debabrata Seth, Anjan Chakraborty, and Nilmoni Sarkar; “*Dynamics of Solvation and Rotational Relaxation of Coumarin 153 in Ionic Liquid Confined Nanometer-Sized Microemulsions*”, *J. Phys. Chem. B*, **109**, 5753 (2005)
- 42 Prasun K. Mandal and Anunay Samanta; “*Fluorescence Studies in a Pyrrolidinium Ionic Liquid: Polarity of the Medium and Solvation Dynamics*”, *J. Phys. Chem. B*, **109**, 15172 (2005)
- 43 Aniruddha Paul, Prasun Kumar Mandal and Anunay Samanta; “*How transparent are the imidazolium ionic liquids? A case study with 1-methyl-3-butylimidazolium hexafluorophosphate, [bmim][PF₆]*”, *Chem. Phys. Lett.* **402**, 375 (2005)
- 44 Aniruddha Paul, Prasun Kumar Mandal, and Anunay Samanta; “*On the Optical Properties of the Imidazolium Ionic Liquids*”, *J. Phys. Chem. B* **109**, 9148 (2005)
- 45 Sang-Woo Kim, Shizuo Fujita, Shigeo Fujita; “*Self-organized ZnO quantum dots on SiO₂/Si substrates by metalorganic chemical vapor deposition*”, *Appl. Phys. Lett.* **81** 5036 (2002)
- 46 Birks JB; “*Photophysics of Aromatic Molecules*”, Wiley-Interscience: London, 1970
- 47 Alexander P. Demchenko; “*The red-edge effects: 30 years of exploration*”, *Luminescence*, **17**, 19 (2002)
- 48 Joseph R. Lakowicz and Susan Keating-Nakamoto; “*Red-edge excitation of fluorescence and dynamic properties of proteins and membranes*”, *Biochemistry*, **23**, 3013 (1984)
- 49 Bernard Valeur and Gregorio Weber; “*Anisotropic rotations in 1-naphthylamine. Existence of a red-edge transition moment normal to the ring plane*”, *Chem. Phys. Lett.*, **45**, 140 (1977)
- 50 G Weber and M Shinitzky; “*Failure of Energy Transfer between Identical Aromatic Molecules on Excitation at the Long Wave Edge of the Absorption Spectrum*”, *Proc. Natl. Acad. Sci. U S A*, **65**, 823 (1970)
- 51 K. Itoh and T. Azumi; “*Shift of emission band upon excitation at the long wavelength*

- absorption edge. I. A preliminary survey for quinine and related compounds*”, Chem. Phys. Lett., **22**, 395 (1973)
- 52 Ken-ichi Itoh and Tohru Azumi; “*Shift of the emission band upon excitation at the long wavelength absorption edge. II. Importance of the solute–solvent interaction and the solvent reorientation relaxation process*”, J. Chem. Phys., **62**, 3431 (1975)
- 53 Lakowicz J R; “*Principles of Fluorescence Spectroscopy*”, Plenum Press: New York, 1999
- 54 Amitabha Chattopadhyay and Sushmita Mukherjee; “*Red Edge Excitation Shift of a Deeply Embedded Membrane Probe: Implications in Water Penetration in the Bilayer*”, J. Phys. Chem. B, **103**, 8180 (1999)
- 55 H. S. Bhatti, Atul Gupta, N. K. Verma and Sunil Kumar; “*Optical characterization of ZnO nanobelts*”, Journal of Materials Science: Materials in Electronics, **17**, 4 (2006)
- 56 D W Bahnemann, C Kormann and M R. Hoffmann; “*Preparation and Characterization of Quantum Size ZnO: A Detailed Spectroscopic Study*”, J. Phys. Chem., **91**, 3789 (1987)
- 57 Ian K. Smith, Stuart R. Andrews, Graham Williams and Paul A. Holmes; J. Mater. Chem., **6**, 539 (1996)
- 58 A Dvornikov, Y Liang, Peter Rentzepis; “*Dependence of the fluorescence of a composite photochromic molecule on structure and viscosity*”, J. Mater. Chem., **15**, 1072 (2005)
- 59 Kim S W, Fujita S and Fujita S; “*Self-organized ZnO quantum dots on SiO₂/Si substrates by metalorganic chemical vapor deposition*”, Appl. Phys. Lett., **81** 5036 (2002)
- 60 P. Schroer, P. Kruger, J. Pollmann; “*First-principles calculation of the electronic structure of the wurtzite semiconductors ZnO and ZnS*”, Phys. Rev. B, **47**, 6971 (1993)
- 61 Fonoberov V A and Balandin A; “*Origin of UV photoluminescence in ZnO quantum dots: Confined excitons versus surface-bound impurity exciton complexes*”, Appl. Phys. Lett., **85**, 5971 (2004)
- 62 van Dijken A, Meulenkamp E A, Vanmaekelbergh D and Meijerink A; “*The Kinetics of the Radiative and Nonradiative Processes in Nanocrystalline ZnO Particles upon Photoexcitation*”, J. Phys. Chem. B, **104**, 1715 (2000)
- 63 N.Y. Garces, N.C. Giles, L.E. Halliburton, G. Cantwell, D.B. Eason, D.C. Reynolds, L.C. Look; “*Production of nitrogen acceptors in ZnO by thermal annealing*”, Appl. Phys. Lett. **80**, 1334 (2002)
- 64 A.B. Djurisic et.al.; “*Photoluminescence and Electron Paramagnetic Resonance of ZnO Tetrapod Structures*”, Adv. Funct. Mater. **14**, 856 (2004)
- 65 P.S. Xu, Y.M. Sun, C.S. Shi, F.Q. Xu, H.B. Pan; “*The electronic structure and spectral properties of ZnO and its defects*”, Nucl. Instrum. Methods B; **199**, 286 (2003)
- 66 J.Z. Wang, G.T. Du, Y.T. Zhang, B.J. Zhao, X.T. Yang, D.L. Liu; “*Luminescence properties of ZnO films annealed in growth ambient and oxygen*”, J. Crystal Growth., **263**, 269 (2004)



Chapter 3

Size dependent enhancement of nonlinear optical properties in nano colloids of ZnO

Abstract

Results of the investigations carried out on the third-order nonlinearity in ZnO nano colloids with particle size in the range 6– 18 nm by z-scan technique are included in this chapter. ZnO nano colloids show negative nonlinearity and good nonlinear absorption behaviour at 532 nm. The observed optical nonlinearity is explained on the basis of two photon absorption followed by free carrier absorption. The third-order optical susceptibility ($\chi^{(3)}$) increases with increasing particle size (R) due to the size dependent enhancement of exciton oscillator strength. In the weak confinement regime, R^2 dependence of $\chi^{(3)}$ is obtained for ZnO nano colloids. Nonlinear susceptibility is highly fluence dependent and it becomes quadratic in nature for large particle size. The optical limiting response is also studied as a function of particle size.

The results of this chapter are published in
Litty Irimpan et.al., Journal of Applied Physics **103**, 033105 (2008)
[Virtual Journal of Nanoscale Science & Technology, February 25, 2008]

3.1 Introduction

The linear and nonlinear optical properties of semiconductors are the subject of much current theoretical and experimental interest¹. Amongst the various nonlinear optical (NLO) materials investigated, wide bandgap semiconductors, especially zinc oxide (ZnO) have attractive nonlinear properties that make them ideal candidates for NLO based devices. Nanosized ZnO in the form of quantum dots, nano wires, nano belts, etc are referred to as the material of 21st century².

Most of the nonlinear optical devices rely mainly on higher order susceptibility of materials, viz., $\chi^{(3)}$. There are a number of nano-sized organic nonlinear optical materials and semiconductor structures of low dimension are a new entry into the field of nonlinear optics. The second and third harmonic generation in ZnO microcrystalline thin films has already been reported³. Bulk ZnO crystals have been investigated for NLO properties by z-scan technique itself⁴. However, very little work has been done in NLO properties of ZnO quantum dots and its nano colloids because semiconductor nanoparticles in solution with well-controlled size, shape, and surface properties are difficult to obtain⁵. Moreover, the volume fraction of crystallites in a stable solution is usually very small. As a consequence, the resultant nonlinear response is relatively weak. Due to the speciality of the synthesis route adopted in our present investigation, the volume fraction of nano particles increases with particle size. Hence high nonlinear absorption at larger particle size can be expected and this in turn excites our interest in investigating the nonlinear optical properties of ZnO nano colloids. Z-scan is a simple and accurate method to study the NLO properties of materials. Hence, in the present investigation our focus is on the third order NLO susceptibility of this wide bandgap semiconductor, employing the technique of z-scan.

In ZnO, the exciton Bohr radius is 2 nm, which is roughly 4 times that of CuCl, and one can investigate confinement effects and size dependence of $\chi^{(3)}$ over a wide range of crystallite sizes⁶. This chapter deals with a detailed study of the size dependent optical nonlinearity in ZnO nanocolloids over a range of 6-18 nm.

3.2 Theory

The electronic structure as a function of size is discussed both theoretically and experimentally in chapter 2. When the crystallite size is reduced to the order of an exciton Bohr radius a_B , quantum size effects appear and drastic changes in optical properties are expected. Nonlinear optical properties in nanocrystals have been investigated for the different confinement regimes.

In the strong-confinement regime, the photo-excited electron and hole are individually confined. Theoretical and experimental works have revealed that the state-filling effect accounts for the optical nonlinearity in this regime⁷. The size dependence of third-order susceptibility $\chi^{(3)}$ has also been studied, but the results are inconsistent; a larger nonlinear susceptibility for a larger size has been found for CdS_xSe_{1-x} nanocrystals by the saturation spectroscopy and degenerate four-wave mixing (DFWM) measurements, while Roussignol *et al.* have shown that larger $\chi^{(3)}$ values are obtained with decreasing sizes for the same material⁷⁻⁸.

In the weak-confinement regime, the coulomb interaction between the electron and hole yields an exciton and it is confined as a quasiparticle. The optical nonlinearity arises from the exciton-exciton interaction, which results in a deviation from the harmonicity of the boson-like exciton within the nanocrystal. The size dependent enhancement of nonlinear susceptibility has been investigated theoretically⁹⁻¹⁰ as well as experimentally¹¹⁻¹². The effect of very large oscillator strength is brought out only in the weak confinement regime.

In the weak confinement regime, the size quantization of the exciton is brought out and consider a quantum sphere of radius R. The electronic excited state, ψ_n is described by the Frenkel exciton as,

$$\psi_n = \sum_j F_n(j) W_j^e(r_j) \prod_{(i \neq j)} W_i^h(r_i) \quad (3.1)$$

where W_j^h and W_j^e are Wannier functions of the valence and conduction bands respectively and $F_n(j)$ is the envelope function in the quantum sphere and is given by

$$F_n(j) = \left[\frac{2}{N} \right]^3 \sin\left[\frac{\pi n_x j_x}{N} \right] \sin\left[\frac{\pi n_y j_y}{N} \right] \sin\left[\frac{\pi n_z j_z}{N} \right] \quad (3.2)$$

where N is the number density, the quantum numbers $n=(n_x, n_y, n_z)$ and the site index $j=(j_x, j_y, j_z)$ are chosen from positive integers between 1 and N and. The ground state of the quantum sphere is given by,

$$\psi_g = \prod_{(i)} W_i^h(r_i) \quad (3.3)$$

The transition dipole moment to the excited states, ψ_n from the ground state, ψ_g is evaluated for the Frenkel exciton in the weak confinement regime⁹.

$$\begin{aligned} \langle \psi_n | P | \psi_g \rangle &= \sum_j F_n(j) \langle W_j^e(r_j) | p_j | W_j^h(r_j) \rangle \\ &= p_{eh} \left[\frac{2}{N} \right]^{\frac{2}{3}} \cot\left[\frac{\pi n_x}{2N} \right] \cot\left[\frac{\pi n_y}{2N} \right] \cot\left[\frac{\pi n_z}{2N} \right] \end{aligned} \quad (3.4)$$

where P is a component of the dipole moment operator and $P = \sum_i p_i$ and

$\langle W_j^e(r_j) | p_j | W_j^h(r_j) \rangle = p_{eh} \delta_{jj^1}$. δ_{jj^1} denotes the well localized electron hole relative motion at the same unit cell, u and p_{eh} is the effective dipole

moment of the exciton . The transition dipole moment to the lowest excited state (n_x, n_y, n_z)=(1,1,1) is

$$\langle \psi_{111} | P | \psi_g \rangle = \left[\frac{2\sqrt{2}}{\pi} \right]^3 p_{eh} N^{3/2} \quad (3.5)$$

For the transition to such a low excited state (n_x, n_y, n_z) as $n_x, n_y, n_z \ll N$,

$$\langle \psi_n | P | \psi_g \rangle = \left[\frac{2\sqrt{2}}{\pi} \right]^3 \frac{p_{eh} N^{3/2}}{(n_x, n_y, n_z)} \quad (3.6)$$

Then the oscillator strength, f_n per quantum spheres is given by

$$f_n = \frac{2m}{\hbar} \omega_n |p_{eh}|^2 \left[\frac{2\sqrt{2}}{\pi} \right]^6 \frac{N^3}{(n_x, n_y, n_z)^2} \quad (3.7)$$

where m and ω_n are the mass and angular frequency of the exciton respectively. The oscillator strength is given by

$$F_n = f_n \frac{u^3}{\pi a_B^3} \quad (3.8)$$

where the length of unit cell, u is R/N and R is the size of the quantum sphere⁹.

$$F_n = \frac{2m}{\hbar} \omega_n |p_{eh}|^2 \left[\frac{2\sqrt{2}}{\pi} \right]^6 \frac{R^3}{\pi a_B^3 (n_x, n_y, n_z)^2} \quad (3.9)$$

Thus theoretical studies have shown that the confinement of excitonic envelope wave function due to the infinite barrier potential gives rise to the enhancement in oscillator strength for an exciton within the nanocrystal by a factor of R^3/a_B^3 and hence $\chi^{(3)}$ depends on the crystallite size⁹. Such a giant oscillator strength effect has been confirmed for CuCl nanocrystals. The radiative decay rate of confined excitons is proportional to $R^{2.1}$ for the glass matrix¹³ and R^3 for the NaCl crystal matrix¹⁴. The validity of the size dependent enhancement effect is limited by the long wavelength

approximation and a nonlocal theory applicable to the mesoscopic system larger than the wavelength has been developed¹⁰. The important role of the giant oscillator strength effect in the size dependent enhancement of optical nonlinearity has been experimentally shown for CuCl nanocrystals¹².

As the quantum-confined exciton system can be modeled as a two level atomic system, the imaginary part of $\chi^{(3)}$ is given by¹⁵

$$\text{Im}(\chi^{(3)}) = \left[\frac{e^2}{2m\omega_n} \right]^2 \hbar N F_n^2 \frac{T_1}{\Gamma_h^2} \quad (3.10)$$

where T_1 and Γ_h are the longitudinal relaxation time and homogeneous width, respectively, and F_n and N are the oscillator strength and the number density of nanocrystals, respectively. The detailed study measuring the susceptibility on resonance and the relaxation parameters T_1 and Γ_h revealed that the oscillator strength exhibits a $R^{2.2}$ dependence on particle size for CuCl nanocrystals¹⁵.

The oscillator strength increases with the size of the particle as long as the excited state is coherent. However, an exciton in a bulk crystal behaves almost as a harmonic oscillator which does not show enhanced nonlinear optical response. Deviation of the electronic excitation from an ideal harmonic oscillator increases as the size of the microcrystallite decreases. Thus the enhancement originates from two conflicting concepts. One is due to the size dependent exciton oscillator strength and the other enhancement comes from the deviation of the electronic excitation from the ideal harmonic oscillator. In the weak confinement regime, as the particle size increases, the optical nonlinearity increases till the excited state is coherent due to the size dependent exciton oscillator strength. After that, the optical nonlinearity decreases with increase in particle size since the deviation from ideal harmonic oscillator decreases with increase in particle

size. As a result, there is an optimum size for obtaining the most effective optical nonlinearity in the weak confinement regime.

3.3 Nonlinear optical properties of nano colloids of ZnO

Colloids of nano ZnO are synthesized by a modified polyol precipitation method¹⁶⁻¹⁸ as described in chapter 2. We have employed the single beam z-scan technique with nanosecond laser pulses to measure the nonlinear optical absorption and refraction properties of ZnO nano colloids and observed that the colloids exhibit large nonlinear effects. A detailed theory of z-scan technique¹⁸⁻²⁰ is described in chapter 1.

A Q-switched Nd:YAG laser (Spectra Physics LAB-1760, 532 nm, 7 ns, 10 Hz) is used as the light source. The sample is moved in the direction of light incidence near the focal spot of the lens with a focal length of 200 mm. The radius of the beam waist ω_o is calculated to be 35.4 μm . The Rayleigh length, $z_o = \pi\omega_o^2/\lambda$ is estimated to be 7.4 mm which is much greater than the thickness of the sample cuvette (1mm) and an essential prerequisite for z-scan experiments. The transmitted beam energy, reference beam energy and their ratio are measured simultaneously by an energy ratiometer (Rj7620, Laser Probe Corp.) having two identical pyroelectric detector heads (Rjp735). The linear transmittance of the far field aperture S, defined as the ratio of the pulse energy passing the aperture to the total energy is measured to be approximately 0.21. The whole experimental set up is automated using LabView program. The z-scan system is calibrated using CS_2 as a standard. The effect of fluctuations of laser power is eliminated by dividing the transmitted power by the power obtained at the reference detector¹⁸.

3.4 Size dependent enhancement of third order nonlinear susceptibility

3.4.1 Open aperture z-scan

Figure 3.1 gives the open aperture z-scan traces of ZnO colloids of different particle sizes at a typical fluence of 866 MW/cm^2 . The open aperture curve exhibits a normalized transmittance valley, indicating the presence of induced absorption in the colloids¹⁸.

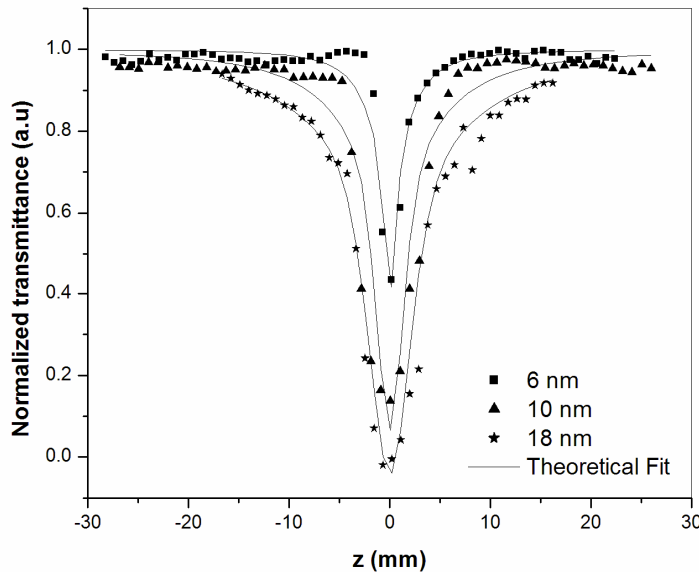


Figure 3.1: The open aperture z-scan traces of ZnO colloids of different particle sizes at a typical fluence of 866 MW/cm^2

The data are analyzed by using the procedure described by Sheik Bahae *et. al*¹⁹ for two photon absorption process and the nonlinear absorption coefficient β is obtained by theoretical fitting as described in chapter 1 using matlab program. From the value of β , the imaginary part of third order susceptibility, $\text{Im}(\chi^{(3)})$ is calculated.

3.4.2 Closed aperture z-scan

Figure 3.2 gives the closed aperture z-scan traces of ZnO colloids of different particle sizes at a fluence of 866 MW/cm^2 . The closed-aperture curve exhibited a peak-to-valley shape, indicating a negative value of the nonlinear refractive index¹⁸. It is observed that the peak-valley of closed-aperture z-scan satisfied the condition $\Delta z \sim 1.7 z_0$, thus confirming the presence of cubic nonlinearity¹⁹. The value of nonlinear refractive index and real part of nonlinear susceptibility are obtained by the theoretical fit from the results of divided z-scan curve as described in chapter 1.

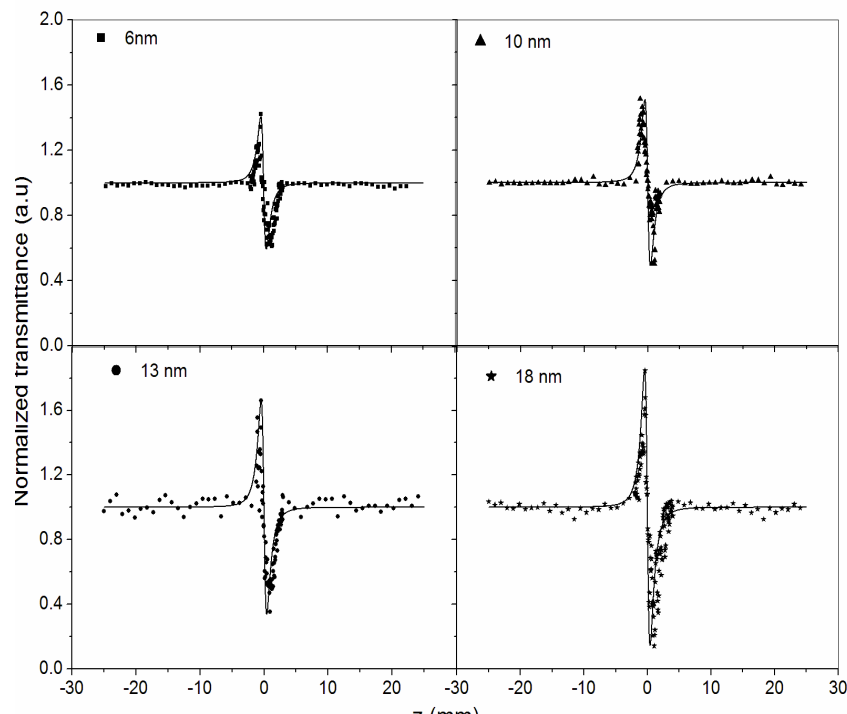


Figure 3.2: The closed aperture z-scan traces of ZnO colloids of different particle sizes at a fluence of 866 MW/cm^2

The obtained values of nonlinear optical properties of ZnO colloids of different particle sizes at a fluence of 866 MW/cm^2 are shown in table 3.1.

The enhancement of nonlinear optical properties with increasing dimension in the weak confinement regime essentially originates from the size dependent enhancement of oscillator strength of coherently generated excitons⁹. Since the exciton is confined in a quantum dot, the confinement of excitonic wave function is expected to give rise to enhancement of the oscillator strength per quantum dot by a factor of R^3/a_B^3 . This size dependent oscillator strength was experimentally confirmed in CuCl quantum dots¹³⁻¹⁴. Such oscillator strength effect will result in an enhancement of the nonlinear susceptibility¹². Hence the observed enhancement of nonlinear optical properties with increase in particle size in our present investigation can be attributed to the size dependent enhancement of exciton oscillator strength.

R (nm)	β (cm/GW)	n_2 $\times 10^{-10}$ esu	$\text{Im}(\chi^{(3)})$ $\times 10^{-10}$ esu	$\text{Re}(\chi^{(3)})$ $\times 10^{-10}$ esu	$ \chi^{(3)} $ $\times 10^{-10}$ esu
6	42.4	-6.3	0.2	-1.3	1.3
10	231	-7.8	1.0	-1.7	2.0
13	487.2	-11.7	2.1	-2.5	3.3
18	2085.2	-13.1	9.0	-2.8	9.4

Table 3.1 : Measured values of nonlinear absorption, nonlinear refraction and nonlinear susceptibility of ZnO colloids at an intensity of 866MW/cm²

In order to obtain the crystallite size dependence of the third-order susceptibility, the R dependence of $\chi^{(3)}$ is shown in figure 3.3. This dependence helps us to write $\log(\chi^{(3)}) = 2\log R - 0.024$ and $\chi^{(3)} \approx R^2$.

The data show a general trend of increasing $\chi^{(3)}$ values with increasing radius from $R=6\text{-}18$ nm. When we apply a least-squares fit, a size dependence of R^2 is obtained indicating an enhancement of more than two orders of magnitude. This dependence is in good agreement with that observed for CdS, CuCl and CuBr nanocrystals^{12, 15, 18, 21}.

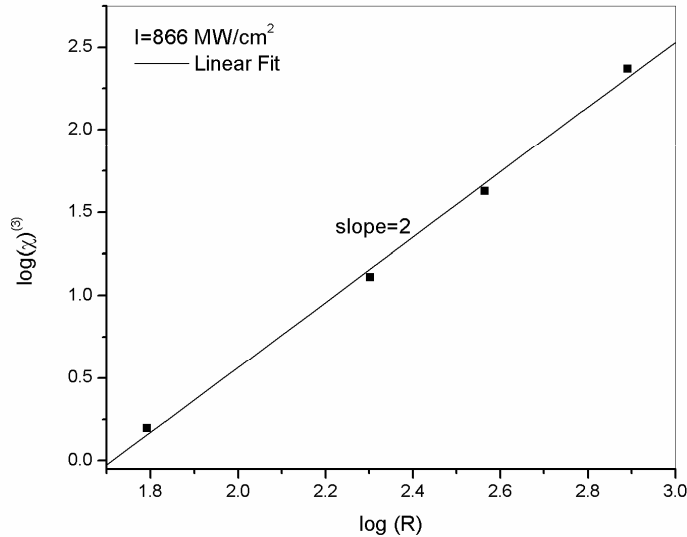


Figure 3.3: The third order susceptibility as a function of particle size for ZnO nano colloids. The straight line with a slope of 2 indicates the R^2 dependence

3.5 Fluence dependence of third order nonlinear susceptibility

The open and closed aperture z-scan curve of ZnO colloid of size 6nm at different input fluences is shown in figure 3.4. We can see that nonlinear optical properties are highly fluence-dependent¹⁸. The results show three orders of enhancement for the nonlinear absorption coefficient from the reported value of 5cm/GW for bulk ZnO²².

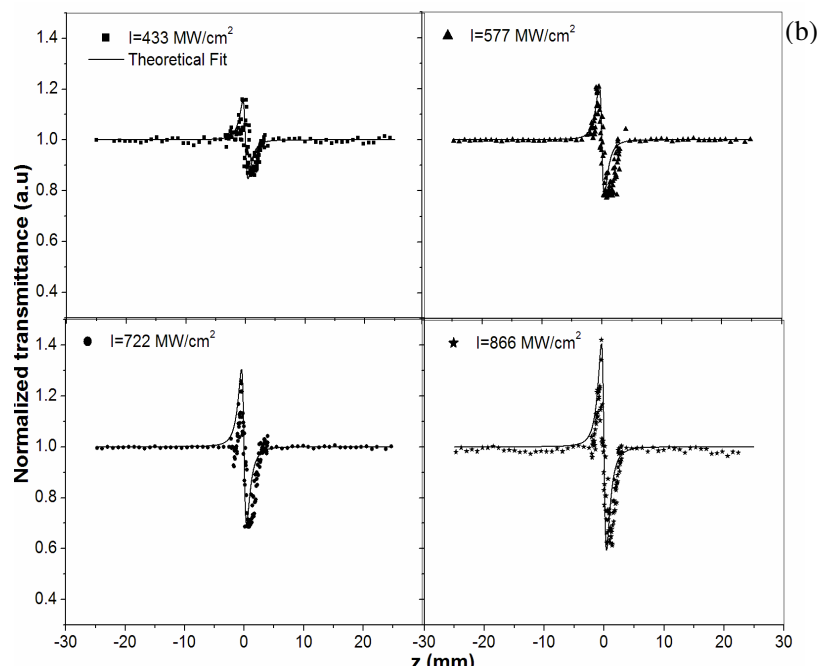
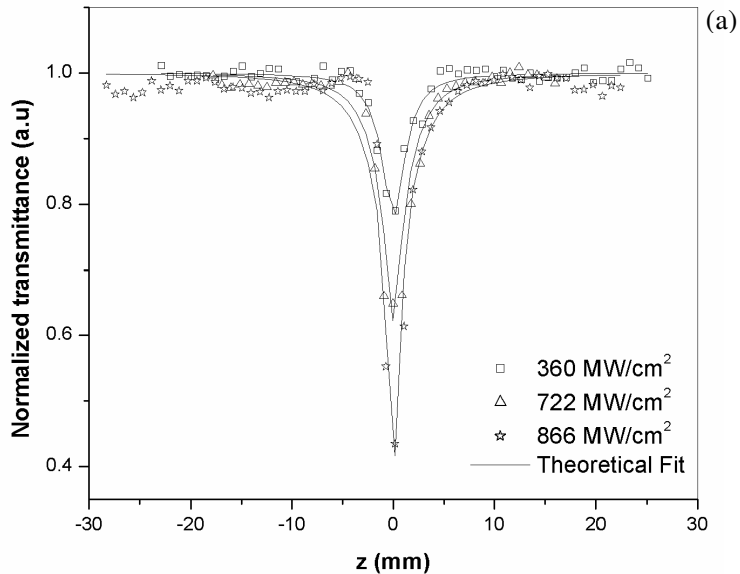


Figure 3.4 (a): Open aperture (b): Closed aperture z -scan curves of ZnO colloid of size 6 nm at different input fluences

It has been reported that the reduced dimensionality of the particles resulted in considerable enhancement of the second-order susceptibility $\chi^{(2)}$ in thin films of ZnO³. Similar results in the third order nonlinear parameters were evident in our measurements also.

The theory of two photon absorption process fitted well with the experimental curve infers that TPA is the basic mechanism. The dependence of nonlinear absorption with input intensity is due to TPA as clearly seen from log q versus log I plot shown in figure 3.5. The parameter q is the depth of the open aperture z-scan curve obtained from the theoretical fit and is a measure of the intensity dependent absorption and I is the irradiance at the focus.

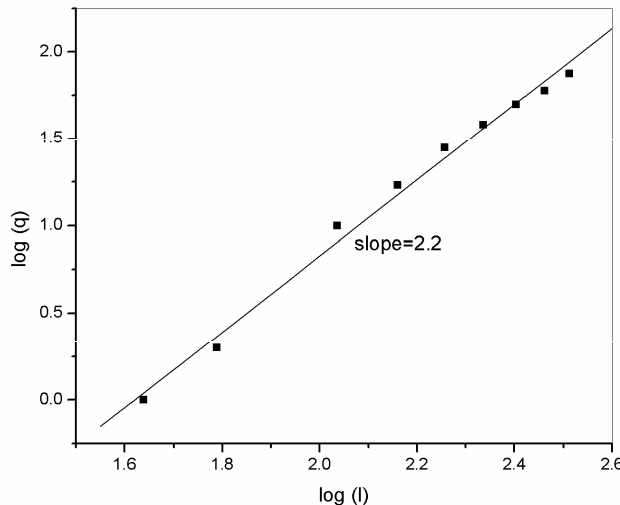


Figure 3.5: Variation of $\log q$ as a function of $\log I$ for ZnO colloid of size 18 nm.

Slope of the plot in figure 3.5 gives 2.2 which infers that TPA is the basic mechanism and there is the possibility of higher order nonlinear

processes such as free carrier absorption (FCA) contributing to induced absorption¹⁸. The free carrier life time of ZnO is reported to be 2.8 ns⁴. Hence there is a strong possibility that the 7 ns pulses used in the present study is exciting the accumulated free carriers generated by TPA by the rising edge of the pulse.

Figure 3.6 shows the variation of nonlinear susceptibility with irradiance for ZnO colloids of different particle sizes. Results show that $\chi^{(3)}$ is a function of intensity of laser radiation which can be written as

$$\chi^{(3)} = \chi_0^{(3)} + \chi_1^{(3)} I + \chi_2^{(3)} I^2 \quad (3.11)$$

For lower fluence and colloids with small size, $\chi^{(3)}$ is independent of intensity indicating that it is a third order effect resulting from two photon absorption (TPA). For colloids of larger particle size and at higher fluences, $\chi^{(3)}$ becomes a nonlinear function of intensity¹⁸.

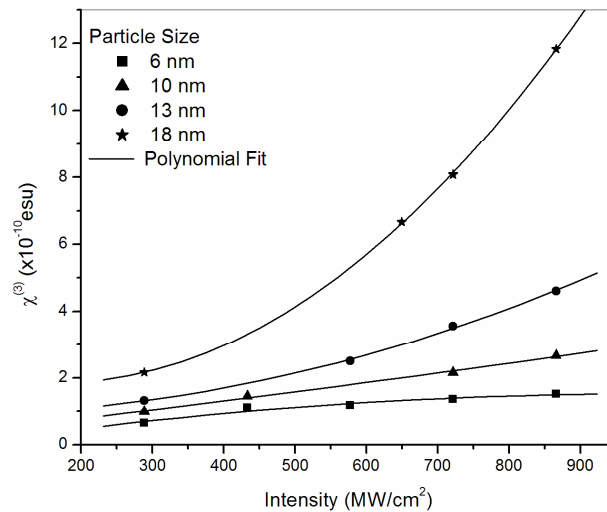


Figure 3.6: Variation of nonlinear susceptibility with irradiance for ZnO colloids of different particle sizes

This nonlinear dependence of $\chi^{(3)}$ with intensity is clearly shown in figure 3.6 indicating the occurrence of higher order nonlinear processes such as free-carrier absorption. Considering all these factors and also that we used nanosecond excitation pulses, it is reasonable to assume that TPA and weak FCA are the important mechanisms contributing to induced absorption in our samples¹⁸.

The values of $\chi^{(3)}$ measured at room temperature by degenerate four wave mixing technique on CuBr nanocrystals range from 8×10^{-11} to 1.1×10^{-9} esu for $R=2.7\text{-}42$ nm and are comparable to the results presented here^{15,18}. In this chapter, we report the experimental evidence for the enhancement of third order nonlinear susceptibility due to the size dependent oscillator strength of confined excitons, which was theoretically predicted by Hanamura⁹. The enhancement of $\chi^{(3)}$ for thin nanocrystalline films compared to microcrystalline films of ZnO was attributed to the nanosized structure of the film²³. Recently significant (~500 times) enhancement of nonlinear refractive index with respect to the bulk value has been observed for polymer capped ZnO nanocrystals with an estimated average size of 4 nm²⁴. The third-order nonlinear optical response of these PVP capped ZnO nanoparticles in a dilute solution is reported to be of the order of 6.3×10^{-11} esu. This value is at least two orders of magnitude greater than that of the bulk ZnO. This remarkable enhancement in the third-order nonlinear optical response may be related to the exciton confinement and optical Stark effects⁵.

It is worth noting that certain representative third-order nonlinear optical materials, such as CuO chain compounds²⁵, Ag₂S/CdS nanocomposites²⁶, Metallophthalocyanines²⁷, porphyrins²⁸, organic dyes²⁹, organic polymers³⁰, organic coated quantum dots³¹, metal clusters³² etc., yielded values of order of 10^{-10} to 10^{-14} esu for $\chi^{(3)}$ at a wavelength of 532 nm. These values are lower by one order of magnitude in comparison to the

value of $\chi^{(3)}$ obtained in the present investigation. Thus, the real and imaginary parts of third-order nonlinear optical susceptibility measured by the z-scan technique revealed that the ZnO colloids investigated in the present study have good nonlinear optical response and could be chosen as ideal candidates with potential applications for nonlinear optics.

3.6 Optical limiting

Optical power limiting is operated through the nonlinear optical processes of nanomaterials³³. However, the great potentials of nanomaterials as optical power limiters have just begun to be recognized. An important term in the optical limiting measurement is the limiting threshold. It is obvious that the lower the optical limiting threshold, the better the optical limiting material.

3.6.1 Optical limiting and open aperture z-scan

The optical limiting property occurs mostly due to absorptive nonlinearity³⁴. Thus it is possible to generate optical limiting curves from open aperture z-scan data. It is because while the sample is translated through the focus of the Gaussian beam, the sample experiences variation in the incident fluence levels. From the value of fluence at focus, the fluence

values at other positions could be calculated, $I(z) = \frac{E}{\pi\omega^2(z)t}$, using the

standard equations for Gaussian beam waist, $\omega^2(z) = \omega_0^2 \left(1 + \frac{z^2}{z_0^2}\right)$ where

the beam waist radius at focus, $\omega_0 = \frac{f\lambda}{D}$, f being the focal length of the

lens, D and λ the radius and wavelength of the beam respectively, E is the energy per pulse and t is the pulse width. The plot of fluence versus transmittance represents the optical limiting curve and figure 3.7 illustrates the influence of nanoparticle size on the optical limiting response.

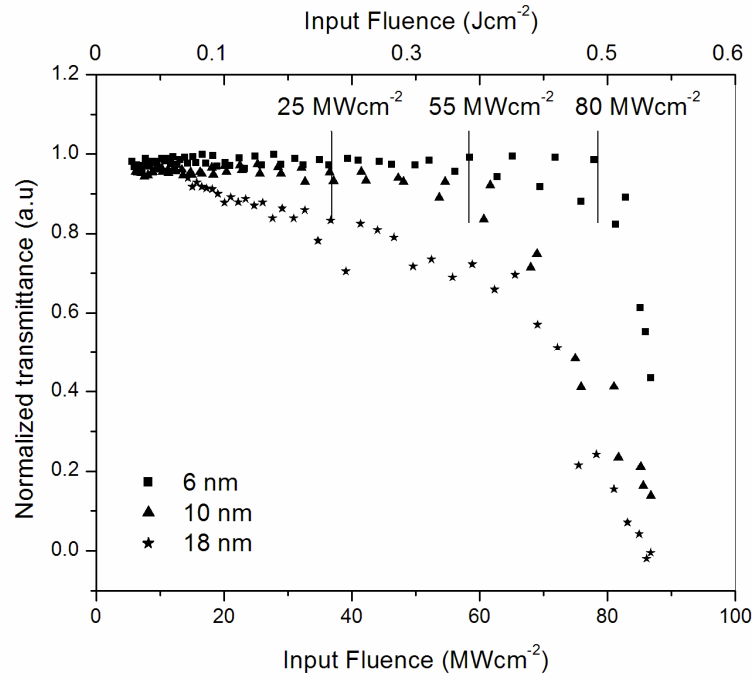


Figure 3.7: Optical limiting curves of ZnO colloids of different particle sizes generated from open aperture z-scan data.

The arrow in the figure 3.7 indicates optical limiting threshold which is the approximate fluence at which the normalized transmission begins to deviate from linearity. The optical limiting threshold is found to be high in the case of ZnO colloids of size 6 nm (80 MW/cm^2) in comparison to the ZnO colloids of size 10 nm (55 MW/cm^2) and ZnO colloids of size 18 nm (25 MW/cm^2). These values are comparable to the reported optical limiting threshold for CdS nano colloids^{18, 21}. Particle size has a significant effect on the limiting performance of ZnO nano colloids. Increasing particle size reduces the limiting threshold and enhances the optical limiting performance. From the measured values of β for the colloids, it can be seen

that the colloids with larger particle size is a better nonlinear absorber and hence a good optical limiter.

3.7 Conclusions

Nonlinear optical properties of ZnO semiconductor nano colloids are investigated for optical power self-limiting application. ZnO nano colloids show negative nonlinearity and good nonlinear absorption behaviour at off resonance wavelength. The observed optical nonlinearity is explained on the basis of two photon absorption followed by free carrier absorption. We have investigated the variation of optical nonlinearity as a function of size and an R^2 dependence of nonlinear susceptibility is obtained for ZnO nano colloids. Nonlinear susceptibility is highly fluence dependent and it becomes quadratic in nature for large particle size. The observed optical nonlinearities are very high compared to the value of bulk ZnO. The optical limiting response of ZnO nano colloids, in the diameter range of 6–18 nm, increases with the increase of particle size.

3.8 References

- 1 Y Kayanuma; “*Quantum-size effects of interacting electrons and holes in semiconductor microcrystals with spherical shape*”, Phys. Rev. B **38**, 9797(1988)
- 2 Zhong Lin Wang; *Materials Today* **7** (6), June (2004)
- 3 Gang Wang, G T Kiehne, G K L Wong, J B Kettersson, X Liu, and R P H Chang; “*Large second harmonic response in ZnO thin films*”, Appl. Phys. Lett. **80** (3), 401, (2002)
- 4 X J Zhang, W Ji and S H Tang; “*Determination of optical nonlinearities and carrier lifetime in ZnO*”, J.Opt. Soc. Am. B **14**, 1951-1955 (1997)
- 5 Lin Guo, Shihe Yang, Chunlei Yang, Ping Yu, Jiannong Wang, Weikun Ge and George K L Wong; “*Highly monodisperse polymer-capped ZnO nanoparticles: Preparation and optical properties*”, Appl. Phys. Lett. **76** (20), 2901 (2000)
- 6 H L Cao, X F Qian, Q Gong, W M Du, X D Ma and Z K Zhu; “*Shape- and size-controlled synthesis of nanometre ZnO from a simple solution route at room temperature*”, Nanotechnology **17**, 3632 (2006)
- 7 P Roussignol, D Ricard and C Flytzanis; “*Quantum confinement mediated enhancement of optical kerr effect in CdS_xSe_{1-x} semiconductor microcrystallites*”, Applied Physics B: Lasers and Optics **51**, 437 (1990)

- 8 D W Hall and N F Borrelli; “*Absorption saturation in commercial and quantum-confined CdSexSI-x-doped glasses*”, J. Opt. Soc. Am. B **5**, 1650 (1988)
- 9 E. Hanamura; “*Very large optical nonlinearity of semiconductor microcrystallites*”, Phys. Rev. B **37**, 1273 (1988)
- 10 H Ishihara and K Cho; “*Cancellation of size-linear terms in the third-order nonlinear susceptibility: Frenkel excitons in a periodic chain*”, Phys. Rev. B **42**, 1724 (1990)
- 11 Y Masumoto, M Yamazaki and H Sugawara; “*Optical nonlinearities of excitons in CuCl microcrystals*”, Appl. Phys. Lett. **53**, 1527 (1988)
- 12 Takumi Kataoka, Takashi Tokizaki and Arao Nakamura; “*Mesoscopic enhancement of optical nonlinearity in CuCl quantum dots: Giant-oscillator strength effect on confined excitons*”, Physical Review B **48**, 2815 (1993)
- 13 A Nakamura, H Yamada and T Tokizaki; “*Size-dependent radiative decay of excitons in CuCl semiconducting quantum spheres embedded in glasses*”, Phys. Rev. B **40**, 8585 (1989)
- 14 T Itoh, M Furumiya and C Gourdon; “*Size-dependent radiative decay time of confined excitons in CuCl microcrystals*”, Solid State Commun. **73**, 271 (1990)
- 15 Yingli Li, Masaki Takata and Arao Nakamura; “*Size-dependent enhancement of nonlinear optical susceptibilities due to confined excitons in CuBr nanocrystals*”, Physical Review B **57**, 15 (1998)
- 16 Didier Jezequel, Jean Guenot, Noureddine Jouini and Fernand Fievet; “*Submicrometer zinc oxide particles: Elaboration in polyol medium and morphological characteristics*”, J.Mater.Res. **10**, 77, (1995)
- 17 Eric W Seelig, Betty Tang, Alexey Yamilov, Hui Cao and R P H Chang; “*Self-assembled 3D photonic crystals from ZnO colloidal spheres*”, Materials Chemistry and Physics **80**, 257 (2002)
- 18 Litty Irimpan, Bindu Krishnan, A Deepthy, V P N Nampoori and P Radhakrishnan; “*Size dependent enhancement of nonlinear optical properties in nano colloids of ZnO*”, Journal of applied physics **103**, 033105 (2008)
- 19 M S Bahae, A A Said and E W van Stryland; “*High-sensitivity, single-beam n_2 measurements*”, Opt Lett, **14**, 955 (1989)
- 20 M S Bahae, A A Said, T H Wei, D J Hagan and E W Van Stryland; “*Sensitive measurement of optical nonlinearities using a single beam*”, IEEE J. Quantum Electron. **14**, 760 (1990)
- 21 Wenling Jia, Elliot P Douglas, Fenggi Guo and Wenfang Suna; “*Optical limiting of semiconductor nanoparticles for nanosecond laser pulses*”, Appl. Phys. Lett. **85** (26), 6326 (2004)
- 22 CRC Handbook of Laser Science and Technology: Optical Materials, edited by M. J. Weber ~CRC Press, Boca Raton, FL, (1997)

- 23 R Adair, L L Chase and S A Payne; “*Nonlinear refractive index of optical crystals*”, Phys. Rev. B **39**, 3337 (1989)
- 24 H Cao, J Y Xu, E W Seelig and R P H Chang; “*Microlaser made of disordered media*”, Appl. Phys. Lett. **76**, 2997 (2000)
- 25 A Maeda, M Ono, H Kishida, T Manako, A Sawa, M Kawasaki, Y Tokura and H Okamoto; “*Third-order nonlinear susceptibility spectra of CuO chain compounds investigated by the Z-scan method*”, Phys. Rev. B **70**, 125117 (2004)
- 26 M Y Han, W Huang, C H Chew, L M Gan, X J Zhang and W Ji; “*Large Nonlinear Absorption in Coated Ag₂S/CdS Nanoparticles by Inverse Microemulsion*”, J. Phys. Chem. B **102**, 1884 (1998)
- 27 J W Perry, L R Khundkar, D R Coulter, T H Wei, E W Van Stryland and D J Hagan; “*Excited State Absorption and Optical Limiting in Solutions of Metallophthalocyanines*”, Proceedings of the NATO workshop on Organic Materials for Nonlinear Optics and Photonics, La Rochelle, France, Aug. 26-31, 1990
- 28 G Wood, M Miller and A Mott; “*Investigation of tetrabenzo porphyrin by the Z-scan technique*”, Opt. Lett. **20**, 973 (1995)
- 29 S N R Swatton, K Welford, S Till and J Sambles; “*Nonlinear absorption of a carbocyanine dye 1,1',3,3,3',3'-hexamethylindotricarbocyanine iodide using a Z-scan technique*”, Appl. Phys. Lett. **66**, 1868 (1995)
- 30 C S Winter, R J Manning, S N Oliver and C A S Hill; “*Measurement of the large optical nonlinearity of nickel dithiolenone doped polymers*”, Opt. Commun. **90**, 139 (1992)
- 31 H P Li, B Liu, C H Kam, Y L Lam, W X Que, L M Gan, C H Chew and G Q Xu; “*Femtosecond Z-scan investigation of nonlinear refraction in surface modified PbS Nanoparticles*”, Opt.Mater. **14**, 321 (2000)
- 32 S Shi, W Ji, and S H Tang; “*Synthesis and optical limiting capability of cubane-like mixed metal clusters (n-Bu₄N)3[MoAg₃BrX₃S₄] (X = Cl and I)*”, J. Am. Chem Soc. **116**, 3615 (1994)
- 33 Y Sun, J E Riggs, K B Henbest and R B Martin; “*Nanomaterials as optical limiters*”, J. Nonlinear Optical Physics & Materials **9**, 481 (2000)
- 34 F M Qureshi, S J Martin, X Long, D D C Bradley, F Z Heneri, W J Balu, E C Smith, C H Wang, A K Kar and H L Anderson; “*Optical limiting properties of a zinc porphyrin polymer and its dimer and monomer model compounds*”, Chem. Phys. **231**, 87 (1998)



Chapter 4

Spectral and NLO characteristics of Self assembled films of ZnO

Abstract

The third order nonlinear optical properties of self assembled films formed from ZnO colloidal spheres are investigated and are compared with those of ZnO thin films deposited by sol-gel process as well as pulsed laser ablation. ZnO thin films clearly exhibit a negative nonlinear index of refraction at 532 nm and the observed nonlinear refraction. The colloids and films developed by dip coating as well as pulsed laser ablation exhibit induced absorption whereas the self assembled film exhibits saturable absorption. These different nonlinear characteristics can be mainly attributed to the saturation of linear absorption of the ZnO defect states and electronic effects when the colloidal solution is transformed into self assembled films. ZnO colloids and self assembled films show two emission bands. The presence of pronounced visible fluorescence in the self assembled film confirms the presence of surface defect states. We also report our investigations on the intensity, wavelength and size dependence of saturable and induced absorption of ZnO self assembled films and colloids. Values of the imaginary part of third order susceptibility are calculated for particles of size in the range 20–300 nm at different intensity levels ranging from 40 to 325 MW/cm² within the wavelength range of 450–650 nm. The wavelength dependence of figure of merit, which specifies the magnitude of nonlinear absorption for unit value of linear absorption, is calculated and this helps in comparing the absorptive nonlinearities at various excitation wavelengths.

The results of this chapter are published in
Litty Irimpan et.al., Optics Communications, **281**, 2938 (2008)
Litty Irimpan et.al., Applied Physics B: Lasers and Optics, **90**, 547 (2008)

4.1 Introduction

The search for new nonlinear optical materials with high optical nonlinearities is gaining interest both from research as well as industrial point of view. The essential requirements of good photonic materials are their large and ultrafast nonlinearity, synthetic flexibility and ease of processing. In recent years, wide bandgap semiconductors have been subjected to extensive studies because of the rising interest in the development of new nonlinear optical materials for potential applications in integrated optics. Impressive progress has been made in fabricating nonlinear optical waveguides from several nonlinear optical single crystals, which tend to be rather expensive. ZnO is an interesting wurtzitic II-VI wide bandgap semiconductor combined with high excitonic gain and large excitonic binding energy¹. The optical properties of this material are currently the subject of tremendous investigations, in response to the industrial demand for optoelectronic devices that could operate at short wavelengths. There is a significant demand for thin film nonlinear optical materials, which can be integrated into an optoelectronic device. Recent studies have revealed that ZnO based self assembled films can act as photonic crystals.

Photonic crystals show a great deal of application in numerous types of devices in 1, 2, and 3D structures. Due to its promising applications such as integrated optical circuits and thresholdless lasers, photonic crystals have been extensively investigated². Numerous techniques have been devised in an effort to produce periodic arrays of dielectric materials that can exhibit a photonic stop band. The fabrication of photonic crystals that work in the visible or near-infrared range is still a challenging topic. The principal method involves semiconductor fabrication technology, which includes lithography, layering, and etching processes. Several sophisticated methods have been developed, but they require expensive and large scale equipment³. One of the simplest techniques of fabricating photonic crystals involves

colloidal self-assembly, wherein, monodisperse colloidal spheres will spontaneously assemble into periodic arrays under certain circumstances. Zinc Oxide is a promising candidate for optically active self assembled photonic crystals⁴.

Most of the work performed in the area of self-assembled 3D photonic crystals has involved a few materials which are readily available as monodisperse colloidal spheres in sizes appropriate for photonic crystals including SiO₂ and polymers, such as polystyrene and PMMA⁵. In addition, while some studies have been performed in which emissive materials are added to the photonic crystal matrix⁶, no work has explored the properties of photonic crystals formed directly from optically active materials. Van Blaaderen et al. have produced a number of interesting emissive materials such as monodisperse colloidal spheres including Er³⁺ doped SiO₂, dye-doped PMMA, and SiO₂/ZnS core/shell structures⁷. ZnO is a promising candidate for optically active self-assembled photonic crystals because of its higher refractive index (2–2.2 in the visible regime) compared to other materials (1.4–1.5 for SiO₂ and most polymers). In addition, ZnO has been found to be an efficient emitter⁸, exhibiting lasing behavior in the near UV region ($\lambda \approx 385$ nm).

Accordingly, designing novel ZnO material and, in particular, well defined anisotropic and highly oriented 3D large arrays is of great importance for fundamental research as well as for various fields of industrial and high technology applications. The thermodynamically stable crystallographic phase of this polar non-transition metal oxide is wurtzite and occurs in nature as the mineral Zincite (although scarcely as natural single crystal). ZnO has a hexagonal lattice, with an a:c axial ratio of 1:1.6. Its ionic and polar structure can be described as a hexagonal close packing (HCP) of oxygen and zinc atoms in point group 3m and space group *P6₃mc* with zinc atoms in tetrahedral sites⁹. The occupancy of four of the eight tetrahedral

sites of HCP arrays controls the structure. The hexagonal unit cell contains two formula units, and the crystal exhibits a basal polar plane (001h) and two types of low-index faces, a nonpolar (1h00) face (and C6V symmetric ones) and a tetrahedron corner-exposed polar (001) face. The “low-symmetry” nonpolar faces with 3-fold coordinated atoms are the most stable ones. Additionally, there is no center of inversion in the wurtzite structure, and therefore, an inherent asymmetry along the *c*-axis is present allowing the growth of anisotropic crystallites¹⁰.

An intense radiation can induce a profound change on the absorption property of a material, resulting in the intensity dependent transmittance, which is the so called nonlinear absorption¹¹. Nonlinear absorption can be classified into two types: (i) transmittance increases with increasing optical intensity; this case corresponds to the well known saturable absorption (SA); (ii) transmittance reduces with increasing optical intensity; this type corresponds to induced absorption which includes two photon absorption (TPA), multiphoton absorption, and reverse saturable absorption (RSA). Different effects originating from different physical mechanisms can lead to a variety of different applications. For instance, SA materials have been used extensively in short-pulsed laser generations¹² as crucial passive mode-locking or *Q*-switching elements. Thus, it is paramount to fully characterize saturable performance, in which a typical figure of merit is the saturable intensity. SA characteristics depend on the inherent properties of a material and the parameters such as wavelength, intensity, and pulse duration of the laser used. To characterize nonlinear absorption, the open aperture *z*-scan technique, which was first pioneered by Sheik-Bahae *et al.*, has been extensively used¹³. Recently, an open aperture *z*-scan theory for the materials with simultaneous two and three photon absorption has been developed, which allows us to identify and determine the two and three photon absorption coefficients from a single open aperture *z*-scan trace¹⁴. The SA

properties of some materials are observed experimentally and analyzed theoretically¹⁵. The theory allows a straightforward estimation of the saturable intensity using the SA model for a material by fitting the experimental data. We also discuss the possible mechanisms of SA. When experiment on the characterization of the saturable absorption is performed by using a pulsed laser, if the nonlinear response time of the samples is much shorter than the laser pulse width, one can assume that the nonlinear effect depends on the instantaneous intensity inside the sample.

The studies on nonlinear processes in photonic materials are significant in the context of their technological applications, especially in areas such as passive optical power limiting, optical switching, and the design of logic gates. However, the switching to saturable absorption in ZnO self assembled films from induced absorption in colloids have not been explored and reported yet. In this chapter, we report our investigations on the size, intensity and wavelength dependence of saturable and induced absorption of ZnO self assembled films and colloids using 10 Hz, 5-7 ns pulses from a tunable laser by z-scan method¹⁶⁻¹⁷. Values of the imaginary part of third order susceptibility are calculated for particles of size in the range 20-300 nm at different intensity levels ranging from 40 to 325 MW/cm² within the wavelength range of 450–650 nm.

4.2 Theory

An intense radiation can induce a profound change on the absorption property of a material, resulting in the intensity dependent transmittance called nonlinear absorption¹¹. The propagation through the sample is given by

$$\frac{dI}{dz} = -\alpha(I)I \quad (4.1)$$

where $\alpha(I)$ is the intensity dependent absorption coefficient. z and

I are the propagation distance and the optical intensity inside the saturable absorption sample, respectively

Nonlinear absorption can be classified into two types: (i) transmittance reduces with increasing optical intensity corresponding to induced absorption; (ii) transmittance increases with increasing optical intensity corresponding to saturable absorption (SA)

4.2.1 Induced absorption

Induced absorption is characterized by decrease of transmittance with increase of the input energy. TPA is also referred to as induced absorption and there are various mechanisms leading to this process¹³. In the presence of TPA, the optical nonlinearity is described by the equation

$$\alpha(I) = \alpha_0 + \beta I \quad (4.2)$$

where α_0 and β are the linear and nonlinear absorption coefficients respectively.

4.2.2 Saturable absorption

Saturable absorption is characterized by an increase in transmittance with increase in input energy. When the beam propagates through a thin saturable absorber, the optical nonlinearity is described by the equation¹⁶,

$$\alpha(I) = \frac{\alpha_0}{1 + \left(\frac{I}{I_s}\right)} \quad (4.3)$$

where I_s is the saturation intensity. Substituting this in equation (4.1) and integrating between the limits I_0 to I_L gives

$$\ln \frac{I_L}{I_0} = -\alpha_0 L - \left(\frac{I_L - I_0}{I_0} \right) \quad (4.4)$$

This can be solved numerically to get the transmission of the sample, I_L . If excitation intensity I_0 is greater than I_s , we can consider SA as a third order

process and in such cases $-\alpha_0/I_s$ is equivalent to nonlinear absorption coefficient β which will then give $\text{Im}(\chi^{(3)})$.

4.3 Synthesis

4.3.1 self assembled films of ZnO

Zinc Oxide is a promising candidate for photonic devices. Colloids of nano ZnO for the present studies are synthesized by a modified polyol precipitation method¹⁶⁻¹⁷ as described in chapter 2. One of the simplest techniques of fabricating photonic crystals of ZnO involves colloidal self-assembly, wherein, monodisperse colloidal spheres will spontaneously assemble into periodic arrays under certain circumstances. Films are then produced from the ZnO colloidal spheres using a sedimentation self assembly process by the technique of drop casting onto a pre-heated glass substrate maintained at a temperature of 120°C.

4.3.2 Thin films of ZnO through sol-gel process

In this method, deposition is carried out by the sol gel technique on commercially available glass substrate by the process of dip coating¹⁷. A stable hydrolysed solution is prepared using stoichiometric quantities of zinc acetate dissolved in diethanolamine and a cleaned substrate is immersed into this solution for thirty seconds at a controlled rate of 5 cm/min. The film is then kept for drying in a furnace for nearly 15 minutes at a temperature of 150°C and annealed for half an hour at a temperature of 600°C, to get good quality crystalline homogenous oxide films.

4.3.3 Thin films of ZnO through pulsed laser ablation

ZnO films are prepared by laser ablation of sintered ZnO target in the presence of an ambient gas at room temperature and a pressure of 500 mbar using the second harmonic of a Q-switched Nd:YAG laser¹⁷. The second harmonic beam from the Nd:YAG laser provide 300 mJ pluses of 7

ns pulse width at a repetition rate of 10 Hz. The laser beam is focused using a spherical convex lens on to the surface of the sample kept inside a stainless steel vacuum chamber through a glass window. The target is fixed at an angle of 45^0 with respect to the laser beam and is rotated at a constant rate during laser deposition, so that pitting of the target surface by the laser beam is uniform. The chamber gas environment during pulsed laser deposition (PLD) consisted of an oxygen partial pressure of 0.008 mbar and the deposition is carried out for duration of one hour at a laser beam power of 50mW.

4.4 Absorption spectroscopy

Figure 4.1(a) gives the room temperature absorption spectra of the ZnO colloid and self assembled film of size 20 nm and figure 4.1(b) shows that of ZnO thin films.

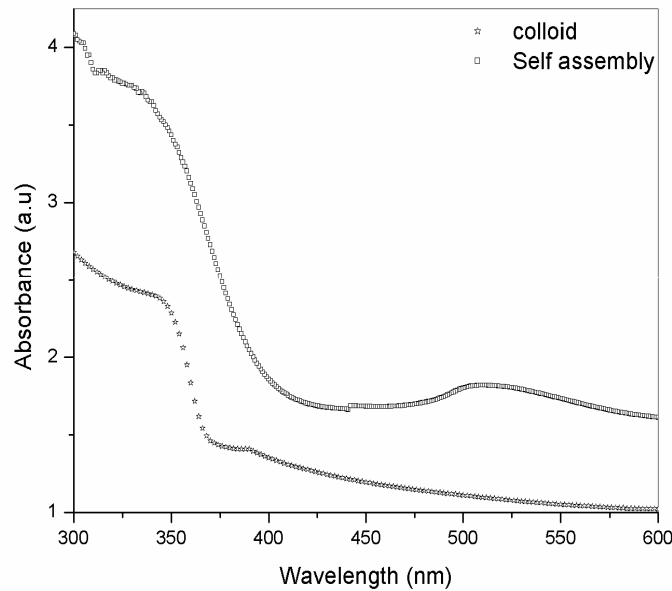


Figure 4.1(a): Absorption spectra of ZnO colloid and self assembled film

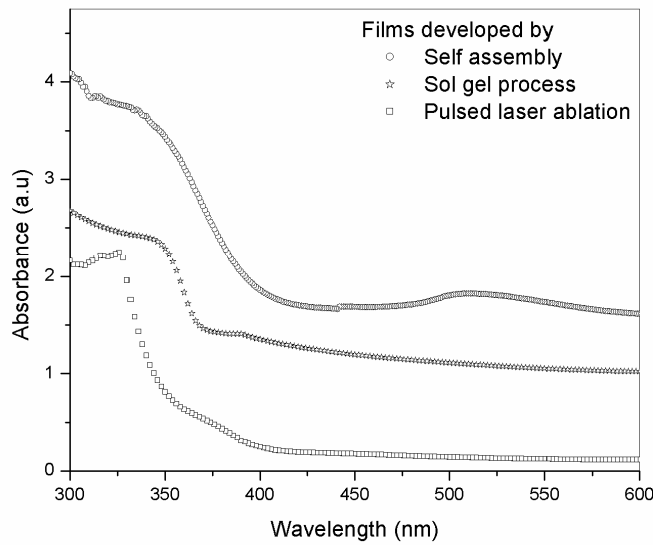


Figure 4.1(b): Absorption spectra of ZnO films

The excitonic peak of the colloid and the films developed by dip coating as well as pulsed laser ablation is found to be blue shifted from that of the bulk ZnO and can be attributed to the confinement effects¹⁸. The breadth of the absorption edge of the self assembled film indicates that there exists defect-related transitions¹⁶⁻¹⁷. Defects usually create discrete electronic states in the bandgap, and therefore influence both optical absorption and emission processes. The two most common defects in ZnO are likely to be oxygen and zinc vacancies and the visible band in the absorption spectrum can be related to the presence of these defect states in the self assembled film.

4.5 Optical bandgap

The direct bandgap are estimated from absorption spectrum as described in chapter 2.

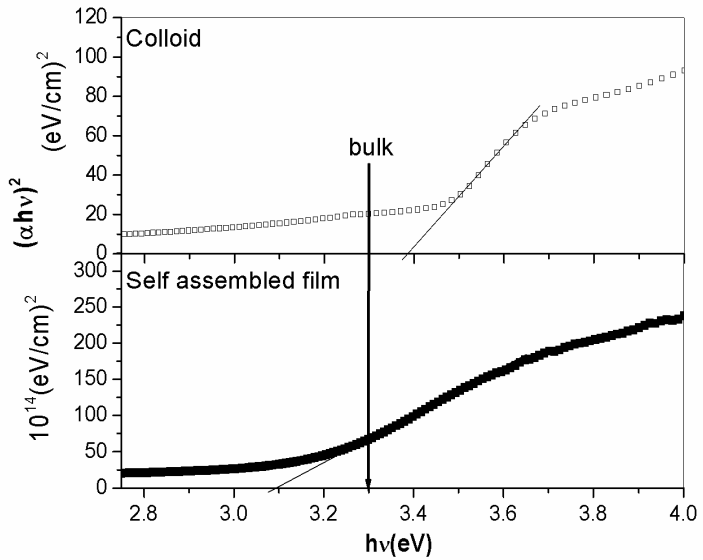


Figure 4.2(a): Optical bandgap of ZnO colloid and self assembled film

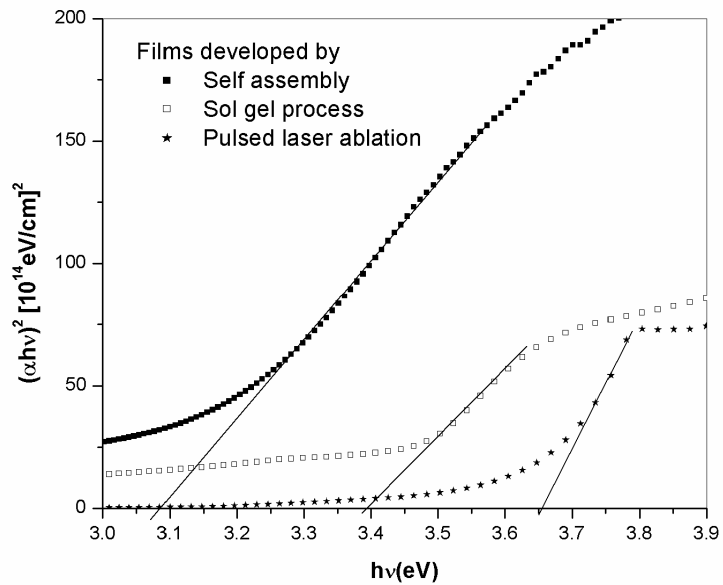


Figure 4.2(b): Optical bandgap of ZnO thin films

The optical bandgap (E_g) of colloidal and films of ZnO is found to be shifted from that of the bulk as shown in figure 4.2. The bandgap of self assembled film is reduced to 3.1eV from that of bulk (3.3 eV) whereas the bandgap energy of the colloid and that of the films developed by dip coating as well as pulsed laser ablation are higher than that of the bulk¹⁶⁻¹⁷.

4.6 X-ray diffraction

The self assembled film and powder extracted from the colloid are characterized by x-ray diffraction. Typical XRD pattern of self assembled film is shown in figures 4.3. The XRD pattern of powder extracted from ZnO colloid is shown in chapter 2. The diffraction pattern and interplane spacings can be well matched to the standard diffraction pattern of wurtzite ZnO, demonstrating the formation of wurtzite ZnO nanocrystals. The particle diameter d is calculated using the Debye–Scherer formula¹⁹ as described in chapter 2. The XRD peak at 36° gives the ZnO particle diameter of 18 and 20 nm for the colloid and film respectively.

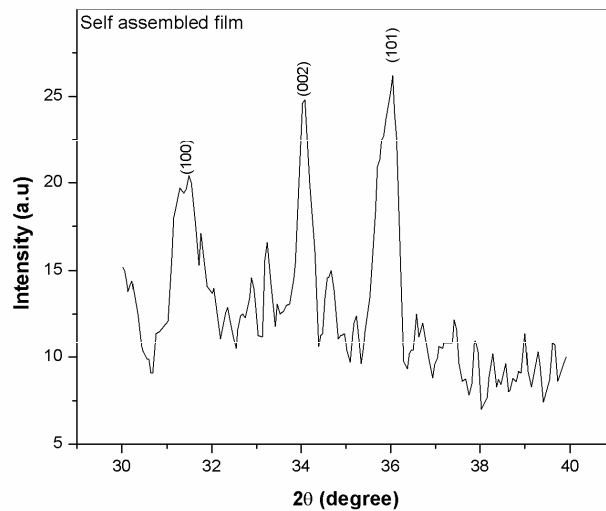


Figure 4.3: XRD pattern of ZnO self assembled film

Both colloid and film show three major orientations, viz., (100), (002) and (101). The (101) orientation is reported to be the prominent peak having the lowest surface energy and other orientations require more thermal energy to develop. The (002) direction is not the direction of fastest growth for ZnO. This we infer from the fact that the (002) faces of ZnO are the ones with the highest surface energy and these faces, according to basic crystal growth theory should, therefore, be among the faces of lowest growth rate²⁰. But the relative intensity for the (002) orientation in self assembled film is observed to be higher compared to the colloidal spheres. In lattice mismatched epitaxial growth, it is well known that the increase of the length of *c* axis causes the decrease of the length of *a* axis. This means that ZnO thin film has a tensile built-in strain and this can be relaxed by providing sufficient thermal energy²⁰.

The (002) peak is observed at a diffraction angle (2θ) of 34.45^0 in the powder extracted from colloid and its line width is about 0.60. The diffraction angle from the (002) plane of bulk ZnO powder²¹ is 34.4^0 and its line width is 0.20. On the other hand, the diffraction angle from the (002) plane of self assembled film is 34.06^0 and its linewidth is 0.80. Thus for self assembled films, a shift of the (002) diffraction angle towards lower angles and an increase in linewidth are also observed. Considering all these observations and the reduction of bandgap of self assembled films, we can conclude that there exist a strong correlation between the electronic structure and the geometrical structure of the ZnO arrays.

The crystallinity of self assembled film is poor compared to powder. Earlier observations have revealed that crystallinity of ZnO thin film was improved by annealing at high temperatures. Hence it is possible to develop other orientations by annealing at high temperatures and the mechanical properties of the self assembled film can be improved after heat treatment. Although ZnO self assembled films can act as photonic crystals,

unfortunately, we are not able to observe photonic crystal. Optimization of self assembled films to get photonic crystals is one of the promising areas for future works.

4.7 Scanning electron microscopy

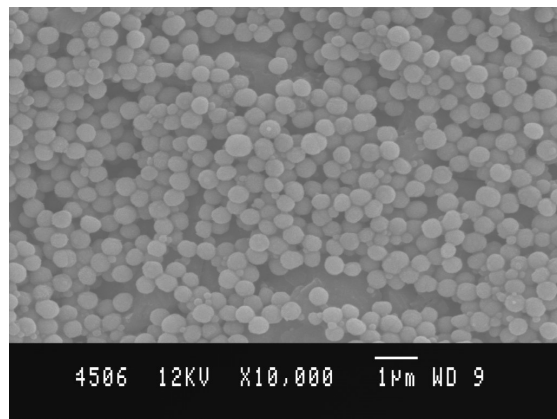


Figure 4.4: SEM image of ZnO self assembled film on silica substrate

To compare the monodispersity of the self assembled colloidal spheres with the actual values, the structure of the self assembled films is recorded using a scanning electron microscope (SEM, S-4300 Hitachi). The SEM image for a self assembled film on silica substrate is shown in figure 4.4 which indicates the presence of monodispersed ZnO spheres with an average particle size of 300 nm.

4.8 Fluorescence spectroscopy

Figure 4.5 shows the fluorescence spectra of ZnO colloid and self assembled film of size 20 nm for an excitation wavelength of 325 nm. From the figure it is clear that two emission bands are present, a UV emission band and another in the green region¹⁶⁻¹⁷. The UV band has been assigned to the bandgap fluorescence and the visible band is mainly due to surface defect states. The presence of pronounced visible fluorescence in the self assembled film confirms the origin of 530 nm emissions due to the presence of surface

defect states. Defects create discrete electronic states and therefore influence optical properties.

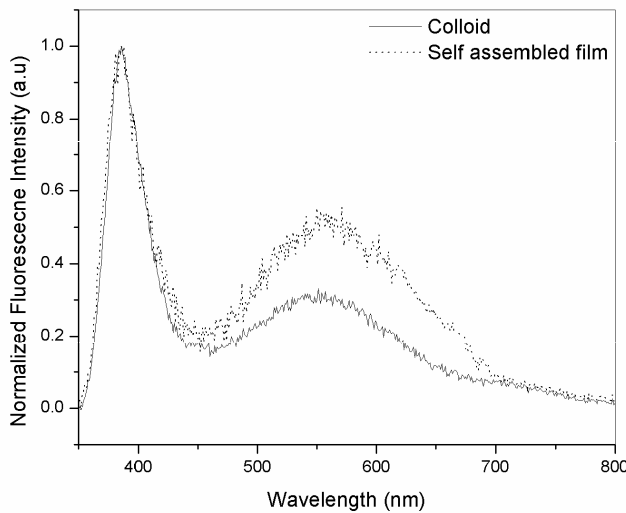


Figure 4.5: Fluorescence spectra of ZnO colloid and self assembled film for an excitation wavelength of 325 nm

4.9 Nonlinear optical characterization

One of the important applications of nano ZnO is in the field of photonic materials. The third order nonlinear optical properties of ZnO colloids and films are investigated using z-scan technique and are explained in chapter 3. Following studies describe the NLO properties of colloids and films of ZnO.

4.9.1 Open aperture z-scan

Typical results of the open aperture z-scan measurements of the films and colloid which correspond to the far-field normalized transmittance as a function of the distance from the lens focus at an intensity of 220 MW/cm^2 are shown in figure 4.6. The open aperture curve exhibits a

normalized transmittance valley, indicating the presence of induced absorption in the case of colloid and films which are developed by dip coating as well as pulsed laser ablation and a transmittance peak, indicating the presence of saturable absorption, in the case of self assembled film¹⁶⁻¹⁷.

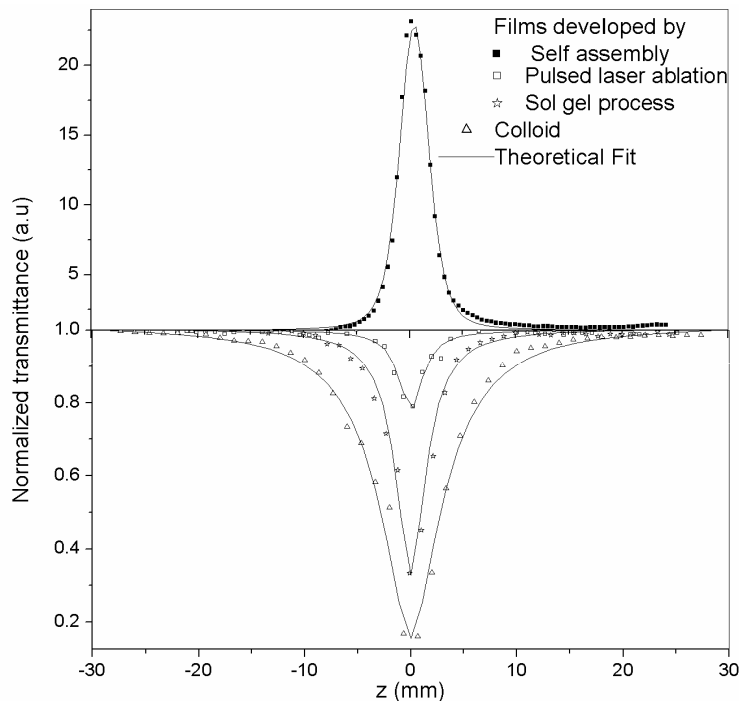


Figure 4.6: Open aperture z-scan traces of ZnO thin films and colloid at an intensity of 220 MW/cm^2 for an irradiation wavelength of 532 nm

In general, induced absorption can occur due to a variety of processes. The theory of two photon absorption process fitted well with the experimental curve infers that TPA is the basic mechanism and the possibility of free carrier absorption (FCA) contributing to induced absorption is explained in chapter 3. Considering all these factors and also that we used nanosecond excitation pulses, it is reasonable to assume that TPA followed by weak FCA are the important mechanisms contributing to

induced absorption in our colloid as well as dip coated and laser ablated samples¹⁶⁻¹⁷.

The switching of saturable absorption behaviour in self assembled ZnO from induced absorption in colloidal ZnO is an interesting effect and can be used for applications such as optical pulse compression, optical switching and laser pulse narrowing²². The z-scan data shows that, along with moving the self assembled film towards the focus, the increase in the laser intensity induces saturation of the ground state absorption, which results in a transmittance increase (SA process).

The self assembled film exhibits saturation of absorption and bleaching and possesses a larger absorption coefficient than the other films and is more susceptible to thermal effects. For semiconductor materials, heat tends to reduce the fermi energy level and thereby, increase the number of carriers in the conduction band. This, in turn, depletes the ground level and induces bleaching in the ground state absorption, which results in SA process. The origin of optical nonlinearity is not only dependent on polarization response of bound electrons but also from conduction electrons in semiconductors. From figure 4.2, it is clear that the bandgap of the self assembled film is reduced to 3.1eV from that of the bulk (3.3 eV) and the laser intensity induces bleaching in the ground state absorption, which results in SA process. But the bandgap energies of the colloid and other 2 films are higher than the bulk which leads to induced absorption. These different nonlinear phenomena in the self assembled films can be attributed to the electronic transitions involving defect states¹⁶⁻¹⁷.

The sensitivity of ZnO to impurities as well as native defects with respect to electronic properties is well known²³. The breadth of the absorption edge of the self assembled film indicates that there are defect-related transitions in this case. The negative β value in ZnO thin films are

reported to be due to the saturated absorption of the defect states²³. A similar explanation can hold for our self assembled films also. Thus the saturable absorption in self assembled films can be attributed to saturation of linear absorption of the ZnO defect states.

Generally ZnO exhibits induced absorption. In the self assembled film, the strong SA and the absence of induced absorption implies that the absorption cross-section of ground state is much larger than the absorption cross-section of excited state. All RSA materials possess a higher absorption cross-section of excited states compared to that of the ground state at the excitation radiation wavelength. Interestingly they will also give a positive value for the imaginary part of susceptibility $\text{Im}(\chi^{(3)})$ which is actually a measure of the induced absorption. On the other hand, a saturable absorber has a negative value for $\text{Im}(\chi^{(3)})$. The most important application of these materials is in optical limiting and to be used as protective material for sensitive devices.

4.9.2 Closed aperture z-scan

Figure 4.7 gives the closed aperture z-scan traces of ZnO colloid and films at an intensity of 220 MW/cm² for an irradiation wavelength of 532 nm. The closed aperture curve exhibited a peak to valley shape, indicating a negative value of the nonlinear refractive index n_2 . The sign of nonlinear refractive index of all the samples remain negative whereas the absorptive nonlinearity reverses its sign when the material changes from colloid to self assembled film¹⁶⁻¹⁷.

It is observed that the peak-valley of closed aperture z-scan satisfied the condition $\Delta z \sim 1.7 z_0$, thus confirming the presence of pure electronic nonlinearity²⁴. The major mechanism behind nonlinear refraction is two photon absorption and ZnO exhibits negative nonlinear refractive indices at 532 nm since the bandgap of bulk ZnO is 3.3 eV. It is reported that all

materials exhibit a sign change of the nonlinear refraction at about 2/3 of the bandgap²⁵. There is no change in the sign of the nonlinear refractive index as the bandgap lies within the range 3.1-3.7 eV for the different samples and the sign change can be expected at near 600 nm. The SA in self assembled films can be attributed to bleaching of defect states and this does not affect the nonlinear refraction and hence there is no change in the sign of nonlinear refractive index whereas the absorptive nonlinearity for the self assembled film exhibits a trend which is reverse to that of the bulk. TPA always exists, even when saturable absorption appears to overlie this mechanism in self assembled films¹⁶⁻¹⁷.

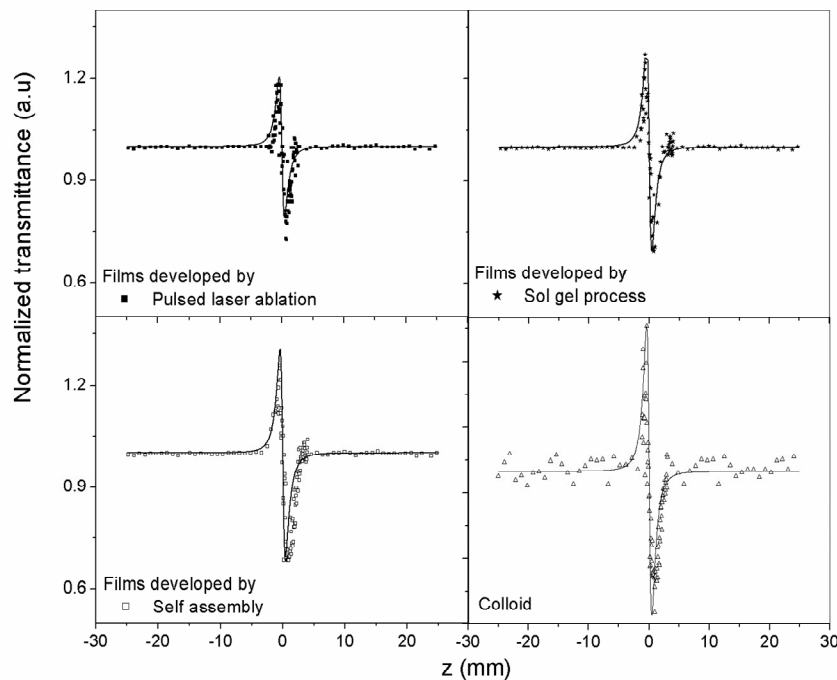


Figure 4.7: Closed aperture z-scan traces of ZnO thin films and colloid at an intensity of 220 MW/cm² for an irradiation wavelength of 532 nm

4.9.3 Nonlinear optical parameters

The nonlinear absorption coefficient, refractive index and third order susceptibility of ZnO films at an intensity of 220 MW/cm² for a wavelength of 532 nm are tabulated in table 4.1. When it is a saturable absorber, a more useful parameter to extract from the transmission measurements is the saturation intensity I_S, which is also given in the table¹⁶⁻¹⁷. These values are within an error of 7% contributed mainly by the uncertainty in intensity measurements on the sample and the fitting error.

Films developed by	β	I _S	n ₂	Im($\chi^{(3)}$)	Re($\chi^{(3)}$)	$\chi^{(3)}$
	x10 ⁻⁵ m/W	GW/cm ²	x10 ⁻⁵ esu	x10 ⁻⁶ esu	x10 ⁻⁶ esu	x10 ⁻⁶ esu
Sol-gel process	4.6	-	-2.6	2.0	-5.5	5.9
Pulsed laser ablation	0.8	-	-1.9	0.3	-3.9	4.0
Self assembly	-	0.4	-2.8	-0.6	-5.9	5.9

Table 4.1: Measured values of nonlinear absorption coefficient, saturation intensity, nonlinear refractive index and third order susceptibility of ZnO films at an intensity of 220 MW/cm² for an irradiation wavelength of 532 nm

Based on these measurements we found that the imaginary part of the susceptibility is an order of magnitude smaller than the value for the real part of the susceptibility function. This means that the refraction effect is stronger than the absorption. One should be very careful while comparing the susceptibility values available in literature. These values vary to a great extent depending on the excitation wavelength, pulse duration, experimental

technique, concentration of the molecular species in the sample etc. The values of $\chi^{(3)}$ obtained for colloids are compared with the reported values in chapter 3. The values of $\chi^{(3)}$ measured at room temperature by femtosecond degenerate four wave mixing technique on ZnO microcrystalline thin films²⁶ range from 10^{-4} to 10^{-7} esu. The β values obtained are quite high, and are of the same order of magnitude as those obtained for ZnO-Cu and ZnO-Mg nanocomposite films^{23, 27}. Thus, the real and imaginary parts of third order nonlinear optical susceptibility measured by the z-scan technique revealed that the ZnO colloid and films investigated here have good nonlinear optical response and could be chosen as ideal candidates with potential applications in nonlinear optics¹⁶⁻¹⁷.

4.9.4 Size dependence

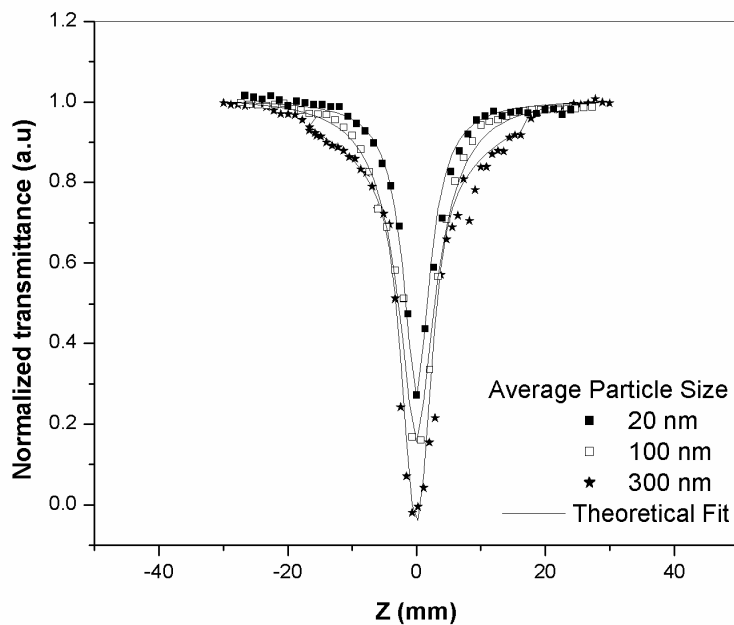


Figure 4.8(a): Open aperture z-scan traces of ZnO colloids of different particle sizes at an intensity of 220 MW/cm^2 for a wavelength of 532 nm

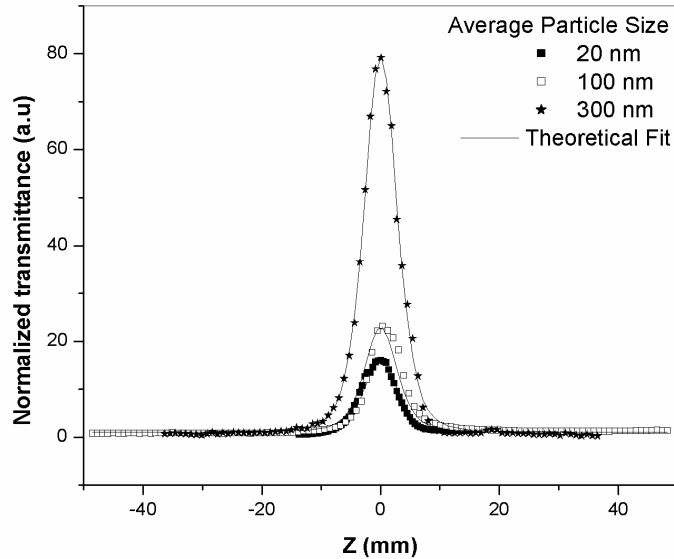


Figure 4.8(b): Open aperture z-scan traces of ZnO self assembled films of different particle sizes at an intensity of 220 MW/cm^2 for an irradiation wavelength of 532 nm

ZnO colloid and film for different particle sizes at an intensity of 220 MW/cm^2 for an irradiation wavelength of 532 nm are shown in figure 4.8 (a) and (b) respectively. The colloids exhibit RSA and the films show SA at all particle sizes from $20\text{-}300 \text{ nm}$. The enhanced nonlinear optical properties of ZnO colloids with increase in particle size are due to strong two photon absorption. The susceptibility is size dependent, without showing a saturation behavior in the size range studied in our investigation¹⁶. The enhancement of nonlinear optical properties with increasing dimension in the weak confinement regime essentially originates from the size dependent enhancement of oscillator strength of coherently generated excitons and is explained in detail in chapter 3.

4.9.5 Fluence dependence

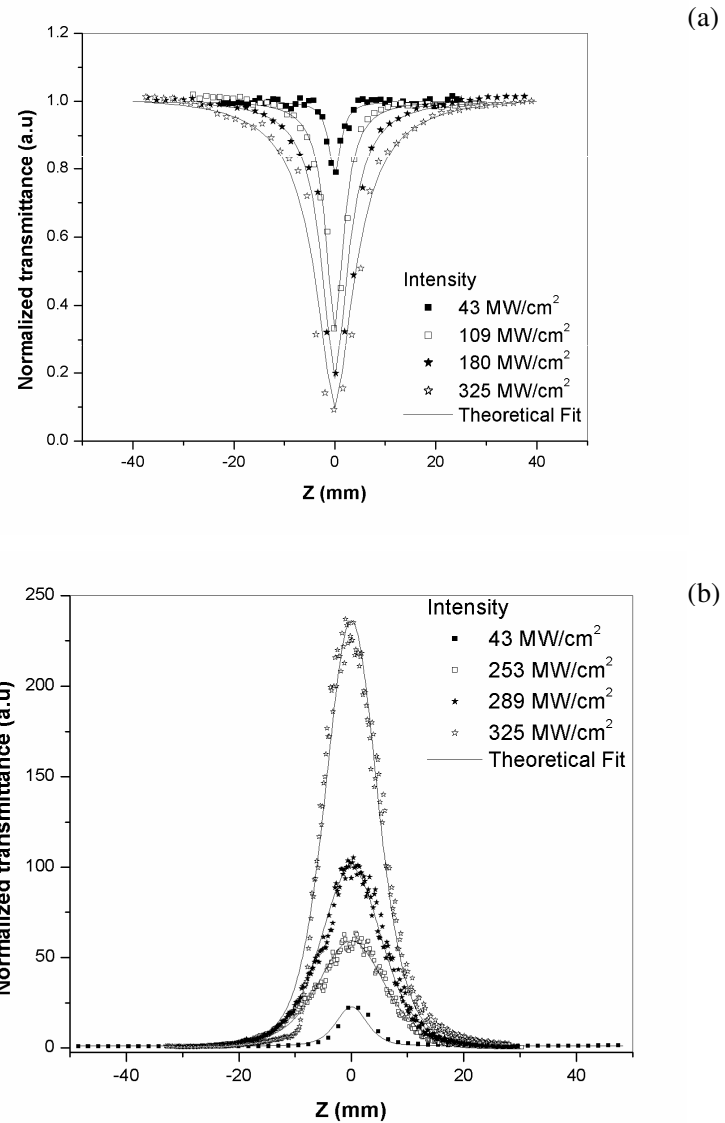


Figure 4.9: Open aperture z-scan curves of (a): ZnO colloid (b): ZnO self assembled films of size 300 nm at a wavelength of 532 nm for different irradiation intensities

The open aperture z-scan curves of ZnO colloid and self assembled film of size 300 nm at a wavelength of 532 nm for different irradiation intensities are shown in figure 4.9(a) and (b) respectively. We can see that nonlinear optical properties are highly irradiance dependent. The colloid shows induced absorption at all intensities under investigation. The results show three orders of enhancement from the reported value of 5cm/GW for bulk ZnO²⁸. It has been reported that the reduced dimensionality of the particles resulted in considerable enhancement of the second-order susceptibility $\chi^{(2)}$ in thin films of ZnO²⁹. Similar results in the third order nonlinear parameters are evident in our measurements also¹⁶.

Now we will evaluate the saturation intensity of the self assembled film and attempt to interpret its SA behavior. We use the SA model described in equation (4.3) to fit our experimental open aperture z-scan trace displayed in figure 4.9(b), with only one adjustable parameter (I_S) and it is in good arrangement with the experimental data. The theoretical fitting give the respective I_S to be within a range of 0.12-0.52 GW/cm², for different intensity levels of I_0 ranging from 40 to 325 MW/cm² respectively. The results certainly imply that the self assembled films show only SA behavior¹⁶. It is well known that the theoretical model could describe the SA effect in a homogeneous broadening two level system very well. In the self assembled film, the strong SA and the absence of induced absorption imply that the absorption cross-section of ground state is much larger than the absorption cross-section of excited state.

4.9.6 Spectral dependence

The nature of nonlinear absorption in ZnO is dependent on the wavelength of the excitation beam¹⁶. It is seen that the material exhibits induced absorption for all wavelengths under investigation when it is in colloidal form.

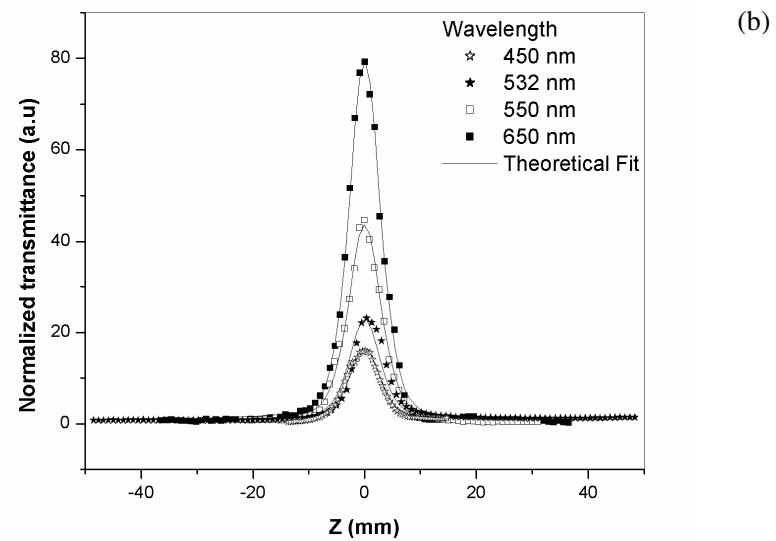
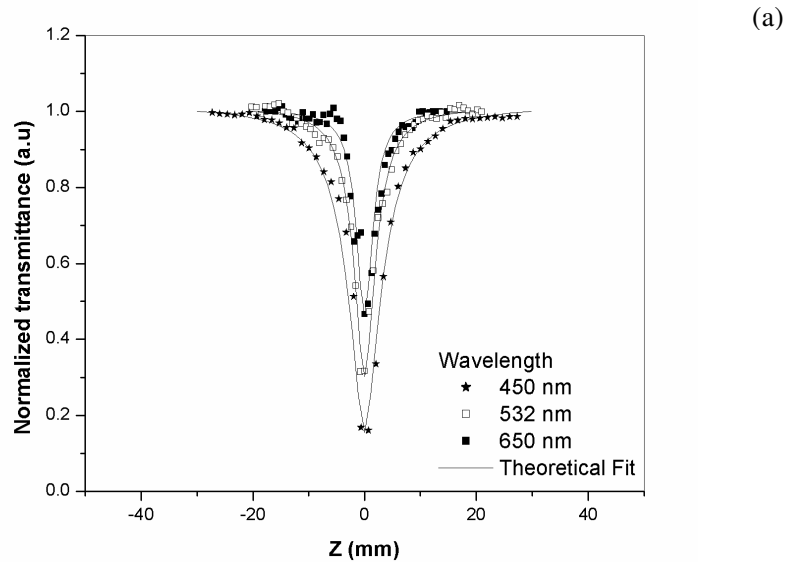


Figure 4.10: Open aperture z-scan curves of (a): ZnO colloid (b): ZnO self assembled films of size 300 nm at an intensity of 220 MW/cm² for different irradiation wavelengths

The self assembled film exhibits SA and the material does not exhibit any sign of absorptive nonlinearity for all wavelengths under investigation. This interesting feature is illustrated in figure 4.10 (a) and (b). However, it can be concluded that the nonlinear absorption changes from induced absorption to SA when the material changes from colloidal form to self assembled film.

4.9.7 Variation of imaginary part of susceptibility

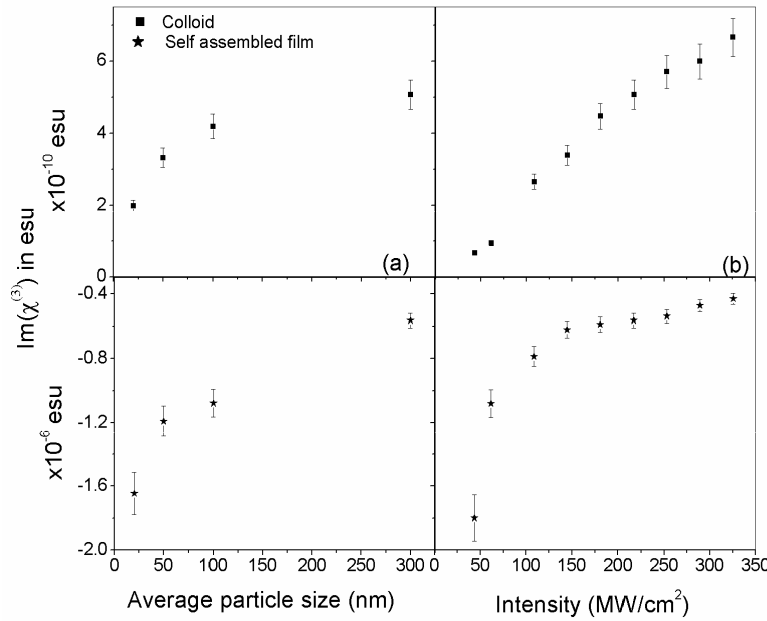


Figure 4.11: Vatriation of imaginary part of susceptibility with

(a) Particle size (b) Intensity

All materials exhibiting RSA possess a higher absorption cross-section of excited states (σ_e) compared to that of the ground state (σ_g) at the excitation radiation wavelength³⁰. Interestingly they will also give a positive value for the imaginary part of susceptibility $\text{Im}(\chi^{(3)})$ which is

actually a measure of the induced absorption. On the other hand, a saturable absorber has a negative value for $\text{Im}(\chi^{(3)})$. The calculated values of $\text{Im}(\chi^{(3)})$ as a function of size and intensity are shown in figure 4.11(a) and 4.10(b) respectively and it is found that susceptibility increases with particle size and intensity¹⁶.

4.9.8 Figure of merit

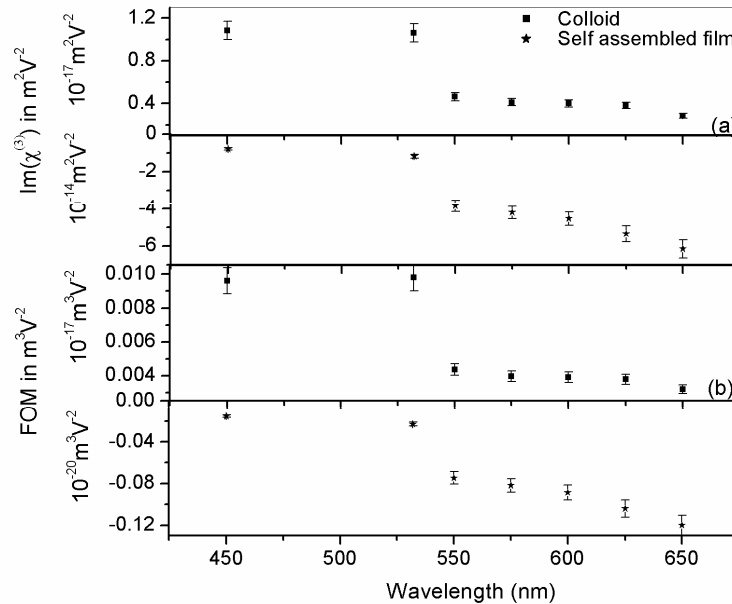


Figure 4.12:(a) Imaginary part of susceptibility as a function of wavelength (b) Figure of merit as a function of wavelength

The calculated values of $\text{Im}(\chi^{(3)})$ as a function of wavelength are shown in figure 4.12(a). It will be useful to define a figure of merit (FOM) for these types of materials as the ratio $\text{Im}(\chi^{(3)})/\alpha_0$, which specifies the magnitude of nonlinear absorption for unit value of linear absorption loss. FOM as a function of wavelength is plotted in figure 4.12(b) and it is found

that FOM is larger in the region between 450 and 550 nm. It helps in comparing the absorptive nonlinearities at various excitation wavelengths¹⁶.

The most important application of these materials is in optical limiting and as a saturable absorber. Since these properties are spectral dependent, it is more common to use another figure of merit, σ_e / σ_g , which is the ratio of excited to ground state absorption cross-section. The value of σ_g can be obtained from the linear absorption spectrum using Beer's law.

To evaluate σ_e we need to analyze the z-scan signal in a manner, as suggested by Wei *et al.*³¹ and the work in the direction will be taken up as a future project.

4.10 Conclusions

ZnO colloids and self assembled films show two emission bands; an ultraviolet emission band and another in the green region. The presence of pronounced visible fluorescence in the self assembled film confirms the presence of surface defect states. The nonlinear optical properties of self assembled films formed from ZnO colloidal spheres have been investigated and compared with those of films developed by sol-gel process and pulsed laser ablation using z-scan technique. ZnO colloids and thin films clearly exhibit a negative nonlinear index of refraction at 532 nm and the observed nonlinear refraction is attributed to two photon absorption followed by free carrier absorption. Although the absolute nonlinear values for these films are comparable, there is a change in absorptive nonlinearity of the films. The colloid and films developed by dip coating as well as pulsed laser ablation exhibit induced absorption whereas the self assembled film exhibits saturable absorption. This behaviour can be attributed to the saturation of linear absorption of the ZnO defect states. In the self assembled film, the strong SA and the absence of RSA implies that the absorption cross-section of ground state is much larger than the absorption cross-section of excited state. We

report our investigations of intensity, wavelength and size dependence of saturable and induced absorption of ZnO self assembled films and colloids. Values of the imaginary part of third order susceptibility are calculated for particles of size in the range 20-300 nm at different intensity levels ranging from 40 to 325 MW/cm² within the wavelength range of 450–650 nm. The wavelength dependence of figure of merit is calculated which helps in comparing the absorptive nonlinearities at various excitation wavelengths.

4.11 References

- 1 S. A. Studenikin, M. Cocivera, W. Kellner, and H. Pascher; “*Band-edge photoluminescence in polycrystalline ZnO films at 1.7 K*”, J. Lumin. **91**, 223 (2000)
- 2 O. Painter, R.K. Lee, A. Scherer, A. Yariv, J.D. O’Brien, P.D. Dapkus and I. Kim; “*Two-Dimensional Photonic Band-Gap Defect Mode Laser*”, Science **284**, 1819 (1999)
- 3 H.B. Sun, S. Matsuo and H. Misawa; “*Three dimensional photonic crystal structures achieved with two- photon-absorption photopolymerization of resin*”, Appl. Phys. Lett. **74**, 786 (1999)
- 4 Eric W Seelig, Betty Tang, Alexey Yamilov, Hui Cao and R P H Chang; “*Self-assembled 3D photonic crystals from ZnO colloidal spheres*”, Materials Chemistry and Physics **80**, 257 (2002)
- 5 S H Park, Y N Xia; “*Assembly of Mesoscale Particles over Large Areas and Its Application in Fabricating Tunable Optical Filters*”, Langmuir **15**, 266 (1999)
- 6 S G Romanov, T Maka, C M S Torres, M Muller and R Zentel; “*Emission in a SnS2 inverted opaline photonic crystal*”, Appl. Phys. Lett. **79**, 731 (2001)
- 7 K P Velikov and A van Blaaderen; “*Synthesis and Characterization of Monodisperse Core-Shell Colloidal Spheres of Zinc Sulfide and Silica*”, Langmuir **17**, 4779 (2001)
- 8 H Cao, J Y Xu, D Z Zhang, S H Chang, S T Ho, E W Seelig, X Liu and R P H Chang; “*Spatial Confinement of Laser Light in Active Random Media*”, Phys. Rev. Lett. **84**, 5584 (2000)
- 9 N Fujimura, T Nishihara, S Goto, J Xu and T Ito; “*Control of preferred orientation for ZnO_x films: control of self-texture*”, J. Cryst. Growth **130**, 269 (1993)
- 10 Lionel Vayssières, Karin Keis, Sten-Eric Lindquist and Anders Hagfeldt; “*Purpose-Built Anisotropic Metal Oxide Material: 3D Highly Oriented Microrod Array of Zinc*”, J. Phys. Chem. B **105**, 3350 (2001)
- 11 R. L. Sutherland, *Handbook of Nonlinear Optics*, Chap. 9 (Marcel Dekker, New York, 1996)

- 12 Y X Fan, J L He, Y G Wang, S Liu, H T Wang and X Y Ma; “*2-ps passively mode-locked Nd:YVO₄ laser using an output-coupling-type semiconductor saturable absorber mirror*”, Appl. Phys. Lett. **86**, 101103 (2005)
- 13 M S Bahae, A A Said, T H Wei, D J Hagan and E W Van Stryland; “*Sensitive measurement of optical nonlinearities using a single beam*”, IEEE J. Quantum Electron. **26**, 760 (1990)
- 14 B Gu, J Wang, J Chen, Y X Fan, J P Ding and H T Wang; “*Z-scan theory for material with two- and three-photon absorption*”, Opt. Express **13**, 9230 (2005)
- 15 J He, W Ji, G H Ma, S H Tang, H I Elim, W X Sun, Z H Zhang and W S Chin; “*Excitonic nonlinear absorption in CdS nanocrystals studied using Z-scan technique*”, J. Appl. Phys. **95**, 6381 (2004)
- 16 Litty Irimpan, A Deepthy, Bindu Krishnan, V P N Nampoori and P Radhakrishnan; “*Nonlinear optical characteristics of self assembled films of ZnO*” Applied Physics B: Lasers and Optics (2008), doi: 10.1007/s00340-007-2886-1
- 17 Litty Irimpan, A Deepthy, Bindu Krishnan, L M Kukreja, V P N Nampoori and P Radhakrishnan; “*Effect of self assembly on the nonlinear optical characteristics of ZnO thin films*” Optics Communications (2008) doi:10.1016/j.optcom.2008.01.029
- 18 D.L. Moreno, E.D. Rosa-Cruz, F.J. Cuevas, L.E. Regalado, P. Salas, R. Rodriguez and V.M. Castano; “*Refractive index measurement of pure and Er³⁺-doped ZrO₂–SiO₂ sol-gel film by using the Brewster angle technique*”, Opt. Mat. **19**, 275 (2002)
- 19 Lin Guo, Shihe Yang, Chunlei Yang, Ping Yu, Jiannong Wang, Weikun Ge, and George K. L. Wong; “*Highly monodisperse polymer-capped ZnO nanoparticles: Preparation and optical properties*”, Appl. Phys. Lett. **76**, 2901 (2000)
- 20 J G E Gardeniers, Z M Rittersm and G J Burger; “*Preferred orientation and piezoelectricity in sputtered ZnO films*”, J. Appl. Phys. **83**, 7844 (1998)
- 21 A Kuroyanagi ; “*Properties of Aluminum-Doped ZnO Thin Films Grown by Electron Beam Evaporation*”, Jpn. J. Appl. Phys. **28**, 219 (1989)
- 22 Y B Band, D J Harter and R Bavli; “*Optical pulse compressor composed of saturable and reverse saturable absorbers*”, Chem. Phys. Lett. **126**, 280 (1986)
- 23 Ja-Hon Lin, Yin-Jen Chen, Hung-Yu Lin, and Wen-Feng Hsieh; “*Two-photon resonance assisted huge nonlinear refraction and absorption in ZnO thin films*” J. Appl. Phys. **97**, 033526 (2005)
- 24 M S Bahae, A A Said and E W van Stryland; “*High-sensitivity, single-beam n₂ measurements*”, Opt. Lett. **14**, 955 (1989)
- 25 Sheik-Bahae, M Hutchings, D C Hagan, D J Van, Stryland E W; “*Dispersion of bound electron nonlinear refraction in solids*”, IEEE JQE **27** (1991) 1296
- 26 W Zhang, H Wang, K S Wong, Z K Tang, G K L Wong and J Ravinder; “*Third-order*

- optical nonlinearity in ZnO microcrystallite thin films”, Appl. Phys. Lett.* **75**,3321 (1999)
- 27 C S Suchand Sandeep, Reji Philip, R Satheeshkumar and V Kumar; “*Sol-gel synthesis and nonlinear optical transmission in $Zn_{(1-x)}Mg_xO$ ($x \leq 0.2$) thin films”* *Appl. Phys. Lett.* **89**, 063102 (2006)
- 28 *CRC Handbook of Laser Science and Technology: Optical Materials*, edited by M. J. Weber ~CRC Press, Boca Raton, FL, (1997)
- 29 Gang Wang, G T Kiehne, G K L Wong, J B Ketterson, X Liu, and R P H Chang, “*Large second harmonic response in ZnO thin films”, Appl. Phys. Lett.*, **80**, 401 (2002)
- 30 P J Gonçalves, I E Borissevitch, L de Boni, N M Barbosa Neto, J J Rodrigues, Jr. and S C Zlio, XXVI Encontro Nacional de Física da Matéria Condensada, 2003 Caxambu. XXVI ENFMC-Annals of Optics, Vol. V5 (2003)
- 31 T H Wei, D J Hagan, M J Sence, E W Stryland, J W Perry and D R Coulter; “*Direct measurements of nonlinear absorption and refraction in solutions of phthalocyanines”, Appl. Phys. B: Lasers and optics* **54**, 46 (1992)



Chapter 5

Effect of Annealing on the spectral and NLO characteristics of thin films of nano ZnO

Abstract

The annealing effect on the spectral and nonlinear optical characteristics of ZnO thin films deposited on quartz substrates by sol gel process is investigated. As the annealing temperature increases from 300-1050°C, there is a decrease in the bandgap which indicates the changes of the interface of ZnO. Systematic studies on nano crystallites have indicated the presence of luminescence due to excitonic emissions when excited with 255 nm as well as significant contribution from surface defect states when excited with 325 nm. The intensity of UV peak remains the same while the intensity of the visible peak increases with increase in annealing temperature. The mechanism of the luminescence is discussed. Nonlinear optical response of these samples is studied using nanosecond laser pulses at off-resonance wavelengths. The nonlinear absorption coefficient increases from 2.9×10^{-6} m/W to 1.0×10^{-4} m/W when the annealing temperature is increased from 300°C to 1050 °C, mainly due to the enhancement of interfacial state and exciton oscillator strength. The third-order optical susceptibility $\chi^{(3)}$ increases with increase in annealing temperature (T) within the range of our investigations. In the weak confinement regime, $T^{2.5}$ dependence of $\chi^{(3)}$ is obtained for ZnO thin films. The role of annealing temperature on the optical limiting response is also studied.

The results of this chapter are published in
Litty Irimpan et.al., “Effect of annealing on the spectral and nonlinear optical
characteristics of thin films of nano ZnO” Journal of Applied Physics 2008 (In Press)

5.1 Introduction

ZnO as a compound semiconductor has drawn considerable attention for its excellent piezoelectric and optical properties¹ which make it useful to develop the fabrication of integrated acousto-optic devices and ultraviolet photonic devices². Because of its intrinsic thermal stability, ZnO is a good candidate for high temperature optoelectronic devices. ZnO films grown on silicon³⁻⁴, sapphire⁴⁻⁷, LiNbO₃^[8], GaAs^[9] and quartz¹⁰⁻¹² substrates have been studied and the properties such as photoluminescence^{3, 13-14}, optical absorption^{4,7,10,12} and optical nonlinearities^{6,11,15-17} have been investigated. ZnO films have been prepared using various techniques like sol-gel process, laser ablation⁴, laser deposition¹¹, electron beam evaporation⁷, molecular-beam epitaxy⁶ and sputtering^{3,5,9,10,12}. It has been found that the substrate temperature¹⁸, sputtering power^{5,19}, oxygen partial pressure^{5,20} and post-treatments^{10,12,21} may significantly influence the structure and optical properties of the films, since the electrical and the optical properties are strongly affected by the interface and the structure of the films. In this chapter, we present the effect of annealing on the spectral and nonlinear optical properties of the ZnO films on quartz substrates annealed within the temperature range of 300-1050°C.

5.2 Theory

As the temperature increases, the particle size increases due to thermal expansion. Over small temperature ranges, the fractional thermal expansion of uniform linear objects is proportional to the temperature change²². Different substances expand by different amounts and hence the knowledge of expansion coefficient is necessary to quantify the thermal expansion. The change in temperature determines the fractional change in length and hence the relationship governing the linear expansion of a long thin rod of length L_0 can be written as,

$$\Delta L = L_0 \alpha \Delta T \quad \text{and} \quad L = L_0 [1 + \alpha \Delta T] \quad (5.1)$$

where, ΔL is the change in length for a temperature change ΔT and α is the linear expansion coefficient. Area expansion is like a photographic enlargement.

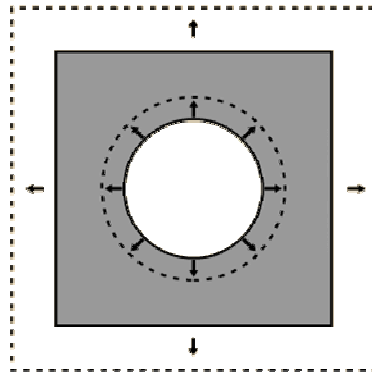


Figure 5.1 Thermal expansion of a material

Thermal expansion of an area, A can be calculated from the linear expansion coefficient.

$$A = L^2 = L_0^2 [1 + 2\alpha \Delta T + \alpha^2 \Delta T^2] \approx A_0 [1 + 2\alpha \Delta T] \quad (5.2)$$

and the expanded volume has the form,

$$V = L^3 = L_0^3 [1 + 3\alpha \Delta T + 3\alpha^2 \Delta T^2 + \alpha^3 \Delta T^3] \approx V_0 [1 + 3\alpha \Delta T] \quad (5.3)$$

since in most cases the quadratic and cubic terms in the above expression can be neglected because of the fact that the typical expansion coefficient is of the order of parts per million per degree celsius²². Every linear dimension increases by the same percentage with a change in temperature, including holes. This assumes that the expanding material is uniform. Thus as the temperature increases, the particle size increases and the size dependent enhancement of exciton oscillator strength is explained in detail in chapter 3.

Optical bandgap reductions with increase in temperature mainly arise from the change of the lattice constant²³. The temperature dependence of bandgap is given by²⁴

$$E_g(T) = E_g - \frac{\alpha\Theta}{2} \left[\sqrt[p]{1 + \left(\frac{2T}{\Theta} \right)^p} - 1 \right] \quad (5.4)$$

where α is the slope parameter, Θ is the average phonon temperature and p is the phonon dispersion parameter. Varshini approximation²⁵ is often employed using empirical parameters A and B is given by

$$E_g(T) = E_g - \frac{AT^2}{B+T} \quad (5.5)$$

For ZnO, the empirical Varshini parameters A and B are calculated to be 5.05×10^{-4} and 900 respectively²⁶ upto 300K.

5.3 Synthesis

The ZnO films are deposited on quartz substrates at room temperature by the technique of spin coating. A stable hydrolysed solution is prepared using stoichiometric quantities of zinc acetate dissolved in isopropyl alcohol and the solution is used for spin coating ZnO thin films on quartz substrates by rotating the deposition system at 2000 rotations per minute. The series of samples are then dried at 110°C for half an hour and then placed in a furnace for annealing. The samples are annealed at temperatures of 300°C , 600°C , 750°C , 850°C , 950°C and 1050°C and marked as a-300, b-600, c-750, d-850, e-950, f-1050 respectively. The samples are held at each temperature for three hours in air and then cooled to room temperature slowly with a cooling rate of 0.1°C per minute.

5.4 Absorption spectroscopy

Figure 5.2 gives the room temperature absorption spectra of the ZnO thin films. When the samples are held at each temperature for a short duration of less than one hour, there is no change in the absorption spectrum

since the temperature driven aggregation regains its original size with slow cooling. But when the samples are held at each temperature for a long duration of much greater than one hour followed by slow cooling, there exist an irreversible change in particle size which increases with increase in annealing temperature. The excitonic peak is found to be blue shifted (370-350 nm) with decrease in particle size with respect to that of bulk ZnO and this could be attributed to the confinement effects²⁷.

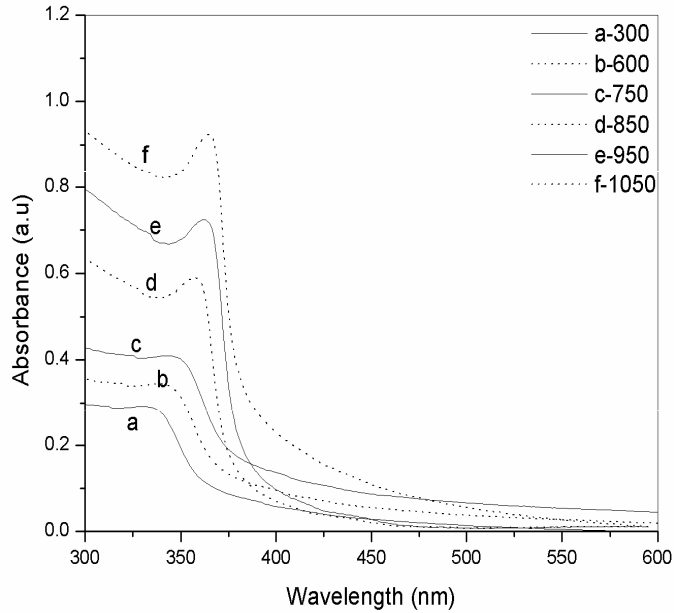


Figure 5.2: Absorption spectra of the ZnO thin films on quartz substrate at different annealing temperatures

By the quantum size effect in nanosized semiconductors, the bandgap increases when the size of the particle is decreased, resulting in a blueshift of the absorption bands. An order of magnitude estimate of the

particle size is possible from the absorption spectra and it is calculated as described in chapter 2.

The ZnO crystallite size increases exponentially from about 4 nm to 85 nm with the rise of the annealing temperature from 300 to 1050 °C as shown in figure 5.3. The quadratic term in equation 5.3 cannot be neglected since the thermal expansion coefficient²⁸ of ZnO is of the order of $7 \times 10^{-6} \text{ K}^{-1}$ and hence we get a nonlinear change in particle size with annealing temperature. In ZnO, the exciton Bohr radius is 2 nm and hence the average particle size of ZnO thin films comes under weak confinement²⁹ regime ($R > a_B$).

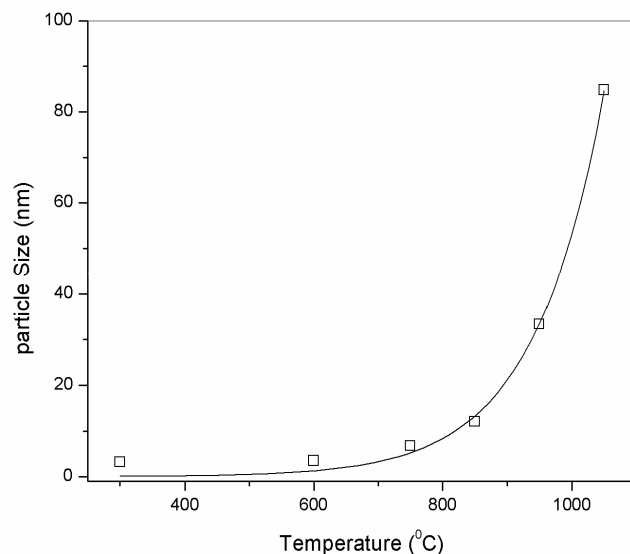


Figure 5.3: Variation of particle size as a function of annealing temperature for ZnO thin films

5.5 Optical bandgap

The direct bandgap is estimated from absorption spectrum as described in chapter 2. The absorption peak of the films shifted towards

lower energy at a higher annealing temperature. The optical bandgap (E_g) is found to be temperature dependent and there is a decrease in the bandgap of the semiconductor with increase in the annealing temperature as shown in figure 5.4. As the films are annealed at a higher temperature the crystallites began to move and tend to agglomerate easily. As a result, the bandgaps of the nanocomposites decrease with increasing annealing temperature.

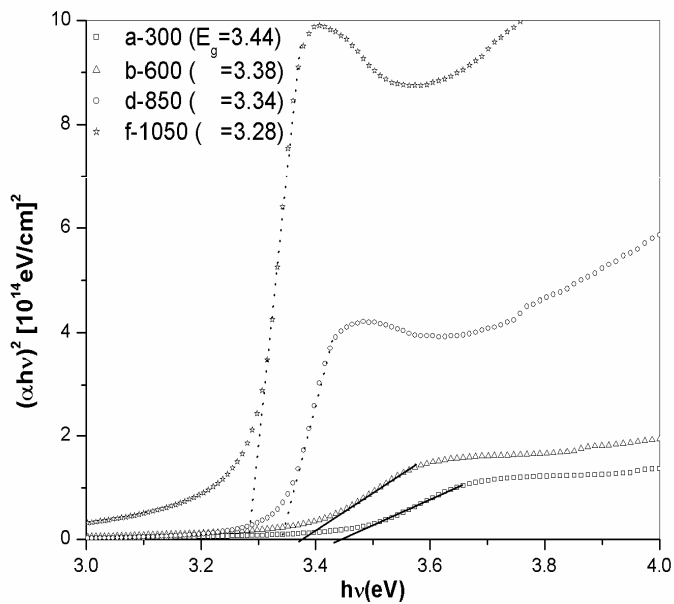


Figure 5.4: Optical bandgap of ZnO thin films at different annealing temperatures. Value of optical bandgap is given in the bracket in the inset legend

The shift of bandgap energy is related to the structural property. Since ZnO thin film has a tensile built-in strain, it can be relaxed by providing sufficient thermal energy. If the tensile strain is relaxed, the bandgap energy is decreased. The bandgap is found to vary in the range 3.28-

3.44 eV in the range of annealing temperatures from 300-1050°C and is in agreement with the reported value³⁰.

5.6 Fluorescence spectroscopy

The fluorescence spectra of nano ZnO colloids of different particle size for an excitation wavelength of 255 nm are shown in figure 5.5. Figure shows multiple emission peaks at 390 nm, 420 nm, 490 nm and 530 nm. Additional shoulders at 455 nm, 570 nm and 600 nm are present along with the emission peaks. These may be attributed to transition from various excited state energy levels of exciton to the ground level corresponding to $R \gg a_B$ case and the series of peaks can be modelled as a particle in a box problem as described in chapter 2.

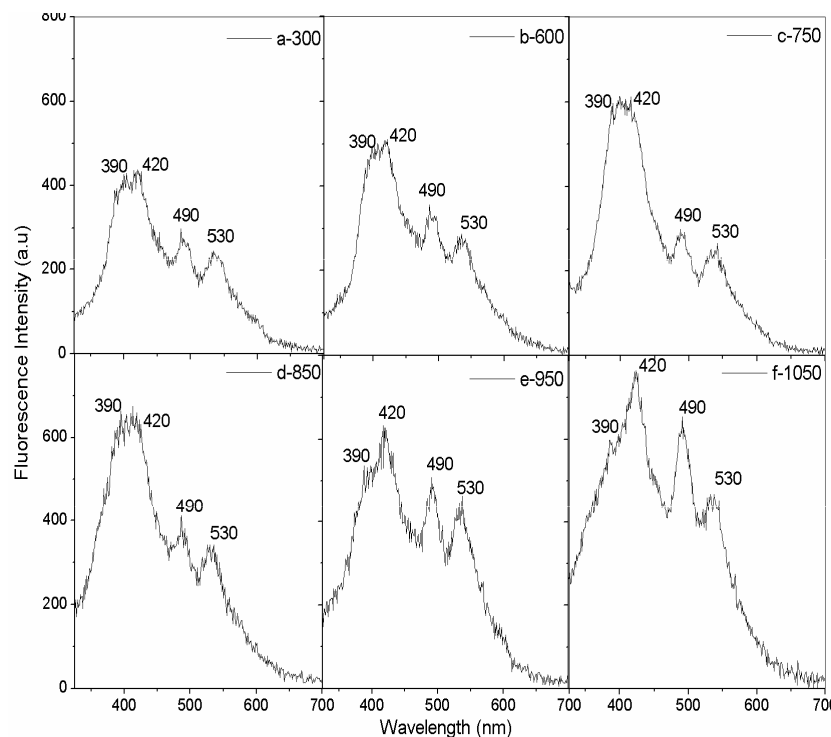


Figure 5.5: Fluorescence spectra of ZnO thin films at different annealing temperatures for an excitation wavelength of 255 nm

Figure 5.6 shows the fluorescence spectra of ZnO thin films annealed at different temperatures from 300-1050°C for an excitation wavelength of 325 nm. From the figure it is clear that two emission bands are present, a UV emission band and another in the green region. The transitions from different excited states of excitons may be weakened at this higher excitation wavelength and a broad visible emission due to surface defect states become more pronounced at 325 nm excitation wavelength. The UV band has been assigned to the bandgap fluorescence and the visible band is mainly due to surface defect states.

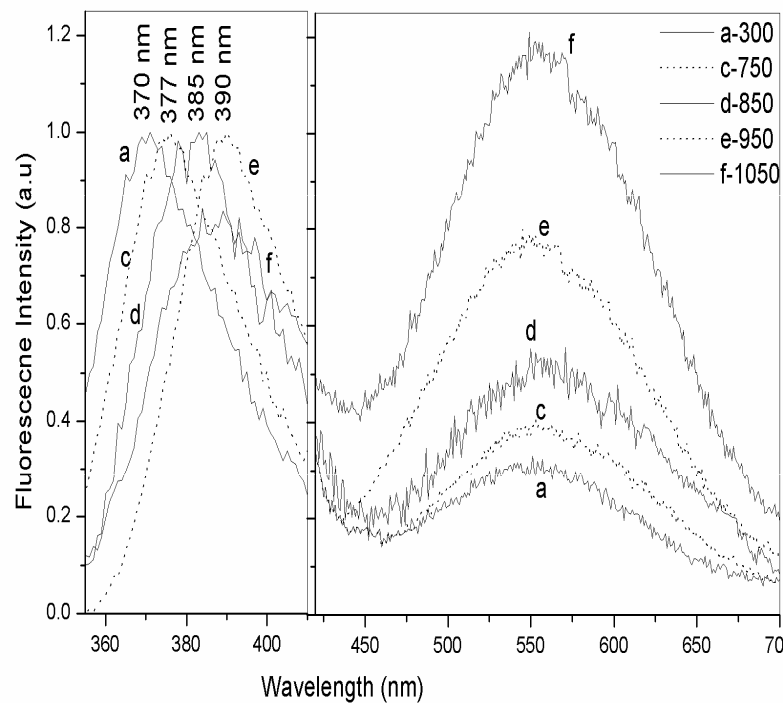
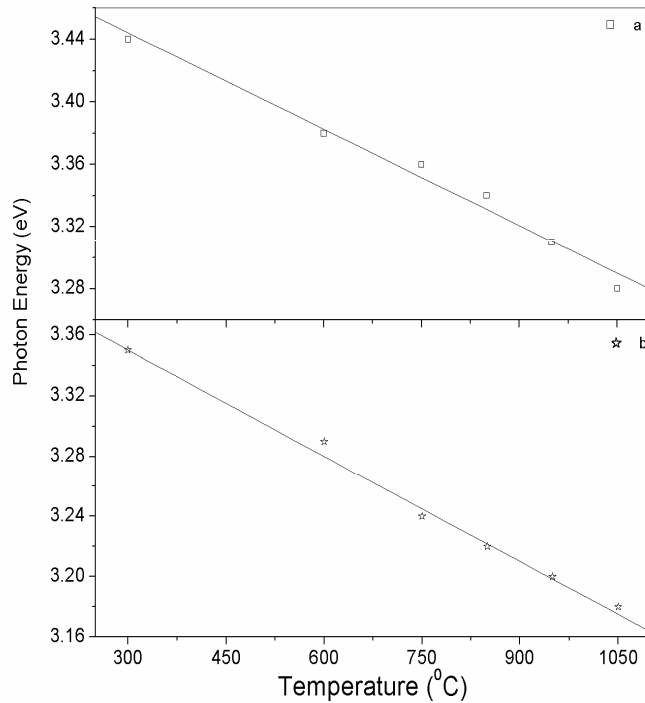


Figure 5.6: Fluorescence spectra of ZnO thin films at different annealing temperatures for an excitation wavelength of 325 nm

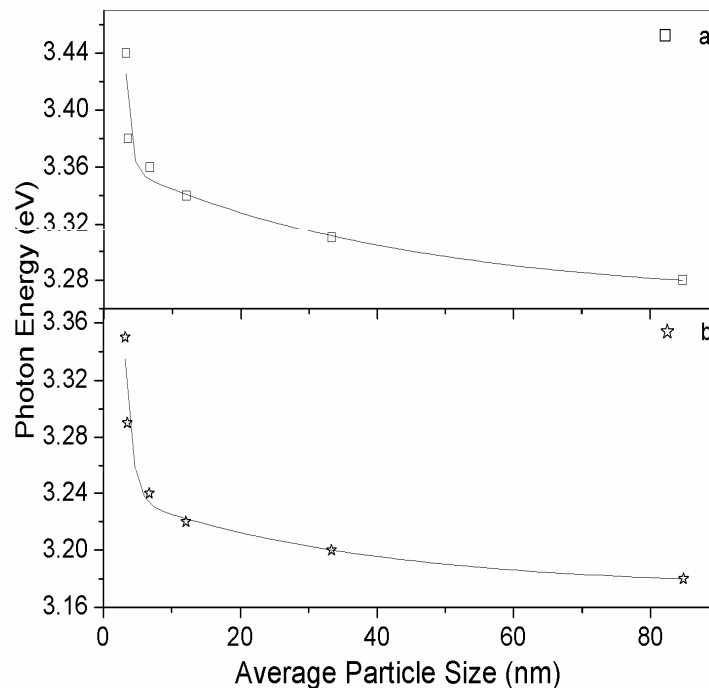
As the annealing temperature increases, this UV band undergoes a red shift with increase in particle size as in the case of absorption spectrum. For the intrinsic luminescence of ZnO nanoparticles, it is generally known that the formation of nanoparticles causes a red shift in the PL spectra due to quantum size effect³¹. The UV emission peak is shifted from 3.34 to 3.18 eV due to the shift of the optical bandgap from 3.44 to 3.28 eV and it clearly indicates that the origin of UV emission is the near band edge emission.

Figure 5.7(a) shows the bandgap change as a function of annealing temperature. Figure 5.7(b) shows the energy of the band to band transition as a function of the annealing temperature. Similarly figure 5.8(a) and 5.8(b) shows the bandgap change and energy of band to band transition respectively as a function of particle size.



*Figure 5.7:The dependence of annealing temperature on
(a) bandgap (b) band to band emission*

As clearly seen in figures 5.7 and 5.8, the red shift in the UV emission with annealing temperature (particle size) closely follows the red shift in the band edge, indicating that the two are related. Mean cluster size could be principally derived from the absorption measurements and the ZnO crystallite size increases exponentially from about 4 nm to 85 nm with the rise of the annealing temperature from 300 °C to 1050 °C as shown in figure 5.3. This allows us to reconstruct the size distribution curves from the fluorescence spectrum.



*Figure 5.8: The dependence of average particle size on
 (a) bandgap (b) band to band emission*

The intensity of the UV emission remains the same whereas the intensity of the green emission increases with annealing temperature. However, there is a decrease in the UV luminescence intensity at an

annealing temperature of 1050°C and this can be mainly because of the formation of interstitial vacancies when the films annealed at a high temperature.

As the annealing temperature increases, the intensity of green luminescence increases. The intensity of green emission becomes even stronger than that of UV emission at a annealing treatment of 1050°C . The intensity variation of green luminescence is systematically studied as a function of annealing temperatures in order to investigate the emission mechanism. The increase of green luminescence after annealing treatment means the increase of singly ionized oxygen vacancies according to the result of Vanheusden *et al.*³². Due to its *n*-type semiconductor nature, the most defects in ZnO are Zn interstitials and oxygen vacancies. The Zn interstitials in ZnO are easily ionized, and electrons produced by ionized Zn interstitials contribute to electrical conductivity and the number of Zn interstitials decreases probably due to Zn evaporation at increasing annealing temperatures³³. However, the number of oxygen vacancies increases with increase in annealing temperature. Therefore, the intensity of green luminescence increases with increase in annealing temperature. ZnO nanopowders and thin films also show green luminescence after they were annealed in oxygen, nitrogen or air³³.

The inset of figure 5.9 shows the variation of green photoluminescence (PL) intensity depending on annealing temperature. The intensity of green emission dramatically increases above an annealing temperature of 750°C . Figure 5.9 shows a break at a transition temperature of 740°C , suggesting a change in mechanism from a low temperature ($300\text{-}650^{\circ}\text{C}$) activated process to a high temperature ($750\text{-}1050^{\circ}\text{C}$) activated process. An indication of this change in process exists in the literature³⁴⁻³⁵. The practical significance of this observation is that it would now require

caution in extrapolating the high temperature data to represent behaviour in the low temperature regime.

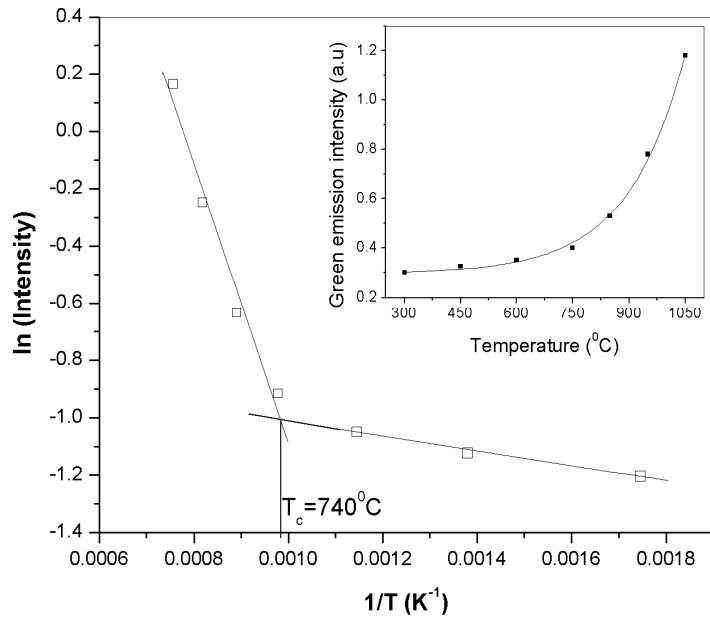


Figure 5.9: Variation of green PL intensity with annealing temperature

From these results, it is considered that many oxygen vacancies are generated due to the large lattice mismatch between the film and the substrate and provides high surface energy during the annealing process at and above the transition temperature of 740°C . Therefore the green emission related to the donor level is dominant due to the increase of oxygen vacancies (V_O^{2-}).

5.6.1 Luminescence mechanism

Figure 5.10 shows the emission mechanism of UV and visible luminescence of ZnO films. UV luminescence is caused by the transition from near conduction band edge to valence band. As temperature increases,

shift of UV luminescence is observed from 3.34 to 3.18 eV due to the shift of the optical energy gap from 3.44 to 3.28 eV. The green luminescence is mainly due to surface defect states. The UV luminescence center is not related to visible luminescence center. If green luminescence is related to the deep acceptor level, UV luminescence should have decreased as green luminescence increased. Based on these results, it can be concluded that the green luminescence of ZnO is not due to the transition from near band edge to deep acceptor level in ZnO but mainly due to the transition from deep donor level to valence band. But at 1050°C , the UV intensity decreases. This may be attributed to the transition from near band edge to deep acceptor level due to zinc vacancies ($\text{V}_{\text{Zn}}^{2+}$).

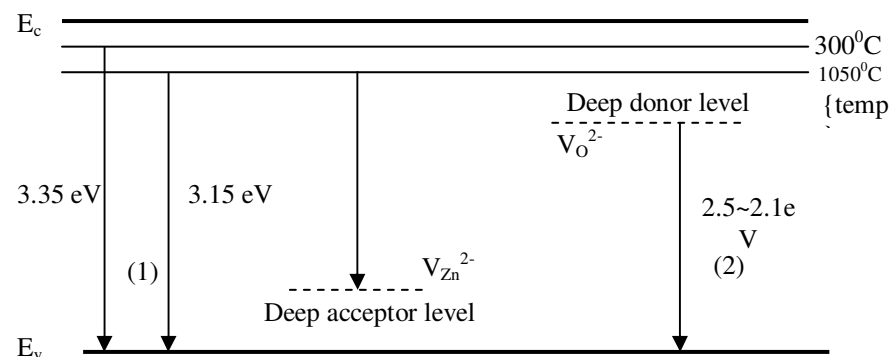


Figure 5.10: The UV and visible photoluminescence mechanism of ZnO

(1) transition from near conduction band edge to valence band

(2) transition from deep donor level to valence band

5.7 Nonlinear optical characterization

The third order nonlinear optical properties of thin films of nano ZnO are investigated using the z-scan technique and are explained in chapter 3. Film thickness is evaluated to be in the range of 60–100 nm. Figure 5.11

gives the open aperture z-scan traces of ZnO films annealed at different temperatures at a typical fluence of 300 MW/cm^2 . The open aperture curve exhibits a normalized transmittance valley, indicating the presence of induced absorption in the ZnO thin films.

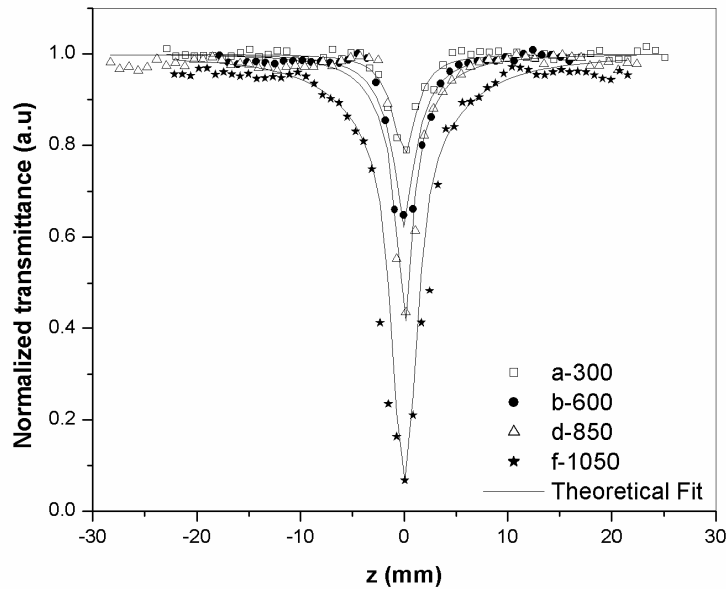


Figure 5.11: The open aperture z-scan traces of ZnO thin films at different annealing temperatures at a fluence of 300 MW/cm^2

Figure 5.12 gives the closed aperture z-scan traces of ZnO films annealed at different temperatures at a fluence of 300 MW/cm^2 . The closed aperture curve exhibited a peak-to-valley shape, indicating a negative value of the nonlinear refractive index n_2 . It is observed that the peak-valley of the closed-aperture z-scan satisfied the condition $\Delta z \sim 1.7 z_0$, thus confirming the presence of cubic nonlinearity³⁶.

The enhancement of nonlinear optical properties with increasing dimension in accordance with increasing annealing temperature in the weak

confinement regime essentially originates from the size dependent enhancement of oscillator strength of coherently generated excitons and is explained in detail in chapter 3. The susceptibility is size dependent, without showing a saturation behavior in the size range studied in our investigation.

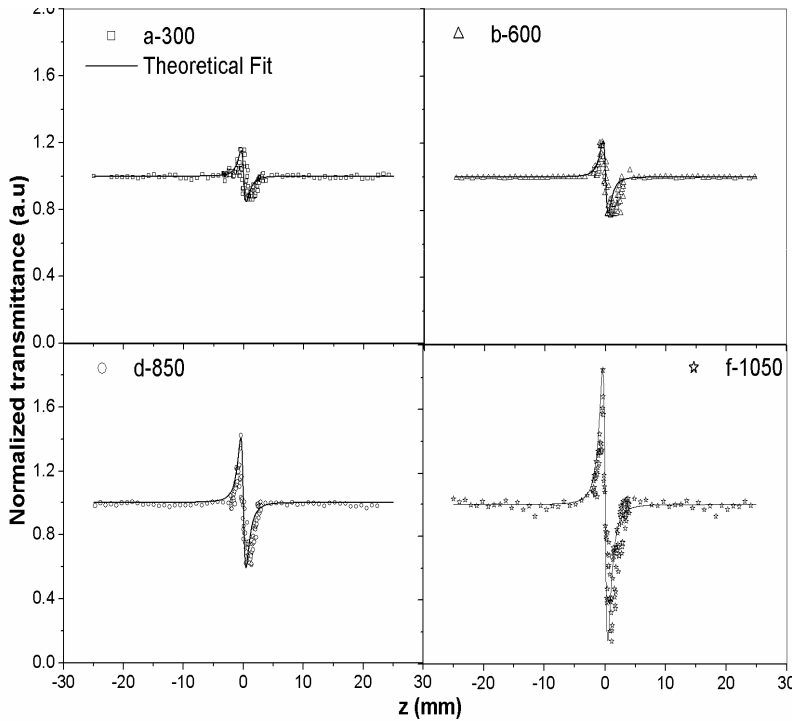


Figure 5.12: The closed aperture z-scan traces of ZnO thin films at different temperatures at a fluence of 300 MW/cm²

The experimentally obtained values of nonlinear parameters at an intensity of 300 MW/cm² are shown in table 5.1. The nonlinear absorption coefficient is reported to increase from 1.2×10^{-9} m/W to 1.1×10^{-8} m/W when the annealing temperature rises from 950°C to 1050°C for ZnO microcrystalline films developed by sputtering technique³⁰. The enhancement of nonlinear coefficients for our thin nanocrystalline films compared to microcrystalline films of ZnO is attributed to the nanosized structure of the

films since it has been reported that the reduced dimensionality of the particles resulted in considerable enhancement of the second-order susceptibility $\chi^{(2)}$ in thin films of ZnO³⁷. Similar results in the third order nonlinear parameters are evident in our measurements also. Thus, the real and imaginary parts of third-order nonlinear optical susceptibility measured by the z-scan technique revealed that the ZnO thin films investigated in the present study have good nonlinear optical response and could be chosen as ideal candidates with potential applications in nonlinear optical devices.

Annealing temperature °C	β 10^{-6} m/W	n ₂ 10^{-5} esu	Im($\chi^{(3)}$) 10^{-6} esu	Re $\chi^{(3)}$ 10^{-6} esu	$ \chi^{(3)} $ 10^{-6} esu
300	2.9	-1.1	0.1	-2.3	2.3
600	6.9	-1.5	0.3	-3.1	3.2
750	13.8	-2.1	0.6	-4.5	4.6
850	19	-2.8	0.8	-6	6.1
950	51.8	-3.5	2.2	-7.5	7.8
1050	103.7	-5.9	4.5	-12.6	13.4

Table 5.1: Measured values of nonlinear absorption coefficient, nonlinear refractive index and third order susceptibility of ZnO thin films at an intensity of 300 MW/cm² for an irradiation wavelength of 532 nm at different annealing temperatures

Figure 5.13 shows the variation of $\chi^{(3)}$ as a function of annealing temperature. The data shows an exponential increase of $\chi^{(3)}$ values with increasing temperature and the values range from 2.3×10^{-6} to 1.3×10^{-5} esu for T=300-1050°C. For the samples annealed below 750 °C, the absolute value

of $\chi^{(3)}$ does not change significantly, but for ones annealed above 750 °C, the $\chi^{(3)}$ value increases rapidly with the increase of the annealing temperature. At lower temperatures and for films with small size, $\chi^{(3)}$ is small indicating that it is a third order effect³⁶ resulting from two photon absorption (TPA). For films of larger particle size and at higher temperatures, $\chi^{(3)}$ becomes very large indicating the occurrence of higher order nonlinear processes such as free carrier absorption. For samples annealed at higher temperatures, the $\chi^{(3)}$ value increases rapidly because of the interdiffusion of the SiO₂ substrates and ZnO films and interfacial state enhancement³⁰.

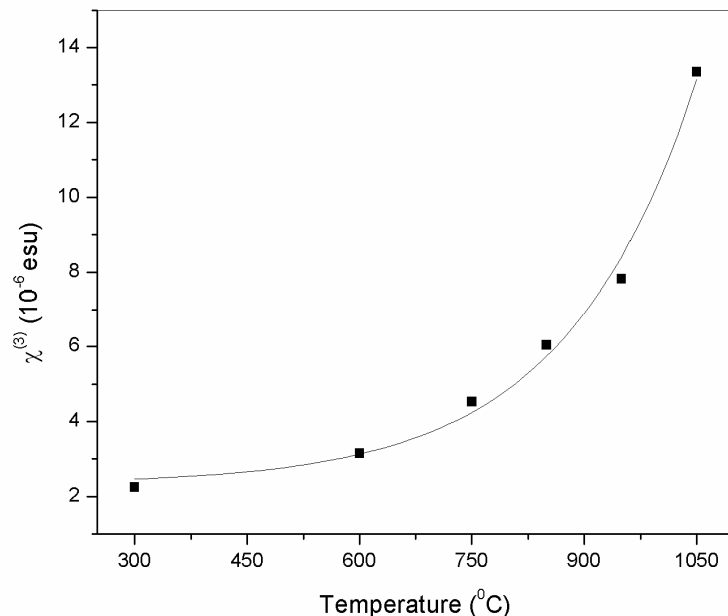


Figure 5.13: Variation of $\chi^{(3)}$ as a function of annealing temperature

For samples annealed at 1050°C, the $\chi^{(3)}$ value is one order of magnitude larger than that at 950°C due to the interfacial state enhancement. Furthermore, as the ZnO nanocrystallites are melted into the SiO₂ substrate, the local field effect and the interband transition of electrons from the

interfacial state to the unoccupied state near the Fermi level will greatly enhance the nonlinear absorption³⁸.

In order to obtain the annealing temperature and particle size dependence of the third-order susceptibility, $\ln(T)$ and $\ln(R)$ are plotted against $\ln(\chi^{(3)})$ and are shown in figure 5.14. When we apply a least-squares fit, a temperature dependence of $T^{2.5}$ and a size dependence of R^2 is obtained indicating an enhancement of more than two orders of magnitude. From the graph, $\ln(\chi^{(3)}) \approx 2\ln(T)$ and $\chi^{(3)} \approx T^{2.5}$

$$\ln(\chi^{(3)}) \approx 2\ln(R) \text{ and } \chi^{(3)} \approx R^2$$

This dependence is in good agreement with that observed for CdS, CuCl and CuBr nanocrystals and ZnO colloids³⁹⁻⁴².

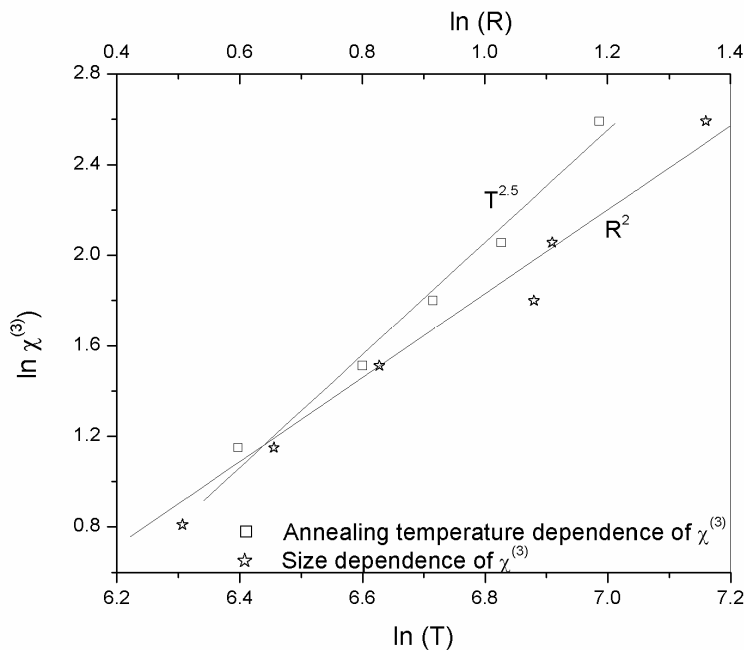


Figure 5.14: Dependence of $\chi^{(3)}$ as a function of annealing temperature and particle size for ZnO thin films. The straight lines indicate $T^{2.5}$ and R^2 dependence

5.8 Optical limiting

Optical limiters are devices that transmit light at low input fluences or intensities, but become opaque at high inputs. To examine the effect of annealing on optical limiting property of thin films of nano ZnO, the nonlinear transmission of the film is studied as a function of input fluence for different annealing temperatures. The optical limiting property occurs mostly due to absorptive nonlinearity and can be generated from z-scan traces⁴³. Figure 5.15 illustrates the influence of annealing temperature on the optical limiting response.

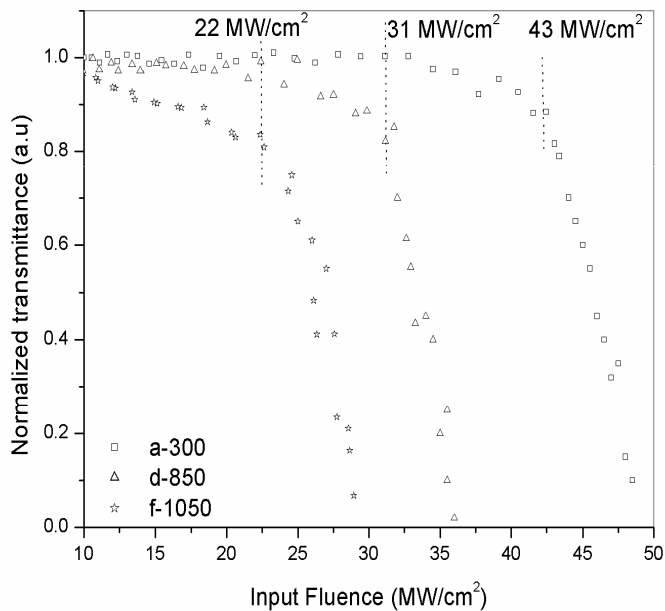


Figure 5.15: Optical limiting curves of ZnO thin films at different annealing temperatures

It is obvious that the lower the optical limiting threshold, the better the optical limiting material. The optical limiting threshold is found to be

high in the case of ZnO films annealed at a temperature of 300°C (43 MW/cm^2) in comparison with the ZnO films annealed at a temperature of 850°C (31 MW/cm^2) and ZnO films annealed at a temperature of 1050°C (22 MW/cm^2). These values are comparable to the reported optical limiting threshold for ZnO nano colloids of different particle size^{39, 42}. Annealing temperature and hence particle size has a significant effect on the optical limiting performance of ZnO films. Increasing the annealing temperature reduces the limiting threshold and enhances the optical limiting performance. From the measured values of β for the ZnO films, it can be seen that the film annealed at a higher temperature and having larger particle size is a better nonlinear absorber and hence a good optical limiter.

5.9 Conclusions

The annealing effect on the spectral and nonlinear optical characteristics of ZnO thin films deposited on quartz substrates by sol gel process is investigated. As the annealing temperature increases from $300-1050^{\circ}\text{C}$, there is a decrease in the bandgap which indicates the changes of the interface of ZnO with substrate. Systematic studies on nano crystallites have indicated the presence of luminescence due to excitonic emissions when excited with 255 nm as well as significant contribution from surface defect states when excited with 325 nm. The intensity of UV peak remains the same while the intensity of the visible peak increases with increase in annealing temperature. The mechanism of the luminescence suggests that UV luminescence of ZnO thin films is related to the transition from conduction band edge to valence band, and green luminescence is caused by the transition from deep donor level resulting from oxygen vacancies to valence band. Nonlinear optical response of these samples is studied using nanosecond laser pulses at an off-resonance wavelength for optical limiting applications. The third order nonlinear susceptibility increases from 2.3×10^{-6} to $1.3 \times 10^{-5} \text{ esu}$ when the annealing temperature rises from 300°C to 1050°C ,

mainly due to the enhancement of interfacial state and exciton oscillator strength. We have experimentally studied optical nonlinearity as a function of temperature and a $T^{2.5}$ dependence of nonlinear susceptibility is obtained for thin films of nano ZnO. Optical limiting response is temperature dependent and the film annealed at higher temperature and having larger particle size is a better nonlinear absorber and hence a good optical limiter.

5.10 References

- 1 W D Hunt; “*Isomorphic surface acoustic waves on multilayer structures*”, J. Appl. Phys. **89**, 3245 (2001)
- 2 H Cao, Y G Zhao, S T Ho, E W Seelig, Q H Wang and R P H Chang, “*Random Laser Action in Semiconductor Powder*”; Phys. Rev. Lett. **82**, 2278 (1999)
- 3 J G Ma, Y C Liu, R Mu, J Y Zhang, Y M Lu, D Z Shen, and X W Fan; “*Method of control of nitrogen content in ZnO films: Structure and photoluminescence properties*”, J. Vac. Sci. Technol. B **22**, 94 (2004)
- 4 V Srikant and D R Clarke; “*Optical absorption edge of ZnO thin films: the effect of substrate*”, J. Appl. Phys. **81**, 6357 (1997)
- 5 I Sayago, M Aleixandre, A Martinez, M J Fernandez, J P Santos, J Gutierrez, I Gracia and M C Horrillo; “*Structure studies of Zinc oxide films grown by RF magnetron sputtering*”, Synth. Met. **148**, 37 (2005)
- 6 W L Zhang, H Wang, K S Wong, Z K Tang, G K L Wong, R Jain; “*Third-order optical nonlinearity in ZnO microcrystallite thin films*”, Appl. Phys. Lett. **75**, 3321 (1999)
- 7 N R Aghamalyan et.al.; “*Influence of thermal annealing on optical and electrical properties of ZnO films prepared by electron beam evaporation*”, Semicond. Sci. Technol. **18**, 525 (2003)
- 8 C L Jia, K M Wang, X L Wang, X J Zhang, F Lu; “*Formation of c-axis oriented ZnO optical waveguides by r-f magnetron sputtering*”, Opt. Express **13**, 5093 (2005)
- 9 M K Ryu, S H Lee, M S Jang, G N Panin and T W Kang; “*Postgrowth annealing effect on structure and optical properties of ZnO films grown on GaAs substrates by the radio frequency magnetron sputtering technique*”, J. Appl. Phys. **92**, 154 (2002)
- 10 R J Hong, J B Huang, H B He, Z X Fan and J D Shao; “*Influence of different post-treatments on the structure and optical properties of zinc oxide thin films*”, Appl. Surf. Sci. **242**, 346 (2005)
- 11 J H Lin, Y J Chen, H Y Lin and W F Hsieh; “*Two-photon resonance assisted huge nonlinear refraction and absorption in ZnO thin films*”, J. Appl. Phys. **97**, 033526 (2005)

- 12 V Gupta and A Mansingh; “*Influence of post-deposition annealing on the structural and optical properties of sputtered zinc oxide film*”, J. Appl. Phys. **80**, 1063 (1996)
- 13 Y W Hong and J H Kim; “*The electrical properties of Mn₃O₄-doped ZnO*”, Ceram. Int. **30**, 1301 (2004)
- 14 D H Zhang, Q P Wang and Z Y Xue; “*Photoluminescence of ZnO films excited with light of different wavelength*”, Appl. Surf. Sci. **207**, 20 (2003)
- 15 G M Jia, G Z Zhang, W H Xiang and J B Ketterson, “*Measurement of the Third-order Nonlinear Optical Coefficient of ZnO Crystals by Using ICCD-Z-Scan*”, Chin. Phys. Lett. **21**, 1356 (2004)
- 16 X J Zhang, W Ji and S H Tang; “*Determination of optical nonlinearities and carrier lifetime in ZnO*”, JOSAB **14**, 1951 (1997)
- 17 X Zhang, H Fang, S Tang, W Ji, “*Determination of two-photon-generated free-carrier lifetime in semiconductors by Z-scan technique*”, Appl. Phys. B **65**, 549 (1997)
- 18 S S Lin, J L Huang and D F Liil; “*Effect of substrate temperature on the properties of Ti-doped ZnO films by simultaneous rf and dc magnetron sputtering*”, Mater. Chem. Phys. **90**, 22 (2005)
- 19 X H Yu, J Ma, F Ji, Y H Wang, X J Zhang, C F Cheng and H L Ma; “*Effects of sputtering power on the properties of ZnO:Ga films deposited by r. f. magnetron-sputtering at low temperature*”, J. Cryst. Growth **274**, 474 (2005)
- 20 R J Hong, H J Qi, J B Huang, H B He, Z X Fan and J D Shao; Thin Solid Films **473**, 58 (2005)
- 21 Z B Fang, Z J Yan, Y S Tan, X Q Liu and Y Y Wang; “*Influence of post-annealing treatment on the structure properties of ZnO films*”, Appl. Surf. Sci. **241**, 303 (2005)
- 22 <http://hyperphysics.phy-astr.gsu.edu/hbase/hframe.html>
- 23 Joachin Piprek; “*Semiconductor optoelectronic devices: Introduction to physics and simulation*”, Academic press, Elsevier -USA (2003)
- 24 R Passler; Phy. Stat. Solidi (b) **216**, 975 (1999)
- 25 Y P Varshni; “*Temperature dependence of the energy gap in semiconductors*” Physica **34**, 149 (1967)
- 26 C Jagadish and S J Pearton; “*ZnO: bulk, thin films and nanostructures: Processing, properties and applications*” Elsevier (2006)
- 27 D Luna-Moreno, E De la Rosa-Cruz, F J Cuevas, L E Regalado, P Salas, R Rodríguez and V M Castano; “*Refractive index measurement of pure and Er³⁺-doped ZrO₂–SiO₂ sol-gel film by using the Brewster angle technique*”, Opt. Mat., **19**, 275 (2002)
- 28 V Kumar and B S R Sastry; “*Thermal expansion coefficient of binary semiconductors*”, Cryst. Res. Technol. **36** (6), 565 (2001)
- 29 H L Cao, X F Qian, Q Gong, W M Du, X D Ma and Z K Zhu; “*Shape- and size-controlled synthesis of nanometre ZnO from a simple solution route at room*

- temperature*”, Nanotechnology **17**, 3632 (2006)
- 30 Y B Han, J B Han, S Ding, D J Chen and Q Q Wang “*Optical nonlinearity of ZnO microcrystallite enhanced by interfacial state*”, Opt. Express, **13** (23), 9211 (2005)
- 31 Litty Irimpan, A Deepthy, Bindu Krishnan, V P N Nampoori and P Radhakrishnan, J. Appl. Phys. **102**, 063524 (2007)
- 32 K. Vanheusden, W. L. Warren, C. H. Seager, D. R. Tallant, J. A. Voigt, and B. E. Gnade; “*Mechanisms behind green photoluminescence in ZnO phosphor powders*”, J. Appl. Phys., **79**, 7983 (1996)
- 33 J.Z. Wang, G.T. Du, Y.T. Zhang, B.J. Zhao, X.T. Yang, D.L. Liu; “*Luminescence properties of ZnO films annealed in growth ambient and oxygen*”, J. Crystal Growth., **263**, 269 (2004)
- 34 T K Gupta,W D Straub; “*Effect of annealing on the ac leakage components of the ZnO varistor. I. Resistive current*” J. Appl. Phys. **68**, 845 (1990)
- 35 V Gavryushin, G Raciukaitis, D Judožbalis, A Kazlauskas and V Kubertavicius; “*Characterization of intrinsic and impurity deep levels in ZnSe and ZnO crystals by nonlinear spectroscopy*” J. Cryst. Growth, **138**, 924 (1994)
- 36 M S Bahae, A A Said and E W van Stryland; “*High-sensitivity, single-beam n_2 measurements*”, Opt Lett, **14**, 955 (1989)
- 37 Gang Wang, G. T. Kiehne, G. K. L. Wong, J. B. Ketterson, X. Liu, and R. P. H. Chang; “*Large second harmonic response in ZnO thin films*”, Appl. Phys. Lett. **80**, 401, (2002)
- 38 R. G. Xie, J. Q. Zhuang, L. L. Wang, W. S. Yang, D. J. Wang, T. J. Li and J. N. Yao, “A WO₃/ZnO nanoparticle composite system with high photochromic performance,” Chem. J. Chinese U. **24**, 2086 (2003)
- 39 W Jia, E P Douglas, Fenggi Guo and Wenfang Suna; “*Optical limiting of semiconductor nanoparticles for nanosecond laser pulses*”, Appl. Phys. Lett. **85** (26), 6326 (2004)
- 40 Takumi Kataoka, Takashi Tokizaki and Arao Nakamura, “*Mesoscopic enhancement of optical nonlinearity in CuCl quantum dots: Giant-oscillator strength effect on confined excitons*”, Physical Review B, **48**, 2815 (1993)
- 41 Yingli Li, Masaki Takata and Arao Nakamura; “*Size-dependent enhancement of nonlinear optical susceptibilities due to confined excitons in CuBr nanocrystals*”, Physical Review B, **57**, 15 (1998)
- 42 Litty Irimpan, Bindu Krishnan, A Deepthy, V P N Nampoori and P Radhakrishnan; Journal of applied physics **103**, 033105 (2008)
- 43 F. M. Qureshi, S.J. Martin, X. Long, D.D.C. Bradley, F.Z. Heneri, W.J. Balu, E.C. Smith, C.H. Wang, A.K. Kar and H.L. Anderson; “*Optical limiting properties of a zinc porphyrin polymer and its dimer and monomer model compounds*”, Chem. Phys., **231**, 87 (1998)



Chapter 6

Spectral and NLO characteristics of ZnO nanocomposites

Abstract

The spectral and nonlinear optical properties of ZnO based nanocomposites prepared by colloidal chemical synthesis are investigated. Very strong UV emissions are observed from ZnO-Ag, ZnO-Cu and ZnO-SiO₂ nanocomposites. The strongest visible emission of a typical ZnO-Cu nanocomposite is over ten times stronger than that of pure Cu due to transition from deep donor level to the copper induced level. The optical band gap of ZnO-CdS and ZnO-TiO₂ nanocomposites is tunable and emission peaks changes almost in proportion to changes in band gap. Nonlinear optical response of these nanocomposites is studied using nanosecond laser pulses from a tunable laser in the wavelength range of 450-650 nm at resonance and off-resonance wavelengths. The nonlinear response is wavelength dependent and switching from RSA to SA has been observed at resonant wavelengths. Such a change-over is related to the interplay of plasmon/exciton band bleach and optical limiting mechanisms. The observed nonlinear absorption is explained through two photon absorption followed by weak free carrier absorption, interband absorption and nonlinear scattering mechanisms. The nonlinearity of the silica colloid is low and its nonlinear response can be improved by making composites with ZnO and ZnO-TiO₂. The increase of the third-order nonlinearity in the composites can be attributed to the enhancement of exciton oscillator strength. This study is important in identifying the spectral range and the composition over which the nonlinear material acts as an RSA based optical limiter. These nanocomposites can be used as optical limiters and are potential materials for the light emission and for the development of nonlinear optical devices with a relatively small limiting threshold.

The results of this chapter are published in

1. Litty Irimpan, V P N Nampoori and P Radhakrishnan; “*Spectral and nonlinear optical characteristics of nanocomposites of ZnO-Ag*” Chemical Physics Letters **455** (4-6), 265-269 (2008)
2. Litty Irimpan, V P N Nampoori and P Radhakrishnan; “*Spectral and nonlinear optical characteristics of nanocomposites of ZnO-CdS*” Journal of Applied Physics **103**, 094914 (2008)
3. Litty Irimpan, Bindu Krishnan, V P N Nampoori and P Radhakrishnan; “*Luminescence tuning and enhanced nonlinear optical properties of nanocomposites of ZnO-TiO₂*” Journal of Colloids and Interface Science **324** (1-2), 99-104 (2008)
4. Litty Irimpan, Bindu Krishnan, V P N Nampoori and P Radhakrishnan; “*Nonlinear optical characteristics of nanocomposites of ZnO-TiO₂-SiO₂*” Optical Materials, 2008 DOI:10.1016/j.optmat.2008.05.009
5. Litty Irimpan, V P N Nampoori and P Radhakrishnan; “*Enhanced luminescence and nonlinear optical properties of nanocomposites of ZnO-Cu*” Journal of Materials Research 2008 (in press)
6. Litty Irimpan, Bindu Krishnan, V P N Nampoori and P Radhakrishnan; “*Linear and nonlinear optical characteristics of ZnO-SiO₂ nanocomposites* ” Applied Optics, 2008 (in press)

*“If I have made any valuable discoveries, it has been owing
to patient attention that to any other talent”*

: Issac Newton

6.1 Introduction

The field of nanocomposite materials has been widely recognized as one of the most promising and rapidly emerging research areas¹⁻². There are some material designs to strengthen and toughen ceramics by using composite techniques to incorporate particulate, whisker or platelet reinforcement. Recent investigations have shown that ceramic composites having nano-sized metal particulate dispersions show excellent optical, electrical and mechanical properties³. Promising applications are expected or have already been realized in many fields of technology such as optical and electronic materials, solid electrolytes, coating technology and catalysis. Significant investigations have been done in the photophysical and photochemical behavior of single and multicomponent metal and semiconductor nanoclusters¹. Such composite materials are especially of interest in developing efficient light-energy conversion systems and optical devices. For example, photoinduced deposition of noble metals such as Pt or Au on semiconductor nanoclusters has often been employed to enhance their photocatalytic activity².

With many advantages such as low cost, nontoxicity and stability, ZnO is becoming a very promising *n*-type oxide semiconductor. Most of the work has been devoted to the electrical and fluorescent properties of ion-doped zinc oxide materials⁴, while only a few reports can be found using ZnO as the matrix for nanoparticle composite films⁵. These nanocomposites may lead to optically functional properties. In this study, therefore, the nanocomposite techniques are applied to improve the spectral and optical properties of ZnO^[6-9].

Optical nonlinearity of metal nanoparticles in a semiconductor has attracted much attention because of the high polarisability and fast nonlinear response that can be utilised in making them as potential optical devices^{1,10}. It is well known that noble metal nanoparticles show an absorption due to

surface plasmon resonance (SPR) in the visible region¹. Out of various metal nanoparticles, silver, copper and gold are extensively studied in colloids, thin films and in different glass matrices for their nonlinear optical properties¹¹.

In recent years, interest in the synthesis, characterization, and application of colloidal “quantum dot” semiconductor materials has grown markedly¹². Nanocrystals of cadmium sulfide are by far the most studied system among all the semiconducting nanocrystals¹³. The bulk CdS has a direct band gap of 2.4 eV at 300 K, and the typical Bohr exciton diameter of CdS is around 5.8 nm; consequently, CdS nanocrystals in the size range of 1–6 nm show sizable quantum confinement effects with remarkably different optical properties. The size dependent, unusual optical and electronic properties of these nanocrystals have been studied in detail using a wide variety of experimental and theoretical techniques¹⁴. Nanoscale composite materials containing titanium oxides are interesting because of their potential applications in optoelectronic devices and the bulk TiO₂ has a direct band gap¹⁵ of 3.2 eV. A great deal of research effort has been focused on both synthesis of TiO₂ nanocomposites, and on their linear optical properties. Recently the nonlinear optical properties of such materials have also received attention. A large, reverse saturable type of nonlinear absorption is observed in polystyrene maleic anhydride-TiO₂ nanocomposites with a continuous wave He-Ne laser beam¹⁶.

Extensive investigations of the photoluminescence and the third order optical nonlinearities of nanometer-sized semiconductor materials have demonstrated interesting physical properties and potential applications. The absorption and luminescent properties of TiO₂, CdS and PbS particles can be easily tuned by selecting appropriate matrix materials¹⁷. Recently, a microemulsion technique has been developed to prepare semiconductor nanocomposites such as ZnS/CdSe, ZnSe/CdSe, ZnS/CdS or TiO₂-SiO₂ in a core-shell structure¹⁸. Chemically synthesized semiconductor

nanocomposites offer necessary and basic materials promising colour-tunable, flexible, all-purpose chromophore systems, in which the strong quantum confinement effect of the carriers leads to unique, size dependent linear and nonlinear optical properties¹⁹.

The synthesis of new nonlinear optical materials based on transparent semiconductor and insulator that contain metal nanoparticles is nowadays of great interest for applications in nonlinear optics¹. For optical limiting applications it is necessary that the sample possess low linear losses and high nonlinear losses. Nonlinear losses can be due to multiphoton absorption, reverse saturable absorption, nonlinear scattering, and self-action of laser radiation²⁰ (Kerr and thermal self-focusing and self-defocusing).

Soon after the reporting of stimulated UV emission of ZnO at room temperature, ZnO attracted the people's attention as an UV laser material². Effective UV random lasing has been observed from patterned p-SiC(4H)/i-ZnO–SiO₂ nanocomposite films under optical excitation²¹. UV random lasing can be achieved in these composites because the appropriate patterning of ZnO clusters enhances the optical quality (i.e., higher gain and lower loss) of the random media. However, the improvement of UV emission and the simplification of growth techniques are still very important. Different metal particles, organic nanocrystals and fullerenes doped in sol-gel glasses and silica composites are well studied for optical limiting applications^{1,3}. It is also known that doping significantly improves the limiting performance of ZnO.

In this chapter we present the spectral and nonlinear optical properties of ZnO-Ag, ZnO-Cu, ZnO-CdS, ZnO-TiO₂, ZnO-SiO₂ and ZnO-TiO₂-SiO₂ nanocomposites. Ag and Cu are selected to prepare metal-semiconductor nanocomposites with ZnO, because of their interesting optical properties in the visible range which gives rise to wide applications in optoelectronic devices. Our results show that ZnO-CdS and ZnO-TiO₂

nanocomposites possess bandgap engineering, fluorescence tuning, very large optical nonlinearity and have a great potential for optical switching and optical communications. The nonlinearity of the silica colloid is low and its optical limiting response can be improved by making composites with ZnO and ZnO-TiO₂ which gives rise to wide applications in optoelectronic devices.

6.2 Theory

A crucial step in designing modern optoelectronic devices is the realization of bandgap engineering to create barrier layers and quantum wells in device heterostructures²². In order to realize such optoelectronic devices, modulation of the bandgap is required. To boost the concentration of electrons and holes, impurity atoms are introduced into the semiconductor crystal²³. The energy gap of the semiconductor A_xZn_{1-x}O (where A=Mg, Cd) is determined by the following equation²⁴,

$$E_g(x) = (1-x)E_{ZnO} + xE_{AO} - bx(1-x) \quad (6.1)$$

where b is the bowing parameter and E_{ZnO} and E_{AO} are the bandgap energies of compounds AO and ZnO respectively. The bowing parameter depends on the difference in electronegativities of the end binaries ZnO and AO.

High carrier concentrations in conduction and valence bands lead to bandgap reduction due to enhanced carrier-carrier interaction²⁵. The reduction in bandgap, ΔE_g can be derived from many-body theory²⁶ as a function of the static dielectric constant ϵ_{st} , rest mass of electron m₀, the effective masses m_c and m_v, the number density N (N=n=p) and the temperature T. It is given by

$$\Delta E_g = -C \left[\frac{\epsilon_{st}^5}{N} \left(m_0 \frac{m_c + m_v}{m_c m_v} + BT^2 \frac{\epsilon_{st}}{N} \right) \right]^{1/4} \quad (6.2)$$

where the fit parameters C and B are $3.9 \times 10^{-5} \text{ eVcm}^{3/4}$ and $B = 3.1 \times 10^{12} \text{ cm}^{-3} \text{ K}^{-2}$ respectively.

Heavy doping also leads to bandgap narrowing caused by carrier-carrier interaction as well as by distortion of the crystal lattice²⁷. For Si, the bandgap reduction as a function of doping density N_{dop} is given by²⁸

$$\Delta E_g \text{ (meV)} = -6.92 \left[\ln\left(\frac{N_{dop}}{0.13}\right) + \sqrt{\left(\ln\left(\frac{N_{dop}}{0.13}\right)\right)^2 + 0.5} \right] \quad (6.3)$$

Both bandgap reduction mechanisms add up and they are often hard to separate.

6.3 ZnO-Ag

6.3.1 Synthesis

Colloids of nano ZnO are synthesized by a modified polyol precipitation method as described in chapter 2. The molar concentration of precursor solution is 0.025 M and a heating rate of 4°C per minute is employed for the formation of ZnO at a temperature of 120°C. The silver nano colloids are prepared by a conventional reduction method²⁹. The method of preparation involves the reduction of a silver nitrate in H₂O with 1% sodium citrate near boiling temperature. The molar concentration of precursor solution is 0.025 M. The concentration of sodium citrate employed for the reduction is kept low to avoid the presence of excess citric acid in the silver suspension. The solution is kept on boiling for one hour to get a monodisperse stable colloid.

The ZnO-Ag nanocomposites are prepared via colloidal chemical synthesis by mixing certain amounts of colloids of Ag to ZnO at 120°C during its preparation stage and stirred for 1 hour at that temperature. The volume fraction of Ag is changed keeping the volume of ZnO constant. The samples having the ZnO-xAg composition of (x=) 0.1%, 0.5%, 1%, 2%, 5% are named as ZnO-0.1Ag, ZnO-0.5Ag, ZnO-1Ag, ZnO-2Ag and ZnO-5Ag respectively.

6.3.2 Absorption spectroscopy

Optical absorption measurement is an initial step to observe the single colloid and metal-semiconductor nanocomposite behaviour. Figure 6.1 gives the room temperature absorption spectra of the ZnO-Ag nanocomposites. The excitonic peak of ZnO colloid is found to be blue shifted with respect to that of bulk ZnO which could be attributed to the confinement effects³⁰. For silver nanocolloid, the surface plasmon absorption (SPA) band lies in the 410 nm region. Although the conduction and valence bands of semiconductors are separated by a well-defined band gap, metal nanoclusters have close-lying bands and electrons move quite freely. The free electrons give rise to a surface plasmon absorption band in metal clusters, which depends on both the cluster size and chemical surroundings¹. The plasmon band of metal particles as explained on the basis of Mie theory involves dipolar oscillations of the free electrons in the conduction band that occupy energy states near the Fermi level¹.

The pronounced dependence of the absorption band gap on the size of the semiconductor nano crystals and SPA band on the size of metal nano crystals is used to determine the particle size. An order of magnitude estimate of the particle size is possible from the absorption spectra. The size of ZnO and Ag nanocolloids are in the range of 10-20 nm. The presence of excitonic peak and SPA band itself indicates that the composites are of nanometer size. The size evolution of nanocomposites may also have some relation with optical characteristics in addition to the composition and is a possible direction for future studies.

For small volume fraction of Ag, the composite exhibits the characteristics of ZnO with a red shift in the excitonic peak. On the other hand, the ZnO-2Ag nanocomposite exhibits both the semiconductor and metallic behaviour with a blue shift in plasmon band. Optical absorption spectra indicate presence of a well-defined ZnO excitonic feature along with

the Ag surface plasmon absorption feature³¹ at 400 nm. The optical absorption spectra of the clusters show a gradual shift in absorbance towards the visible region, over which an extremely weak surface plasmon resonance is superposed.

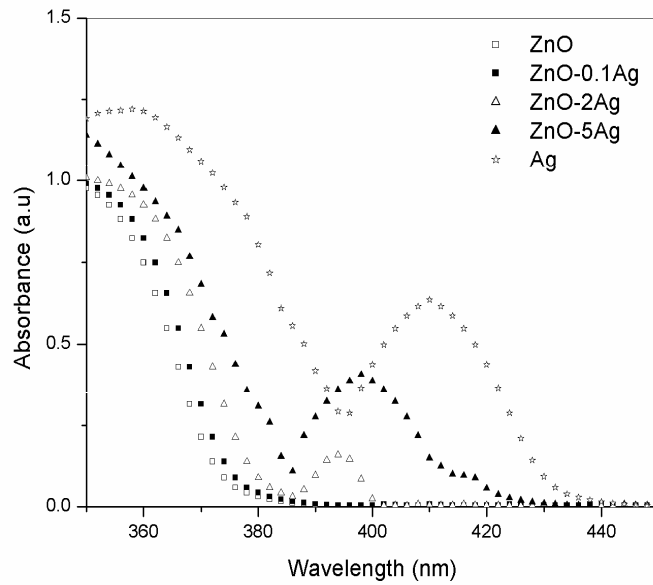


Figure 6.1: Absorption spectra of ZnO-Ag nanocomposites

The surface plasmon absorption band of metal nanoclusters is very sensitive to the surface-adsorbed species and dielectric of the medium. For example, Γ and $C_6H_5S^-$ ions result in damping of the surface plasmon band of colloidal silver particles³². Alternately, one can also observe bleaching of the surface plasmon band with electrons deposited from radiolytically produced radicals, which cause a blue shift and narrowing of the plasmon band. A more detailed discussion on the damping effects caused by surrounding material can be found elsewhere¹. When the volume fraction of

Ag increases beyond 2%, the surface plasmon peak is shifted towards 410 nm. It has been established that the shift of the SPA band of silver observed is a result of the accumulation of excess electrons on the ZnO/Ag particles which leads to equalization of the potentials of the conduction zones of the semiconductor and the metallic components of the nanocomposite³³.

6.3.3 Fluorescence spectroscopy

Photoluminescence spectra of all samples measured at room temperature are shown in figure 6.2. The intensities of the emission peaks depend on the volume fraction of Ag of the samples. ZnO and ZnO-0.1Ag have only 385 nm emission, but the intensity of the peak of ZnO-0.1Ag is much stronger than that of ZnO. ZnO-1Ag has the strongest UV emission centered at 375 nm. ZnO-2Ag has UV emission centered at 365 nm, which can be fitted to two peaks centered at 348 and 382 nm. ZnO-5Ag and Ag have only a peak at 348 nm.

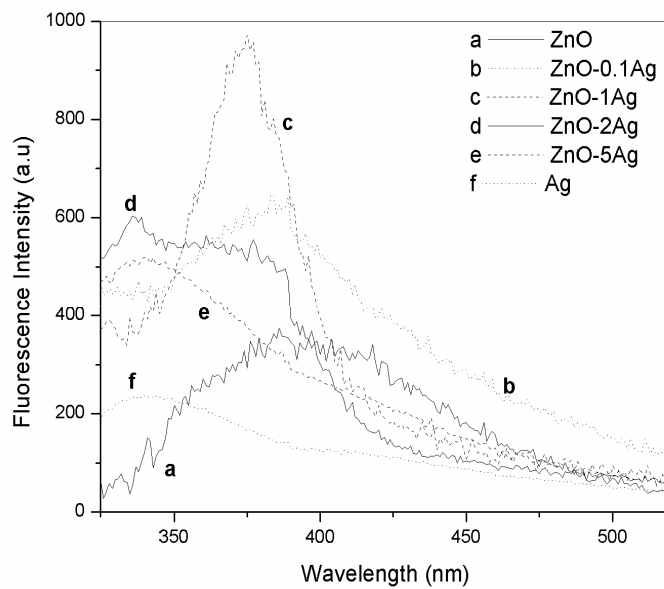


Figure 6.2: Fluorescence spectra of ZnO-Ag nanocomposites

Figure 6.3 shows the PL intensity as a function of the silver content. It is clear that the intensity of this peak increases with the increasing amount of the Ag and Zn acceptors. When the ZnO colloid is overdoped by Ag, the Ag_2O nanoclusters appears and hence there is reduction in PL intensity³⁴. The emission of ZnO at 385 nm can be attributed to exciton transition. An undoped ZnO colloid has insufficient holes and so restricted exciton concentration. After Ag doping, Ag acceptors bring more holes to make the concentration of the excitons increase, so that the UV emission is enhanced accordingly as shown in Figure 6.2.

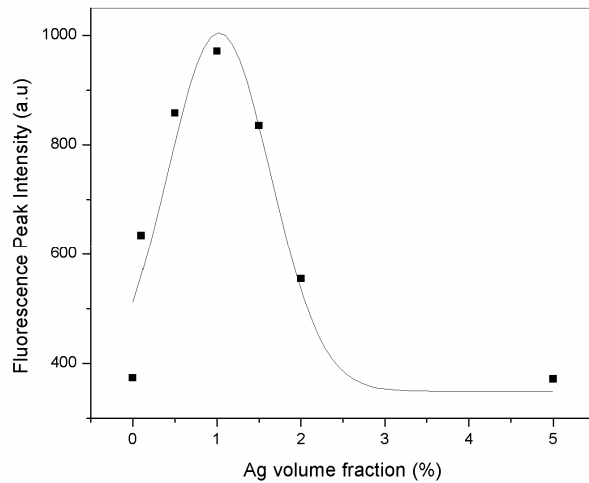


Figure 6.3: The fluorescence intensity of UV peak as a function of the volume fraction of silver in ZnO-Ag nanocomposites

Nanostructural semiconductor materials generally have more holes accumulated on its surface or in the interface than common semiconductor material³⁵. Therefore, there are many holes existing in the interface between Ag nanoclusters and ZnO grains. The electrons in ZnO arrive at the interface easily because of their short mean free paths and the Coulomb forces. Based

on quantum confinement effects, plenty of excitons can be formed. Then the UV emission due to exciton transition is enhanced.

The optical absorption spectroscopy and photoluminescence studies reveal the reaction mechanism at the junction. A two-fold enhancement of steady state luminescence of rhodamine 6G has been observed when it is doped with silver³⁶. The presence of silver aggregates cause substantial depolarization of the luminescence and the electromagnetic interaction between Ag surface plasmons and dye molecules can result, under certain conditions, in an enhanced fluorescence quantum efficiency and photostability of the dye. The strongest UV emission of a certain ZnO–Ag film is reported to be over ten times stronger than that of a pure ZnO film and the enhancement of UV emission is caused by excitons formed at the interface between Ag nanoclusters and ZnO grains³⁴. For ZnO-Ag nanocomposites, the strongest UV emission is over three times that of pure ZnO.

6.3.4 Nonlinear optical characterization

The third order nonlinear optical properties of ZnO nanocomposites are investigated using the z-scan technique explained in chapter 1. Figure 6.4 shows the nonlinear absorption of ZnO-Ag nanocomposites at a typical fluence of 300 MW/cm² for a wavelength of 532 nm. Interestingly, ZnO and Ag colloids show a minimum nonlinearity, while the ZnO-Ag nanocomposites clearly exhibit a larger induced absorption behavior. The nonlinear absorption coefficient increases substantially in the nanocomposites, as compared to pure ZnO and Ag colloids and can be attributed to the enhancement of exciton oscillator strength. Similar increase is also reported in bimetallic and core-shell nanocomposites, as compared to pure metals³⁷.

Different processes, like two photon absorption, free carrier absorption, transient absorption, interband absorption, photoejection of

electrons and nonlinear scattering are reported to be operative in nanoclusters. In general, induced absorption can occur due to a variety of processes. The theory of two photon absorption process fitted well with the experimental curve infers that TPA is the basic major mechanism. The possibility TPA induced free carrier absorption³⁸ (FCA) is explained in chapter 3. But FCA is weak compared to TPA and hence the corresponding contribution in the z-scan curves is relatively less. Silver nanoparticles are well known materials for nonlinear optical applications because of their subpicosecond time response of third-order optical nonlinearity. Transient absorption and nonlinear absorptive mechanisms are reported to lead to optical limiting in the case of Ag nanoparticles³⁹.

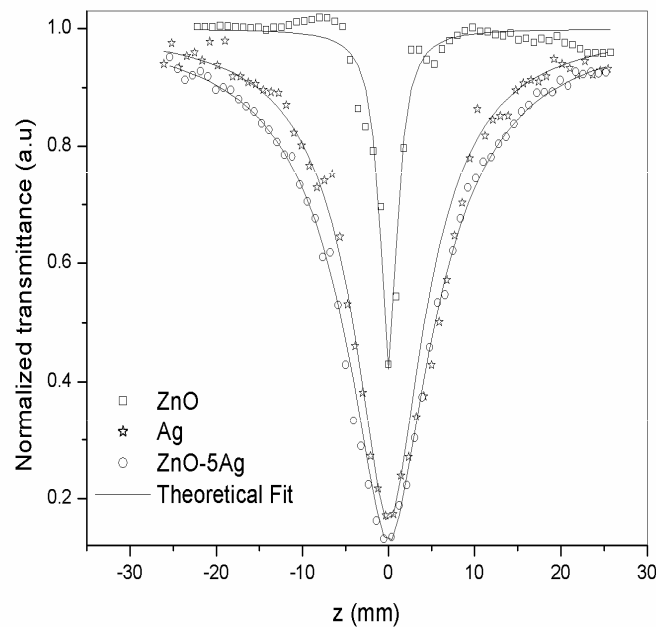


Figure 6.4: Open aperture z-scan traces of ZnO-Ag nanocomposites at an intensity of 300 MW/cm^2 for an irradiation wavelength of 532 nm

The surface plasmon band is sensitive to laser excitation. The plasmon band of metal particles as explained on the basis of Mie theory involves dipolar oscillations of the free electrons in the conduction band that occupy energy states near the Fermi level¹. Once these electrons are excited by a laser pulse, they do not oscillate at the same frequency as that of the unexcited electrons, thus causing the plasmon absorption band to bleach⁴⁰. In our case, the excitation energy (532 nm or 2.3 eV) is lower than the Ag SPR (410 nm or 3.02 eV) and as such the plasmon absorption is not possible. No plasmon bleach effects are seen when the samples are excited with nanosecond laser pulses at 532 nm. Instead, a reduced transmission behavior is observed, which fits to a two photon absorption mechanism. A laser pulse can cause an intraband or interband absorption in the metal nanoparticle system, depending on the excitation wavelength and incident intensity⁴¹. In our case, the excitation energy (532nm or 2.3 eV) is lower than the interband threshold from d level to p levlel ($E_{dp}=2.5$ eV), and hence interband absorption is not possible⁴². We propose that this nonlinearity is caused by two photon absorption followed by weak free carrier absorption occurring in the nanocomposites.

Figure 6.5 gives the closed aperture z-scan traces of ZnO-Ag nanocomposites at a fluence of 300 MW/cm². It is observed that the closed-aperture z-scan satisfies the condition $\Delta z \sim 1.7 z_0$, thus confirming the presence of pure electronic third order nonlinearity⁴³.

The peak–valley trace in a closed aperture z-scan shows that these samples have self-defocusing (negative, $n_2<0$) nonlinearity, though earlier reports with picosecond pulsed lasers have shown positive nonlinearity for individual Ag nanoclusters⁴⁴. Though laser-induced permanent sign reversal of the nonlinear refractive index is reported in Ag nanoclusters in soda-lime glass, we have not observed any such permanent effect⁴⁵ either in the intensity ranges (150-400 MW/cm²) studied using the second harmonics of a

Q-switched Nd:YAG laser or within the wavelength range 450-650 nm studied using a tunable laser (Quanta Ray MOPO, 5 ns, 10 Hz). The nanocomposites exhibit reverse saturable absorption at all wavelengths and good nonlinear absorption, which increases with increasing input intensity. The nonlinear refractive index (n_2) increases substantially in the nanocomposites, as compared to pure ZnO and Ag colloids. The dramatically enhanced nonlinear refractive response is due to the enhanced electromagnetic field existing in the interface between Ag nanoclusters and ZnO grains⁴⁶. Since n_2 increases with absorption, thermal nonlinearity is also taken into account. It is reported that if the thermal contributions are to dominate, then there will be increase in n_2 with increase of absorption⁴⁷.

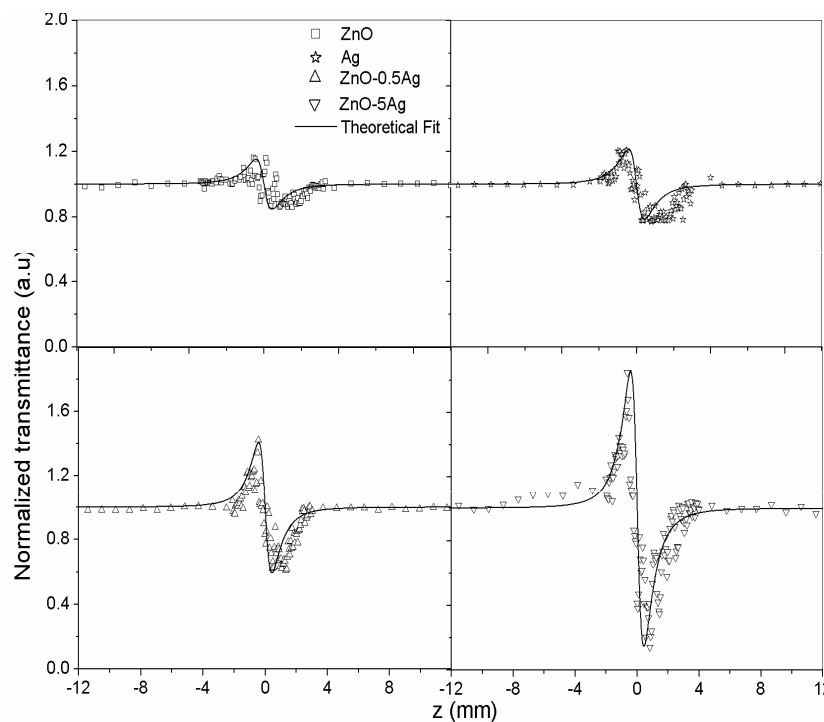


Figure 6.5: Closed aperture z-scan traces of ZnO-Ag nanocomposites at an intensity of 300 MW/cm^2 for an irradiation wavelength of 532 nm

The obtained values of nonlinear parameters of ZnO-Ag nanocomposites are given in table 6.1. The nonlinear refractive index of pure Ag colloid at 532 nm is reported to be of the order of 10^{-16} to $10^{-17} \text{ m}^2/\text{W}$. The nonlinear coefficients of Ag films are about one order of magnitude larger than that of Ag colloids⁴⁸. It is worth noting that certain materials, such as CuO chain compounds, Ag₂S/CdS nanocomposites, organic coated quantum dots and metal clusters yielded values of order of 10^{-9} to 10^{-14} m/W for nonlinear absorption coefficient^{18,49} at a wavelength of 532 nm. These values are comparable to the values of nonlinear optical parameters obtained for nanocomposites in the present investigation. Thus, the nonlinear absorption coefficient and nonlinear refractive index measured by the z-scan technique reveals that the ZnO-Ag nanocomposites investigated in the present study have good nonlinear optical response and could be chosen as ideal candidates with potential applications in nonlinear optical devices.

ZnO-Ag Nanocomposites	β cm/GW	n_2 $10^{-17} \text{ m}^2/\text{W}$
ZnO	20.7	-1.5
Ag	121	-2.9
ZnO-0.1Ag	138.2	-4.4
ZnO-0.5Ag	155.5	-5.9
ZnO-1Ag	172.8	-7.3
ZnO-2Ag	190.1	-11
ZnO-5Ag	207.4	-12.3

Table 6.1: Measured values of nonlinear absorption coefficient and nonlinear refractive index of ZnO-Ag nanocomposites at an intensity of 300 MW/cm² for an irradiation wavelength of 532 nm

6.3.5 Optical limiting

To examine the viability of ZnO-Ag nanocomposites as optical limiters, the nonlinear transmission of the colloids are plotted as a function of input fluence derived from open aperture z-scan trace. Figure 6.6 illustrates the influence of volume fraction of silver in ZnO-Ag nanocomposites on the optical limiting response.

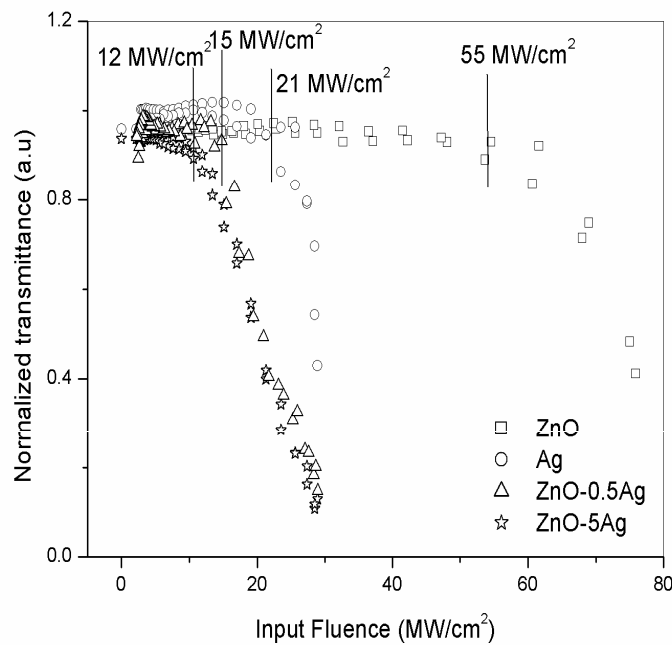


Figure 6.6: Optical limiting response of ZnO-Ag nanocomposites

The arrow in the figure indicates the approximate fluence at which the normalized transmission begins to deviate from linearity. The optical limiting threshold is found to be high in the case of ZnO colloids (55 MW/cm^2) in comparison with that of Ag colloids (21 MW/cm^2). These values are comparable to the reported optical limiting threshold for CdS and

ZnO nano colloids^{50,51}. ZnO-Ag nanocomposites are found to be good optical limiters compared to ZnO and Ag and the optical limiting threshold of ZnO-5Ag nanocomposite is observed to be 12 MW/cm². Nanocomposites have a significant effect on the limiting performance and increasing the volume fraction of Ag reduces the limiting threshold and enhances the optical limiting performance.

6.4 ZnO-Cu

6.4.1 Synthesis

The copper nanocolloids are prepared by a hydrolysis method⁵². The method of preparation involves the hydrolysis of copper sulphate in H₂O near boiling temperature. The solution is kept on boiling for one hour to get a monodisperse stable colloid. The molar concentration of the precursor solution is 0.025 M. The ZnO-Cu nanocomposites are prepared by colloidal chemical synthesis by mixing certain amount of Cu colloid with ZnO colloid at 120°C during its preparation stage and stirred for 1 hour at that temperature. The volume fraction of Cu is changed keeping the volume of ZnO constant. The samples having ZnO-xCu composition with (x=) 0.1-5% are named as ZnO-0.1Cu to ZnO-5Cu respectively.

6.4.2 Absorption spectroscopy

Figure 6.7 gives the room temperature absorption spectra of the ZnO-Cu nanocomposites. For copper nanocolloid, the surface plasmon absorption band (SPA) lies in the 560 nm region. The size of ZnO and Cu nanocolloids are in the range of 10-30 nm. For small volume fraction of Cu, the composite exhibits the characteristics of ZnO with a red shift in the excitonic peak. On the other hand, the ZnO-1.5Cu nanocomposite exhibits both the semiconductor and metallic behaviour. Optical absorption spectra indicate presence of well-defined ZnO excitonic feature along with the Cu surface plasmon absorption feature³¹ at 545 nm. The optical absorption

spectra of the clusters show a gradual shift in absorbance towards UV region, over which an extremely weak surface plasmon resonance is superposed.

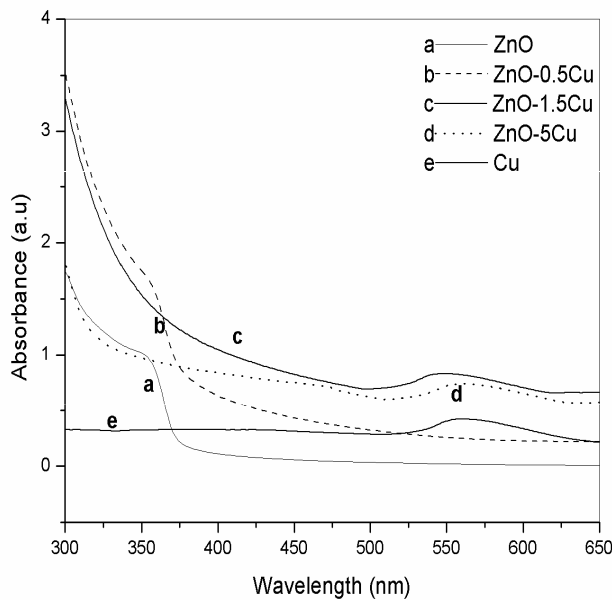


Figure 6.7: Absorption spectra of ZnO-Cu nanocomposites

When the volume fraction of Cu increases beyond 1.5%, the surface plasmon peak is shifted towards 560 nm and it has been established that the shift of the plasma band of Cu observed is a result of the accumulation of excess electrons on the ZnO/Cu particles which leads to equalization of the potentials of the conduction zones of the semiconductor and the metallic components of the nanocomposites³³.

6.4.3 Fluorescence spectroscopy

Photoluminescence spectra of all samples measured at room temperature are shown in Figure 6.8. ZnO and ZnO-0.5Cu have only emissions at 385 nm, but the intensity of the peak of ZnO-0.5Cu is much

stronger than that of ZnO. ZnO-0.5Cu has the strongest UV emission which is over three times stronger than that of ZnO. It is clear that the intensity of this peak increases with the increasing amount of the Cu and Zn acceptors.

At small volume fractions, Cu acts as a sensitizer in the nanocomposites. ZnO-1Cu has UV and visible emissions. As the volume fraction of Cu increases beyond 0.5%, intensity of UV peak decreases and visible peak increases. When the ZnO colloid is overdoped by Cu, the CuO nanoclusters appears which will introduce defect states due to anion vacancies and hence there is reduction in PL intensity and increase in visible intensity³⁴. ZnO-5Cu and Cu have only visible peak centered at 550 nm. It is obvious that the intensity of 550 nm peak agrees with the content of Cu nanocolloids.

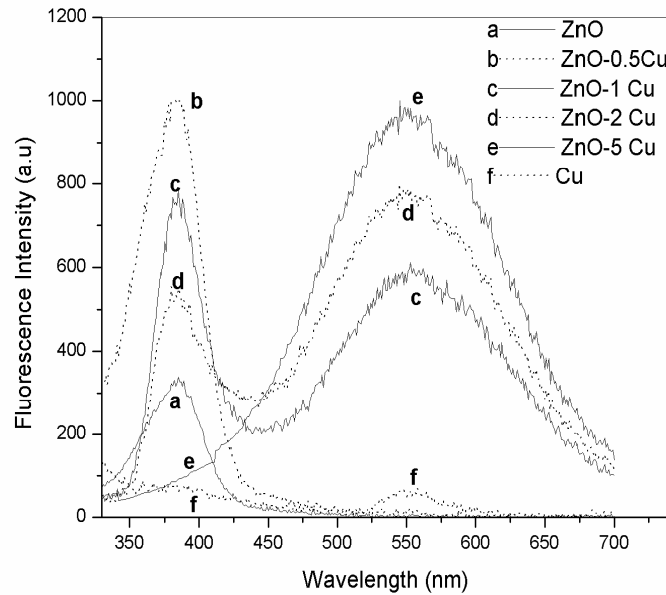


Figure 6.8: Fluorescence spectra of ZnO-Cu nanocomposites

At larger volume fractions of Cu in the nanocomposites, ie, when ZnO is overdoped by Cu, defect states due to anion vacancies are introduced and hence there is ten times enhancement in visible emission compared to that of Cu. The intensity of green emission becomes stronger than that of UV emission in the composite after certain volume fraction of Cu. The intensity variation of green luminescence is systematically observed depending on the volume fraction of Cu in order to investigate the emission mechanism. This difference could be mainly because UV luminescence is degraded by excessively oxidized layer formed on the surface and the grain boundary⁵³ of ZnO and Cu.

Copper doped ZnO is a strong luminescent material and the green emission is due to copper induced levels. The transition mechanism for copper doped ZnS has been thoroughly discussed by Suzuki and Shionoya⁵⁴. They attributed it to donor–acceptor transitions. The donor level is due to Al³⁺ used as the coactivator and acceptor levels are due to Cu²⁺ in the excited state under the UV radiation. When excited, the levels of Cu²⁺(3 d⁰ configuration) are split into ²t₂ and ²e states with ²t₂ lying in the higher position. In our experiments no coactivator is used so that one can rule out the presence of donor levels due to Al³⁺. We do not observe any other impurities which would introduce donor levels. Another model to explain the green luminescence due to copper in zinc sulphide is recently proposed by Peka and Schulz⁵⁵. Green copper luminescence in their model is due to a transition from the conduction band of ZnS to the “t₂” level of excited Cu²⁺ in the ZnS band gap.

Figure 6.9 shows the luminescence mechanism in ZnO-Cu nanocomposites in which the doping introduces defect levels due to anion vacancies. Impurities such as sodium, copper, lead, potassium, nickel, cadmium, iron, etc. can lead to impurity levels in the band gap and lead to luminescence⁵². Without doping, radiative transition occurs from near

conduction band to the valence band. In case of Cu doped ZnO nanocomposites, enhancement of visible luminescence is due to transition from defect level to the copper induced t_2 level.

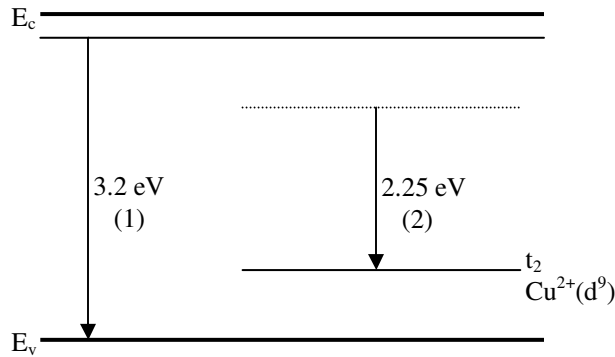


Figure 6.9: Luminescence mechanism of ZnO-Cu nanocomposites

- (1) transition from near conduction band edge to valence band
- (2) transition from deep donor level to t_2 induced level

6.4.4 Nonlinear optical characterization

Figure 6.10 shows the nonlinear absorption of ZnO-Cu nanocomposites at a typical fluence of 300 MW/cm^2 for an irradiation wavelength of 532 nm. The open-aperture curve exhibits a normalized transmittance valley, indicating the presence of reverse saturable absorption in the colloids. The obtained values of nonlinear absorption coefficient β at an intensity of 300 MW/cm^2 are shown in table 6.2.

The nonlinear absorption coefficient increases substantially in the nanocomposites, as compared to pure ZnO and Cu colloids. The theory of two photon absorption process fitted well with the experimental curve which suggests that TPA is the basic mechanism. There is the possibility of FCA, but it is weak compared to TPA and hence the corresponding contribution in the z-scan curves is relatively less.

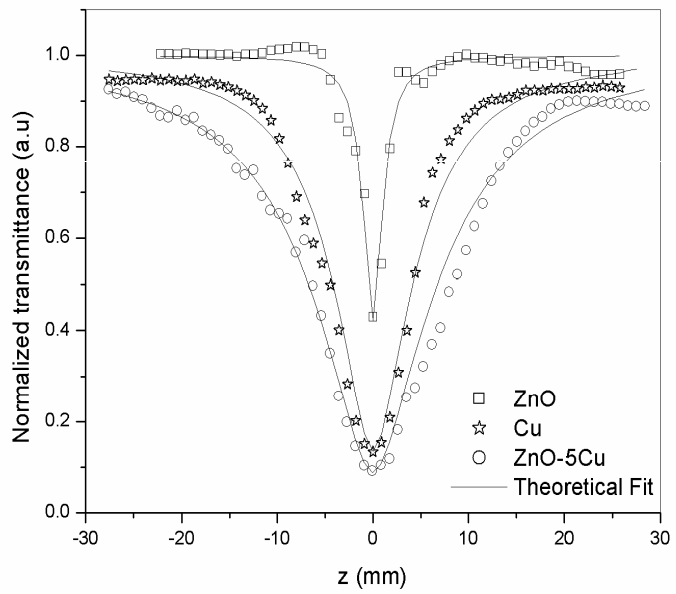


Figure 6.10: Open aperture z-scan traces of ZnO-Cu nanocomposites at an intensity of 300 MW/cm^2 for an irradiation wavelength of 532 nm

A laser pulse can cause an intraband or interband absorption in the metal nanoparticle system, depending on the excitation wavelength and incident intensity. The electrons thus excited are free carriers possessing a whole spectrum of energies, both kinetic and potential, immediately after the absorption leading to the bleaching of the ground state plasmon band. This process is accompanied by the nascent excited state showing a transient absorption due to the free carrier absorption⁴¹. The possibility of photo-ejection of electrons, which is an ultrafast phenomena occurring by a two photon or multiphoton absorption process, should also be considered as a contributing factor leading to nonlinear absorption, since the excitation photons in the visible region are usually not energetic enough for

monophotonic electronic ejection. In our case, the excitation energy (532nm or 2.3 eV) is higher than the interband threshold of copper from d level to p level (571 nm $E_{dp}=2.17$ eV), and hence interband absorption accompanied by the absorption of free carriers generated in the conduction band is possible. Strong optical limiting properties because of interband absorption are reported in different nanoparticle systems⁴². Thus we propose that the observed nonlinearity is caused by two photon induced weak free carrier absorption and interband absorption mechanisms occurring in the nanocomposites.

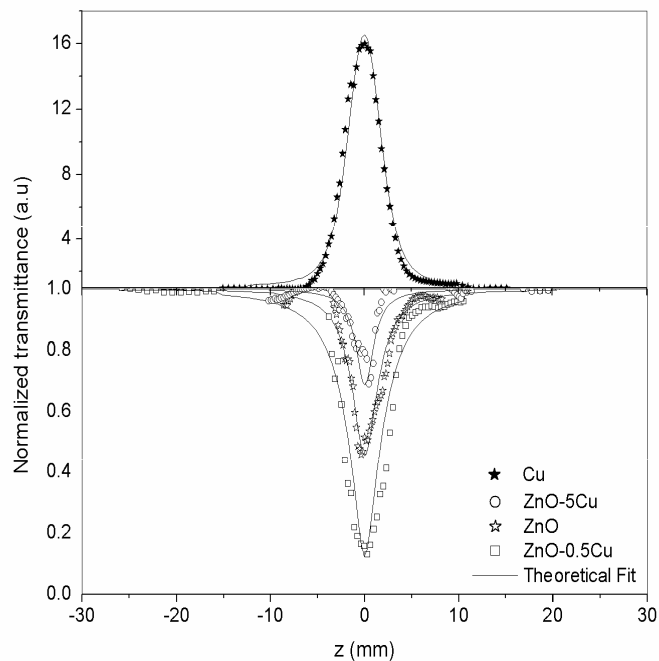


Figure 6.11: Open aperture z-scan traces of ZnO-Cu nanocomposites at an intensity of 300 MW/cm² for an irradiation wavelength of 570 nm

Figure 6.11 shows the nonlinearity observed at 570 nm at a fluence of 300 MW/cm². An absorption saturation behavior is found in Cu colloid.

However, the saturation changes over to induced absorption in all other ZnO colloids and ZnO-Cu nanocomposites. Such a change-over in the sign of the nonlinearity is related to the interplay of plasmon band bleach and optical limiting mechanisms, as found from earlier studies on metal nanoparticles in liquid and glass media^{41,56}. Such behavior can generally be modeled by defining an intensity dependent nonlinear absorption coefficient $\alpha(I)$, which is a sum of independent positive and negative transmission coefficients⁵⁷

$$\alpha(I) = \frac{\alpha}{1 + \left(\frac{I}{I_s}\right)} + \beta I \quad (6.4)$$

where I_s is the saturation intensity.

The surface plasmon band is sensitive to laser excitation. These aspects have been addressed in several recent spectroscopic investigations⁴⁰. Plasmon bleach effects are seen when the Cu nanocolloids are excited at its SPR with nanosecond laser pulses of 570 nm. So increased transmission behavior is observed for Cu nanocolloids, which fits to a saturable absorption mechanism. The saturation changes over to induced absorption in all the other ZnO colloids and ZnO-Cu nanocomposites. For small volume fraction of Cu, the nonlinear absorption coefficient increases substantially in the nanocomposites, as compared to pure ZnO. ZnO-0.5Cu exhibits maximum nonlinear absorption at 570 nm since ZnO features dominates till that composition as clearly exhibited in absorption spectra. When the volume fraction of Cu increases beyond 0.5% the nonlinear absorption coefficient decreases with increase in Cu composition due to the effect of plasmon bleach. Thus the nonlinearity of the ZnO-Cu nanocomposites is related to the interplay of plasmon band bleach and optical limiting mechanisms at 570nm.

Figure 6.12 shows the nonlinear absorption at 650 nm. At this off-resonant excitation wavelength there is no local field enhancement within the

particles, and hence the nonlinearity is less at this wavelength. Interestingly, colloids containing only Cu or ZnO nanoparticles show a minimum nonlinearity at this wavelength, while the composites clearly exhibit a larger induced absorption behavior.

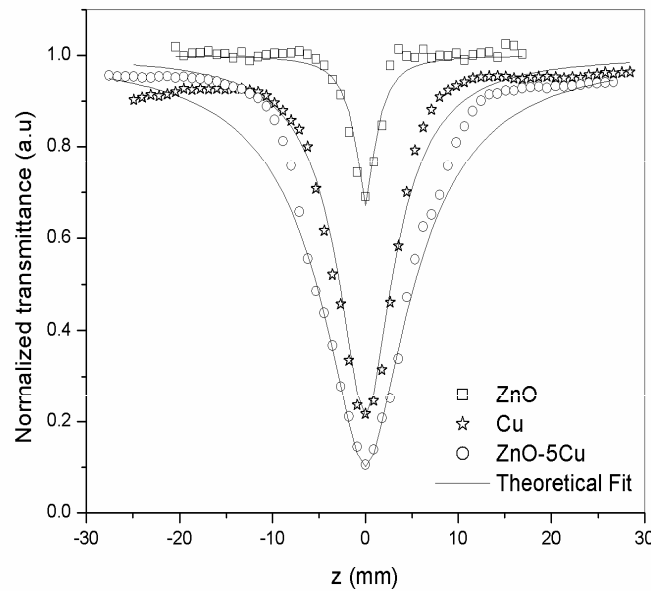


Figure 6.12: Open aperture z-scan traces of ZnO-Cu nanocomposites at an intensity of 300 MW/cm^2 for an irradiation wavelength of 650 nm

Figure 6.13 gives the closed aperture z-scan traces of ZnO-Cu nanocomposites at a fluence of 300 MW/cm^2 . It is observed that the peak–valley of closed-aperture z-scan satisfied the condition $\Delta z \sim 1.7 z_0$, thus confirming the presence of pure electronic third order nonlinearity⁴³. The peak–valley trace in a closed aperture z-scan shows that these samples have self-defocusing (negative, $n_2 < 0$) nonlinearity, though earlier reports with picosecond pulsed lasers have shown positive nonlinearity for individual Cu

nanoclusters⁴⁴. The nonlinear refractive index increases substantially in the nanocomposites, as compared to pure ZnO and Cu colloids. The enhanced nonlinear refractive response is due to the enhanced electromagnetic field existing in the interface between Cu nanoclusters and ZnO grains⁴⁶. Since n_2 increases with absorption, thermal nonlinearity is also taken into account⁴⁷.

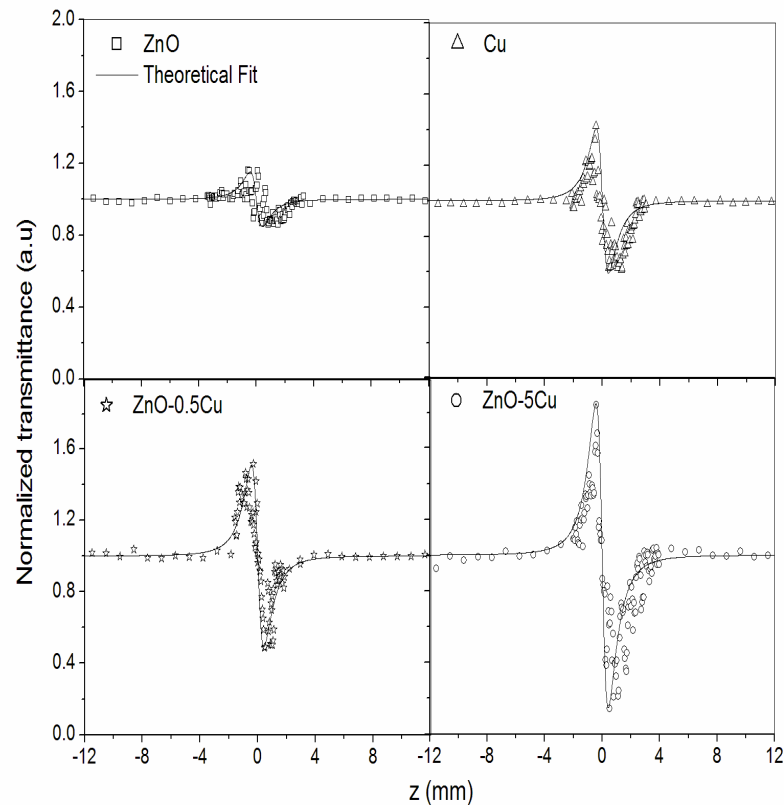


Figure 6.13: Closed aperture z-scan traces of ZnO-Cu nanocomposites at an intensity of 300 MW/cm² for an irradiation wavelength of 532 nm

The obtained values of nonlinear parameters of ZnO-Cu nanocomposites are given in table 6.2. The nonlinear absorption coefficient of CuO chain compounds and metal clusters yielded values of order of 10^{-9}

to 10^{-14} m/W for nonlinear absorption coefficient^{18,49} at a wavelength of 532 nm. These values are comparable to the values of nonlinear optical parameters obtained for nanocomposites in the present investigation.

ZnO-Cu nanocompo sites	Nonlinear absorption coefficient				Nonlinear refractive index
	532 nm	570nm		650 nm	
	β cm/GW	β cm/GW	I_s GW/cm ²	β cm/GW	n_2 $10^{-17} \text{m}^2/\text{W}$
ZnO	20.7	17.3		6.7	-1.5
Cu	145.2	-	0.04	76.0	-5.9
ZnO-0.1Cu	172.8	131.3		103.7	-6.6
ZnO-0.5Cu	190.1	179.7		121.0	-7.3
ZnO-1.5Cu	248.8	138.2		145.2	-9.5
ZnO-2Cu	276.5	29.4		190.1	-11.0
ZnO-5Cu	293.8	5.4		241.9	-12.3

Table 6.2: Measured values of nonlinear absorption coefficient, saturation intensity and nonlinear refractive index of ZnO-Cu nanocomposites at an intensity of 300 MW/cm² for different irradiation wavelengths

6.4.5 Optical limiting

Figure 6.14 illustrates the influence of volume fraction of copper in ZnO-Cu nanocomposites on the optical limiting response. The optical limiting threshold is found to be high in the case of ZnO colloids (55 MW/cm²) in comparison with the Cu colloids (10 MW /cm²). ZnO-Cu nanocomposites are found to be good optical limiters compared to ZnO and

Cu and the optical limiting threshold of ZnO-5Cu nanocomposites is observed to be 3 MW/cm^2 . Nanocomposites have a significant effect on the limiting performance and increasing the volume fraction of Cu reduces the limiting threshold and enhances the optical limiting performance.

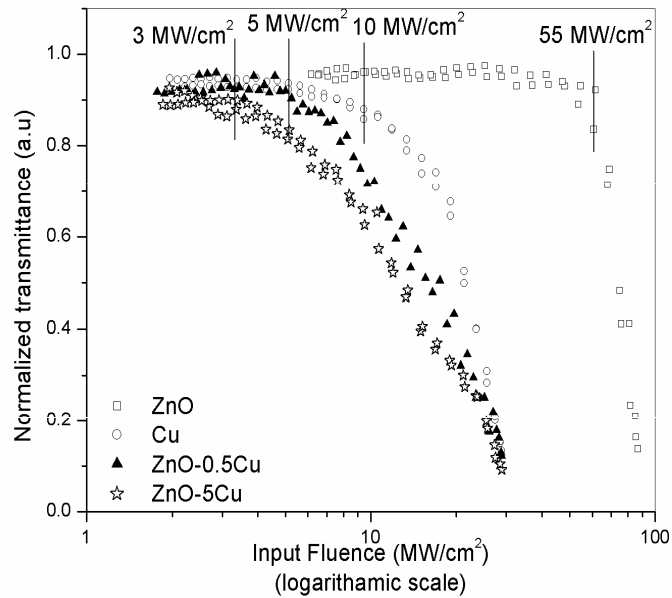


Figure 6.14: Optical limiting response of ZnO-Cu nanocomposites

6.5 ZnO-CdS

6.5.1 Synthesis

The CdS nanocolloids are prepared by chemical method⁵⁸. $\text{Cd}(\text{NO}_3)_2 \cdot 4\text{H}_2\text{O}$ (Merck, India) and NH_2CSNH_2 (Merck, India) are used as the precursors for the incorporation of Cd and S, respectively. These precursors are dissolved in 2-propanol and distilled water under stirring. The solution is kept on stirring for one hour to get a monodisperse stable colloid. The molar concentration of the precursor solution is 0.025 M. The ZnO-CdS

nanocomposites are prepared by colloidal chemical synthesis by mixing certain amount of CdS colloid to ZnO colloid and stirred for 1 hour. The volume fraction of CdS is changed keeping the volume of ZnO constant. The samples having $ZnO-xCdS$ composition with ($x=$) 0.1-5% are named as $ZnO-0.1CdS$ to $ZnO-5CdS$ respectively.

6.5.2 Absorption spectroscopy

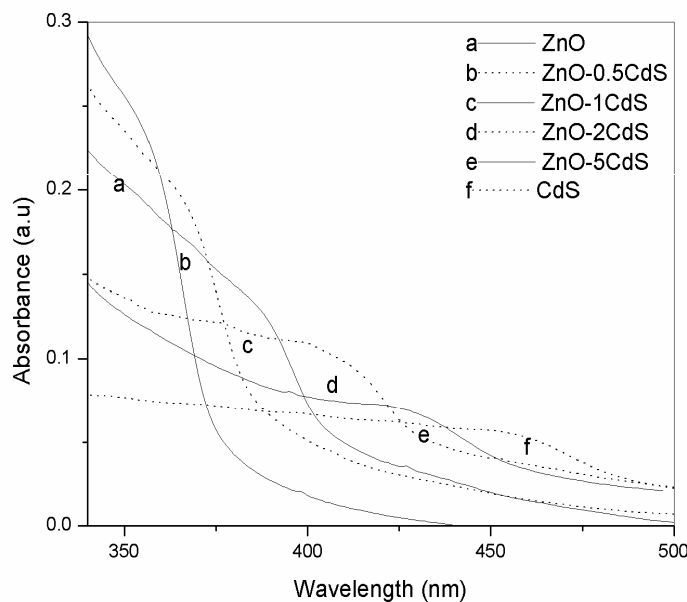


Figure 6.15: Absorption spectra of ZnO - CdS nanocomposites

Figure 6.15 gives the room temperature absorption spectra of the ZnO - CdS nanocomposites. The excitonic peak of ZnO and that of CdS colloids are found to be blue shifted with respect to their bulk which could be attributed to the confinement effects³⁰. From the shift of absorption edge, the size of ZnO and CdS nanocolloids are calculated to be in the range of 10-12 nm. The presence of excitonic peak itself indicates that the composites are of

nanometer size. It is seen that the absorption edge corresponding to the nanocomposites gets red shifted as a function of the CdS content.

6.5.3 Optical bandgap

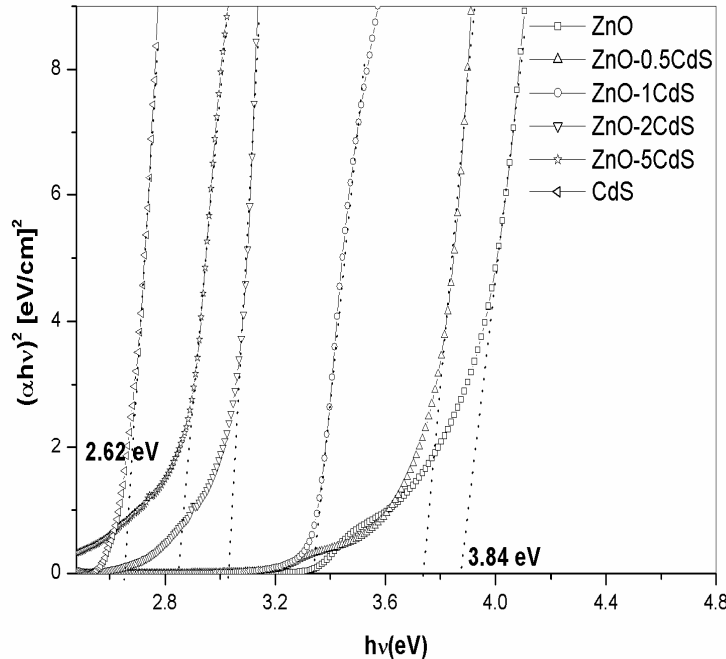


Figure 6.16: Optical band gap of ZnO-CdS nanocomposites

The direct bandgap of ZnO-CdS nanocomposites is estimated from the graph of $h\nu$ versus $(\alpha h\nu)^2$. The optical band gap (E_g) is found to be dependent on the composition and there is a decrease in the band gap of the semiconductor with an increase in the volume fraction of CdS in the nanocomposites as shown in figure 6.16. E_g changes from 3.84 eV for ZnO to 2.62 eV for CdS almost in proportion to the composition of CdS. Within the range of compositions studied, the optical bandgap is tunable from 2.62

eV to 3.84 eV. The bandgap engineering⁵⁹ in ZnS-CdS is reported to be from 2.58 to 3.91 eV.

6.5.4 Fluorescence spectroscopy

Photoluminescence spectra of all the samples measured at room temperature are shown in Figure 6.17.

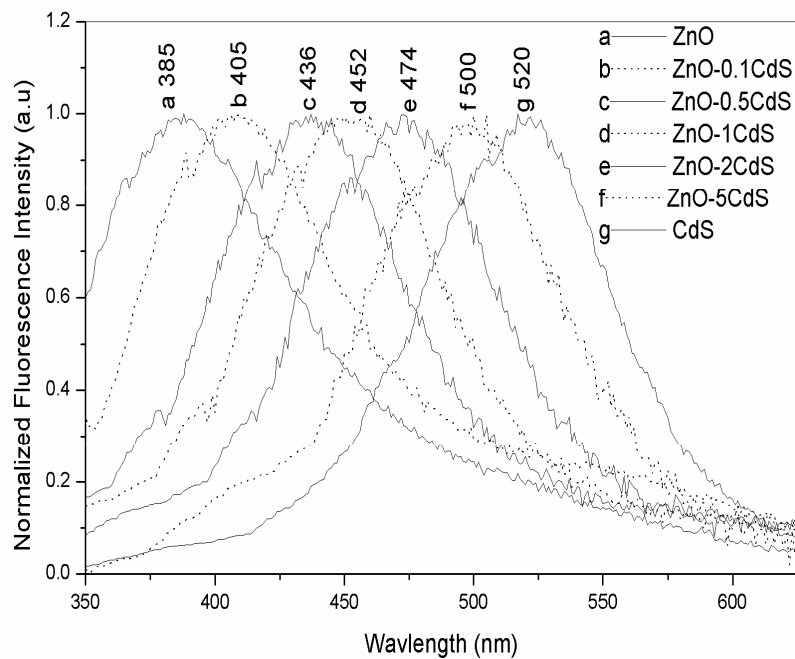


Figure 6.17: Fluorescence spectra of ZnO-CdS nanocomposites

The 385 nm emission is the near band edge emission of ZnO and the 520 nm emission is the near band edge emission peak of CdS. Emission peaks of ZnO-CdS nanocomposites changes from 385 nm to 520 nm almost in proportion to changes in E_g . It is possible to obtain a desired luminescence colour from UV to green by simply adjusting the composition.

The tuning of luminescence⁵⁹ in ZnS-CdS is reported to be from blue to red in proportion to change in E_g .

6.5.5 Nonlinear optical characterization

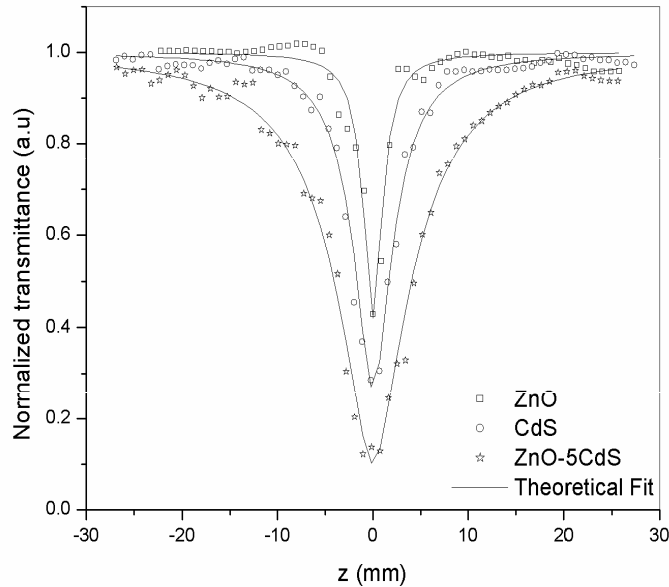


Figure 6.18: Open aperture z-scan traces of ZnO-CdS nanocomposites at an intensity of 300 MW/cm^2 for an irradiation wavelength of 532 nm

Figure 6.18 shows the nonlinear absorption of ZnO-CdS nanocomposites at a typical fluence of 300 MW/cm^2 for an irradiation wavelength of 532 nm . The obtained nonlinearity is found to be of the third order, as it fits to a two photon absorption (TPA) process. The nonlinear absorption coefficient increases substantially in the nanocomposites, as compared to pure ZnO and CdS colloids due to the enhancement of exciton oscillator strength¹². The larger nonlinear absorption in semiconductors such as ZnSe, ZnO, and ZnS is reported to be due to two photon induced free

carrier absorption³⁸ along with TPA. The enhancement of nonlinear absorption in $\text{Ag}_2\text{S}-\text{CdS}$ nanocomposites in comparison with the CdS nanoparticles is reported to be due to free carrier absorption and the free carrier life time of ZnO is determined to be a few nanoseconds¹⁸. Thus we propose that the observed nonlinearity is caused by two photon absorption followed by weak free carrier absorption in the nanocomposites.

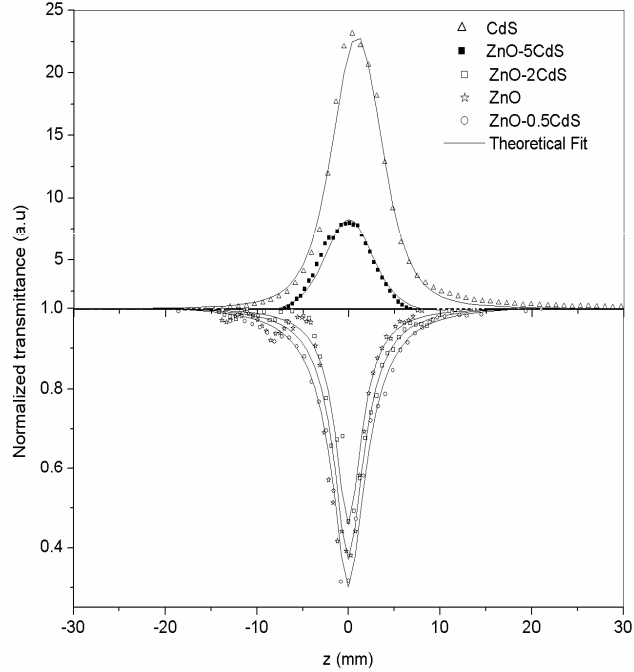


Figure 6.19: Open aperture z-scan traces of ZnO-CdS nanocomposites at an intensity of 300 MW/cm^2 for an irradiation wavelength of 450 nm

Figure 6.19 shows the nonlinearity observed for 450 nm at a fluence of 300 MW/cm^2 . An absorption saturation behavior is found in CdS colloid and ZnO-5CdS nanocomposites. However, all the other ZnO colloids and ZnO-CdS nanocomposites exhibit induced absorption at this wavelength. Such a change-over in the sign of the nonlinearity is related to the interplay of

exciton band bleach and optical limiting mechanisms, as found from earlier studies of semiconductor nanoparticles⁶⁰.

The excitonic peak is sensitive to laser excitation. As the particle size is reduced, a series of nearby transitions occurring at slightly different energies in the bulk are compressed by quantum confinement into a single, intense transition in a quantum dot. Therefore, the oscillator strength of the nanoparticle is concentrated into just a few transitions and the strong exciton bleaching can be expected. Exciton bleach effects are seen when the CdS nanocolloids are excited at excitonic resonance with nanosecond laser pulses of 450 nm. So increased transmission behavior is observed for CdS nanocolloids, which fits to a saturable absorption mechanism. On the other hand, ZnO colloids exhibit induced absorption at this wavelength. For small volume fraction of CdS, the nonlinear absorption coefficient increases substantially in the nanocomposites, as compared to pure ZnO. ZnO-0.5CdS exhibits maximum nonlinear absorption at 450 nm and can be attributed to the enhancement of exciton oscillator strength¹². When the volume fraction of CdS increases beyond 0.5% the nonlinear absorption coefficient decreases with increase in the volume fraction of CdS and it becomes a saturable absorber at and above 5% CdS due to the interplay of exciton bleach and optical limiting mechanisms. The excitonic bleaching of the CdS nanocolloids originates from the transition between the ground state $1S(e)$ and the lowest excited state $1S_{3/2}(h)$ since the excitation at 450 nm corresponds to the absorption close to the resonance of the $1S(e)-1S_{3/2}(h)$ excitonic transition⁶⁰. Thus the nonlinearity of the ZnO-CdS nanocomposites is related to the interplay of exciton bleach and optical limiting mechanisms at 450 nm. The great potential of using the ZnO-CdS nanocomposite lies in the fact that the composition of the constituent elements can be readily altered to optimize the desired NLO properties either as a saturable absorber or as a reverse saturable absorber.

Figure 6.20 gives the closed aperture z-scan traces of ZnO-CdS nanocomposites at a fluence of 300 MW/cm^2 . It is observed that the peak-valley of closed-aperture z-scan satisfied the condition $\Delta z \sim 1.7 z_0$, thus confirming the presence of pure electronic third order nonlinearity⁴³. The peak–valley trace in a closed aperture z-scan shows that these samples have self-defocusing (negative, $n_2 < 0$) nonlinearity, though earlier reports have shown positive nonlinearity for individual CdS nanoclusters prepared by laser ablation⁶¹. The nonlinear refractive index increases substantially in the nanocomposites, as compared to pure ZnO and CdS colloids and can be attributed to the enhancement of exciton oscillator strength¹². Since n_2 increases with absorption, thermal nonlinearity is also taken into account⁴⁷.

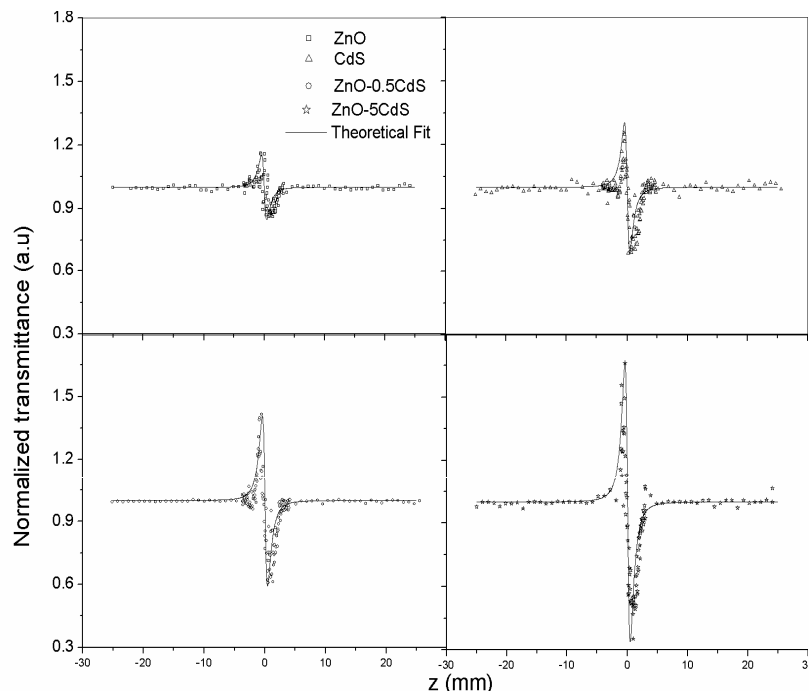


Figure 6.20: Closed aperture z-scan traces of ZnO-CdS nanocomposites at an intensity of 300 MW/cm^2 for an irradiation wavelength of 532 nm

The obtained values of nonlinear optical parameters of ZnO-CdS nanocomposites are given in table 6.3. The nonlinear refractive index of the pure semiconductor nano colloids at 532 nm are reported to be of the order of 10^{-16} to $10^{-17} \text{ m}^2/\text{W}$. The third order nonlinear absorption coefficient of CdS nanocrystals⁶² are reported to be of the order of $10^{-10} \text{ m}/\text{W}$. Ag₂S-CdS nanocomposites yielded values of order of 10^{-9} to $10^{-14} \text{ m}/\text{W}$ for nonlinear absorption coefficient^{18,49} at a wavelength of 532 nm. These values are comparable to the values of nonlinear optical parameters obtained for nanocomposites in the present investigation.

ZnO-CdS nanocomposites	Nonlinear absorption coefficient			Nonlinear refractive index
	450nm		532 nm	532 nm
	β cm/GW	I _s GW/cm ²	β cm/GW	n ₂ $10^{-17} \text{ m}^2/\text{W}$
ZnO	51.8		20.7	-1.5
CdS		0.20	51.8	-4.4
ZnO-0.5CdS	131.3		62.2	-5.9
ZnO-1CdS	34.6		155.5	-6.9
ZnO-2CdS	17.3		207.4	-8.9
ZnO-5CdS		0.04	242.0	-11.0

Table 6.3: Measured values of nonlinear absorption coefficient, saturation intensity and nonlinear refractive index of ZnO-CdS nanocomposites at an intensity of $300 \text{ MW}/\text{cm}^2$ for different irradiation wavelengths

6.5.6 Optical limiting

Figure 6.21 illustrates the influence of volume fraction of CdS in ZnO-CdS nanocomposites on the optical limiting response. The optical

limiting threshold is found to be high in the case of ZnO colloids (55 MW/cm^2) in comparison with the CdS colloids (20 MW/cm^2). ZnO-CdS nanocomposites are found to be good optical limiters compared to ZnO and CdS and the optical limiting threshold of ZnO-5CdS nanocomposites is observed to be 7 MW/cm^2 . Nanocomposites have a significant effect on the limiting performance and increasing the volume fraction of CdS reduces the limiting threshold and enhances the optical limiting performance.

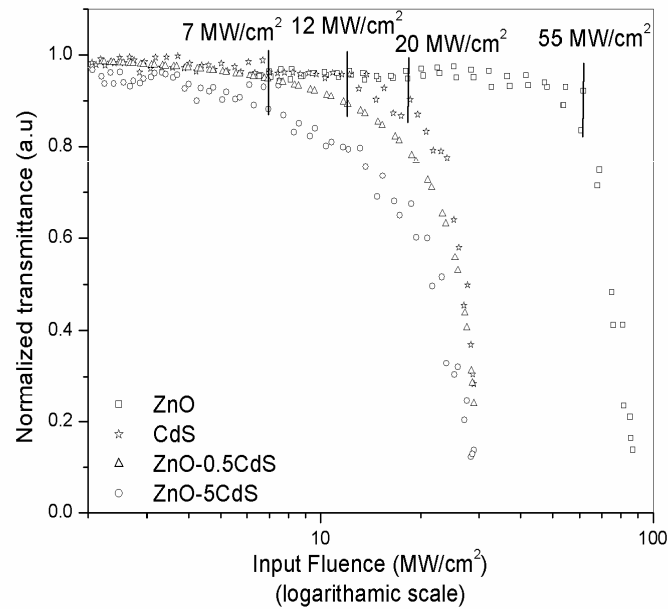


Figure 6.21: Optical limiting response of ZnO-CdS nanocomposites at 532nm

6.6 ZnO-TiO₂

6.6.1 Synthesis

The TiO₂ nanocolloids are prepared by hydrolysis method⁶³. Titanium tetrabutoxide (Aldrich) is used as the precursor. In a typical

synthesis, 0.025M titanium tetrabutoxide is dispersed in distilled water under stirring. The solution is kept on stirring for one hour to get a monodisperse stable colloid. The ZnO-TiO₂ nanocomposites are prepared by colloidal chemical synthesis by mixing certain amount of TiO₂ colloid to ZnO colloid and stirred for 1 hour. The volume fraction of TiO₂ is changed keeping the volume of ZnO constant. The samples having ZnO-xTiO₂ composition with (x=) 0.1-5% are named as ZnO-0.1TiO₂ to ZnO-5TiO₂ respectively.

6.6.2 Absorption spectroscopy

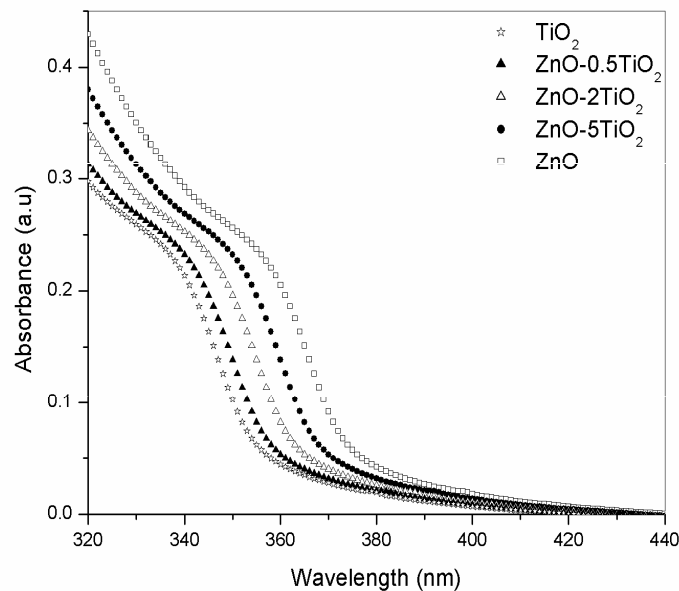


Figure 6.22: Absorption spectra of ZnO-TiO₂ nanocomposites

Figure 6.22 gives the room temperature absorption spectra of the ZnO-TiO₂ nanocomposites. The excitonic peak of ZnO and that of TiO₂ colloids are found to be blue shifted with respect to their bulk which could be attributed to the confinement effects³⁰. From the shift of the absorption band

edge, the size of ZnO and TiO₂ nanocolloids are calculated to be in the range of 8-10 nm. The presence of excitonic peak itself indicates that the composites are of nanometer size. It is seen that the absorption edge corresponding to the nanocomposites gets red shifted as a function of the TiO₂ content compared to pure TiO₂.

6.6.3 Optical bandgap

The direct bandgap of ZnO-TiO₂ nanocomposites is estimated from the graph of $h\nu$ versus $(\alpha h\nu)^2$. The optical band gap (E_g) is found to be dependent on the composition and there is a decrease in the band gap of the nanocomposite with an increase in volume fraction of TiO₂ compared to pure TiO₂ as shown in figure 6.23.

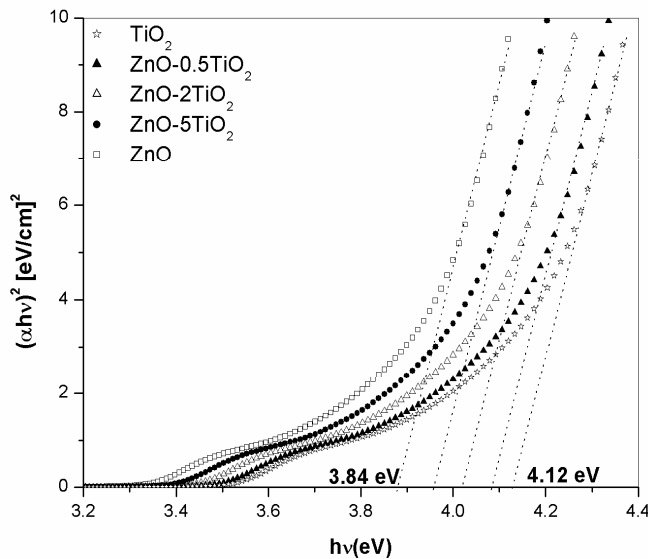


Figure 6.23: Optical band gap of ZnO-TiO₂ nanocomposites

This is because higher carrier concentrations in conduction and valence bands lead to bandgap reduction due to enhanced carrier-carrier

interaction as well as by the distortion of the crystal lattice since the optical properties of the nano colloids strongly depend on the micro-structure of the materials. Both bandgap narrowing mechanisms add up and they are often hard to separate²³. E_g changes from 3.84 eV to 4.12 eV almost in proportion to the composition of TiO_2 .

6.6.4 Fluorescence spectroscopy

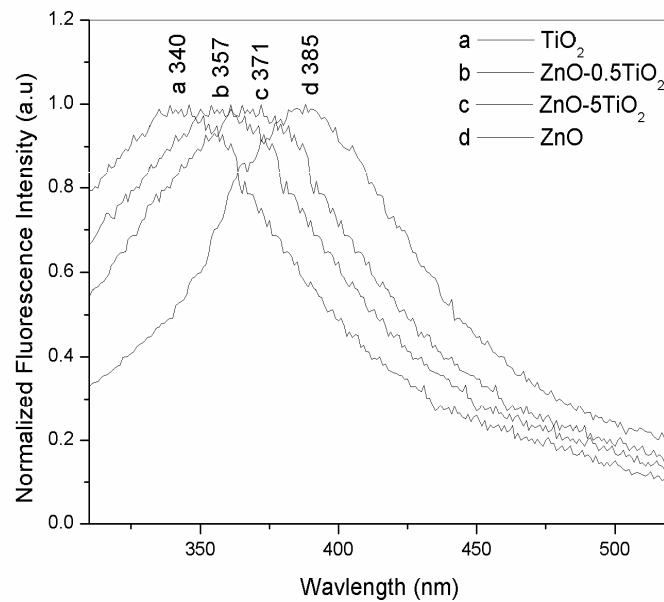


Figure 6.24: Fluorescence spectra of $\text{ZnO}-\text{TiO}_2$ nanocomposites

Photoluminescence spectra of all samples for an excitation wavelength of 300 nm measured at room temperature are shown in Figure 6.24. The 385 nm emission is the near band edge emission of ZnO and the 340 nm emission is the near band edge emission peak of TiO_2 . Emission peaks of $\text{ZnO}-\text{TiO}_2$ nanocomposites changes from 340 nm to 385 nm almost

in proportion to changes in E_g . It is possible to obtain a desired wavelength of UV luminescence by simply adjusting the composition.

6.6.5 Nonlinear optical characterization

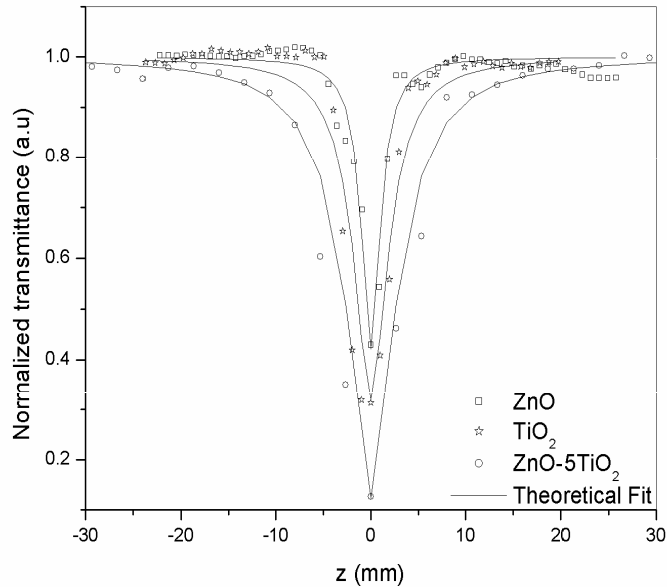


Figure 6.25: Open aperture z-scan traces of ZnO-TiO₂ nanocomposites at an intensity of 300 MW/cm² for an irradiation wavelength of 532 nm

Figure 6.25 shows the nonlinear absorption of ZnO-TiO₂ nanocomposites at a typical fluence of 300 MW/cm² for an irradiation wavelength of 532 nm. ZnO and TiO₂ colloids show a minimum nonlinearity, while the ZnO-TiO₂ nanocomposites clearly exhibit a larger induced absorption behavior and can be attributed to the enhancement of exciton oscillator strength¹². The obtained nonlinearity is found to be of the third order, as it fits to a two photon absorption (TPA) process. The nanosecond pulses can excite the accumulated free carriers generated by

TPA in ZnO. But the free carrier absorption is weak compared to TPA and hence the corresponding contribution in the z-scan curves is relatively less. The large optical nonlinearities in the nanosized particles containing TiO₂ are reported to be due to TPA⁶⁴. Thus we propose that the observed nonlinearity is caused by two photon absorption followed by weak free carrier absorption in the nanocomposites.

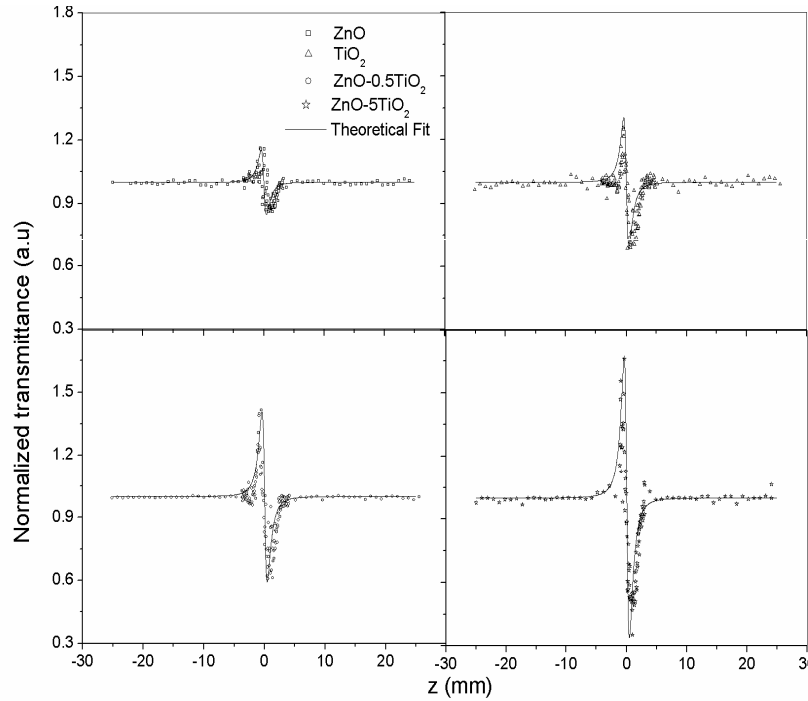


Figure 6.26: Closed aperture z-scan traces of ZnO-TiO₂ nanocomposites at an intensity of 300 MW/cm² for an irradiation wavelength of 532 nm

Figure 6.26 gives the closed aperture z-scan traces of ZnO-TiO₂ nanocomposites at a fluence of 300 MW/cm². It is observed that the peak-valley of closed-aperture z-scan satisfied the condition $\Delta z \sim 1.7 z_0$, thus confirming the presence of pure electronic third order nonlinearity⁴³. The peak–valley trace in a closed aperture z-scan shows that these samples have

self-defocusing (negative, $n_2 < 0$) nonlinearity, though earlier reports with 780 nm picosecond pulsed lasers have shown positive nonlinearity for PMMA-TiO₂ nanocomposites⁶⁵. The nonlinear refractive index increases substantially in the nanocomposites, as compared to pure ZnO and TiO₂ colloids and can be attributed to the enhancement of exciton oscillator strength¹². Since n_2 increases with absorption, thermal nonlinearity is also taken into account⁴⁷.

ZnO-TiO ₂ nanocomposites	β cm/GW	n_2 $10^{-17} \text{m}^2/\text{W}$
ZnO	20.7	-1.5
TiO ₂	77.8	-2.9
ZnO-0.1 TiO ₂	86.4	-4.1
ZnO-0.5 TiO ₂	100.2	-6.0
ZnO-1 TiO ₂	121.0	-6.9
ZnO-2 TiO ₂	138.2	-8.9
ZnO-5 TiO ₂	180.0	-10.3

Table 6.4: Measured values of nonlinear absorption coefficient and nonlinear refractive index of ZnO-TiO₂ nanocomposites at an intensity of 300 MW/cm² for an irradiation wavelength of 532 nm

The obtained values of nonlinear optical parameters of ZnO-TiO₂ nanocomposites are shown in table 6.4. The third order optical nonlinearity, n_2 of TiO₂ nanocrystalline particles dispersed in SiO₂ is found to be 10^{-12} esu at 532 nm with nanosecond laser pulses⁶⁶. The two photon absorption coefficient of TiO₂ nanocrystal is reported to be 14 cm/GW at 532 nm and these values are comparable to the value of β obtained for nanocomposites in the present investigation⁶⁶. Thus, the nonlinear absorption

coefficient and nonlinear refractive index measured by the z-scan technique reveals that the ZnO-TiO₂ nanocomposites investigated in the present study have good nonlinear optical response and could be chosen as ideal candidates with potential applications in nonlinear optics.

6.6.6 Optical limiting

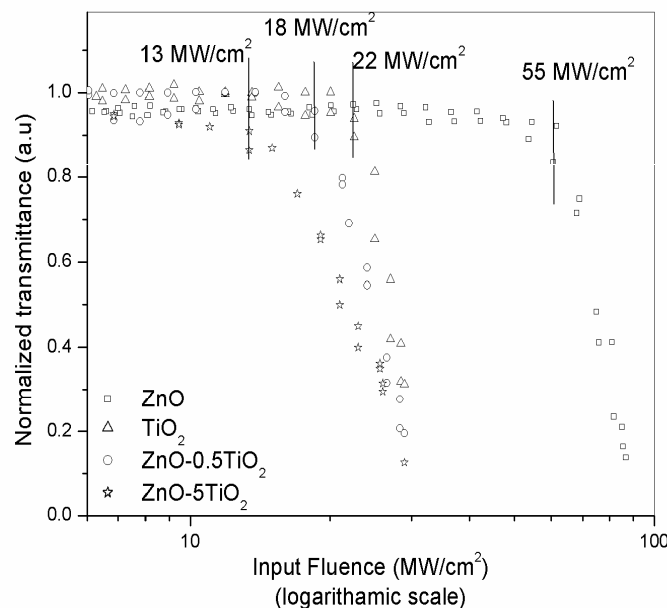


Figure 6.27: Optical limiting response of ZnO-TiO₂ nanocomposites

Figure 6.27 illustrates the influence of volume fraction of TiO₂ in ZnO-TiO₂ nanocomposites on the optical limiting response. The optical limiting threshold is found to be high in the case of ZnO colloids (55 MW/cm²) in comparison with the TiO₂ colloids (22 MW /cm²). ZnO-TiO₂ nanocomposites are found to be good optical limiters compared to ZnO and TiO₂ and the optical limiting threshold of ZnO-5TiO₂ nanocomposites is observed to be 13 MW/cm². Nanocomposites have a significant effect on the

limiting performance and increasing the volume fraction of TiO_2 reduces the limiting threshold and enhances the optical limiting performance.

6.7 ZnO-SiO₂

6.7.1 Synthesis

A stable nanocolloid of SiO_2 particles dispersed in water has been obtained from Aldrich Chemical Company. The ZnO-SiO₂ nanocomposites are prepared by colloidal chemical synthesis by mixing certain amount of SiO_2 colloid to ZnO colloid at 120°C during its preparation stage and stirred for 1 hour at that temperature. The nonlinearity of the silica colloid is low and its nonlinear response can be improved by making composites with ZnO and hence the volume fraction of ZnO is changed keeping the volume of SiO_2 a constant. The samples having $x\text{ZnO-SiO}_2$ composition of ($x=$) 0.1-5% are named as 0.1ZnO-SiO₂ to 5ZnO-SiO₂ respectively.

6.7.2 Absorption spectroscopy

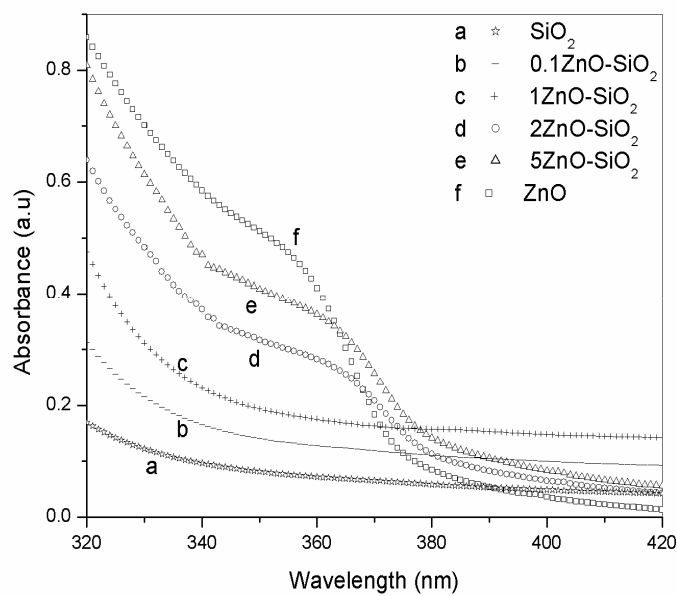


Figure 6.28: Absorption spectra of ZnO-SiO₂ nanocomposites

Figure 6.28 gives the room temperature absorption spectra of the ZnO-SiO₂ nanocomposites. The excitonic peak of ZnO colloid is found to be blue shifted with respect to that of bulk ZnO which could be attributed to the confinement effects³⁰. There is a change in absorption with the ZnO content and as the volume fraction of ZnO increases beyond 2%, the excitonic peak exhibits its signature. It is seen that the absorption edge corresponding to the nanocomposites gets red shifted and the exciton oscillator strength increases as a function of the ZnO content consistent with published reports⁶⁵.

6.7.3 Fluorescence spectroscopy

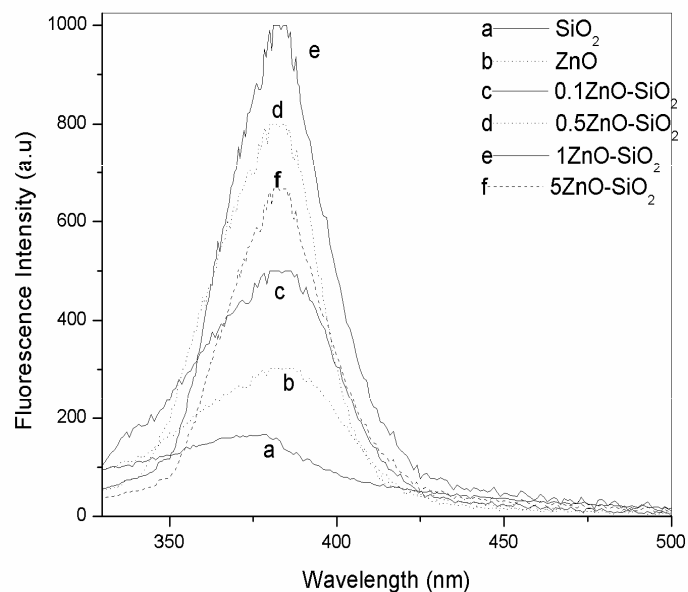


Figure 6.29: Fluorescence spectra of ZnO-SiO₂ nanocomposites

Photoluminescence spectra of all the samples measured at room temperature are shown in Figure 6.29. The intensities of the emission peaks depend on the volume fraction of ZnO present in the samples. ZnO and ZnO-

SiO_2 composites exhibit emission at 385 nm, but the fluorescence intensity of the composites is much stronger than that of ZnO . 1ZnO-SiO_2 has the strongest UV emission centered at 385 nm. The increase of the UV emission can be attributed to the enhancement of the exciton oscillator strength¹².

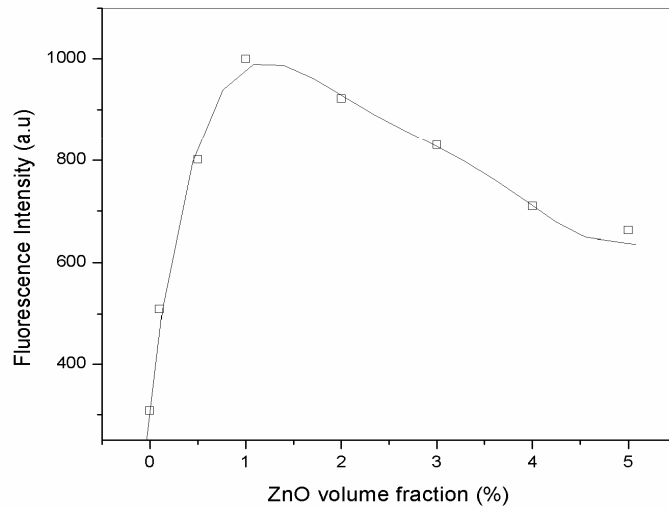


Figure 6.30: The fluorescence intensity of UV peak as a function of the volume fraction of ZnO in ZnO-SiO_2 nanocomposites

Figure 6.30 shows the PL intensity as a function of the ZnO content. It is clear that the intensity of this peak increases with the increasing amount of the Zn acceptors. As the volume fraction of ZnO increases, the formation of aggregates decreases the fluorescence emission⁶⁷. This can be related to the phenomenon of re-absorption and emission at higher concentrations which ultimately reduces the fluorescence emission. As the volume fraction increases, the low frequency tail of the absorption spectrum of the sample overlaps with the high frequency end of its fluorescence spectrum. The fluorescence from the excited state is reabsorbed by the ground state. This

process increases with increase in volume fraction, which results in decrease of fluorescence. The formation of aggregates quenches the fluorescence emission by collision or long range non-radiative energy transfer. The emission of ZnO at 385 nm can be attributed to exciton transition. As the volume fraction of ZnO increases, the exciton oscillator strength increases, so that the UV emission is enhanced accordingly as shown in figure 6.29. Nanostructural semiconductor materials generally have more holes accumulated on its surface or in the interface than common semiconductor materials³⁵.

6.7.4 Nonlinear optical characterization

Figure 6.31 shows the nonlinear absorption of ZnO-SiO₂ nanocomposites at a typical fluence of 300 MW/cm².

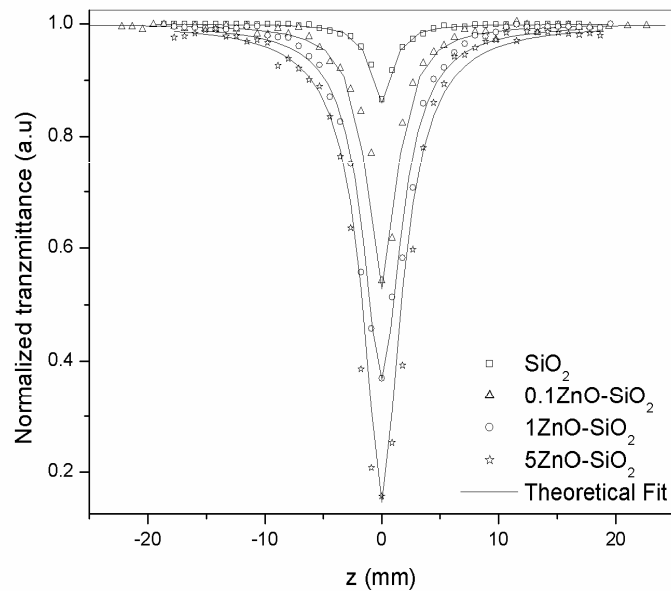


Figure 6.31: Open aperture z-scan traces of ZnO-SiO₂ nanocomposites at an intensity of 300 MW/cm² for an irradiation wavelength of 532 nm

The nonlinear absorption coefficient increases substantially in the nanocomposites, as compared to pure ZnO and SiO₂ colloids. It is reported that the nonlinear absorption coefficient increases in the core-shell silica nanocomposites, as compared to pure nanoparticles³⁷. The large values of the third-order nonlinearity can be attributed to the enhancement of exciton oscillator strength¹².

The obtained nonlinearity is found to be of the third order, as it fits to a two photon absorption process. The nanosecond pulses can excite the accumulated free carriers generated by TPA in ZnO. But the free carrier absorption is weak compared to TPA and hence the corresponding contribution in the z-scan curves is relatively less. It is possible that nonlinear scattering dominates two photon absorption on the silica colloids and the presence of nonlinear scattering reduces the two photon absorption coefficient in silica colloids⁶⁸. Both the linear and the nonlinear absorption of wide-band silica colloids in the visible and the near-infrared ranges are known to be negligible if the input intensity is well below the breakdown threshold⁶⁸. Therefore, two-photon absorption contribution is expected to be very small in silica colloids because the total input intensity is relatively small compared to the breakdown threshold. Hence we propose that the nonlinearity in ZnO-SiO₂ nanocomposites is caused by two photon absorption followed by weak free carrier absorption and nonlinear scattering.

Figure 6.32 gives the closed aperture z-scan traces of ZnO-SiO₂ nanocomposites at a fluence of 300 MW/cm². The closed-aperture curve exhibits a peak-valley shape, indicating a negative value of the nonlinear refractive index n_2 . It is observed that the peak-valley of closed-aperture z-scan satisfied the condition $\Delta z \sim 1.7 z_0$, thus confirming the presence of pure electronic third order nonlinearity⁴³. The peak-valley trace in a closed aperture z-scan shows that these samples have self-defocusing (negative, $n_2 < 0$) nonlinearity, though earlier reports with nanosecond pulsed lasers have

shown positive nonlinearity for fused silica due to the mechanism of electrostriction⁶⁹.

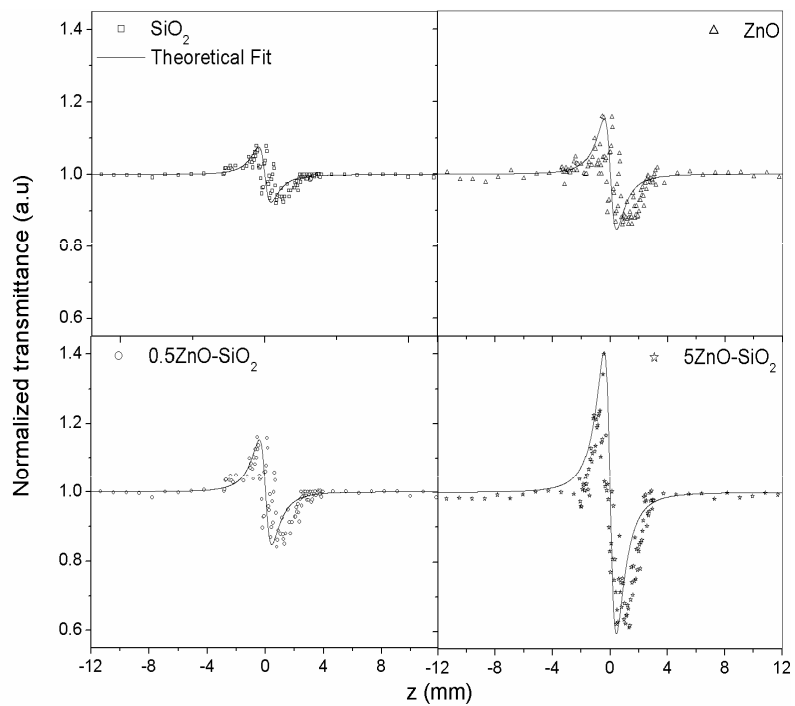


Figure 6.32: Closed aperture z-scan traces of ZnO-SiO₂ nanocomposites at an intensity of 300 MW/cm² for an irradiation wavelength of 532 nm

We suggest that the possible physical origin of the nonlinear refraction of ZnO-SiO₂ composites is mainly a two photon absorption process and partially nonlinear scattering and weak thermal effects in the nanosecond time domain. It is reported that the difference between the third-order optical susceptibilities for z-scan and four wave mixing (FWM) is due to scattering from the surface of silica nanoaerogels in the z-scan measurements²⁴. We have not observed any sign reversal of the nonlinear refractive index either in the intensity ranges (150-400 MW/cm²) studied using the second harmonics of a Q-switched Nd:YAG laser or within the

wavelength range 450-650 nm studied using a tunable laser (Quanta Ray MOPO, 5 ns, 10 Hz). The nanocomposites exhibit induced absorption at all wavelengths and good nonlinear absorption, which increases with increase in input intensity. The nonlinear refractive index increases substantially in the nanocomposites, as compared to pure ZnO and SiO₂ colloids. The large enhancement of the third-order nonlinearity of the silica aerogel is reported to be due to the quantum confinement effect of bound electrons, which is induced by the nanostructure nature of the sample⁷⁰.

ZnO-SiO ₂ nanocomposites	β cm/GW	n ₂ $10^{-17} \text{m}^2/\text{W}$
ZnO	20.7	-1.5
SiO ₂	1.7	-0.9
0.1ZnO-SiO ₂	12.1	-2.2
0.5ZnO-SiO ₂	27.7	-3.1
1ZnO-SiO ₂	41.5	-4.4
2ZnO-SiO ₂	86.4	-5.0
5ZnO-SiO ₂	138.2	-5.9

Table 6.5: Measured values of nonlinear absorption coefficient and nonlinear refractive index of ZnO-SiO₂ nanocomposites at an intensity of 300 MW/cm² for an irradiation wavelength of 532 nm

In the present investigations, the obtained values of nonlinear optical parameters of ZnO-SiO₂ nanocomposites are shown in table 6.5. The third-order nonlinear susceptibility of silica nanoaerogels is estimated to be $9.6 \times 10^{-19} \text{ m}^2/\text{V}^2$ ($6.9 \times 10^{-11} \text{ esu}$) from FWM measurements⁷⁰. In the case of fused silica, the nonlinear refractive index is reported to be quite small, roughly $3 \times 10^{-20} \text{ m}^2/\text{W}$, which is about two order of magnitude below the nonlinear refractive index of most of the materials usually studied with the z-

scan method⁷⁰. The core-shell silica nanocomposites yielded values of the order of 10^{-9} to 10^{-14} m/W for nonlinear absorption coefficient and 10^{-16} to 10^{-20} m²/W for nonlinear refractive index at a wavelength of 532 nm. These values are comparable to the value of β and n_2 obtained for nanocomposites in the present investigation.

6.7.5 Optical limiting

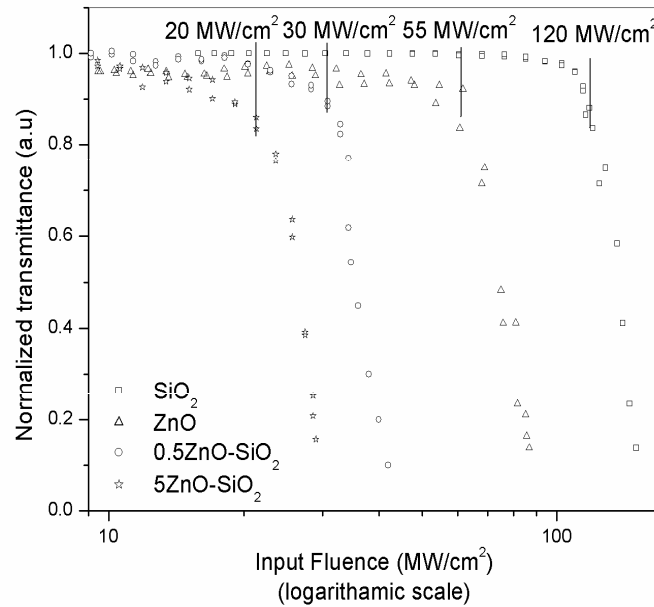


Figure 6.33: Optical limiting response of ZnO-SiO₂ nanocomposites generated from open aperture z-scan traces at 532 nm

Figure 6.33 illustrates the influence of volume fraction of ZnO in ZnO-SiO₂ nanocomposites on the optical limiting response. The optical limiting threshold is found to be very low in the case of ZnO colloids (55 MW/cm²) in comparison with that of the silica colloids (120 MW /cm²). ZnO-SiO₂ nanocomposites are found to be good optical limiters compared to

ZnO and SiO₂ and the optical limiting threshold of 5ZnO-SiO₂ nanocomposites is observed to be 20 MW/cm². Nanocomposites have a significant effect on the limiting performance and increasing the volume fraction of ZnO reduces the limiting threshold and enhances the optical limiting performance.

6.8 ZnO-TiO₂-SiO₂

6.8.1 Synthesis

The ZnO-TiO₂-SiO₂ nanocomposites are prepared by colloidal chemical synthesis by mixing fixed amount of TiO₂ and SiO₂ colloids to ZnO colloid at 120°C during its preparation stage and stirred for 1 hour at that temperature. The volume fraction of ZnO is changed keeping the volume of TiO₂ and SiO₂ a constant. The samples having xZnO-TiO₂-SiO₂ composition of (x=) 1-5% are named as 1ZnO-TiO₂-SiO₂ to 5ZnO-TiO₂-SiO₂ respectively.

6.8.2 Absorption spectroscopy

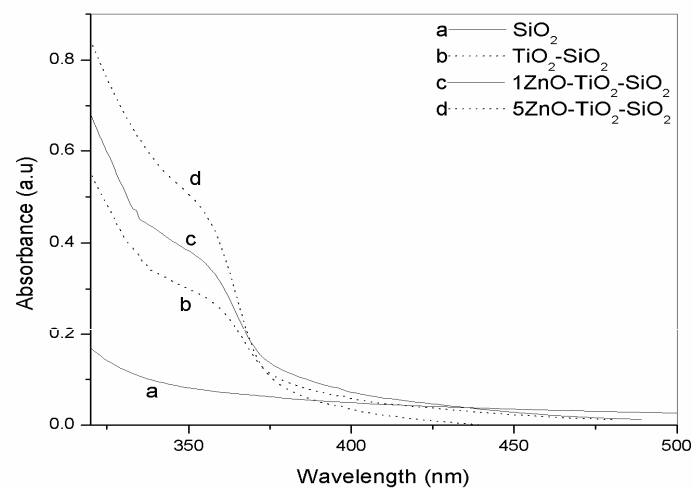


Figure 6.34: Absorption spectra of ZnO-TiO₂-SiO₂ nanocomposites

Figure 6.34 gives the room temperature absorption spectra of the ZnO-TiO₂-SiO₂ nanocomposites. There is a change in absorption with the ZnO content and as the volume fraction of ZnO increases, the excitonic peak exhibits its signature³⁰. It is seen that the absorption edge corresponding to the nanocomposites gets red shifted and the exciton oscillator strength increases as a function of the ZnO content consistent with published reports⁶⁵.

6.8.3 Nonlinear optical characterization

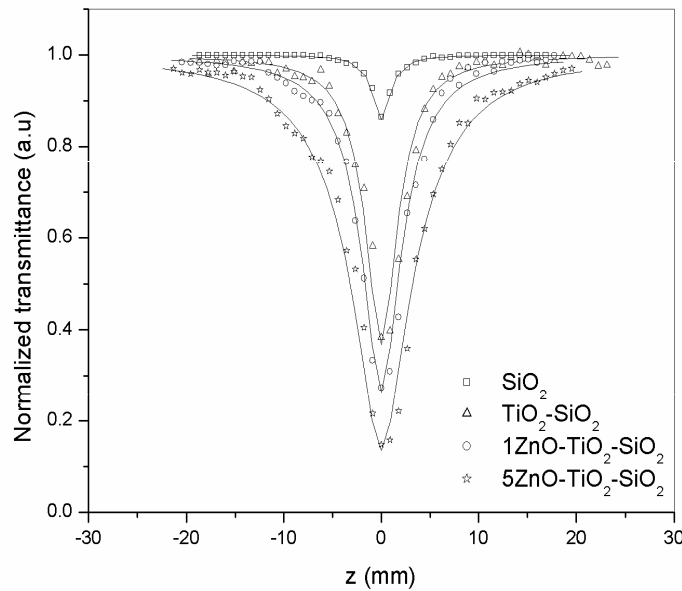


Figure 6.35: Open aperture z-scan traces of ZnO-TiO₂-SiO₂ nanocomposites [intensity of 300 MW/cm², wavelength = 532 nm]

Figure 6.35 shows the nonlinear absorption of ZnO-TiO₂-SiO₂ nanocomposites at a typical fluence of 300 MW/cm². The nonlinear absorption coefficient increases substantially in the nanocomposites, as

compared to pure SiO_2 colloids. The large values of the third-order nonlinearity can be attributed to the enhancement of exciton oscillator strength¹². We propose that this nonlinearity is caused by two photon absorption followed by weak free carrier absorption and nonlinear scattering occurring in the nanocomposites.

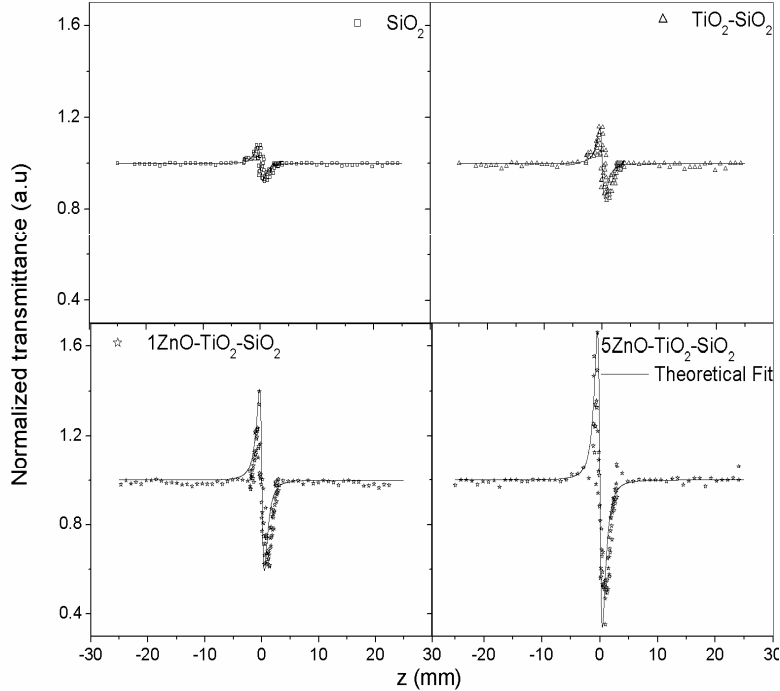


Figure 6.36: Closed aperture z-scan traces of $\text{ZnO-TiO}_2\text{-SiO}_2$ nanocomposites[$I = 300 \text{ MW/cm}^2$, irradiation wavelength = 532 nm]

Figure 6.36 gives the closed aperture z-scan traces of $\text{ZnO-TiO}_2\text{-SiO}_2$ nanocomposites at a fluence of 300 MW/cm^2 . The closed-aperture curve exhibits a peak-valley shape, indicating a negative value for the nonlinear refractive index n_2 . It is observed that the peak-valley of closed-aperture z-scan satisfied the condition $\Delta z \sim 1.7 z_0$, thus confirming the presence of pure electronic third order nonlinearity⁴³. We suggest that the possible physical

origin of the nonlinear refraction of ZnO-TiO₂-SiO₂ nanocomposites is mainly due to two photon absorption process and partially due to nonlinear scattering and weak thermal effects in the nanosecond time domain. We have not observed any sign reversal of the nonlinear refractive index either in the intensity ranges (150-400 MW/cm²) studied using the second harmonics of a Q-switched Nd:YAG laser or within the wavelength range 450-650 nm studied using a tunable laser (Quanta Ray MOPO, 5 ns, 10 Hz).

ZnO-TiO ₂ -SiO ₂ nanocomposites	β cm/GW	n ₂ $10^{-17} \text{m}^2/\text{W}$
SiO ₂	1.7	-0.9
TiO ₂ -SiO ₂	27.7	-3.1
1ZnO-TiO ₂ -SiO ₂	51.8	-3.8
2ZnO-TiO ₂ -SiO ₂	86.4	-5.0
3ZnO-TiO ₂ -SiO ₂	110.6	-6.7
5ZnO-TiO ₂ -SiO ₂	155.5	-9.5

Table 6.6: Measured values of nonlinear absorption coefficient and nonlinear refractive index of ZnO-TiO₂-SiO₂ nanocomposites at an intensity of 300 MW/cm² for an irradiation wavelength of 532 nm

The obtained values of nonlinear optical parameters of ZnO-TiO₂-SiO₂ nanocomposites are shown in table 6.6. The nanocomposites exhibit induced absorption at all wavelengths and good nonlinear absorption, which increases with increase in input intensity. The nonlinear refractive index increases substantially in the nanocomposites, as compared to pure SiO₂ colloids.

6.8.4 Optical limiting

Figure 6.37 illustrates the influence of volume fraction of ZnO in ZnO-TiO₂-SiO₂ nanocomposites on the optical limiting response. The optical

limiting threshold is found to be very low in the case of $\text{TiO}_2\text{-SiO}_2$ colloids (21 MW/cm^2) in comparison with that of the silica colloids (120 MW/cm^2). $\text{ZnO-TiO}_2\text{-SiO}_2$ nanocomposites are found to be good optical limiters compared to ZnO , TiO_2 and SiO_2 and the optical limiting threshold of $5\text{ZnO-TiO}_2\text{-SiO}_2$ nanocomposites is observed to be 11 MW/cm^2 . Nanocomposites have a significant effect on the limiting performance and increasing the volume fraction of ZnO reduces the limiting threshold and enhances the optical limiting performance.

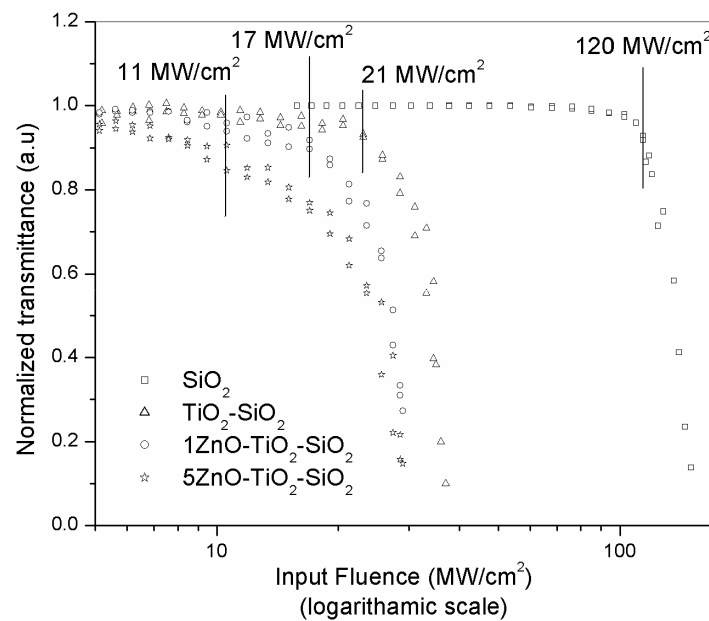


Figure 6.37: Optical limiting response of $\text{ZnO-TiO}_2\text{-SiO}_2$ nanocomposites

6.9 Conclusions

The spectral and nonlinear optical properties of ZnO based nanocomposites prepared by colloidal chemical synthesis are investigated and are summarized in the following table.

Nanocomposites	Emission mechanism	Third order Optical Nonlinearity
ZnO-Ag	Strong UV emission	Negative nonlinearity and induced absorption due to TPA followed by weak FCA at 532 nm
ZnO-Cu	UV and Visible emission	Negative nonlinearity at 532 nm Switching from SA to RSA as the excitation wavelength changes from the surface plasmon resonance to off-resonance wavelengths Off-resonance wavelength: TPA followed by weak FCA and interband absorption Resonance wavelength: Plasmon band bleach and optical limiting
ZnO-CdS	Emission peaks changes from 385-520 nm in proportion to changes in E_g from 2.62-3.84 eV	Negative nonlinearity at 532 nm Switching from SA to RSA as the excitation wavelength changes from the excitonic resonance to off-resonance wavelengths Off-resonance wavelength: TPA followed by weak FCA Resonance wavelength: Exciton bleach and optical limiting mechanisms
ZnO-TiO ₂	Emission peaks 340-385nm E_g from 3.84-4.12 eV	Negative nonlinearity and induced absorption due to TPA followed by weak FCA at 532 nm
ZnO-SiO ₂	Strong UV emission	Negative nonlinearity and induced absorption due to TPA followed by weak FCA and nonlinear scattering at 532 nm
ZnO-TiO ₂ -SiO ₂	-	Negative nonlinearity and induced absorption due to TPA followed by weak FCA and nonlinear scattering at 532 nm

The large values of the third-order nonlinearity in the composites can be attributed to the enhancement of exciton oscillator strength. Thus ZnO based nanocomposites are potential materials for the light emission and for the development of nonlinear optical devices with a relatively small limiting threshold.

6.10 References

- 1 Kreibig U, Vollmer M; “*Optical Properties of Metal Clusters*”; Springer: Berlin, 1995
- 2 Bernhard Kraeutler, Alien J Bard; “*Heterogeneous Photocatalytic Preparation of Supported Catalysts. Photodeposition of Platinum on TiO₂ Powder and Other Substrates*”;
JACS **100**, 4317 (1978)
- 3 T Sekino, T Nakajima, S Ueda and K Niihara; “*Reduction and Sintering of a Nickel-Dispersed-Alumina Composite and Its Properties*”; *J. of the American Ceramic Society*, **80**,1139 (1997)
- 4 A. E. Hichou, A. Bougrine, J. L. Bubendorff, J. Ebothe, M. Addou, and M Troyon; “*Structural, optical and cathodoluminescence characteristics of sprayed undoped and fluorine-doped ZnO thin films*”, *Semicond. Sci. Technol.* **17**, 607 (2002)
- 5 X. H. Wang, J. L. Shi, S. G. Dai, and Y. Yang; “*A sol-gel method to prepare pure and gold colloid doped ZnO films*”, *Thin Solid Films*, **429**, 102 (2003)
- 6 Litty Irimpan, A Deepthy, Bindu Krishnan, V P N Nampoori and P Radhakrishnan, ‘*Size dependent fluorescence spectroscopy of nanocolloids of ZnO*’; *J. Appl. Phys.* **102**, 063524 (2007)
- 7 D M Bagnall, Y F Chen, Z Zhu, T Yao, S Koyama, M Y Shen and T Goto; “*Optically pumped lasing of ZnO at room temperature*”; *Appl. Phys. Lett.* **70**, 2230 (1997)
- 8 U Ozgur, Ya I Alivov, C Liu, A Teke, M A Reschchikov, S Dogan, V Avrutin, S J Cho and H Morkoc; “*A comprehensive review of ZnO materials and devices*”; *J. Appl. Phys.* **98**, 041301 (2005)
- 9 A Tsukazaki et.al.; “*Repeated temperature modulation epitaxy for p-type doping and light-emitting diode based on ZnO*”; *Nat. Mater.* **4**, 42 (2005)
- 10 Y Sun, J E Riggs, K B Henbest and R B Martin; “*Nanomaterials as optical limiters*”, *J. Nonlinear Opt. Physics & Materials*, **9** 481 (2000)
- 11 Uchida K et.al.; “*Optical nonlinearities of a high concentration of small metal particles dispersed in glass:copper and silver particles*”; *J.Opt. Soc. Am. B, Opt. Phys.* **11**, 1236 (1994)
- 12 A P Alivisatos; “*Perspectives on the Physical Chemistry of Semiconductor Nanocrystals*”;

- J. Phys. Chem. **100**, 13226 (1996)
- 13 L E Brus; “*A simple model for the ionization potential, electron affinity, and aqueous redox potentials of small semiconductor crystallites*”, J. Chem. Phys. **79**, 5566 (1983)
- 14 M V Rama Krishna and R A Friesner; “*Exciton spectra of semiconductor clusters*”, Phys. Rev. Lett. **67**, 629 (1991)
- 15 N Suzuki, Y Tomita and T Kojima; “*Holographic recording in TiO₂ nanoparticle-dispersed methacrylate photopolymer films*” Appl. Phys. Lett. **81**, 4121 (2002)
- 16 S X Wang et.al.; “*Two-photon absorption and optical limiting in poly(styrene maleic anhydride)/TiO₂ nanocomposites*”, Phys. Lett. A **281**, 59 (2001)
- 17 P Yang, C F Song, M K Lu, X Yin, G J Zhou, D Xu and D R Yuan; “*The luminescence of PbS nanoparticles embedded in sol-gel silica glass*”, Chem. Phys. Lett., **345**, 429 (2001)
- 18 M Y Han, W Huang, C H Chew, L M Gan, X J Zhang and W Ji; “*Large Nonlinear Absorption in Coated Ag₂S/CdS Nanoparticles by Inverse Microemulsion*”; J. Phys. Chem. B 1998, **102**, 1884-1887
- 19 A Nakamura, Y L Lee, T Kataoka, and T Tokizaki; ”*Mesoscopic enhancement of optical nonlinearity in semiconducting quantum dots: CuCl and CuBr microcrystals*” J. Lumin., **60–61**, 376 (1994)
- 20 Litty Irimpan, A Deepthy, Bindu Krishnan, V P N Nampoori and P Radhakrishnan; “*Nonlinear optical characteristics of self assembled films of ZnO*” Applied Physics B: Lasers and Optics, **90**, 547 (2008)
- 21 E S P Leong and S F Yu; “*UV Random Lasing Action in p-SiC(4H)/i-ZnO-SiO₂ Nanocomposite/n-ZnO:Al Heterojunction Diodes*”, Advanced Materials, **18** (13) , 1685 (2006)
- 22 Chennupati Jagadish and Stephen J Pearton; “*Zinc oxide: bulk, thin films and nanostructures: Processing, properties and applications*” Elsevier (2006)
- 23 Joachin Piprek; “*Semiconductor optoelectronic devices: Introduction to physics and simulation*”, Academic press, Elsevier -USA (2003)
- 24 J A Van Vechten and T K Bergstresser; “*Electronic structures of semiconductor alloys*”, Phys. Rev. B **1**,3351 (1970)
- 25 W W Chow and S W Koch; “*Semiconductor laser fundamentals*” Berlin: Springer (1999)
- 26 R Zimmermann; “*Many particle theory of highly excited semiconductors*” Leipzig: Teubner Verlagsgesellschaft (1998)
- 27 V Palankavski, G Kaiblunger Grujin and S Selberherr; “*Study of dopant dependent bandgap narrowing in compound semiconductor devices*”, Mater. Sci. Eng. B, **66**, 46 (1999)
- 28 D B M Kaassen, J W Slotboom and B C de Graff; “*Unified apparent bandgap narrowing in n and p type silicon*”, Solid. Stat. Electron. **35**, 125 (1992)
- 29 Litty Irimpan, V P N Nampoori and P Radhakrishnan; “*Spectral and nonlinear optical*

- characteristics of nanocomposites of ZnO-Ag”* Chemical physics letters, **455**, 265 (2008)
- 30 D.L. Moreno, E.D. Rosa-Cruz, F.J. Cuevas, L.E. Regalado, P. Salas, R. Rodriguez, V.M. Castano, “*Refractive index measurement of pure and Er³⁺-doped ZrO₂-SiO₂ sol-gel film by using the Brewster angle technique*”, *Opt. Mat.*, **19**, 275 (2002)
- 31 Shashikant Patole, M Islam, R C Aiver and Shailaja Mahamuni; “*Optical studies of ZnO/Ag nanojunctions*”; *J Mater Sci.* **41**, 5602–5607 (2006)
- 32 Linnert T, Mulvaney, P, Henglein A; “*Surface chemistry of colloidal silver: surface plasmon damping by chemisorbed iodide, hydrosulfide (SH-), and phenylthiolate*”; *J. Phys. Chem.* **97**, 679 (1993)
- 33 A L Stroyuk, V V Shvalagin and S Ya Kuchmii; “*Photochemical Synthesis, Spectral-Optical and Electrophysical Properties of Composite Nanoparticles of ZnO/Ag*”; *Theoretical and Experimental Chemistry*, **40**, 98 (2004)
- 34 Li Duan, Bixia Lin, Weiyi Zhang, Sheng Zhong, and Zhuxi Fua; “*Enhancement of ultraviolet emissions from ZnO films by Ag doping*”, *Appl. Phys. Lett.* **88**, 232110 (2006)
- 35 L. D. Zhang and J. M. Mou, “*Nanomaterials and Nanostructures*” (Scientific, Beijing, China, 2001)
- 36 R Reisfeld, M Eyal and D Brusilovsky; “*Luminescence enhancement of rhodamine 6G in sol-gel films containing silver aggregates*”; *Chemical Physics Letters*, **153**, 210-214 (1988)
- 37 B Karthikeyan, M Anija and Reji Philip; “*In situ synthesis and nonlinear optical properties of Au:Ag nanocomposite polymer films*”; *Appl. Phys. Lett.* **88**, 053104 (2006)
- 38 X J Zhang, W Ji, and S H Tang; “*Determination of optical nonlinearities and carrier lifetime in ZnO*”, *J.Opt. Soc. Am. B*, **14**, 1951 (1997)
- 39 Kamat P V, Flumiani M and Hartland G V; “*Picosecond dynamics of silver nanoclusters. Photoejection of electrons and fragmentation*”; *J. Phys. Chem. B* **102**, 3123 (1998)
- 40 Temer S Ahmadi, Stephan L Logunov and Mostafa A El Sayed; “*Picosecond Dynamics of Colloidal Gold Nano particles*”; *J. Phys. Chem.* **100**, 8053 (1996)
- 41 Philip R, Ravindra Kumar G, Sandhyarani N and Pradeep T; “*Picosecond optical nonlinearity in monolayer-protected gold, silver, and gold-silver alloy nanoclusters*”; *Phys. Rev. B, Condens. Matter*, **62** (19), 13160–13166 (2000)
- 42 Qu S, Song Y, Liu H, Wang Y, Gao Y, Liu S, Zhang X, Li Y and Zhu D; “*A theoretical and experimental study on optical limiting in platinum nanoparticles*”; *Opt. Commun.* **20**, 3283 (2002)
- 43 M S Bahae, A A Said and E W van Stryland; “*High-sensitivity, single-beam n₂ measurements*”, *Opt Lett.* **14**, 955 (1989)
- 44 Hamanaka Y, Nakamura A, Omi S, Del Fatti N, Vallee F, and Flytzanis C; ‘*Ultrafast response of nonlinear refractive index of silver nanocrystals embedded in glass*’, *Appl. Phys. Lett.* **75** (12), 1712–1714(1999)

- 45 Osborne, Jr. D.H., Haglund, Jr. R.F., Gonella, F., and Garrido, F. "Laser-induced sign reversal of the nonlinear refractive index of Ag nanoclusters in soda-lime glass"; Appl. Phys. B, Lasers and Opt. **66**, 517–521 (1998)
- 46 Wang Gang, Zhang Yu, Cui Yiping, Duan Muyun and Liu Mi; "Study on the non-linear refraction of silver nanoparticles with aggregation effect"; Opt. commun. **249**, 311 (2005)
- 47 P. Prem Kiran, G. De and D. Narayana Rao, "Nonlinear optical properties of copper and silver nanoclusters in SiO_2 sol-gel films"; IEE Proc.-Circuits Devices Syst., Vol. **150** (6), 559 (2003)
- 48 Guang Yang, Dongyi Guan, Weitian Wang, Weidong Wu and Zhenghao Chen; "The inherent optical nonlinearities of thin silver films"; Optical Materials, **25** (4), 439-443 (2004)
- 49 S. Shi, W. Ji, and S.H. Tang; "Synthesis and optical limiting capability of cubane-like mixed metal clusters (n -Bu₄N)3[MoAg₃ BrX₃S₄] (X = Cl and I)", J. Am. Chem Soc., **116**, 3615-3616 (1994)
- 50 Wenling Jia, Elliot P Douglas, Fenggi Guo and Wenfang Suna; "Optical limiting of semiconductor nanoparticles for nanosecond laser pulses", Appl. Phys. Lett. **85** (26), 6326 (2004)
- 51 Litty Irimpan, Bindu Krishnan, A Deepthy, V P N Nampoori and P Radhakrishnan; "Size dependent enhancement of nonlinear optical properties in nano colloids of ZnO", Journal of applied physics **103**, 033105 (2008)
- 52 A A Khosravi, M Kundu, L Jatwa, S K Deshpande, U A Bhagwat, M Sastry and S. K. Kulkarni; "Green luminescence from copper doped zinc sulphide quantum particles", Appl. Phys. Lett., **67**, 18 (1995)
- 53 H S Kang, J S Kang, S S Pang, E S Shim and S Y Lee; "Variation of light emitting properties of ZnO thin films depending on post-annealing temperature" Mater. Sci. Eng. B, **102**, 313 (2003)
- 54 A Suzuki and S Shionoya; "Mechanism of the Green-Copper Luminescence in ZnS Crystals. I. Direct Evidence for the Pair Emission Mechanism"; J. Phys. Soc. Jpn. **31**, 1455 (1971)
- 55 P Peka and H J Schulz; "Empirical one-electron model of optical transitions in Cu-doped ZnS and CdS", Physica B **193**, 57 (1994)
- 56 B Karthikeyan, J Thomas and R Philip; "Optical nonlinearity in glass-embedded silver nanoclusters under ultrafast laser excitation"; Chem. Phys. Lett. **414**, 346 (2005)
- 57 Y Gao, X Zhang, Y Li, H Liu, Y Wang, Q Chang, W Jiao and Y Song; "Saturable absorption and reverse saturable absorption in platinum nanoparticles" Opt. Commun. **251**, 429 (2005)
- 58 S K Panda et.al.; "Optical and microstructural characterization of CdS-ZnO nanocomposite thin films prepared by sol-gel technique", J. Phys. D: Appl. Phys. **37** 628-

- 633 (2004)
- 59 Shigeo Shionoya and William M Yen, Phosphor handbook (CRC press, New York, 1999)
- 60 J He, W Ji, G H Ma, S H Tang, H I Elim, W X Sun, Z H Zhang and W S Chin; “*Excitonic nonlinear absorption in CdS nanocrystals studied using Z-scan technique*”, *J. Appl. Phys.*, **95**, 11 (2004)
- 61 R A Ganeev et.al.; “*Investigation of nonlinear refraction and nonlinear absorption of semiconductor nanoparticle solutions prepared by laser ablation*”, *J. Opt. A: Pure Appl. Opt.* **5**, 409 (2003)
- 62 N. Venkatram, R. Sai Santosh Kumar, and D. Narayana Rao; “*Nonlinear absorption and scattering properties of cadmium sulphide nanocrystals with its application as a potential optical limiter*” *J. Appl. Phys.* **100**, 074309 (2006)
- 63 Robson Fernandes de Farias, “*Synthesis of TiO₂ (Anatase) by Sol–Gel Process Performed in Metal Chlorides Saturated Aqueous Solutions*” *Journal of Colloid and Interface Science*, **239**, 584 (2001)
- 64 A Penzkofer and W Falkenstein; “*Direct determination of the intensity of picosecond light pulses by two-photon absorption*” *Opt. Commun.* **17**, 1 (1976)
- 65 H. I. Elim, W. Ji, A. H. Yuwono, J. M. Xue and J. Wang; “*Ultrafast optical nonlinearity in poly.methylmethacrylate-TiO₂nanocomposites*” *Appl. Phys. Lett.*, **82** (16) 2691 (2003)
- 66 Yuichi Watanabe, Masato Ohnishi, and Toshio Tsuchiya; “*Measurement of nonlinear absorption and refraction in titanium dioxide single crystal by using a phase distortion method*”, *Appl. Phys. Lett.* **66** (25) 3431 (1995)
- 67 Achamma Kurian, K P Unnikrishnan, Pramod Gopinath, V P N Nampoori and C P G Vallabhan, “*Study of energy transfer in organic dye pairs using thermal lens technique*”, *J. Nonlinear Opt. Phys. & Mats.*, **10**, 415 (2001)
- 68 Sun, J P Longtin and P M Norris; “*Ultrafast laser micromachining of silica aerogels*” *J. Non-Cryst. Solids* **281**, 39 (2001)
- 69 Thomas Olivier, Franck Billard and Hassan Akhouayri, “*Nanosecond Z-scan measurements of the nonlinear refractive index of fused silica*”, *Optics Express*, **12** (7), 1377 (2004)
- 70 J T Seo, S M Ma, Q Yang, L Creekmore, H Brown, R Battle, K Lee, A Jackson, T Skyles, B Tabibi, K P Yoo, S Y Kim, S S Jung and M Namkung, “*Large Optical Nonlinearity of Highly Porous Silica Nanoaerogels in the Nanosecond Time Domain*”, *Journal of the Korean Physical Society*, **48**, 1395 (2006)



Chapter 7

Conclusions and future prospects

Abstract

This chapter deals with the summary of the work reported in this thesis along with an outline of the future prospects. The spectral and nonlinear optical characteristics of nano ZnO and its composites are investigated. The fluorescence behaviour of nano colloids of ZnO has been studied as a function of the excitation wavelength and there is a red shift in emission peak with excitation wavelength. Systematic studies on nano ZnO have indicated the presence of luminescence due to excitonic emissions when excited with 255 nm as well as significant contribution from surface defect states when excited with 325 nm. In the weak confinement regime, the third-order optical susceptibility $\chi^{(3)}$ increases with increasing particle size (R) and annealing temperature (T) and a R^2 and $T^{2.5}$ dependence of $\chi^{(3)}$ is obtained for nano ZnO. ZnO nanocomposites exhibit negative nonlinear index of refraction which can be attributed to two photon absorption followed by weak free carrier absorption. The self assembled films of ZnO exhibit saturable absorption due to saturation of linear absorption of ZnO defect states and electronic effects. ZnO based nanocomposites are potential materials for enhanced and tunable light emission and for the development of nonlinear optical devices with a relatively small optical limiting threshold.

*“Do not go where the path may lead, go instead where
there is no path and leave a trail”
: Ralph Waldo Emerson*

7.1 Synthesis

Scaling down of feature sizes into the nanometer range is a common trend in advanced compound semiconductor devices, and the progress of the nano-fabrication technology along this line has opened up exciting possibilities of constructing novel quantum devices for which the operations are directly based on the quantum mechanics.

ZnO possess very large exciton binding energy which makes the material very attractive both from scientific point of view and optical device application aspect. One of the first attempts to produce II-VI nanocrystals is by the method of colloidal chemical synthesis. Chemical method has many advantages such as relatively low precipitation temperature, scope of capping thereby providing a way for size selection and relatively low cost of fabrication. In the present studies, ZnO is prepared by two different chemical routes such as polyol method and sol-gel method using different capping agents like poly vinyl pyrrolidone (PVP) and poly ethylene imine (PEI).

Both fast nucleation and slow growth dynamics should be adjusted to obtain monodisperse nanocrystals. Large efforts are presently being made to prepare highly monodisperse nanocrystals. The process of self assembly allows us to tune the quantum dot size and improve the size and shape uniformity of the optically active quantum dots. Self assembled ZnO films are prepared by modified polyol synthesis. Scanning electron micrograph of our self assembled films shows that this process is very effective in giving monodisperse ZnO. Although ZnO self assembled films can act as photonic crystals, unfortunately, we are not able to observe photonic crystal properties. Optimization of self assembled films to get photonic crystals is one of the promising areas for future work.

The potential applications of ZnO thin films in optoelectronic devices slowly transformed the present “art” of thin film fabrication into an

established science. In our studies, we have used thin films of nano ZnO prepared by pulsed laser ablation, sol-gel process and spin coating. The optical bandgap of self assembled ZnO film is reduced to 3.1eV from that of the bulk (3.3 eV) whereas the bandgap energies of the colloids and other films developed by pulsed laser ablation, sol-gel process and spin coating are higher than that of the bulk. Thus there exists a strong correlation between the electronic structure and the geometrical structure of the ZnO thin films and hence is an interesting area for future theoretical research. The crystallinity of ZnO thin films can be improved by annealing at high temperatures.

The field of nanocomposites has been widely recognized as one of the most promising and rapidly emerging research areas. In our studies, the ZnO based nanocomposites such as ZnO-Ag, ZnO-Cu, ZnO-CdS, ZnO-TiO₂, ZnO-SiO₂ and ZnO-TiO₂-SiO₂ are prepared by colloidal chemical method.

Suggestions for quantum dot and quantum wire devices (transistors, lasers, information storage, etc.) have been around for quite some time, but there are still physics and technology based issues that will determine whether they have any practical importance. Various kinds of techniques such as lithography, etching, ion implantation etc. have been reported and demonstrated to realize quantum nanostructures. With all the above achievements, a lot of improvements are required in the presently fabricated quantum nanostructures for their size, size fluctuation, density and so on. These points are particularly important when we think of practical device applications. For this purpose, more detailed understanding of growth of structures in microscopic and macroscopic scales are necessary. However, this in turn suggests that there are still a lot of possibilities to be explored for the formation of quantum nanostructures. Significant efforts in the last few years have been aimed at controlling conductivity and improving crystal quality. However in order to realize ZnO devices, problems related to

additional material process and process development issues must be addressed.

7.2 Optical properties

All the exciton problems attracting interests recently are related to quantum many-body problems and to non-equilibrium dynamics far from the thermal equilibrium. For eg, the exciton-lattice interactions lead to the self-trapping phenomena, the randomness can induce the exciton weak localization, or the exciton-photon interaction results in the exciton squeezing. These effects and their dimensionality open new field in nanophotonics.

7.2.1 Fluorescence spectroscopy

We have highlighted the size and excitation wavelength dependence of the fluorescence behaviour in nano colloids of ZnO. The size dependent optical bandgap is systematically investigated and there is red shift in optical bandgap with increase in particle size. The fluorescence maximum shifts towards red as the excitation wavelength is increased. This observation has been attributed to the presence of energetically different associated forms of the constituent molecules and the slow rate of the excited state relaxation process in these media. The high polarity and viscosity of the medium slows down the relaxation of the excited state. In summary, the inefficient energy transfer between the upper and the lower vibrational levels of the excited state of these particles owing to the short fluorescence lifetime is primarily responsible for the excitation wavelength dependent spectral shift of ZnO colloids.

Fluorescence spectra consist of emissions in the UV and visible regions. Apart from the known bandgap emissions at 380 nm and impurity dominated emissions at 530 nm, emissions in the 420-490 nm range are also observed with increase in particle size. This series of peaks are related to the transition from excited state energy levels of exciton to ground state by

modelling it with a particle in a box problem. The UV band has been assigned to the *bandgap* fluorescence of clusters of different sizes. This allows us to reconstruct the size distribution curves from fluorescence spectroscopy. Systematic studies on nano crystallites have indicated the presence of luminescence due to excitonic emissions when excited with 255 nm as well as significant contribution from surface defect states when excited with 325 nm. The relevant energy levels showing the transitions corresponding to the observed peaks in the emission spectrum of ZnO of particle size 18 nm under 255 nm excitation are calculated.

Effect of annealing on the spectral properties of ZnO thin films are investigated and it is found that the intensity of UV band remains the same while the intensity of the visible band increases with increase in annealing temperature. Very strong UV emissions are observed from ZnO-Ag, ZnO-Cu and ZnO-SiO₂ nanocomposites. The strongest visible emission of a typical ZnO-Cu nanocomposite is over ten times stronger than that of pure Cu due to transition from deep donor level to the copper induced level. The optical bandgaps of ZnO-CdS and ZnO-TiO₂ nanocomposites are tunable and emission peaks changes almost in proportion to changes in bandgap.

7.2.2 Nonlinear optical properties

Nonlinear optical properties of ZnO semiconductor nano colloids and thin films are investigated for optical power self-limiting application. ZnO nano colloids show negative nonlinearity and good nonlinear absorption behaviour at off resonance wavelength. The observed optical nonlinearity is explained on the basis of two photon absorption followed by weak free carrier absorption. In the weak confinement regime, the third-order optical susceptibility $\chi^{(3)}$ increases with increasing particle size (R) and annealing temperature (T) and a R² and T^{2.5} dependence of $\chi^{(3)}$ is obtained for nano ZnO. These studies can be extended to strong confinement regime. Nonlinear susceptibility is highly fluence dependent and it becomes quadratic in nature

for large particle size. The optical limiting response of ZnO nano colloids, in the diameter range of 6–18 nm, increases with the increase of particle size. Optical limiting response is temperature dependent and the film annealed at higher temperature and having larger particle size is observed to be a better nonlinear absorber and hence a good optical limiter.

The nonlinear optical properties of self assembled films formed from ZnO colloidal spheres have been investigated and compared with those of films developed by sol-gel process and pulsed laser ablation using z-scan technique. ZnO colloids and thin films clearly exhibit a negative nonlinear index of refraction at 532 nm. The colloid and films developed by dip coating as well as pulsed laser ablation exhibit induced absorption whereas the self assembled film exhibits saturable absorption. This behaviour can be attributed to the saturation of linear absorption of the ZnO defect states.

The nonlinear optical response of ZnO nanocomposites is wavelength dependent and switching from induced absorption to saturable absorption has been observed at resonant wavelengths. Such a changeover is related to the interplay of bleaching of plasmon/exciton band and optical limiting mechanisms. ZnO based nanocomposites show self-defocusing nonlinearity and good nonlinear absorption behaviour at 532 nm. The observed nonlinear absorption is explained through two photon absorption followed by free carrier absorption, interband absorption and nonlinear scattering mechanisms.

The nonlinearity of the silica colloid is low and its nonlinear response can be improved by making composites with ZnO and ZnO-TiO₂. The increase of the third-order nonlinearity in the composites can be attributed to the enhancement of exciton oscillator strength. This study is important in identifying the spectral range and composition over which the nonlinear material acts as an RSA based optical limiter. These materials can be used as optical limiters and are potential nanocomposite material for the

light emission and for the development of nonlinear optical devices with a relatively small limiting threshold. For a comparison, the optical limiting threshold values are shown in table 7.1.

Compound	Optical limiting threshold MW/cm ²
SiO ₂	120
ZnO	55
TiO ₂	22
Ag	21
CdS	20
Cu	10
5ZnO-SiO ₂	20
ZnO-5TiO ₂	13
ZnO-5Ag	12
5ZnO-TiO ₂ - SiO ₂	11
ZnO-5CdS	7
ZnO-5Cu	3

Table 7.1: Values of optical limiting threshold of ZnO nanocomposites

The size dependence of fluorescence lifetime of nano ZnO can be investigated. When the spherical particles of ZnO are converted into nano rods and nano wires, alteration of the spectral and nonlinear optical characteristics is another possible direction for future studies. The works related to nanocomposite can be done in solid state form and optical limiting threshold can be further reduced for optical device applications. The size and structure evolution of nanocomposites may also have some relation with

optical characteristics in addition to the composition and is a possible direction for future studies

At reduced dimensions, interfaces play far more important and delicate role in quantum devices. Thus, the interfaces of quantum structures should be perfect in the interface atom arrangements and be capable of producing desired potential profiles required for quantum device operation. Additionally, the interface region should be free of ionized impurities and trapping defects such as surface states, interface states and discrete deep levels.

We also need further understanding of the physics of semiconductor nanostructures through the characterization of the optical and electrical properties of unique structures ranging from single isolated quantum dots, arrays of quantum dots to coupled quantum dots. For these reasons, efforts should be continued to seek some breakthrough in the formation of quantum nanostructures not only for the understanding of their physics but also for their device applications.

7.3 Device applications

The successful fabrication of quantum wire and quantum dot structures have enabled scientists to explore novel concepts such as exciton based nonlinear optical effects and confinement effects as well as new concept devices like microcavity lasers and single-electron transistors. The semiconductor research through advanced materials engineering has inspired many ingenious experiments, resulting in observations not only of predicted effects but also of phenomena hitherto totally unknown. Activity at this new frontier of semiconductor physics has in turn given immeasurable stimulus to scientists working in device physics, provoking innumerable new ideas for applications. Thus a new class of transport and optoelectronic devices has emerged.

Many studies about nanoscale effects in recent years have shown that nanoscale semiconductor devices have a good potential for high speed and capacity in telecommunication and information technology. In terms of components, discrete devices consisting of nanoscale semiconductors exhibit quantum mechanical characteristics in device operations, which imply ultrahigh speed switching, ultralarge integrability and multifunctionality. Such components will become more important as the information processing technologies begin to attract more attention, because in system applications quantum devices are expected to increase their share of functions. Semiconductor quantum devices showing functional properties that can serve the above mentioned purposes will therefore have more future prospects.

An important key issue for semiconductor devices is the development of a suitable theory for device analysis and design based on quantum mechanics. Unsolved issues include level structures and wavefunctions of quantum states in dots, many body effects, nature and rates of single electron tunneling, phase coherence, tunneling time, co-tunnelling, current leakage mechanisms, effects of external electromagnetic environments, charge fluctuation and off-set charge, current fluctuation and noise etc. For semiconductor coupled dots, one also needs a theory for quantum mechanical analysis and design of such artificial molecules and their arrays.

Key issues for the future can be summarized as follows:

1. The understanding and design of devices, based on quantum mechanics
2. Further progress on material/fabrication technologies
3. Cooperative efforts from the basic physics level upto system architecture level are vitally important

7.3.1 ZnO based devices

The main issue currently limiting the production of ZnO based devices is that of the achievement of p-type ZnO. ZnO is predicted to be an intrinsic semiconductor since it almost exclusively occurs naturally as n-type. The cause of this inherent doping combined with the difficulty in achieving p-type material is still not directly understood. Recent improvements in the as-grown quality of ZnO material as well as successes with dopant atoms indicate that p-type doping of ZnO is an achievable goal.

Another issue important for the realization of ZnO devices is that of contacts to ZnO. While ohmic contacts to n-type ZnO are relatively easily obtained, the production of good reliable Schottky diodes still remains an issue. Whilst other issues within ZnO exist, these two are by far the most important and currently play a limiting role in the realization of ZnO devices. We are moving ever close to the future in which ZnO will be a viable and integral part of many functional and exotic devices.

"Look at the sky. We are not alone. The whole universe is friendly to us and conspires only to give the best to those who dream and work"
: A P J Abdul Kalam

Curriculum Vitae



Litty Mathew Irimpan,
Irimpan House, Poovathussery,
P O Parakkadavu-683579
Ernakulam, Kerala, India
E-mail: littyirimpan@yahoo.co.in

Litty Mathew Irimpan was born on 23rd September 1978 at Poovathussery, Kerala, India, completed her schooling in 1994 at St. Joseph's Girls' High School Poovathussery. She entered St. Xavier's College for Women, Aluva affiliated to Mahatma Gandhi University and took her Masters degree in Physics in 2001. She completed her Bachelors degree in Education from Jesus Training College affiliated to Calicut University in 2002. For a couple of years, she served as a lecturer in Soccorsso Convent Girls Higher Secondary School, Government Samithy Higher Secondary School and Cochin University of Science and Technology. She joined at the International School of Photonics as a full time research scholar under UGC-JRF scheme on 1st March 2004 under the supervision of Prof. P Radhakrishnan and Prof. V P N Nampoori. She is herewith submitting her thesis entitled "*Spectral and nonlinear optical characterization of ZnO nanocomposites*" in June 2008.